28 May 2010 | $10

Science

Arabia's Ancient Crossroads

AAAS

Seeking Science Standards

Alan I. Leshner is Chief Executive Officer of AAAS and Executive Publisher of *Science*.

Shirley Malcom is Director of AAAS Education and Human Resources Programs.

Jo Ellen Roseman is Director of AAAS Project 2061.

GREAT CONCERN HAS BEEN VOICED FOR AT LEAST 30 YEARS ABOUT THE SAD STATE OF U.S. PRIMARY and secondary education in mathematics, science, engineering, and technology, but little real progress has been made. The most recent findings from the U.S. Department of Education brought no optimism. In 2005, 32% of all U.S. fourth-graders and 41% of eighth-graders scored below expected achievement levels in science. Nearly 30% of entering college students needed remedial science and math courses. However, we are at a moment in U.S. history to finally address one cause of the problems, and the scientific community needs to help capture this unique opportunity.

The many national commissions and studies of science education in the past three decades have consistently identified the same two issues and potential remedies: a need for much better-prepared math and science teachers and for a clear statement of learning goals for science that are the same across the United States. The consistency would remove some of the disadvantages faced by students in states with less rigorous standards, and it would ease students' mobility across state boundaries. It would also help the United States develop robust curriculum and assessment materials and prepare teachers who understand the science to use such tools to help students reach the standards. Nearly all of America's competitor countries have national science education standards and score much higher on international science achievement assessments: U.S. 15-year-olds ranked 21st among students in 30 developed nations in science on the 2006 Programme for International Student Assessment.

Efforts are now under way that can move the United States toward what are often referred to as "common, internationally benchmarked, state-approved standards." In March 2010, the National Governors Association and the Council of Chief State School Officers (CSSO) released a draft of Common Core State Standards for English-language arts and for mathematics. This was followed in April by a call for state assessment systems based on those common standards. Because education in the United States is the responsibility of individual states, with the federal government providing vision and support but not control, this historic call by state leadership for common standards and assessments is momentous indeed. But science education has been left out of this public agenda for standards development. Fortunately, there is a major privately funded, common science education standards development effort taking place. The Carnegie Corporation of New York has funded the U.S. National Academy of Sciences (NAS) to develop a framework for such standards, and then, through work with the educational nonprofit organization Achieve, the standards themselves. The American Association for the Advancement of Science (AAAS) will play a supporting role in both efforts.

But the private effort to develop common standards can only be effective if the scientific community mobilizes to support it. This help is needed in at least three major ways. State and local education leaders need to hear now from the scientific community about the need for a common and coherent set of science education standards. Such urgings should be directed at state and local school boards, CSSOs, and state legislators who may ultimately rule on the use of these standards. Scientists must also participate in the standards development process. The first broad call for their contribution will come from NAS and is expected this summer, when comments will be sought on a draft framework. Once states agree on common science standards, scientists should help schools and teachers implement them, as many educators will have to learn new content, and they will need the help of scientists to support student learning.

A unique time has arrived for achieving the long-needed goal of common, state-level science education standards in the United States, a core component of effective science education reform. But we can only capture this opportunity if the scientific community steps up as a vocal, energetic advocate for common standards, while also becoming an active partner in the development and implementation processes. **– Alan I. Leshner, Shirley Malcom, Jo Ellen Roseman**

10.1126/science.1192334

A bite out of CDC's budget?
1088

Q&A with Francis Collins
1090

CLIMATE CHANGE RESEARCH

Arduous Expedition to Sample Last Virgin Tropical Glaciers

JAKARTA—For 25 years, Lonnie Thompson has longed to take a field crew to Papua, home to the only tropical glaciers west of the Andes and east of Mount Kilimanjaro. The glaciologist at Ohio State University's Byrd Polar Research Center (BPRC) in Columbus wants to retrieve ice from Puncak Jaya, a mountain in Indonesia's Papua Province, to glean insights into ancient climate and compare cores with records from the handful of other tropical glaciers. Next week, Thompson will get that chance—and not a moment too soon, as Papua's glaciers are almost gone. "The ice is melting very fast," says team member Dodo Gunawan, a climatologist at Indonesia's Agency for Meteorology, Climatology, and Geophysics (BMKG). "It's a race against time."

Puncak Jaya is perched at a critical spot in the global climate system: the western edge of the Pacific Warm Pool, which pumps more heat into the atmosphere than any other source on Earth. Gas bubbles, chemical compounds, and organic matter trapped in the ice should offer a window into past cycles of the El Niño–Southern Oscillation (ENSO), the periodic warming of tropical Pacific waters that wreaks havoc on climate, and on its capricious twin, La Niña, which brings cooler water. The ice should also provide clues into past ocean circulation and the Australasian monsoon rhythms.

The Papua project poses daunting logistical challenges, and the payoff is far from certain. It's unknown, for instance, how far back in time the Puncak Jaya climate record runs. What is clear is that this is the last chance to get useful data from Papua, says Thompson, whose team includes colleagues from BPRC, Columbia University's Lamont-Doherty Earth Observatory, and BMKG. "Once the glaciers melt, the history in the ice will be gone forever," he says.

Papua is the final terra nova in tropical glaciology. Thompson's team has hauled back ice from the other comparable glacial fields: Kilimanjaro's summit in Tanzania and several locations in the Peruvian Andes, including one that last year produced a record 195-meter-long core. The Papua ice should complement the Andes record, he says.

The expedition kicked off this week with an arduous and risky 2-day trek through rain forest, home to the Free Papua Movement, a long-running insurgency. The team will acclimate at a base camp some 4200 meters above sea level. Then drilling will commence at Carstensz glacier, 4884 meters high, and nearby Northwall Firn glacier. They plan to drill six cores down to bedrock.

Since photographic records began in 1936, the Puncak Jaya glaciers have beaten a steady retreat, punctuated by a brief expansion from 1997 to 2000. Since then, losses have accelerated. Comparing photos from Puncak Jaya last year and fresh ones from his advance team, Thompson says "the difference is absolutely amazing. There's a clear and present danger of decapitation," or loss of more recent data to melting.

Another unknown is the age of the Puncak Jaya ice. Kilimanjaro's ice cap, a mere 50 meters thick, goes back 11,700 years, into the last Ice Age. But that ice is more than a kilometer higher than Papua's glaciers. One discouraging possibility is that Puncak Jaya's ice began to accumulate only after the Medieval Warm Period ended several hundred years ago, Thompson says.

One challenge will be to get the cores back intact. Unlike treks in the Andes or Kilimanjaro, the team in Papua must make do without pack animals or porters. But they are getting crucial support from PT Freeport Indonesia, a company that operates a gold and copper mine near Puncak Jaya. The company will ferry the drilling equipment to the site by helicopter and then whisk chest freezers full of cores back to Tembagapura, a town halfway up the mountain, where they will be kept in an industrial-sized food locker before a series of flights gets them to Ohio for analysis. "If it wasn't for this city in the clouds, I don't know how we'd get the cores back," Thompson says.

Back in Ohio, the team will use a variety of techniques to date and analyze the ice. The first thing they will look for is radionuclides dispersed by Soviet atom bomb tests in the early 1960s. But even on Kilimanjaro, ablation had stripped away a half-century of ice by 2000. Volcanic dust could peg layers to massive eruptions of Mount Tambora in 1815

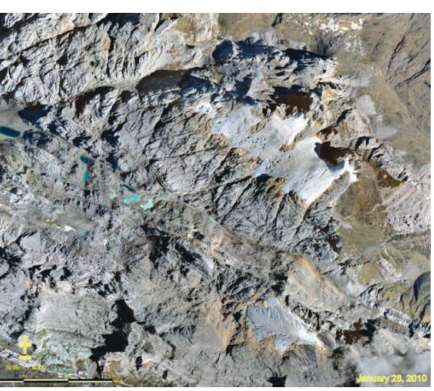

Vanishing act. In a January aerial shot of Puncak Jaya (*above*), Northwall Firn is upper right and Carstensz is lower right. Close up, Northwall Firn appears severely ablated.

CREDITS (LEFT TO RIGHT): COURTESY OF PT FREEPORT INDONESIA; COURTESY OF LONNIE THOMPSON

Published by AAAS

and Krakatau in 1883. Another possibility is to radiocarbon date insects and plants in the ice. And oxygen-18 levels can be compared with well-calibrated cores from Antarctica and Greenland. Gas concentrations are linked to regional temperatures and thus will be vital clues to past climates and the shifting currents of La Niña and El Niño. Core data may also serve as a proxy for the Indonesian Throughflow, which, as part of the global ocean conveyor belt, funnels warm water from the Pacific into the Indian Ocean and varies with ENSO conditions, says Columbia oceanographer and team member R. Dwi Susanto.

The expedition marks a coming of age for climate change research in Indonesia. "For the first time, when we talk about global warming, we will talk about data from our own soil," says Susanto, who is Indonesian. To help build capacity, two Indonesian graduate students at Ohio State will take the lead in analyzing the ice.

Researchers are holding their breath about just what they will find at the top of Puncak Jaya. Thompson, who has a track record of coming back with valuable data, is optimistic. "The beauty of going to a place no one has gone," he says, "is that we are sure to find something unexpected."

–RICHARD STONE

CLIMATE CHANGE

NRC Reports Strongly Advocate Action on Global Warming

The three reports released last week by the National Academies' National Research Council (NRC) had a familiar theme—the human-induced warming of the planet—but the tone, especially as presented to the public, was less familiar. The 2-year effort involving 90 scientists "emphasizes why the United States should act now," Ralph Cicerone, president of the National Academy of Sciences (NAS), said at a public briefing. The reports also have a few words about *how* the nation should act, which might influence a lively debate on a proposed Senate climate bill.

The science supporting the why of action on climate change recalled the 2007 report of the Intergovernmental Panel on Climate Change (IPCC). "Climate change is occurring, Earth is warming," said environmental scientist Pamela Matson of Stanford University in Palo Alto, California, chair of the NRC panel on advancing the science of climate change, one of three separate panels that produced the trio of reports. "These climate changes are largely caused by human activities."

But this was no rehashing of the IPCC report, which has taken considerable flak of late. The new NRC reports draw on the past 5 years of peer-reviewed literature, which was published too late for inclusion in the IPCC analysis, Matson emphasized. They also reflect findings from more than a score of reports from the U.S. Global Change Research Program and earlier efforts from NAS. The membership of the three NRC panels also had little overlap with that of the IPCC's working groups, says economist Gary Yohe of Wesleyan University in Middletown, Connecticut, an IPCC veteran who was on the NRC panel on adapting to climate change. Yohe says he was surprised to find at the panel's inaugural meeting that three-quarters of his fellow members were unfamiliar to him.

Call to action. Ralph Cicerone introduced climate reports detailing why the nation should act now.

Although NRC tasked the panel on limiting the magnitude of future climate change with providing "policy-relevant (but not policy-prescriptive) input," the panel did recommend that "the United States set a future greenhouse gas emissions target in the form of an emissions budget," said panel chair Robert Fri of Resources for the Future in Washington, D.C. And the NAS press release said a "reasonable goal" would be emissions of 170 to 200 gigatons of carbon dioxide equivalent in 2012 through 2050.

In recommending a carbon budget and a target range, the panels "did go farther than IPCC could," says climate scientist Stephen Schneider of Stanford University, who was not involved in the NRC reports. "There were more words like 'should' than you normally have with IPCC." And the press release takes the emission budget goal a step further, noting that it is "a goal that is roughly in line with the range of emission reduction targets proposed recently by the Obama Administration and members of Congress."

But can the report help bolster the proposals' chances of becoming law? "That's the $64,000 question," says ecologist Peter Frumhoff of the Union of Concerned Scientists in Cambridge, Massachusetts. The House of Representatives passed a bill that would probably keep the United States under the emissions budget, but action has been slow in the Senate. There, senators John Kerry (D–MA) and Joe Lieberman (ID–CT) have introduced a package with the same goals as the House version's but more flexibility and with subsidies for nuclear and fossil fuel industries. Senate Majority Leader Harry Reid (D–NV) recently announced a go-slow approach, which might see votes as late as July. But elections loom in the fall, and climate lobbyists worry that the closer elections get, the more hyperpartisan the atmosphere will be.

It's unclear whether science can change that. Myron Ebell of the Competitive Enterprise Institute in Washington, D.C., rattles off a number of Democrats in the House who supported last year's bill but have either publicly repudiated their vote or retired. "Cap-and-trade is dead," he says. Said a Senate staffer: "I'm hoping this will help push the issue, but I don't think we are at a place where scientific reports can find that influence."

–RICHARD A. KERR AND ELI KINTISCH

CREDIT: PATRICIA POOLADI/NAS

PARTICLE PHYSICS

Hints of Greater Matter-Antimatter Asymmetry Challenge Theorists

The universe is chock-full of matter and devoid of antimatter, and physicists can't say why. They think that matter piled up after the big bang thanks to a slight asymmetry, called charge-parity (CP) violation, in the way matter and antimatter behave, but the effects seen so far are too small to do the job. So when a team reported last week that certain particles showed a huge matter-antimatter asymmetry, physicists—and the front page of *The New York Times*—took note, as it could be a sign of new particles. But the marginal result could be a fluke, and theorists say it's difficult to explain why the effect is so big in this study and so small in earlier work on related particles.

"I take this as a provocative result rather than a discovery," says Chris Quigg, a theorist at the Fermi National Accelerator Laboratory (Fermilab) in Batavia, Illinois.

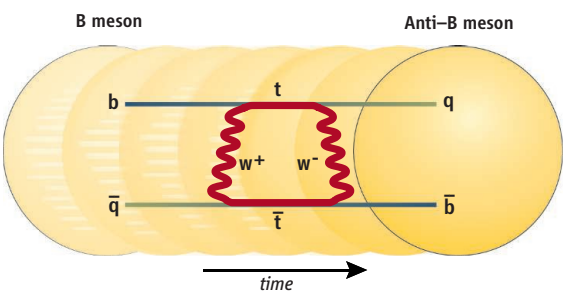

Presto! A B meson becomes an anti–B meson as its quark and antiquark exchange massive W bosons and top quarks.

To spot the asymmetry, experimenters working with Fermilab's D0 particle detector studied particles called B mesons, which flash into existence as Fermilab's Tevatron collider smashes protons into antiprotons. Each B meson contains a massive particle called a bottom quark bound to a lighter antiquark. Bizarrely, it can transform into an anti–B meson containing a bottom antiquark and a light quark through a process called "mixing." If matter and antimatter behaved symmetrically, then the anti–B meson should mix back into a B meson at the same rate, creating an even oscillation. Instead, the D0 team found that a B meson "prefers to exist a little longer in the matter state than the antimatter state," says Fermilab's Dmitri Denisov, co-spokesperson for the team.

The key to the experiment was that B mesons are born in the Tevatron's collisions in meson-antimeson pairs. So if an event contained a pair of B mesons or a pair of anti–B mesons, mixing must have occurred, and the D0 researchers could probe it by tallying such pairs. They did that by exploiting the fact that a B meson can decay into an easily spotted particle called a muon, whereas an anti–B meson decays into an antimuon. Two-muon events outnumbered two-antimuon events by 1%—a bias toward matter 40 times larger than the standard model of particle physics predicts, the team reports in a paper submitted to *Physical Review D*.

Here's the tricky part. B mesons come in two types: B_d mesons that contain a down antiquark and B_s mesons that contain strange antiquark. Counting muon pairs, the D0 team cannot tell the two apart, but studies elsewhere found no similar asymmetry in B_d mesons (although a small asymmetry appeared when B_d mesons were measured another way). So D0 researchers ascribe the skewing they see to the B_s mesons alone.

But it's not easy to whip up extra asymmetry for just B_s mesons. Mixing arises when the bottom quark and the lighter antiquark within a meson exchange other particles, which thanks to quantum uncertainty can be much more massive than the meson itself (see figure). So still-undiscovered massive particles could join in and pump up the asymmetry. But it's hard to explain why they would affect B_s mesons so strongly but leave B_d mesons alone, says Yosef Nir, a theorist at the Weizmann Institute of Science in Rehovot, Israel. "There are models that do it," he says. "But I would say that in the preferred models, the influence on B_s and B_d would be the same."

The result may soon be tested. The more-powerful Large Hadron Collider (LHC) at the European laboratory, CERN, near Geneva, Switzerland, feeds a detector named LHCb that's designed to study B mesons, and it should soon compete with Fermilab's D0 and CDF detectors in "B physics," says Sheldon Stone, an LHCb team member from Syracuse University in New York: "With any luck we will catch them by the end of the year, and by the end of next year we'll be way ahead."

–ADRIAN CHO

CREDIT: ADAPTED FROM FERMILAB

ScienceNOW

From *Science*'s Online Daily News Site

Genetic Discovery Promises to Boost Rice Yields

Some agricultural experts believe worldwide crop yields need to double by 2050 to avert a global food crisis. And improving yields of rice is deemed particularly important because rice is the staple food for nearly half of the world's population. Two groups working independently have now identified a variant of a gene in rice plants that could boost rice yields by 10%, though they must still demonstrate that their experimental breakthrough will pay off in farmers' fields. http://bit.ly/rice-yields

Animal Reserves Can Be Good for People, Too

Creating a national park or other reserve can help protect animals and plants. But what about the people who live in the area? A new study of Costa Rica and Thailand suggests that neighbors are better off economically than people who don't have parks nearby. http://bit.ly/animal-reserves

Body Temperature Time Machine

It's not quite as easy as putting thermometers under their tongues and waiting 30 seconds, but scientists have discovered a way to measure the average body temperature of animals that lived millions of years ago. The findings will help biologists learn more about extinct animals' physiology and give paleoclimatologists a powerful new tool for gauging ancient environmental temperatures. http://bit.ly/bodytemp

Life's Pageant Not So Rich

How many kinds of bugs are there? A new estimate, based on mathematical modeling and a major bug-counting effort in New Guinea, puts the number of arthropod species in the tropics—which account for most of the animal species in the world—at about 3.7 million, well below the 30 million once suggested. The results could help scientists get a better sense of how many species are disappearing in the current human-caused mass extinction. http://bit.ly/species-diversity

Read the full postings, comments, and more at **news.sciencemag.org/sciencenow**.

Published by AAAS

INFECTIOUS DISEASES

Fears of Lax Surveillance if CDC Program Cut

A proposal to stop funneling dollars directly to U.S. surveillance and research for most mosquito and other vector-borne diseases such as West Nile virus and dengue has scientists wringing their hands. They are concerned that if the plan sticks, the country will be ill-prepared to handle new emerging diseases and manage existing ones. The proposal in President Barack Obama's 2011 budget for the U.S. Centers for Disease Control and Prevention (CDC) in Atlanta, combined with a $15.7 million cut for infectious disease work generally, would virtually eliminate the vector-borne program. Currently, CDC funds mosquito testing for a variety of diseases and investigations into patterns of disease spread in the United States.

The budget recommended removing $26.7 million from the vector-borne program, along with $8.6 million from antimicrobial research, and partially offsetting that with an increase of $19.6 million to emerging infectious diseases. Since the cut was recommended earlier this year, several professional groups have urged Congress to override it and continue directing money to vector-borne diseases. If the vector-borne program is eliminated, they argue, CDC would likely respond only when disease surges.

"Everybody's looking for opportunities to save" money, says Ali Khan, acting deputy director at CDC's National Center for Emerging & Zoonotic Infectious Diseases. But although "we do support the president's budget, … if all these dollars are eliminated, there's no doubt this would have a profound effect." As an example of the importance of continued surveillance, some are pointing to the detection of 28 cases of dengue fever in Florida since last fall. These are the first cases in the continental United States since the 1940s, except for a few along the Texas-Mexico border. Although dengue is also raging in Puerto Rico.

Although the cut is a tiny part of CDC's $6.6 billion proposed budget, it has jolted a number of societies into action. The American Society for Microbiology submitted written testimony to Congress last month, as did the American Red Cross and other blood bankers. Other groups focused on epidemiology, public health, and mosquito control have either written to or met with congressional staff. It's not clear yet what impact those objections will have: Congressional appropriators won't finalize the budget until later this year.

Dengue on the upswing. Cases of the disease, transmitted by *Aedes aegypti* mosquitoes, have been rising, but CDC's dengue branch in Puerto Rico is threatened by possible budget cuts.

In the past, the budget has allocated money to vector-borne diseases within the United States as a group and separately to malaria and to Lyme disease; those two are unaffected by the proposed cuts. The vector-borne program is a catchall for many diseases transmitted mostly by mosquitoes, although the list shifts as new conditions surface and some diseases become less common. The current vector-borne program began in 1999 when the first cases of West Nile virus showed up unexpectedly in crows and then people. Its finances have held mostly steady, with occasional cuts in recent years as West Nile cases have dropped in some areas and the virus has faded from public attention. About $13 million of the nearly $27 million is distributed to state and local health departments, and Khan estimates that 100 state employees and 24 at CDC would lose their job if the cuts go through. Most severely affected would be CDC's Dengue Branch in San Juan, Puerto Rico, and another branch of the Division of Vector-Borne Infectious Diseases in Fort Collins, Colorado, which could lose more than half its funding. Rather than allocate money specifically to vector-borne diseases, the 2011 budget recommends a new tack: pooling money for infectious diseases more generally and consolidating the work in one center instead of two.

But many say that removing dedicated funds for vector-borne diseases is shortsighted and could gut the strong surveillance programs that state and local health departments have built, making CDC reactive rather than proactive. "If you're not doing surveillance, … you're going to miss these things until you have a major outbreak," says Laura Kramer, a virologist at the New York State Department of Health in Albany. The current program supports seasonal testing of mosquitoes and other potential vectors, such as ticks, along with testing of dead birds. It has also supported studies into the evolution of West Nile virus and the genetics of the mosquitoes that transmit it.

Justifying all this when there's little illness—West Nile cases plunged last year—leads people to ask, "Why are we doing this?" Kramer says. Although the proposed budget allows money to be funneled back to vector-borne diseases if they resurface, Kramer says that's less efficient than sustaining the program. "The people who have been trained to do the work in the labs and the field aren't going to be there" anymore, she says.

There would be other effects as well. "We rely on [CDC's surveillance] data to mold … our testing policies," says Roger Dodd, vice president of research and development at the American Red Cross in Rockville, Maryland. In times and regions where West Nile is surging, the Red Cross tests every blood unit for the virus rather than pooling blood for a less sensitive test, as it usually does. The Red Cross is also concerned about dengue virus because two transfusion cases have been reported, both in Asia.

Khan says CDC will find money for vector-borne diseases somehow, no matter how the budget shakes out. "This is a priority for us, and we will support" it, he says. "However, we are all very conscious and honest that you can't get all [you need] out of these cuts."

–JENNIFER COUZIN-FRANKEL

CREDITS: COURTESY OF CDC

Published by AAAS

SCIENCE AWARDS

Efforts to Stop UNESCO Science Award in Honor of African Dictator

Unless human-rights organizations score a last-minute victory, one or more life scientists could find themselves in an awkward spot next month: to be awarded a prize by the United Nations Educational, Scientific and Cultural Organization (UNESCO) that is named after one of Africa's most infamous dictators.

As *Science* went to press, behind-the-scenes discussions about the award, named after President Teodoro Obiang Nguema Mbasogo of Equatorial Guinea, were still going on at UNESCO, and nongovernmental organizations (NGOs) were increasing the pressure to stop, or at least postpone, what they see as a major embarrassment. But a UNESCO spokesperson said the five-member jury has already made its choice, and UNESCO Director-General Irina Bokova could adopt their recommendations as early as this week. Prize rules stipulate that up to three researchers, groups, or institutions can share the $300,000 award.

Obiang, who came to power in a 1979 coup against his uncle, has ruled his small West African country of fewer than 1 million people with an iron fist. A U.S. Department of State report issued last year cites many human-rights violations, including unlawful killings by security forces, government-sanctioned kidnappings, systematic torture of prisoners and detainees, and arbitrary arrests. A 2004 U.S. Senate investigation also cited evidence of corruption by Obiang and his family, which enjoys a very lavish lifestyle. Equatorial Guinea became very wealthy after oil was discovered in its waters in the 1990s, but more than half the population still lives in extreme poverty.

The Obiang government proposed the prize for "scientific achievements that improve the quality of human life" in 2007 and put $3 million on the table in award money and administrative costs for the first 5 years. When the proposal came before UNESCO's Executive Board—on which 58 of the agency's 193 member states have a seat—in October 2008, many Western countries opposed it, but they didn't ask for a vote because they knew they would be defeated, says one diplomat. "It was the first African science prize. African countries were all in favor, and they had enough supporters among the G77," a coalition of developing nations, the diplomat says.

The award puts Bokova, a Bulgarian diplomat elected in 2009 on a platform to reform the heavily politicized agency, in a difficult position. She appears to have signaled her own reservations about the idea in a speech at an April meeting of the Executive Board, when she said that she had "received criticism" about the prize, which she had passed on to the board.

Bokova has also asked a task force to look at the procedure for new prizes. She wants "to make sure there is real consensus about the creation of these awards," a spokesperson says. But the review, whose outcomes probably won't be known until this fall, comes too late to affect the Obiang prize. Early this week, Gavin Hayman, campaign director of Global Witness, said he still held out hope that the prize would be canceled or postponed—or that the laureate, or laureates, will refuse it. "It would be a brave person to accept this prize," he adds.

Sylvie Rano, a member of Equatorial Guinea's delegation to UNESCO, says she is "sorry" that NGOs are trying to block the award. But she would not comment further and referred *Science* to President Obiang's office. Rano says Obiang plans to come to Paris for the June ceremony if his agenda permits it.

–MARTIN ENSERINK

Prize fight. A $300,000 award named after president Teodoro Obiang put UNESCO Director-General Irina Bokova in a difficult position.

CREDIT: FABIO RODRIGUES POZZEBOM/ABR/WIKIMEDIA COMMONS

*Science*Insider

From the *Science* Policy Blog

Dedicated team coverage of the Gulf Oil spill included a critical look at the much-ballyhooed risk that the **Loop Current** would drive the oil to Florida. An expert said the amount of oil involved and the predicted behavior of the current made that unlikely. The 20 biologists working for Louisiana have found **oil on the state's beaches** for the first time; experts hope tall reeds can survive the slick on the surface. Scientists explained why so much of the oil has remained **under the surface of the ocean** and when it might rise. http://news.sciencemag.org/oilspill/

In a Q&A, research policy expert Mary Moran explained the rationale behind the PDP+ Fund, proposed by the International Aids Vaccine Initiative and partners. The fund would pool money from government and private sources, and even bonds or grants to support existing "Product Development Partnerships" to develop **treatments for neglected diseases**. Some 140 such efforts exist, said Moran, but they are underfunded and don't last long enough. http://bit.ly/PDPfund

Forty-one prominent anthropologists have written a letter of complaint to the U.S. Department of the Interior about a proposed new **rule on human remains**. The ruling would allow groups to file requests to bury human remains held by scientists at universities or other research institutions even if the groups are unconnected to the remains. http://bit.ly/BurialRule

After the announcement of the creation of a **synthetic genome**, President Barack Obama has ordered a 6-month study of the topic from his bioethics commission. http://bit.ly/SynBioLetter

British scientists appear to have avoided £6 billion (about $9 billon) in cuts to this year's budget passed by the new Conservative–Liberal Democrat governing coalition. The former government had planned to spend £230 million on the UK Centre for Medical Research and Innovation in the 2010–11 budget, but the funding will be allotted more slowly. http://bit.ly/BritFunding

See the full postings and more at **news.sciencemag.org/scienceinsider**.

Published by AAAS

NEWSMAKER INTERVIEW

Francis Collins: On Recruiting Varmus, Discovering Drugs, the Funding Cliff

He may be working a 100-hour week, but human geneticist Francis Collins is clearly enjoying running the National Institutes of Health (NIH). Since he began last August, he has pushed out the door the $10.4 billion that NIH got in last year's stimulus package, fleshed out five strategic themes for NIH (*Science*, 1 January, p. 36), and put his stamp on the president's proposed 2011 budget.

Collins's passion is to expand NIH's emphasis on translational research. He wants to give basic researchers the tools to convert their discoveries into therapies, he says. He is also an enthusiastic proponent of a new drug-development program at NIH called the Cures Acceleration Network. The program, approved for $500 million a year but not yet funded, was added to the health reform bill by biomedical research champion Senator Arlen Specter (D–PA).

Last week in an interview at NIH with several *Science* staffers, Collins said he was "grieving" about Specter's loss in the Democratic primary. He discussed NIH's budget prospects for next year and spoke of his role in luring former NIH director Harold Varmus back to Bethesda to head the National Cancer Institute (NCI).

Here are his comments, edited for brevity and clarity. On *Science* online, this article links to a full transcript.

–JOCELYN KAISER

Q: What has it been like going from directing the genome institute to running the whole NIH?

F.C.: When I ran the genome institute, I felt I could pretty much get my head around most of the major issues that we needed to attend to on any given day. Here, it's quite a stretch. The hours are long; I'm probably working 100 hours a week in an average week.

Q: Regarding the budget and grant funding, you've said that you expect very low success rates in 2011, 15%. What's this going to mean?

F.C.: We don't know what the budget will end up being. Obviously, the signs are not particularly good that the Congress will do better than the president's budget [a 3.2% increase]. Some noises might even indicate that they'll do worse.

We will undoubtedly have to look at draconian things like downward negotiations, which means cutting the budgets of approved grants in order to try to free up dollars to fund more grants. We are trying to protect certain parts of the enterprise. Postdoc training slots, for instance. But I'm sorry, I can't come up with a magic solution here that is going to reduce all of the pain.

Q: Some researchers are worried that your emphasis on translational research and big goals will mean cutting back on investigator-initiated grants.

F.C.: I don't think they should be very worried. Everybody's going to be stressed, so it will be tempting if your grant didn't get funded to look around for some reason other than the fact that it was a tough year budgetarily. The amount of additional funds that might go into focusing on translation are going to be maybe 1% or thereabouts of the overall NIH effort. That shouldn't have a very big effect.

Q: Does that mean 1% less for investigator-initiated research?

F.C.: I would argue that if NIH simply said we're going to keep doing what we've been doing all along, we're not in a very good position then to ask the Administration or the Congress to give us more resources.

The translational goals get a lot of traction with the Congress, with the public. They should. I mean, we're the National Institutes of Health. We are supposed to be coming up with ways to prevent and treat disease.

Q: As part of this, you're investing more and more in drug discovery and development. Why?

F.C.: Let's talk about TRND [Therapeutics for Rare and Neglected Diseases]. In terms of dollars, it's pretty puny. Fiscal year 2010: $24 million. What's in the president's budget for FY '11 is $50 million. On the scale of $31 billion to $32 billion, it is a pretty tiny blip.

It is high-risk for sure. Why should we do it at all? Well, if you're talking about rare diseases, or diseases of the developing world that don't have much of an economic market, if the government doesn't get invested in those therapeutic efforts, they're not going to happen.

We've arrived at the point scientifically where we've discovered the molecular basis of hundreds of diseases, and academic investigators [can] turn that into a high-throughput screen that yields up a small molecule that looks like it might be promising. And what TRND offers is to go one step beyond that into the preclinical phase to take some of those promising compounds and see whether you could get them all the way to FDA approval and a clinical trial. … So all of that I think is very defensible.

Q: Have genomewide association studies (GWAS) paid off?

F.C.: We're approaching 1000 validated genetic variations associated with a common disease. Most of them with very small odds ratios [as a cause of disease]. So probably not of much use for making predictions about future risk.

But I see no reason why there should be any connection at all between the strength of a variant as far as its risk on future illness and whether it is pointing you towards a target that could be very valuable for new drug development. So I think we have 1000 new drug targets sitting in front of us. I get

CREDIT: COURTESY OF THE NATIONAL INSTITUTES OF HEALTH

Published by AAAS

a little bit frustrated when people say, "Oh, GWAS has been a bust."

Q: Was it hard to persuade Harold Varmus to come back [to NIH]?

F.C.: You know, initially Harold was helping with the search process. Which had to be informal because this was a presidential appointment, but he obviously knew the field and so he and a few others were helping me with the trolling of the landscape. After a couple, three, months, it became more and more clear to all of us that there was a really perfect candidate right there in our midst.

Obviously, this is a big investment for him to come back to NIH, for a guy who loves New York City, and to take this on. But he's got a lot of ideas, a lot of fire in the belly. It's going to be wonderful having him here.

Q: There seems to be paranoia that you and Varmus want to take away the special status of NCI.

F.C.: The [Institute of Medicine] in [a] report back in 2003 concluded that the special status of the NCI has been more of a negative than a positive. So what is it that people are worried about here? That not having the ability to submit the bypass budget is going to have a big effect on cancer research? As far as I can tell, the bypass budget has no effect on anything.

Are they worried that not having a presidentially appointed institute director is going to do damage to the leadership of the institute? Well, look back over time and you decide whether that presidential appointment, which means it becomes a political issue, has been a good thing or not. I think Harold and I have the same view here, that this is a big place with a lot of smart people, and the best outcomes are generally when you don't have walls between parts of the organization that prevent people from learning from each other.

Q: How much time do you get in your own lab?

F.C.: I try to be over there on Monday mornings. I have about 10 people in my lab, three projects: diabetes, progeria, and asthma. It's great for me, it's like a wonderful respite from dealing with lots of other issues to actually look at data and talk to young scientists about where they're going. And I would argue it also makes me a little bit more effective as an NIH director to be anchored in the reality of what science is all about instead of just reading it in journals. It works out. It wouldn't work out if I wasn't willing to work 100 hours a week.

NATIONAL INSTITUTES OF HEALTH

Lowering the Boom on Financial Conflicts

After a year of review, the National Institutes of Health (NIH) has unveiled a plan for cracking down on conflicts of interest in biomedical research. Pressured by Congress, NIH last week released proposed changes to a 15-year-old regulation affecting everybody who receives U.S. Public Health Service money—about 40,500 grantees. The changes would require researchers to report more financial information to their employers, have the institutions and not researchers decide when a conflict exists, and make some of the reported information public.

NIH Director Francis Collins explained that although "partnerships between NIH-funded researchers and industry are essential," public trust is essential, too. Even if it means more paperwork, "we cannot afford to take any chances with the integrity of the research process."

Watchdog groups and the Association of American Medical Colleges (AAMC) generally praised the revisions. Senator Charles Grassley (R–IA), who has been investigating conflicts in academic medicine, called the changes "an important step in the right direction."

NIH is responding to growing controversy over the influence of drug money in biomedicine, including allegations by Grassley's staff that several NIH-funded psychiatrists failed to disclose consulting income (*Science*, 3 July, p. 28). The revised rules would lower the threshold for "significant," hence reportable, outside income or equity from $10,000 to $5000 and remove entirely the 5% threshold for reportable equity in a nonpublicly traded company. Investigators would inform their institutions about all significant financial interests related to their "institutional responsibilities"—so that administrators, not the investigator, would decide if any are related to a specific NIH-funded project.

For the first time, institutions would have to send NIH a detailed report on the amount of money involved and how the conflict is being managed. This would help NIH make sure institutions are following the regulation, said NIH Acting Deputy Director for Extramural Research Sally Rockey. And institutions would be required to disclose senior investigators' significant conflicts related to an NIH grant to the public on a Web site.

The changes fall short of what some experts wanted. The Institute of Medicine (IOM), for example, had recommended that researchers should report all industry financial relationships to their institutions, with no minimum dollar threshold. The highest level of public disclosure is an open-ended "above $250,000." That means the public won't know if the amount is $250,000 or $2 million, says Allan Coukell of the Pew Prescription Project in Boston. However, Coukell calls the rules "pretty solid" overall.

"It's definitely an improvement in terms of disclosure," agrees Lisa Bero, a conflict-of-interest expert at the University of California, San Francisco. But she points out that responsibility for handling conflicts hasn't changed: It will still lie with institutions—and NIH hasn't given them much specific guidance. For example, the rules don't say that conflicts should be avoided in human subjects research, which IOM and AAMC have urged. "I think there's going to be a lot of variability" in how institutions implement the rules, Bero says.

NIH will take comments for the next 60 days before issuing a final regulation.

–JOCELYN KAISER

Key Changes to PHS Conflict-of-Interest Rule

	Old	New
Reportable interest:	$10,000 or 5% equity	$5000 or any equity in nonpublicly traded company
Conflict determined by:	Investigator	Institution
Public disclosure of conflicts:	No	Yes
Institutions report to NIH:	Existence of conflict, whether managed	Conflict's nature, amount, how managed

Published by AAAS

A Forgotten Corridor Rediscovered

As the world's first civilizations emerged in the 3rd millennium B.C.E., an obscure region in eastern Arabia served as a crucial trade link while developing a surprisingly sophisticated independent culture of its own

BAT, OMAN—To a layperson, the three broken bits of red-and-black pottery, which fit in the palm of one hand, all look similar. But for 31-year-old archaeologist Chris Thornton, each piece tells a remarkable and distinct story of the time when humans first began to travel and trade over a vast area.

One angular piece shows that some 4500 years ago, traders carrying pots created across the sea in Iran's distant Kerman Province came to this small oasis in a remote corner of Oman in southeastern Arabia. A second piece hails all the way from the Indus River civilization, some 1500 kilometers to the east. And the third piece is a local imitation of the imported Indusware, not quite as sophisticated as the original. The modest sherds are clear evidence that in the 3rd millennium B.C.E., this dry and rugged region of the Arabian Peninsula was an important trading crossroads.

Clues like these are remaking our understanding of the first civilizations and the networks that bound them together. The urban centers of Mesopotamia, Iran, and the Indus River were connected in a web encompassing much of southern Asia, including places like Bat that were long considered backwaters. "This is a quite dynamic world filled with people moving about," says archaeologist Gregory Possehl of the University of Pennsylvania, who directs the dig at Bat. "There were a number of chainlike networks. The whole place was quite lively."

That's a far cry from the traditional view in which the world's first civilizations—Egypt, Mesopotamia, and the Indus—were largely isolated by sparsely populated deserts, seas, and mountains. Recent digs in Iran and Central Asia, however, have uncovered a plethora of ancient cities that traded goods and technologies overland with one another and their more famous neighbors (*Science*, 3 August 2007, p. 586). Now discoveries

Rocks of ages. Five-millennia-old Hafit tombs like these dot the rugged hills of Oman.

PHOTO CREDIT: REBECCA GILMOUR

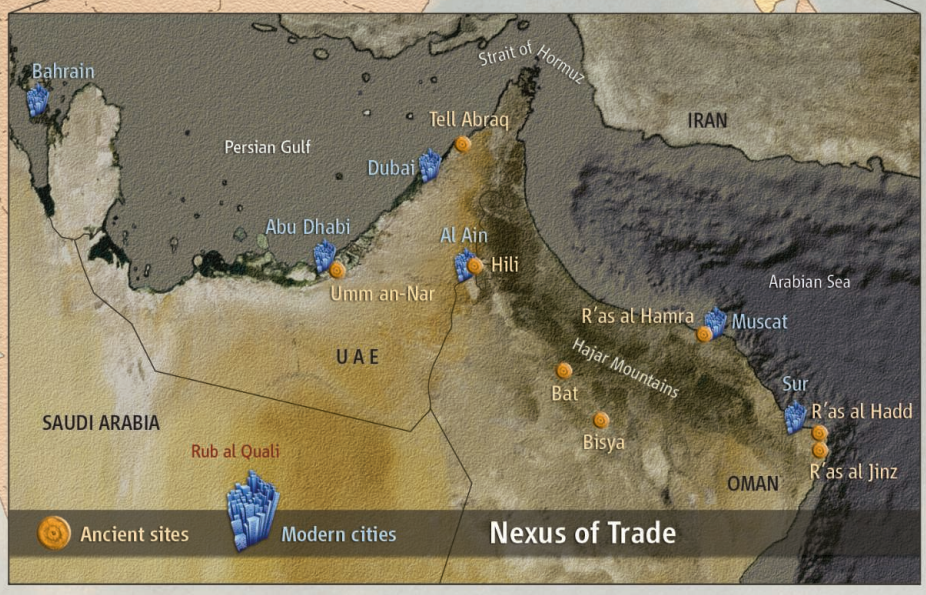

Trading place. Arabia was perfectly positioned to be the linchpin of trade among the world's first great civilizations.

in Oman and the neighboring United Arab Emirates (UAE) are beginning to show that there was a southern sea route as well, which funneled raw materials such as copper and manufactured goods such as textiles across the Arabian Sea and the Persian Gulf.

Those links reached deep into the eastern Arabian Peninsula to sites such as Bat, a modest settlement that by 2400 B.C.E. boasted massive round stone towers and tombs, a clever system to manage scarce water, and exotic goods.

Much is still unknown, including whether Indus traders actually penetrated deep into Arabia, the identities of the sailors who first plied the Indian Ocean, and just how extensive that contact was. But clues continue to emerge from numerous archaeological digs in Oman and the UAE, a region that has become a hotbed of excavation (see p. 1098). Work here and in the western Persian Gulf, Iran, Pakistan, and India reveals that this early Arabian culture was a nexus point for the far-flung civilizations of the 3rd millennium B.C.E. "Arabia is the hinge," says Maurizio Tosi, an archaeologist at the University of Bologna in Italy who has conducted pioneering work in the region.

Sailing away

While vacationing in 1981 on a cliff-ringed beach on the easternmost cape of Arabia, 200 kilometers east of Bat, Tosi stumbled on a 4500-year-old settlement. Over the next decade, he and his late colleague Serge Cleuziou of CNRS in Paris dug the site, called R'as al Jinz, and eventually uncovered ivory combs and potsherds marked with distinctive signs from the Indus River civilization, all buried in a modest mud-brick house.

They also excavated lumps of bitumen, an oil-based substance common in Mesopotamia, covered in barnacles. One piece still had the impressions of rope. The bitumen provided convincing proof for ocean-going boats made from reeds or planks sewn together and slathered with the imported waterproof substance—at the astonishingly early date of 2200 B.C.E. Excavators also found a piece of broken pottery chemically determined to come from Mesopotamia. Thus this single site demonstrated maritime connections with the two largest civilizations of the day.

The finds stunned archaeologists, who had long assumed that mariners did not master the secrets of the Indian Ocean's monsoon winds until 1000 or more years later (see p. 1094). And it forced them to rethink trade connections between the Indus and its western neighbors. When the evidence was presented at a meeting in the early 1980s, "it was a very dramatic moment," recalls New York University's Rita Wright. "We were all dumbfounded."

The discovery put the spotlight on an area mostly neglected by archaeologists. But given its modest houses and size, R'as al Jinz was almost certainly a fishing village rather than an international port. So where did ships from the Indus dock? To find out, researchers have moved a short drive up the dramatic coast to a series of sites at R'as al Hadd, where they are finding even earlier settlements.

Current excavations by Maurizio Cattani, also from the University of Bologna, are exposing a rudimentary settlement dating back to the end of the 4th millennium B.C.E. By 3000 B.C.E.—centuries before Indus goods arrived at R'as al Jinz—the inhabitants here suddenly enclosed a 60-meter-by-40-meter area with a 1.5-meter-high stone wall. The settlers imported clay for their floors and built mud-brick structures using bricks of identical size to those at Hili, a distant oasis town just west of the Oman border in Abu Dhabi. One building exposed this season has a tripartite structure reminiscent of those found in Mesopotamia in that era. "The transformation is so fast," says Cattani. "It went directly from poor huts to stone structures—

Online
sciencemag.org
Podcast interview with author Andrew Lawler

CREDIT: (MAP SOURCE) GOOGLE EARTH

Published by AAAS

Tomb rater. At R'as al Hadd, Cattani seeks clues to Arabia's great transformation.

almost as if it is a kind of colonization, or a push from outsiders."

Just who those outsiders might have been is unclear. The huge number of fish bones—the area is renowned even today for the size and variety of its fish—suggests that inhabitants salted fish to trade with peoples living inland on the southern slopes of Oman's Hajar Mountains. Donkey bones, date pits, and copper pieces are signs of a robust trade with those interior settlements by the middle of the 3rd millennium B.C.E., prior to the arrival of Indus goods. But there is no sign here of a port that might have served oceangoing ships later in the 3rd millennium B.C.E. Tosi and Cattani suspect that it may still lie in the vicinity: The current lagoon has shifted over the millennia, they think, and the port may be lost or lie under the town's medieval fort. But some other archaeologists theorize that international trade here may have been restricted to an exchange of pots for supplies by roving Indus fishers. Indus pots were likely highly prized luxury items, given that Arabians made few ceramics themselves until well into the 3rd millennium B.C.E., typically preferring skins, like their Bedouin descendants. The question of just how extensive the trade here was remains unresolved.

Another puzzle is the sudden sophistication that appears at both coastal sites like R'as al Hadd and R'as al Hamra near Oman's capital of Muscat as well as at interior eastern Arabia settlements like Bat. What Tosi calls "the great transformation" predates the rise of the Indus civilization. Although a scattering of small Mesopotamian pots dating to 3000 B.C.E. demonstrates a link with that society, the changes wrought in Oman appear to have been largely homegrown.

Whatever the extent of trade at R'as al Jinz itself, evidence from elsewhere makes it clear that global trade took off in the middle of the 3rd millennium B.C.E. By then, inhabitants in Oman were apparently ready to participate as important players. Cuneiform tablets from Mesopotamian cities detail huge amounts of copper coming from the land of Magan, believed by many scholars to be Oman. Ports on the Persian Gulf, along the coast of today's UAE, transported metals from deep in the interior, and manufactured goods such as textiles were provided in exchange, says Piotr Steinkeller, an Assyriologist at Harvard University.

Going to Bat

Hints of this ancient trade are emerging in an unlikely spot: Bat, a small village set amid a palm grove deep in Oman's interior. To the

The Shipping News, Circa 2200 B.C.E.

MUSCAT, OMAN—As a team of senior archaeologists watched in horror from the deck of the sultan's yacht, the reed vessel it was accompanying began to sink. The 13-meter-long, 11-ton craft, the *Magan III*, had been launched from the harbor here and was aiming at the Indian port of Mandvi, 1000 kilometers away. But after just several dozen kilometers, the vessel took on water and eventually foundered. The crew was rescued, but the debacle on 7 September 2005 ended an unusual research experiment aimed at understanding how ancient mariners made the passage from the Arabian coast to the Indus River civilization more than 4000 years ago.

The project was sparked by archaeological discoveries that show a maritime link between the Indus, Arabia, and Mesopotamia in what may have been the world's first oceangoing vessels (see main text, p. 1092). But debate continues over the design of what may have been the world's first oceangoing vessels.

Seaworthy. This piece of bitumen documented ancient sea trade.

Boats were used in the Persian Gulf as early as 5000 B.C.E., based on recent excavations in Kuwait. By 2500 B.C.E., pharaohs buried themselves with impressive craft, Mesopotamian tombs contained models of large ships, and Indus sites preserve models and images of boats. In addition, Mesopotamian texts from the 21st century B.C.E. mention construction of massive vessels that consumed huge numbers of palm, tamarisk, and pine trees, along with enormous quantities of reeds, ox hides, goat's hair, and fish oil and asphaltlike bitumen to coat the exterior. The discovery of pieces of what appears to be a large boat on the eastern shore of Oman—the first clear evidence for oceangoing trade, dated to 2200 B.C.E.—inspired a small group of archaeologists and boat builders to try to recreate such a vessel.

The effort differed from Thor Heyerdahl's *Tigris* reed raft, which the Norwegian sailed from Basra, Iraq, to Muscat, and then on to Pakistan in the late 1970s. Many archaeologists dismissed that effort as a stunt that did little to enhance our understanding of ancient technology, given the dearth of data on construction and sailing techniques. The *Magan III* was based instead on the recent finds as well as 400 models, clay seals, and drawings of the 3rd millennium B.C.E.

Unlike a raft, the *Magan III* was made up of reed bundles shaped as planks, with a leather gunwale and a tapered bow and stern. A crew of eight was to subsist on a 2200 B.C.E. diet of dates, honey, pulses, and dried fish during the estimated 10-day voyage. Thomas Vosmer of Muscat, an American-born Australian who specializes in ancient boatbuilding, experimented with several smaller versions before settling on a design; the Omani government agreed to cover construction costs.

With guidance from archaeologists such as Maurizio Tosi of the University of Bologna and Gregory Possehl of the University of Pennsylvania, Vosmer's team set out to build the *Magan III* as authentically as possible. A coating of bitumen, along with calcium

CREDITS: ANDREW LAWLER; JOINT HADD PROJECT

Published by AAAS

Beachcombing. This Indus sherd and ivory comb were found on the Arabian shore at R'as al Jinz.

north and east, the Hajar Mountains form a spine separating the area from the coast along the Gulf of Oman. To the south and west lies the fearsome Empty Quarter, one of the world's harshest deserts, peopled today only by intrepid Bedouins.

Archaeologists have long suspected that this copper-rich region was important to 3rd millennium B.C.E. civilization, given the frequent mention of Magan in cuneiform texts. Until Oman began to open its doors to outsiders after 1970, however, the area's past was almost completely unknown.

When they did begin to explore, archaeologists were amazed by what they found: As many as 100,000 ancient round stone tombs and monuments pepper the region. A series of surveys and excavations conducted across the arc along the southern foothills of the Hajar reveal an advanced indigenous culture previously unknown. In the earliest period that began during about 3100 B.C.E. and is dubbed the Hafit, impressive single-chamber tombs as high as 5 meters were built in lines along ridges of hills and mountains. Some include small, elaborate pots made in Mesopotamia.

Just as at R'as al Hadd and R'as al Hamra on the coast, "there's an explosion of social complexity" by the start of the 3rd millennium B.C.E., says Thornton. During about 2700 B.C.E., at the start of what researchers call the Umm an-Nar culture, more elaborate multichambered stone tombs were built—usually on a plain and sometimes faced with carefully dressed limestone quarried 30 kilometers or more from the site. These were typically common graves in which dozens—and occasionally more than 100—bodies were interred over time; some tombs include valuable objects such as ivory combs, copper daggers and ornaments, gold diadems, silver, gold, carnelian beads, and Indus pottery—all signs of economic prosperity and long-distance connections.

Royal Ghazal, a University of Chicago graduate student working in Oman, says the common burials may reflect attempts to limit social stratification. Despite the wealth, there are few signs of the strict hierarchy typical of graves in ancient Egypt or Mesopotamia. There are only hints about Magan's social and political structure in Mesopotamian texts, such as one in which Naram-Sin, leader of the Akkadian empire circa 2150 B.C.E., boasts of having captured several Magan cities as well as its king. He may have been a temporary leader, because the Umm an-Nar people apparently eschewed the hierarchical systems of contemporary Egypt and Mesopotamia in favor of strong clanlike organizations that still have their echoes in modern Oman.

The tombs carry a wealth of information, but until recently, few settlement sites were

carbonate from crushed seashells and fish oil, made a waterproof seal. The sail was made from hand-woven goat hair. "We had five sea trials for 25 days, and we plugged a lot of holes," recalls archaeologist Alessandro Ghidoni of Muscat, who was a construction supervisor and crew member.

Once on the rough open sea, however, the ship began to take on water in the stern, forcing sailors to abandon ship. By the next day, it had sunk completely. Ghidoni says that the pressure from ocean swells softened the bitumen, creating gaps in the hull. "We sank because it was too flexible," he says. Both he and Vosmer note that the team was under intense pressure to complete the project quickly, contributing to a failure to spot design flaws. Vosmer, who admits that his errors played a role, says now that there was simply not enough data to recreate the vessel faithfully.

As with any good experiment, the *Magan III*'s failure provided new insights. Ghidoni is no longer convinced that reed boats could weather the open sea, and he adds that bitumen was far too valuable a substance to slather liberally on merchant or fishing craft. Sewn-plank boats were more likely the vessel of choice, though finding the necessary wood in either Mesopotamia or Arabia would have been challenging. More likely, he says, ships were built of timber floated down the Indus River. So far, however, no early Bronze Age shipyards there—or in Oman or Mesopotamia—have been found. So the identity of the Bronze Age sailors remains unclear. But for now, says Possehl dryly, "there are no more plans for reed boats." **–A.L.**

Trials at sea. The *Magan III* sank long before it reached India.

CREDITS (TOP TO BOTTOM): JOINT HADD PROJECT; HELEN KIRKBRIDE

Published by AAAS

known that could provide important data on day-to-day life. Archaeologists now are focusing on the dozens of squat stone structures strewn across the southern slopes of the Hajar. Bat hosts one of the largest concentrations of these structures or towers, which average 20 meters across and a few meters high and include half-ton stone blocks. They usually have a well in their center and are frequently divided into small chambers.

Possehl's team is now conducting a thorough examination of three of the five towers at Bat as well as geomorphologic and archaeobotanical studies of the area. Radiocarbon dates on charcoal and other organic material date the structures to between 2800 and 2450 B.C.E. Thornton has found contemporaneous buildings nestled against one tower.

Archaeologists have variously theorized that the towers are fortified wells, watchtowers, platforms, or storage bins. Possehl's team has recently shown that at least two at Bat were built over earlier Hafit settlements and that the tower architecture evolved over time. One of the later structures has vertical crenellations, the only decorative pattern seen on any Umm an-Nar towers. Thornton believes the structures are too low to serve as forts or watchtowers. Instead, he sees them as platforms used for public rituals, "a wonderful expression of social and political complexity."

Although lacking the cities and large populations in other parts of contemporaneous southern Asia, the region shared remarkably similar styles and goods. At Bisya, south of Bat, Jeffery and Jocelyn Orchard of the University of Birmingham in the United Kingdom are working at a site with more than a half-dozen towers, including one they believe had a spiral ramp that led to a long-vanished temple, similar to the temple-topped ziggurats of Mesopotamia. They postulate that the southern Hajar during the Umm an-Nar time was linked through a series of oasis towns, some 200 to 400 hectares in size.

Possehl and Thornton, however, insist that the evidence for towns is still lacking. They see small settlements of farmers and pastoralists who impounded water for growing wheat, barley, and date palms and herded goats. Bat's connection with the outside world is due in large part to geography, says Possehl: It lies at the conjunction of a path over the Hajar to the northern coast of Oman and another that stretches from the Arabian Sea to the east to the Persian Gulf on the west. These trade routes connected Bat to the wider 3rd millennium B.C.E. network.

The wealth of interior Oman derived from local, regional, and international trade centered on copper, limestone, the soft-stone called chlorite, and the hard-stone diorite favored by Sumerian sculptors. Along with Indus pots, carnelian beads manufactured in what is today western India are scattered across the southern Hajar. Perishable goods such as wine, oil, and grains were also likely part of that commerce, though their remains have yet to be proven. And by 2400 B.C.E., "Indus pottery is everywhere," Thornton says, holding out a black-slipped sherd in the team's nearby laboratory.

Grave goods. A restored Umm an-Nar tomb at Bat demonstrates the skill of ancient stone workers.

CREDITS: ANDREW LAWLER

Published by AAAS

Arabian sights. Possehl's team digs near one of the tower structures at Bat.

Whether this means that Indus traders or even potters traversed the arc between the Indian Ocean and the Persian Gulf is controversial. Pots may have been passed along from sites like R'as al Jinz, or Indus traders may have brought them along as they moved into the interior trading for copper. However it happened, "these people have incorporated Indus culture into their own," says Charlotte Marie Cable of Michigan State University in East Lansing, who is part of Possehl's team.

Sophie Méry, an archaeologist at the University of Paris who has closely studied Indus remains in Arabia, matched the clay used to manufacture the vessels with soil from the Indus area around Mohenjo Daro and to the south. Similar analyses demonstrate that other pots were fashioned from local clay in the Indus style, "but the [Hajar] potters did not master the techniques of wheel throwing as the Indus potters did." She finds it unlikely that itinerant Indus potters or traders were making their way across Oman. "I see local networks passing goods on rather than Indus caravans," she says. Others agree. "We don't imagine Indus traders traveling inland," says archaeologist Hans-Peter Uerpmann of the University of Tübingen in Germany, who is digging in the UAE. But Possehl says that the occasional Indus donkey caravan might have worked its way from oasis to oasis. And Daniel Potts of the University of Sydney in Australia thinks it "very likely" that Indus agents as well as local traders were involved in the Arabian economy. The only agreement is that there is not enough data yet to say for sure.

Even if ancient sailors had mastered the seas, why not sail directly from India into the Persian Gulf, bypassing the challenging overland route via Bat? Thomas Vosmer, an expert in ancient boats who lives in Oman, says that contrary winds make it difficult for rudimentary sailing ships to pass through the Strait of Hormuz (see map, p. 1093). And Possehl argues that Oman's copper and other minerals made it worthwhile for at least a limited number to traipse across the paths connecting the oases. To him, the oasis path is a "portage," a land crossing between the two bodies of water.

Broken hinge

Whether Indus traders physically made that trek, there is a consensus among archaeologists that the corridor was an important element in the economic circuit of the 3rd millennium B.C.E., funneling raw materials to Mesopotamia and serving as a transshipment point for Indus goods. On the Persian Gulf coast, at the site near Abu Dhabi called Umm an-Nar which gave the culture its name, inhabitants built a dozen stone houses dating to about 2500 B.C.E., worked copper into usable products, and weighed their goods with a collection of weights corresponding with northern Syrian standards. Along with Indus pottery, archaeologists found the impression made by a northern Syrian cylinder seal, demonstrating links with that distant area.

At other sites such as Tell Abraq, farther north on the coast, locals built a tower 40 meters in diameter between 2200 and 2000 B.C.E. Artifacts testify to links with eastern Iran, Central Asia, Bahrain, the Indus, and Mesopotamia in the late 3rd millennium B.C.E., as well as with important settlements in the interior such as Hili, which is strategically set between Bat and Umm an-Nar. Several Persian Gulf sites include scatterings of Indus pottery, a likely sign of visiting trading boats. These settlements were clearly tied to the ancient emporium of Dilmun, an area mentioned frequently in Mesopotamian texts that likely thrived in today's Bahrain and the adjacent Saudi Arabian coast between Oman and Iraq, explains Harvard's Steinkeller.

Shell game. Marcucci shows off finds at the R'as al Hamra coastal site near Oman's capital.

Tell Abraq continued as a modest port until 500 B.C.E., but most of the other sites along the Hajar corridor underwent a dramatic change during about 2000 B.C.E. "They fell like dominoes," says Uerpmann, though no one knows just why. The important Mesopotamian city of Ur surrendered to invaders at that time, and trade circuits across southwest Asia appear to have disintegrated quickly. Iranian cities collapsed, and the Indus civilization soon fell into ruin. A drying climate, increased warfare, and an unstable economic system may have been factors.

Adrian Parker, an archaeologist at Oxford Brookes University, Headington, in the U.K., sees evidence of a "megadrought" in eastern Arabia during about 2000 B.C.E., based in part on unpublished data showing that vegetation vanished and sand dunes began to move and grow. "The extreme climate would have had significant impact on the copper trade and routes from the Hajar to Mesopotamia," he says. Those data match a radical change in life apparent in Oman and the UAE excavations, where the Umm an-Nar tradition gives way to the Wadi Suq culture at the start of the 2nd millennium B.C.E. Indus pottery in the interior nearly vanishes. Tombs are cruder and have fewer grave goods than the preceding two periods. Locals casually robbed stones from earlier tombs to house their own dead, which Thornton argues demonstrates a dramatic cultural break with the past.

Within a century or two, eastern Arabia reverted to a simpler culture based on agriculture and herding, largely cut off from the outside world. When an Arabian revival came 1000 years later, it was centered far to the west on the lucrative incense trade that moved up the peninsula via Yemen to the Near East (see sidebar, p. 1099). Not until medieval times did the area around Oman once again participate so fully in the global economy. But for that brief millennium in the Bronze Age, this area long ignored by archaeologists was a key player in the emergence of the first civilizations. "There is so much back and forth," says Thornton, tucking his sherds back into a plastic bag at the Bat dig house. "It is much more complicated than we thought."

–ANDREW LAWLER

CREDIT: ANDREW LAWLER

Published by AAAS

Exploring the Virgin Country

Omani soil is providing a bevy of archaeological surprises, but researchers there also struggle with rapid development and a lack of homegrown expertise

MUSCAT, OMAN—Until 1970, Oman rivaled Tibet as one of the world's most inaccessible countries. Even the renowned British explorer Wilfred Thesiger, who spoke fluent Arabic and traveled on camel with Bedouins, was barred from the country 20 years earlier. Few nations on Earth have changed so dramatically since. The sultanate, run by the monarch Qaboos bin Said for the past 40 years, now welcomes not only investors eager to benefit from the country's oil revenues but also archaeologists seeking to study everything from medieval forts to evidence of early oceangoing ships.

A dozen foreign teams are at work in this boomerang-shaped nation, which was a surprisingly sophisticated player in global trade 4000 years ago and also the center of the incense trade (see sidebar, p. 1099). Researchers are taking advantage of a stable political system, generous help from the central government, and a landscape that until recently was remarkably unmarred by modern development. "Here all is visible and untouched; you can find 5th and 4th millennium B.C.E. sites everywhere," marvels Maurizio Cattani, a Paris-based archaeologist and dig director at R'as al Hadd on the country's east coast. "The whole country from north to south is full of archaeological remains," agrees Hassan Mohammad Ali al-Lawati, Oman's director general of archaeology and museums at the Ministry of Culture. "We call ourselves a virgin country."

Yet the quickening pace of development threatens many sites, and local champions of archaeology are few and politically vulnerable. "We don't want to be called anti-development," al-Lawati says during an interview in his Muscat office.

All the same, Oman today is an oasis of Arabian archaeological research. Wary of outsiders, its larger neighbor Saudi Arabia, with which Oman shares a long border and large oil reserves, grants few excavation permits to foreigners, although that country has its own cadre of domestic archaeologists. Meanwhile, political troubles restrict excavations in countries from Yemen to Iran. The United Arab Emirates welcomes archaeologists, but its borders are limited largely to the Persian Gulf shore. Oman, by contrast, not only is vast and archaeologically diverse but also helps foreign teams financially. "We provide logistical support, accommodations in Muscat, workers, cars, petrol, and labor" to supplement funds provided by outside teams, says Biubwa Ali Al-Sabri, who heads the excavation and archaeological department at the ministry. She says that interest in excavating in Oman has increased dramatically since the 1980s.

But development has also increased dramatically since that time. New highways, urban sprawl, copper mining, and beach resorts are the primary threats. Al-Lawati says his ministry, which oversees archaeology, is in a delicate position. "We need schools and roads. And at the same time, we don't want to be soft and spoil our archaeological heritage. But there are a lot of stakeholders."

Those stakeholders include a host of influential members of the government. Several are building seaside villas on a dramatic cape called R'as al Hamra, just a short drive from al-Lawati's office at the Ministry of Culture's headquarters in Muscat. A large new home is rising there on a 5th millennium B.C.E. village that provided the country's earliest evidence of copper, Oman's signature export. In the surrounding few hectares, 10 of 12 prehistoric sites have been destroyed in recent years. One of the surviving sites bordered a mangrove swamp and was difficult to develop; the second was slated to be part of a luxury-home community until Italian archaeologists made a media fuss that stopped the project in 2005.

On that site—now perched next to a luxury hotel—a team led by Lapo Marcucci of the Italian archaeological mission in Oman found 120 graves, nine phases of occupation, and important insights into the transition from a hunter-gathering culture to the more sophisticated Hafit culture that emerged at the end of the 4th millennium B.C.E. This and the other remaining site, which dates from 1000 years earlier, may soon form the nucleus of an innovative archaeological park proposed by a team of Italian architects and landscape designers. Al-Lawati says he hopes to win government approval this year to spend $1.3 million on the first phase of the project. And he cites other successes, such as preventing construction of a copper mine that would have destroyed several prehistoric settlements

CREDIT: DANIEL USHER

Published by AAAS

Ocean view. Development threatens sites such as R'as al Hamra (on promontory to right).

and ensuring that a new highway from Muscat to Sur avoided archaeological sites, even at the cost of millions of dollars and months of construction time.

Such efforts are hampered in part by the lack of homegrown archaeologists. The university in Muscat, the country's leading academic institution, closed its archaeology degree program decades ago and now offers only the occasional course. Those interested in pursuing degrees must go abroad. Two Omani archaeology teams are at work, but their efforts are dwarfed by those of foreign groups. "We are trying to put together a plan with the Ministry of Education" to reestablish a program, al-Lawati says.

One foreign scientist, who requested anonymity, says archaeology in Oman suffers from a tradition of ministries run like fiefdoms, limiting cooperation. With its relatively small budget and political pull, the Ministry of Culture is among the least influential parts of the government. "We always get the smallest share," al-Lawati acknowledges. But he is also confident that new rules requiring archaeological surveys before construction, along with the introduction of archaeological parks, will boost awareness of the country's rich past. A dose of national pride may help as well. "We once had an important civilization," says Al-Sabri. "And we need to know more."

–ANDREW LAWLER

Digging deep. Dhofar's deputy governor, Sheikh Suhaiyl Musallam al-Rojdi (*left*) examines dig by McCorriston's team.

Hot on the Incense Trail

SALALAH, OMAN—A cool mist hangs over the Dhofar Mountains close to the Yemen border, turning bare hillsides an English-meadow green as the rest of Arabia swelters in the summer heat. It is this moisture, the only finger of the Asian monsoon to touch the peninsula, that makes these mountains the perfect habitat for the scraggly frankincense tree, which oozes a gooey and aromatic resin when cut. The tree grows only in this Dhofar region of Oman, its likely ancestral home, and parts of Yemen and Somalia.

Frankincense was the ancient world's most lucrative product, essential in temple rituals throughout the Mediterranean and Southwest Asia, prescribed by doctors for digestive problems, and turned to ash for eyeliner among Egyptian gentry. Yet the origin of its trade remains only dimly understood, in part because the mostly nomadic inhabitants here closely guarded their secret and left few artifacts and no texts behind. Researchers long assumed that the frankincense trade did not flourish until 1000 B.C.E. or later. But a country now welcoming archaeologists is providing an unusual combination of textual evidence, remote-sensing data, and careful excavations (see main text, p. 1098). The data suggest that the trade sprang up far earlier, says archaeologist Juris Zarins, who lives in Dhofar's sleepy provincial capital, Salalah.

According to Zarins, long-distance trade itself—in seashells—began here as early as the 5th or 6th millennium B.C.E. Then, far to the northeast at R'as al Jinz, Italian excavators found what appears to be a frankincense burner dating to about 2200 B.C.E. Resins from Egyptian tombs date to about this time and may signal maritime connections across the Red Sea. For overland travel, donkeys, which by this period were in use, may have made the journey north. And Mesopotamian texts from this same era mention a trade in "aromatics," likely frankincense.

By the height of the Umm an-Nar period at the end of the 3rd millennium B.C.E., when Indus goods were arriving in Arabia and Omani copper was being shipped to Mesopotamia, distant Dhofar and its frankincense seem to have been part of the first international trade system (see p. 1092). "There's abundant evidence of goods exchange," says Joy McCorriston of Ohio State University in Columbus. She and her colleagues are mapping thousands of uncataloged tombs in the region to gather data on population and trade routes.

Both teams are finding evidence that Dhofar's frankincense made it a player in the early economic network. But even as that origin comes to light, the 4-millennia-old tradition is nearing its end. The stalls of Salalah today are still filled with bags of frankincense. But buyer beware. "Now it all comes from Somalia," says Zarins. **–A.L.**

Precious resin. Incense was made from the frankincense tree and burned as early as 2200 B.C.E. (*inset*).

CREDITS (TOP TO BOTTOM): MICHAEL HARROWER; DAVE G. HOUSER/CORBIS; (INSET) JOINT HADD PROJECT

Published by AAAS

The Coastal Indus Looks West

Fortified coastal settlements suggest that the Indus Civilization, once considered an insular society, shipped goods to the east

DHOLAVIRA, INDIA—Most of the year, this small island near the Pakistan border is surrounded by thick salt flats in the estuary called the Rann of Kutch. In late January, the midday heat is already intense, and the land is brown and barren. Yet more than 4000 years ago, architects and engineers designed a vast city here with high stone battlements, deep wells, huge water basins, and wide and straight streets. Extending over 100 hectares and excavated only in the 1990s, the site was clearly an important metropolis during the height of the Indus River, or Harappan, civilization.

And yet Dholavira is hundreds of kilometers from the cities long considered the heart of the Indus River Valley civilization, Harappa and Mohenjo Daro, which lie far upstream on the Indus River in modern-day Pakistan. But recent digs and surveys in India's westernmost province of Gujarat show that sites like Dholavira may be the critical link between the heart of the Indus and Arabia and Mesopotamia in the 3rd millennium B.C.E. At a recent conference in the nearby city of Bhuj, archaeologists compared notes on the mounting evidence that this area played an important role in long-distance trade at the dawn of civilization. "There are more than 60 Harappan sites in Kutch," says Y. S. Rawat, head of archaeology in Gujarat Province. "Most are near the coast, and some are heavily fortified."

Indus passports? Kanmer's odd-shaped pendants may have been related to trade and travel.

There's no doubt there were maritime connections; Indus seals and artifacts have been found on the Arabian coast and in Sumerian port cities like Ur (see p. 1092). And although evidence of foreign material in Indus sites is scarce, seals from the area around today's Bahrain on the Persian Gulf coast have been found at a small site called Lothal, 50 kilometers east of Dholavira and 270 kilometers from Mohenjo Daro. In 1954, Indian excavators here unearthed a massive brick-lined basin that they claimed was a harbor bordered by warehouses. Twice as long as a football field and nearly 40 meters wide, the structure was built in the second half of the 3rd millennium B.C.E., the heyday of trade with the West. But many Western archaeologists don't think it was a harbor. "It was a tank" for storing water,

Shifting currents. Sites in the province of Gujarat in western India are yielding new data on Indus life and trade.

CREDITS (TOP TO BOTTOM): RIHN'S INDUS PROJECT; (MAP SOURCE): GOOGLE EARTH

Published by AAAS

Playing defense. Kanmer's thick walls protected the small settlement from prying eyes.

insists Gregory Possehl, an archaeologist at the University of Pennsylvania. An Italian team led by Dennys Frenez of the University of Bologna in Italy hopes to resolve the matter; recently, they found hints that a wide canal connected the basin with the sea, supporting the port theory.

Meanwhile, a team of Japanese and Indian excavators is focusing on a fortified village called Kanmer that likely housed between 400 and 500 people during its heyday between 2600 B.C.E. and 1900 B.C.E. Behind 20-meter-thick and 10-meter-high walls, residents were busy making tens of thousands of beads from many kinds of stones, such as carnelian, lapis, and agate, which were used in jewelry exported across the region. They also found three unique round pendants carrying Indus script and the familiar Indus image of the unicorn. Dig director Toshiki Osada, an archaeologist with Kyoto's National Institutes for the Humanities, believes the pendants might be a kind of passport used in trade.

In recent years, dozens of Indus sites have come to light in this coastal area, which was once considered on the distant periphery of the Indus. Most are modest in size like Kanmer. "We're finding small sites with massive fortifications, where raw materials are stored," says Osada. He suggests that these settlements were an important link in the chain of commerce reaching from the Himalayas to Mesopotamia. Such fortifications are rare elsewhere in the Indus. Kuldeep Bhan of India's Maharaja Sayajirao University of Baroda, who is excavating a nearby site called Shikarpur, says that the fortifications could be a sign of conflict with locals who refused to adopt Indus ways, or the walls may have helped to protect goods from attackers by land or sea. "Craft may have been heavily controlled," he says. Even today, Bhan notes, there are closely held secrets in Gujarati bead production. Just as excavators in Arabia are seeking the port where Indus traders unloaded their pots, Bhan hopes to find clear evidence of maritime life at Shikarpur, which sits within a few kilometers of the sea. He has found a dozen or so Indus seals but is on the lookout for material that might hint at the multicultural nature of a port town. One of the great mysteries of the 3rd millennium B.C.E. is who built and sailed the ships that connected the Indus, the Persian Gulf, and Mesopotamia. Excavators like Bhan hope this harsh landscape will soon reveal their identities.

–ANDREW LAWLER

CREDIT: MAURIZIO TOSI

PROFILE: MAURIZIO TOSI

'The Cobra' Uncovers Ancient Civilizations—And Cold War Political Secrets

He told colleagues he was looking for ancient lapis lazuli mines. But when Maurizio Tosi crossed into Afghanistan at the height of the war between the Soviet Union and the mujahedin in 1984, his real goal was to locate wooden boxes that had once contained American-supplied Stinger missiles. Those missiles threatened Soviet helicopters, and Moscow was eager to trace the route they had taken into Pakistan.

As Tosi tells it, Soviet operatives asked him to investigate, and the dutiful Marxist, who is also a University of Bologna professor, went to Pakistan and crossed by car into southern Afghanistan, then controlled largely by rebels. Instead of Stinger boxes, however, he saw only masses of child graves, and he decided to swear off the spy business, in which he had participated off and on for 2 decades.

Tosi has been a peripatetic and influential archaeologist, excavating from Iran to Sicily and shaping new ideas about how humans first began to live in cities and trade over vast areas. As a young man, he dug at Shahr-i Sokhta in southeastern Iran, exposing one of the world's largest urban centers in the 3rd millennium B.C.E., far from the known big-three civilizations of Egypt, Mesopotamia, and the Indus. And in 1981, he discovered Indus material in Oman, sparking a revolution in archaeology in that country, and he continues to study connections between the Indus and Arabia (see main text, p. 1100).

The son of a senior government official in Mussolini's fascist Italy, Tosi turned communist as a teenager in Rome during the 1960s and studied paleontology and archaeology. By then, he says, he had already been recruited by the Cominform, the organization that coordinated efforts among Soviet-influenced communist parties. Tosi says he only performed "four or five operations." But the communist connection also served his professional life. A 1969 visit to Moscow introduced him to Soviet archaeologists who were making important discoveries in Central Asia, contacts that proved influential in Tosi's later ideas about interconnected societies.

Cold warrior. Tosi successfully lobbied for a new view of ancient Asia.

When Tosi and the late Serge Cleuziou of the French National Center for Scientific Research in Paris began to work in Oman in the 1980s, they abandoned the old way of seeing the emergence of civilization from a center to a periphery. Instead they postulated a network of linked societies including Mesopotamia, Arabia, Central Asia, and the Indus, each with a unique culture but sharing goods, ideas, and technologies. Tosi helped create a regular conference to discuss what he named the Middle Asian Interaction Sphere, and the idea, once considered fringe, is now mainstream.

Tosi's politics, sharp mind, many wives (including a former Soviet political commissar), and often-brusque personality make him a controversial figure. "A brilliant monster," says one colleague, who declines to be named. Although he has many enemies, few dispute his intellectual capacity. Tosi revels in what he claims is his nickname in the field—the cobra. In his many intellectual contests, he claims victory. "I've been in so many battles and never lost a fight," he boasts.

"Maurizio's contributions have been immense," says archaeologist Philip Kohl of Wellesley College in Massachusetts. "He's one of the smartest and most knowledgeable persons I've ever met, but I also feel he could have accomplished even more if he had control over his personal life. But then he wouldn't be Maurizio."

A heart operation has slowed Tosi of late, but during a recent visit to India he was busy organizing a meeting to bring modern experts in port facilities together with archaeologists to understand how ancient Indus harbors may have operated—and by so doing, forge economic connections between today's Italy and India. "You must have an open mind," says Tosi. "I'm just curious." **–A.L.**

Published by AAAS

Choice and testing won't do 1107

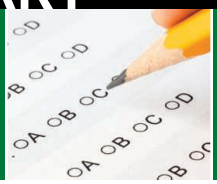

Boosting beige fat 1113

SPORE prize essay 1119

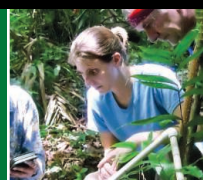

LETTERS | BOOKS | POLICY FORUM | EDUCATION FORUM | PERSPECTIVES

LETTERS

edited by Jennifer Sills

Male Mice Not Alone in Research

THE NEWS FOCUS STORY BY C. WALD AND C. WU, "OF MICE AND WOMEN: THE BIAS IN ANIMAL models" (26 March, p. 1571), is one-sided. We agree that the choice of animal model requires care and that extrapolating data from one sex to the other can be misleading. However, we disagree with their statement that researchers use predominantly male mice because they are "cheaper and easier to work with."

First, many factors influence the choice of research subject. The most obvious are inherent differences in behavior (males fight) and physiology (female hormonal fluctuations); cost (more animals cost more money); and the incidence of strain-specific disorders (such as cancer and epilepsy). Our collective experience is that many researchers select less aggressive females because they can be group-housed to save money. This female bias will persist indefinitely given financial constraints on basic biomedical research, especially in academic laboratories.

Second, "best practice" by U.S. federal regulatory agencies and research institutes as well as industry already requires that animal data used to predict human responses be obtained from both sexes. Examples include analysis of genetically engineered animals for translational medicine (*1*) and preclinical studies to investigate chemical carcinogenicity (*2*) or to develop new drugs (*3*) and pesticides (*4*). Definitive information on the role of gender in human disease must be obtained in humans because of intrinsic interspecies physiological differences, but animal studies remain the essential foundation for designing rational human clinical trials.

Contributing to the issue of identifying whether there is a male or female bias in modern biomedical research is the consistent failure of researchers to report the critical experimental details—age, sex, strain or stock (with correct nomenclature), animal source, husbandry conditions, and health status—that are necessary to interpret studies. Including experienced comparative pathologists as co-investigators or journal reviewers [such as those recruited through the Center for Genomic Pathology (http://ctrgenpath.net)] would substantially enhance study designs and the credibility of data acquisition, analysis, interpretation, and reporting.

BRAD BOLON,[1]* STEPHEN W. BARTHOLD,[2] KELLI L. BOYD,[3] CORY BRAYTON,[4] ROBERT D. CARDIFF,[2] LINDA C. CORK,[5] KATHRYN A. EATON,[6] TRENTON R. SCHOEB,[7] JOHN P. SUNDBERG,[8] JERROLD M. WARD[9]

[1]GEMpath Inc., Longmont, CO 80503, USA. [2]Center for Comparative Medicine, University of California–Davis, Davis, CA 95616, USA. [3]Vanderbilt University Medical Center, Nashville, TN 37232, USA. [4]Johns Hopkins University School of Medicine, Baltimore, MD 21205, USA. [5]Stanford University School of Medicine, Stanford, CA 94305, USA. [6]University of Michigan Medical School, Ann Arbor, MI 48109, USA. [7]University of Alabama at Birmingham, Birmingham, AL 35294, USA. [8]The Jackson Laboratory, Bar Harbor, ME 04609, USA. [9]Global VetPathology, Montgomery Village, MD 20886, USA.

*To whom correspondence should be addressed. E-mail: brad@gempath.net

References

1. C. Brayton, M. Justice, C. A. Montgomery, *Vet. Pathol.* **38**, 1 (2001).
2. U.S. Department of Health and Human Services, National Toxicology Program, "Studies in genetically modified models" (http://ntp.niehs.nih.gov/index.cfm?objectid=0847E178-9BF1-96CA-E620628825490444).
3. U.S. Department of Health and Human Services, Food and Drug Administration (FDA), "Guidance for industry: S6 preclinical safety evaluation of biotechnology-derived pharmaceuticals" (www.fda.gov/downloads/RegulatoryInformation/Guidances/UCM129171.pdf).
4. U.S. Environmental Protection Agency (EPA), Chemical Safety and Pollution Prevention, OCSPP Harmonized Test Guidelines (http://epa.gov/oppts/pubs/frs/publications/Test_Guidelines/series870.htm).

African Researchers Underrepresented

I READ WITH INTEREST THE NEWS FOCUS story "In the shadow of Jane Goodall" (J. Cohen, 2 April, p. 30). I was fascinated by the progress in behavioral research but disconcerted to learn that, 50 years after this research began, only 1 of 18 long-term chimpanzee and bonobo research sites has a lead researcher who is an African scientist. In addition, only one up-and-coming African field manager was profiled in the article. It is possible that some of the foreign research leaders are Africans based elsewhere, but the overall picture is one of the foreign dominance that has persisted for generations. This unfortunate picture casts conservation efforts that accompany research as externally imposed, thereby undermining their effectiveness. It is also self-perpetuating, creating few role models for younger African scientists.

This situation with chimpanzee and bonobo field research is sadly reflective of many areas of science in Africa (*1*, *2*). Because of its long history and impressive growth, this example suggests that the lopsidedness of research leadership in Africa will not be corrected by the traditional research apprenticeship model. Projects necessarily located in Africa must build local human resources to the highest level, even if this means that they will lose their most valued trainees to new, Africa-led projects. Generating local leaders must be a deliverable goal for such projects and one in which funders of long-term research projects need to be invested.

IRUKA N. OKEKE

Department of Biology, Haverford College, Haverford, PA 19041, USA. E-mail: iokeke@haverford.edu

References

1. *Nature* **435**, 1146 (2005).
2. I. N. Okeke, J. Wain, *Nat. Rev. Microbiol.* **6**, 858 (2008).

Published by AAAS

REDD+: Property Rights and Liability

IN THEIR POLICY FORUM "DOES REDD+ threaten to recentralize forest governance?" (16 April, p. 312), J. Phelps *et al*. note that a national approach to Reducing Emissions from Deforestation and Forest Degradation (REDD+) could reverse the gains made from decentralization. However, a national approach is still some way off—instead, the current, rapid roll-out of REDD+ pilot projects (*1*) is likely to dominate the policy agenda in the next few years. For many REDD+ host countries, a "nested" approach may emerge, which incorporates both project- and national-level approaches (*2*). Rather than see a national approach as a threat, it should be viewed as an opportunity to strengthen, innovate, and extend decentralized approaches to governance.

The possible inclusion of REDD+ in a future global compliance system will necessitate clearly defined and allocated REDD+ carbon rights with liability assigned for possible future carbon release into the atmosphere. Assigning liability is not only a precondition for carbon credit fungibility, but is also crucial for ensuring permanence (*3*). Under a project-based approach, REDD+ rights could be allocated to local actors such as landowners, farmers, and communities who could then trade these rights. Given the widespread existence of common property regimes in tropical forest areas (*4*), serious consideration should be given to the creation of common property carbon rights. Ultimate liability for carbon reversal will, however, most likely be assigned to REDD+ credit purchasers—i.e., Annex I countries or firms—if a future compliance system follows the principles as laid out in the Kyoto Protocol (*5*). Where carbon rights are assigned to governments under a national approach, liability could potentially be shared between REDD+ host governments and government buyers (*6*).

The inability to assign liability for carbon reversals to local actors participating in project-level activities therefore implies a need for state involvement at some level if these activities are to be more effective in preventing future carbon reversal. Given that decentralization reforms involve a transfer of rights to forest land and resources to local actors, it could be tailored toward more effective REDD+ policy. In a collaborative management (or co-management) framework, for example, state authorities and local actors share both the management of and the benefits from forest resources (*7*). Hence, liability for carbon reversal could lie with the state, whereas additional incentives, such as REDD+ payments for environmental services, could be transferred to local actors in order to capture the forest carbon externality.

CHARLES PALMER

Department of Geography and Environment, London School of Economics (LSE), Houghton Street, London WC2A 2AE, UK. E-mail: c.palmer1@lse.ac.uk

References

1. E. Sills, E. Myers-Madeira, W. D. Sunderlin, S. Wertz-Kanounnikoff, in *Realising REDD+: National Strategy and Policy Options*, A. Angelsen *et al*., Eds. (Centre for International Forestry Research, Bogor, Indonesia, 2009), pp. 265–279.
2. S. Wertz-Kanaounnikoff, A. Angelsen, in *Realising REDD+: National Strategy and Policy Options*, A. Angelsen *et al*., Eds. (Centre for International Forestry Research, Bogor, Indonesia, 2009), pp. 13–24.
3. R. A. Sedjo, G. Marland, *Clim. Pol.* **3**, 435 (2003).
4. A. Agrawal, A. Chhatre, R. Hardin, *Science* **320**, 1460 (2008).
5. United Nations Framework Convention on Climate Change, Addendum, Part Two, of "Report of the 11th Conference of the Parties serving as the meeting of the Parties to the Kyoto Protocol on its first session," Montreal, Canada, 28 November to 10 December 2005.
6. M. Dutschke, A. Angelsen, in *Moving Ahead with REDD+: Issues, Options and Implications*, A. Angelsen, Ed. (Centre for International Forestry Research, Bogor, Indonesia, 2008), pp. 77–86.
7. L. Carlsson, F. Berkes, *J. Environ. Manage*. **75**, 65 (2005).

TECHNICAL COMMENT ABSTRACTS

Comment on the Paleobiology and Classification of *Ardipithecus ramidus*

Esteban E. Sarmiento

White and colleagues (Research Articles, 2 October 2009, pp. 64–106 and www.sciencemag.org/ardipithecus) reported *Ardipithecus ramidus* as an exclusive member of the human lineage post–African ape divergence. However, their analysis of shared-derived characters provides insufficient evidence of an ancestor-descendant relationship and exclusivity to the hominid lineage. Molecular and anatomical studies rather suggest that *Ar. ramidus* predates the human/African ape divergence.

Full text at www.sciencemag.org/cgi/content/full/328/5982/1105-b

Response to Comment on the Paleobiology and Classification of *Ardipithecus ramidus*

Tim D. White, Gen Suwa, C. Owen Lovejoy

We assigned *Ardipithecus* to the Hominidae based on numerous dental, cranial, and postcranial characters. Sarmiento argues that these characters are not exclusive to hominids, contending that *Ardipithecus* is too old to be cladistically hominid. His alternative phylogeny, however, is unlikely because it requires tortuous, nonparsimonious evolutionary pathways.

Full text at www.sciencemag.org/cgi/content/full/328/5982/1105-c

Comment on the Paleoenvironment of *Ardipithecus ramidus*

Thure E. Cerling, Naomi E. Levin, Jay Quade, Jonathan G. Wynn, David L. Fox, John D. Kingston, Richard G. Klein, Francis H. Brown

White and colleagues (Research Articles, 2 October 2009, pp. 65–67 and www.sciencemag.org/ardipithecus) characterized the paleoenvironment of *Ardipithecus ramidus* at Aramis, Ethiopia, which they described as containing habitats ranging from woodland to forest patches. In contrast, we find the environmental context of *Ar. ramidus* at Aramis to be represented by what is commonly referred to as tree- or bush-savanna, with 25% or less woody canopy cover.

Full text at www.sciencemag.org/cgi/content/full/328/5982/1105-d

Response to Comment on the Paleoenvironment of *Ardipithecus ramidus*

Tim D. White, Stanley H. Ambrose, Gen Suwa, Giday WoldeGabriel

Cerling *et al*. contest our interpretation of the woodland habitat preference of *Ardipithecus ramidus*. However, their reconstruction of a predominantly open grassy environment with riparian woodlands is inconsistent with the totality of the fossil, geological, and geochemical evidence. In the Middle Awash, *Ar. ramidus* fossils are confined to the western half of the sampled Pliocene landscape where the species is associated with woodland to grassy woodland habitat indicators.

Full text at www.sciencemag.org/cgi/content/full/328/5982/1105-e

Verdict Still Out on Biotech Crops

THE TITLE OF THE NEWS OF THE WEEK STORY "Biotech crops good for farmers and environment, Academy finds" (E. Stokstad, 16 April, p. 295) gives the impression that the verdict is in after an unprecedented comprehensive assessment by a National Research Council committee studying the sustainability impacts of genetically engineered (GE) crops on U.S. farms. As the chair of that committee and a scientist who has studied these issues since 1996, I can assure you that it is not.

The committee did indeed find that many farmers planting current GE soybean, cotton,

Published by AAAS

and corn varieties have received substantial economic and environmental benefits from using the first generation of these GE crops. However, as the News story mentions but does not sufficiently emphasize, the report also stresses that these benefits are not universal across farms, some may decline over time, and potential benefits and risks may become more numerous as the technology is applied to more crops. There are substantial gaps in our knowledge about the longer-term environmental, economic, and social effects of current and future GE crops. For example, it is critical that we undertake intensive research to understand the evolution of weed and insect resistance at a landscape scale and the salient social issues surrounding the technologies.

The central take-away message should not be that current GE crops are ushering in a sustainable agriculture in the United States. Rather, the report's recommendations make clear that new information on the full spectrum of sustainability impacts of GE crops should be pursued vigorously to assure progress toward that worthy social goal and avoid unanticipated risks.

DAVID ERVIN

Departments of Economics and Environmental Management, Portland State University, Portland, OR 97207, USA. E-mail: dervin@pdx.edu

Letters to the Editor

Letters (~300 words) discuss material published in *Science* in the previous 3 months or issues of general interest. They can be submitted through the Web (www.submit2science.org) or by regular mail (1200 New York Ave., NW, Washington, DC 20005, USA). Letters are not acknowledged upon receipt, nor are authors generally consulted before publication. Whether published in full or in part, letters are subject to editing for clarity and space.

Immunology Programs Must Include Sepsis

THE NEWS FOCUS STORY "IMMUNOLOGY uncaged" (M. Leslie, 26 March, p. 1573) rightly highlights the need to develop human immunology programs. One day we will be able to better assess the immune system and adapt treatment to our patient's condition. HIV, sclerosis, and cancer will be ideal candidates for this approach. However, I must underline the desperate need to include sepsis—a condition characterized by cataclysmic immune dysfunction—in the list.

There are nearly one million cases of sepsis annually in the United States, and sepsis mortality has remained constant over the years (up to 40 to 50% in septic shock) (*1*, *2*). Anti-inflammatory trials have failed, most likely because they have been extrapolated from observations made in mice that inadequately mirror the immune response occurring in humans (*3*).

The success of future trials relies on our capacity to minutely and globally assess the immune system. We need a human immunology sepsis program that includes cytokine measurement, flow cytometry, microarrays, and functional testing—as reported by Leslie—to define targeted individualized therapy.

GUILLAUME MONNERET

Cellular Immunology Laboratory, Hospices Civils de Lyon, Hôpital E. Herriot, 69437 Lyon, cedex 03, France. E-mail: guillaume.monneret@chu-lyon.fr

References

1. R. S. Hotchkiss, E. I. Karl, *N. Engl. J. Med*. **348**, 138 (2003).
2. G. Monneret, F. Venet, A. Pachot, A. Lepape, *Mol. Med*. **14**, 64 (2008).
3. A. Dyson, M. Singer, *Crit. Care Med*. **37**, S30 (2009).

Published by AAAS

EDUCATION

A Reformer's Change of Heart

William J. Reese

Over the past generation, few institutions in American society have received closer scrutiny and more condemnation from politicians and reformers of every stripe than the public schools. While most institutions—banks, insurance companies, and corporations come to mind—seem far removed from public control, schools attract special attention because of their expansive social reach and ostensible capacity for reform. Reformers on the left expect schools to level the playing field for the poor and disadvantaged; those on the right complain about taxes and pupils' low performance on standardized tests. Legally established by the states but controlled by over 13,000 independent districts, public schools number in the tens of thousands and enroll around 50 million pupils. Their abundance generates a surfeit of anecdotes about their nature and statistics on achievement for the reading, blogging, and viewing public. Much of the news is critical and unkind to pupils and teachers, who seem unable to address America's many deep-seated problems, from racial segregation to the anemic state of academic achievement.

The Death and Life of the Great American School System
How Testing and Choice Are Undermining Education
by Diane Ravitch
Basic Books, New York, 2010. 293 pp. $26.95, C$33.95. ISBN 9780465014910.

Since their origins in the pre-Civil War North, politicians and educators have viewed public schools as a panacea for the ills of society. The greatest early advocate of tax-supported schools, Horace Mann of Massachusetts, claimed in 1848 that the schools were the "great equalizer of the conditions of men—the balance wheel of the social machinery." Expected to assimilate immigrants and teach Christian morality and basic subjects, the schools have long been a basic part of American society, still enrolling around 90% of all eligible youth from kindergarten through high school. But, as Diane Ravitch explains in her feisty analysis of contemporary market-based educational reforms, the schools that long stood the test of time are at a crossroads. Greater privatization of the system seems imminent.

A prominent historian, policy-maker, and public intellectual, Ravitch long aligned herself with conservative school critics but has had a change of heart. *The Death and Life of the Great American School System* is part memoir, explaining her shifting position on market solutions to educational problems, and part jeremiad, warning readers about the ill effects of "No Child Left Behind" (2002), landmark federal legislation endorsed by Kennedy liberals and George W. Bush Republicans alike. With the appointment of Arne Duncan as the Secretary of Education, the Obama Administration has swallowed whole the prevailing ideology about the salutary influence of markets and choice, originally concocted by libertarians, neoconservatives, and Republicans.

Ravitch's engaging book documents her own political odyssey. A lifelong Democrat, she joined the administration of George H. W. Bush in an important post in the Department of Education and affiliated with activists enamored with various forms of "school choice." The collapse of communism and end to the Cold War made market ideals alluring across the political spectrum. By the 1990s, she notes, Bill Clinton's Democratic Leadership Council embraced more market-based reforms, especially charter schools (privately managed "public" schools funded with taxpayer dollars), to address woefully underperforming public schools, particularly in the cities. In theory, deregulation would work wonders, lifting test scores like a bull market. Reflecting the notion that standardized tests and quantitative assessments best judged a school's worth, No Child Left Behind required (under the threat of severe sanctions) that every pupil attain "proficiency" in mathematics and reading by 2014, an impossible goal. But the logic of deregulation by creating more charters seemed irresistible: if schools were free from local bureaucratic rules and forced to compete like McDonald's, scores would rise. Nothing of the sort happened. The law allowed each state to create its own definition of "proficiency," creating laughable claims about rising scores not substantiated by the exam results from the National Assessment of Educational Progress.

A funny thing happened on the way to the revolution. Despite the recent expansion of charter schools, test results did not generally improve—either there or in the regular public schools, which increasingly enrolled more disadvantaged pupils, special education students, and the troublesome and inattentive, all unlikely to lift scores. "No Child" only required testing in mathematics and English, so art, music, history, social studies, and science classes were cut in many school systems. Teachers taught a narrower range of topics even within the tested subjects, undermining learning. Without any evident improvement in test scores, the curriculum narrowed and teaching to the test on the truncated basics became more prevalent.

Through case studies on the fate of market-oriented school reforms in several cities, Ravitch documents the arrogance and naïveté of the new wave of school managers. Largely drawn from the corporate sector, the legal profession, and so forth, these believed they, like corporate CEOs, needed arbitrary power and authority to crack down on teachers, principals, and students. Often flush with huge donations from mega-donors, including the Gates and Walton foundations (themselves

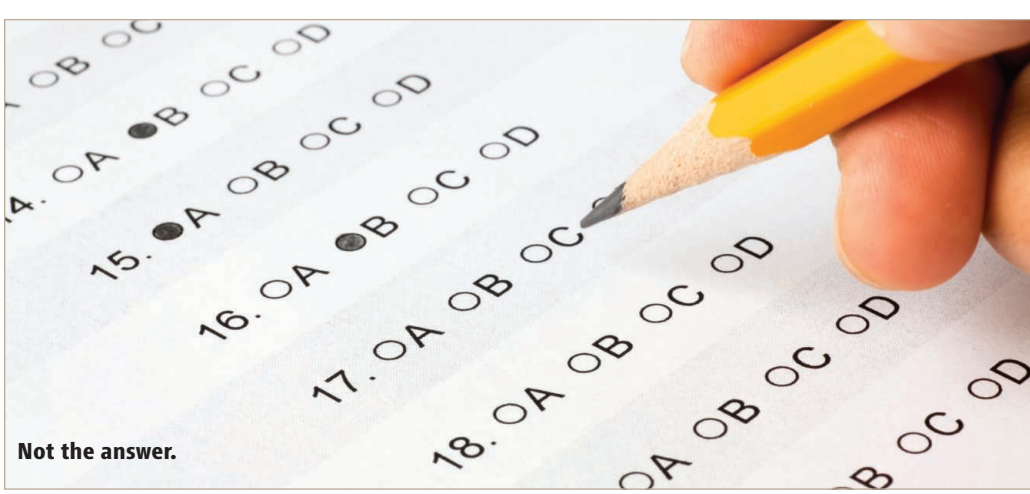

Not the answer.

CREDIT: ISTOCKPHOTO.COM

The reviewer is at the Department of Educational Policy Studies and Department of History, University of Wisconsin, Madison, WI 53715, USA. E-mail: wjreese@wisc.edu

Published by AAAS

accountable to no one), these managers often knew little about teaching or the curriculum but generally blamed teachers' unions for any failures in the schools. They insulted and intimidated teachers and often closed functioning if imperfect neighborhood schools, weakening community ties without doing much to lift school achievement.

The Death and Life of the Great American School System is a sobering narrative by a former advocate of choice and market-inspired educational reforms who had the courage to change her mind. That deregulation of the economy produced the "great recession" and led to massive government bailouts has shaken some citizens' faith in unfettered markets. Unless the current administration changes its educational course, however, America's often-mindless fixation on raising test scores seems likely to continue into the foreseeable future.

10.1126/science.1190046

ANTHROPOLOGY

Cutting a Controversy Down to Size

Robert A. LeVine

Can there ever be an end to the 27-year-old controversy over Margaret Mead's Samoan fieldwork of 1926? The BBC aired a television program on it as recently as 2006, and with *The Trashing of Margaret Mead*, Paul Shankman, a long-time participant in the debate, has made a serious and illuminating attempt at providing the last word. The controversy first flared in 1983, with the publication of Derek Freeman's *Margaret Mead and Samoa* (*1*). Freeman, a respected New Zealand anthropologist, charged that Mead's 1928 best-seller *Coming of Age in Samoa* (*2*) incorrectly described Samoan adolescence and propagated a false view of human nature. Freeman held Mead's Samoan research responsible for the environmentalist bias he attributed to anthropologists' views on the "nature-nurture debate." His charges made the front page of the *New York Times* (*3*) and received wide coverage in the media, including a long (unfavorable) book review in *Science* (*4*). They also set off a long series of academic responses, mostly by specialists on Polynesia, to Freeman's claims.

The reviewer is at the Graduate School of Education, Harvard University, Appian Way, Cambridge, MA 02138, USA. E-mail: bob_levine@gse.harvard.edu

Shankman, an anthropologist at the University of Colorado, has worked extensively in Samoa, published criticisms of Freeman, and argued with him in private. He does not pretend to be neutral, but his heavily researched book sheds new light on the controversy. Mead's reputation is at stake, Shankman emphasizes, rather than any scientific issue.

The Trashing of Margaret Mead
Anatomy of an Anthropological Controversy
by Paul Shankman
University of Wisconsin Press, Madison, 2009. 320 pp. Paper, $29.95. ISBN 9780299234546. e-book, $9.99. ISBN 9780299234539. Studies in American Culture and Thought.

An anthropological pioneer, Mead conducted fieldwork in the Pacific during the 1920s and 1930s that provided early evidence of cultural diversity in childhood and adolescence. She was not an extreme environmentalist; rather, she emphasized an interaction between innate temperament and culture. Her main point—that cultural variations in the experiences of growing up, coming of age, and becoming male and female were substantial enough to warrant scientific examination and public attention—was amply confirmed by more intensive studies conducted around the world after World War II.

Although Mead became a celebrity through her books and talks popularizing cultural anthropology, her work was often sharply criticized by her anthropological colleagues. Within the discipline, she had, particularly after the 1950s, little theoretical influence. By 1978 (when she died at age 77), however, she was appreciated as a founding figure of American anthropology whose flaws represented an early era of the field and whose colorful personality had made her the most famous anthropologist of her time.

Long after the media debate about Freeman's 1983 claims died down, anthropologists who had worked in Polynesia continued to pen articles and books on the topic, most of which criticized Freeman. In a second, 1998 book (*5*), he presented additional evidence that in 1926, the young and inexperienced Mead had been duped by her informants. It too was, under the title "Mead Misrepresented," unfavorably reviewed in these pages (*6*), and Freeman responded with a rejoinder (*7*). He died in 2001, but the Mead-Freeman controversy, like the nature-nuture "debate," still fascinates journalists and the public regardless of what scientists think about it.

Shankman argues that Freeman made inaccurate claims to exaggerate the significance of his attack: He presented himself as unique among anthropologists in daring to criticize Mead. He claimed, incorrectly, that Mead ignored "biology" and the possibility of genetic influence. Freeman also failed to recognize that it was clear long before 1983 that "emotional turmoil" at adolescence was not universal in humans. Therefore, as Robert Levy noted in his book review in *Science* (*4*), Mead's early conclusion was correct regardless of whether or not all her facts were accurate. Freeman seemed not to know that the question of universal adolescent turmoil had long ceased being an issue in anthropology. In Shankman's account, Freeman imagined his critique of Mead to be one of the most important theoretical breakthroughs of the 20th century. The author's unflattering portrait of Freeman, supported by detailed anecdotes and quotations, is central to his argument that the fabricated controversy is largely attributable to one man's unbridled ambition and grandiose fantasies. He concludes: "For reasons that are still not fully understood, Freeman became obsessed with Mead and compromised his own scholarship as he damaged hers."

The Trashing of Margaret Mead offers more of a contextualized history of the controversy in the media rather than an analysis of the scientific issues, although it covers both aspects. It contains an informative introduction to the lives and work of Mead and Freeman, the unfolding of the public discourse about Freeman's first book, and the relevant aspects of Samoan culture. There are innovative chapters on Mead's American audience in the 1920s, what the controversy meant to Samoans, and the "selling of the controversy" (which includes a description of Freeman's 1983 appearance on the Phil Donahue Show). As history, however, the book does not probe as far as it might have the publisher's role in creating the controversy and the relationship of the debate to developmental psychology. Thus there is still room for future attempts at the last word.

References

1. D. Freeman, *Margaret Mead and Samoa: The Making and Unmaking of an Anthropological Myth* (Harvard Univ. Press, Cambridge, MA, 1983).
2. M. Mead, *Coming of Age in Samoa: A Psychological Study of Primitive Youth for Western Civilization* (Morrow, New York, 1928).
3. E. McDowell, *New York Times*, 31 January 1983, p. A1.
4. R. I. Levy, *Science* **220**, 829 (1983).
5. D. Freeman, *The Fateful Hoaxing of Margaret Mead: A Historical Analysis of Her Samoan Research* (Westview, Boulder, CO, 1998).
6. M. Orans, *Science* **283**, 1649 (1999).
7. D. Freeman, *Science* **285**, 50 (1999).

10.1126/science.1189202

CONSERVATION

CITES Designation for Endangered Rosewood in Madagascar

Predicted forest losses and a recent government ban on logging build support for trade protection of Malagasy rosewood.

Meredith A. Barrett,[1]* Jason L. Brown,[2] Megan K. Morikawa,[3] Jean-Noël Labat,[4] Anne D. Yoder[2,5]

Logging in Madagascar, one of the world's most threatened biodiversity hot spots (*1*, *2*), has rapidly increased amid political turmoil since a transitional government assumed power in March 2009 (*1*, *3*). With as much as 90% of the country's primary forest already lost, continued logging will mean species extinctions across all biotic elements of Madagascar's ecosystems, where rates of endemism are unparalleled (*2*, *4*, *5*). We demonstrate immediate risk for rosewood (genus *Dalbergia*) species extinctions and thus the need for protection via international trade regulation under the Convention on International Trade in Endangered Species of Wild Fauna and Flora (CITES). Protection of Malagasy rosewood species, which suffer from targeted logging because of their high value in international markets, would not only avoid their extinction but also extend the benefits of protection to all biota within these threatened ecosystems.

Despite public concern from international parties (*6*), the Malagasy rosewood issue was absent from the March 2010 CITES Conference of Parties (CoP). Yet one day before the meeting's conclusion, the Malagasy government issued a decree prohibiting rosewood logging and export, likely a response to international pressure (*7*). This unexpected, positive change, a window of opportunity in an unstable political climate, combined with the 3-year delay before the next CoP at which species can be voted on for full CITES protection, heightens the potential and urgency for listing of rosewood under CITES Appendix III by the Malagasy authorities (*8*).

Market-Driven Logging Pressure

A conservatively estimated 1137 containers, each carrying an average of 144 rosewood logs and valued at more than U.S. $227.4 million, have been exported from Madagascar since April 2009 (*1*, *9*). Exporters have benefited from the transitional government's exceptions to a previous ban on exportation of unfinished hardwood products (*1*, *3*). The administration legalized rosewood export on 31 December 2009, yet overturned this ruling on 24 March 2010, by banning logging and export of rosewood for the next 2 to 5 years (Decree no. 2010-141) (*7*). The enforceability of the ban is questionable, and the fate of 10 to 15 thousand metric tons of felled rosewood waiting in ports remains uncertain.

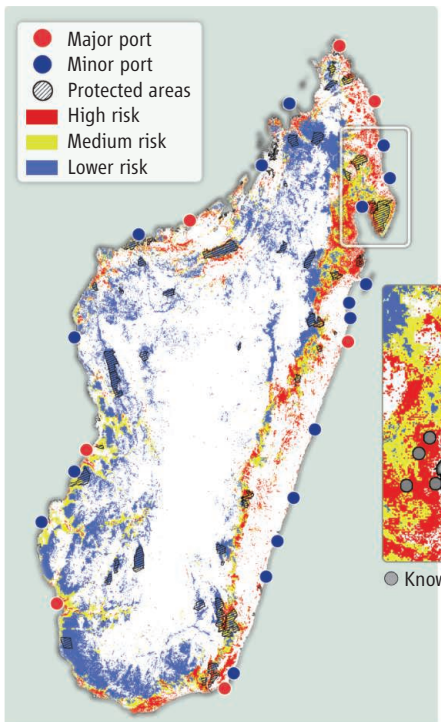

Areas at risk for future illegal rosewood logging in Madagascar. Much known current logging has occurred in the northeast (inset), especially in protected areas (fig. S3).

Rosewood is sought for its rich burgundy color and hard wood, qualities valued for high-end furniture and musical instruments (fig. S1). Most exports have been shipped to China, the world's largest consumer of tropical hardwoods, where an opaque regulatory process and high demand for rosewood furniture have driven the market (*1*, *10*). A rosewood armoire can command $20,000 in China, in stark contrast to the $0.49 a Malagasy laborer earns for each rosewood log extracted (*1*, *11*). Current rosewood market practices not only deprive Malagasy laborers of a living wage but also impair future rural livelihoods by damaging essential ecosystems.

Impacts of Rosewood Logging

Although selective rosewood logging results in less forest loss than clear-cutting, the consequences are still destructive (*12*). Because of the low density of rosewood trees per hectare, loggers must routinely encroach on new territories—up to 20,450 ha have been affected by selective logging in the northeast region thus far (*9*). In order to float dense rosewood logs downstream for export, four or five lighter trees are cut to raft each rosewood log, amounting to hundreds of additional trees daily (fig. S1) (*1*, *9*). Such selective logging facilitates invasion of non-native species, reduces native species diversity (*12*, *13*), and aridifies landscapes, which leads to an increased likelihood of fires (*14*). The loss of nitrogen-fixing by *Dalbergia* results in a reduction in soil fertility (*15*, *16*).

Increased access to forests via logging trails and roads leads to further resource extraction and deforestation, as seen with settlement patterns around logging hot spots in northeastern Madagascar (*7*). Increased fragmentation of forests can amplify environmental stress, impair wildlife and ecosystem health, induce local species extinctions, shift community composition, and lead to significant loss in genetic diversity of isolated populations of endemic animals and plants (*12*, *17*–*19*). Increased forest access has led to the emergence of a bushmeat market in Madagascar (*20*). Hunting and habitat loss will deteriorate conditions for already endangered animal species (*12*). Rosewood extraction undermines the legitimacy of Madagascar's National Parks management, impairing conservation efforts and destabilizing the once-thriving ecotourism industry.

Estimating the Extent of Decline

Using geospatial tools, we modeled eight species of rosewood (*21*) to address the following questions [supporting online material (SOM),

[1]University Program in Ecology, Duke University, Durham, NC 27708, USA. [2]Department of Biology, Duke University, Durham, NC 27708, USA. [3]Trinity College of Arts and Sciences, Duke University, Durham, NC 27708, USA. [4]Département Systématique et Evolution, UMR 7205, Muséum national d'Histoire naturelle, Paris, 75005, France. [5]Duke Lemur Center, Duke University, Durham, NC 27708, USA.

*Author for correspondence. E-mail: meredith.barrett@duke.edu

Published by AAAS

§ 1]: (i) Where are Madagascar's richest areas for rosewood species? (ii) How reduced is the distribution of rosewood versus estimated historic distributions? (iii) Which areas are most vulnerable to further logging? (iv) Is there sufficient evidence and urgency to call for CITES designation of Malagasy rosewood?

Historic distributions extended almost entirely throughout Madagascar (93% coverage), with the highest richness—seven co-occurring species—in northeastern rain forests. Depending on the species and deforestation scenario, distribution reduction ranged from 54 to 98% (fig. S2 and table S2), which demonstrates intense habitat loss. Based on a logging-risk model combining logging access and rosewood presence (SOM, § 1c), we confirmed high logging risk in northeastern protected areas, where lack of enforcement and higher quality, size, and density per hectare of rosewood attract increased logging (*3*). Our analyses forecast that logging could extend throughout the country (see the figure, p. 1109, and fig. S3); we identified 25 protected areas that are at high or medium risk for future logging (fig. S3).

CITES Designation, Government Action

Despite their threatened status (table S2) (*22*), no Malagasy *Dalbergia* species are protected under CITES (*12*). However, three non-Malagasy *Dalbergia* species are currently regulated under CITES (table S2). Brazilian rosewood, listed as vulnerable by the International Union for Conservation of Nature (IUCN), as are several Malagasy species, has benefited from CITES protection since 1992 (*22*). Some claim that much logging shifted from Brazil to Madagascar because of this listing (*23*).

Although CITES may not provide an immediate or comprehensive solution, owing to the lengthy process, difficult implementation, and need for political will (*24*), it nonetheless affords the best protection available (*12*, *25*). The eight species analyzed here satisfy criteria for listing under CITES Appendix I (*8*), primarily because of severe range reductions (table S2). The two endangered rosewood species for which we lacked sufficient data would qualify for Appendix II because of their resemblance to these eight rosewood species (SOM, § 2c, and table S2). Despite participation by Malagasy authorities at the 2010 CoP, little discussion of Malagasy rosewood occurred (*26*). However, an international working group was formed to help Madagascar identify species to evaluate at the next CoP in 2013 (*27*). We urge the Malagasy government to immediately list these 10 rosewood species for limited protection under Appendix III to ensure their existence until they can be listed in Appendix I or II, pending CoP approval in 2013 (SOM, § 2d).

CITES listing of rosewood would signify commitment by the Malagasy government and could provide a consistent legal framework for traders. Any export would require a permit that certifies the specimen was legally collected in a method nondetrimental to species survival. To ensure sustainability, forestry strategies including land-use planning, explicit management policies, chain-of-custody timber tracking, and log DNA bar-coding should be implemented (*24*). International agencies have called upon the government to seize all illegal timber and to use money from its sale within legal markets to start a trust fund for conservation and rural development; however, this may only enhance opportunities for continued corruption (*1*).

Government declaration of high-risk logging areas identified in these analyses (see the figure and fig. S3) will raise awareness about enforcement efforts. The government should consider expansion of the protected area network, but additional funds for park patrols and infrastructure will be essential (*28*).

Role of the International Community

Weak penalties and limited enforcement, as well as difficulties in identifying and tracking illegally sourced specimens, remain fundamental challenges. The international community should raise awareness of the consequences of rosewood logging, place pressure on the Malagasy government to implement improvements, and reduce market demand for illegal wood products. The recently amended U.S. Lacey Act (*29*) bans trade of illegally sourced plant and wood products and requires importers to declare origin and species of all plants. Even so, the United States continues to import $3.5 billion in illegal wood products from China annually (*10*), and European companies have been implicated in recent rosewood export (*1*).

Malagasy forests could offer far greater, renewable economic value when evaluated through innovative markets. Potential revenue of $72 to $144 million per year for Madagascar from a Reducing Emissions from Deforestation and Forest Degradation (REDD) program far exceeds the estimated $9 million in annual conservation funding received before the political unrest (*30*).

Environmental costs of political instability are high; no long-term conservation goals can be achieved in a governmental void. The urgency of illegal rosewood logging demands national and international action to conserve both rural livelihoods and remaining biodiversity habitats.

References and Notes

1. Global Witness, "Investigation into the illegal felling, transport and export of precious wood in SAVA region Madagascar" (Global Witness, London, 2009).
2. N. Myers *et al.*, *Nature* **403**, 853 (2000).
3. D. Schuurman, P. P. Lowry, II, *Madagas. Conserv. Dev* **4**, 98 (2009).
4. A. D. Yoder, M. D. Nowak, *Annu. Rev. Ecol. Evol. Syst.* **37**, 405 (2006).
5. G. J. Harper ***et al.***, *Environ. Conserv.* **34**, 325 (2007).
6. World Wildlife Fund (WWF), Communique (2009); http://wwf.panda.org/wwf_news/news/?166201/International-community-calls-for-action-against-illegal-logging-in-Madagascar.
7. J. Bohannon, *Science* **328**, 23 (2010).
8. CITES consists of three levels of protection that vary in rigor and permitting requirements. Appendix I affords the most protection by effectively stopping all trade with a careful permitting process. Appendix II allows limited nondetrimental trade, with export permits; Appendix III allows less regulated trade, with export permits. Appendix I and II listings require approval of two-thirds of the CoP. Appendix III species can be listed unilaterally by the country of origin, a faster, but less protective, option.
9. L. Wilmé *et al.*, Precious trees pay off—but who pays? An update; www.madagascar-library.com/r/1587.html.
10. W. F. Laurance *et al.*, *Science* **319**, 1184, author reply 1184 (2008).
11. D. Schuurman, *TRAFFIC Bull.* **22**, 49 (2009).
12. E. R. Patel, *Madagas. Conserv. Dev.* **2**, 11 (2007).
13. K. A. Brown, J. Gurevitch, *Proc. Natl. Acad. Sci. U.S.A.* **101**, 6045 (2004).
14. M. A. Cochrane, M. D. Schulze, *Conserv. Biol.* **12**, 948 (1998).
15. B. Favreau *et al.*, *Mol. Ecol. Notes* **7**, 774 (2007).
16. R. Rasolomampianina *et al.*, *Mol. Ecol.* **14**, 4135 (2005).
17. A. C. M. Gillies *et al.*, *Heredity* **83**, 722 (1999).
18. D. J. Rapport, W. G. Whitford, *Bioscience* **49**, 193 (1999).
19. T. R. Gillespie, C. A. Chapman, *Am. J. Primatol.* **70**, 222 (2008).
20. M. A. Barrett, J. Ratsimbazafy, *Nature* **461**, 470 (2009).
21. Ten of the 48 Malagasy ***Dalbergia*** species (SOM, § 2b) are economically and ecologically important and targeted for timber markets (***31***). We had sufficient expert-validated data to estimate historic distributions for 8 of these 10 species (table S1 and fig. S2).
22. IUCN, *IUCN Red List of Threatened Species, Version 2009.2* (IUCN, Gland, Switzerland, 2009).
23. D. Louppe, A. A. Oteng-Amoako, M. Brink, Eds., *Plant Resources of Tropical Africa*, vol. 7(1), *Timbers* (PROTA Foundation, Backhuys Publ., Leiden, Netherlands, 2008), vol. 7(1).
24. A. G. Blundell, *Ecol. Appl.* **17**, 323 (2007).
25. C. H. Keong, *Int. For. Rev* **9**, 805 (2007).
26. K. Neville, T. Rosen, L. Russo, *Earth Negot. Bull.* **21**, 1 www.iisd.ca/cites/cop15/ (2010).
27. CITES, Committee I, Summary Record 6 (Rev. 1), Fifteenth Meeting of the Conference of the Parties (CoP15), Doha, Qatar, 13 to 25 March 2010; www.cites.org/eng/cop/15/sum/E15-Com-I-Rec06.pdf.
28. Only one National Park agent, who does not have enforcement capabilities, tours 100 km^2 of forest, a ratio unfavorably disproportionate to the threat (***11***).
29. 16 U.S. Code of Regulations (U.S.C.) 3371–3378 (2008).
30. L. Hannah *et al.*, *Biol. Lett.* **4**, 590 (2008).
31. J.-N. Labat, J. Moat, in *The Natural History of Madagascar*, S. M. Goodman, J. P. Benstead, Eds. (Univ. of Chicago Press, Chicago, 2003), pp. 346–373.

32. This is Duke Lemur Center publication no 1178. We thank E. Patel, J. Moat, L. Chan, A. Stoertz, M. Turnipseed, C. Welch, A. Heilman, M. Nowak, R. C. Atkinson, and L. Olander. Supported by NSF: M.A.B. (Graduate Research Fellowships Program), J.L.B. (0905905), and A.D.Y. (DEB 0516276). We note the services of Madagascar Institut pour la Conservations des Ecosystèmes Tropicaux (MICET) for ongoing facilitation of research in Madagascar.

Supporting Online Material

www.sciencemag.org/cgi/content/full/328/5982/1109/DC1

10.1126/science.1187740

MEDICINE

Prion Strain Mutation and Selection

Structural compatibility of infecting prion proteins with those of a new host determine whether they will be successfully transmitted.

John Collinge

When the connection was made between bovine spongiform encephalopathy (BSE or "mad cow" disease) and human illnesses in the 1990s, it raised the public profile of the underlying prion diseases as the implications of animal and public health crises, and their economic impacts, became apparent. At the core of these concerns is how prions, the infectious agent, diversify and expand their host range. On page 1154 of this issue, Angers *et al.* (*1*) reveal how this occurs in chronic wasting disease (CWD), a contagious prion disease of wild deer and elk. Its prevalence in the United States raised fears that, like BSE, it might transmit to humans.

Prions cause fatal neurodegenerative diseases of humans and animals such as scrapie in sheep and goats, BSE in cattle, and Creutzfeldt-Jakob disease in humans (*2*). They consist of a rogue form of a protein produced by an infected animal, not by a foreign DNA or RNA genome, and pass from one species to another via dietary and other routes of transmission. Prions are thought to be composed principally or entirely of polymers of misfolded prion protein (known collectively as PrP scrapie or PrP^{Sc}). They propagate by recruiting the normal host prion protein (PrP^{C}) via seeded protein fibrilization. In this process, fragmentation of elongating fibrils leads to an autocatalytic, exponential amplification process that effectively mimics a conventional infectious agent in its ability to invade and colonize susceptible hosts. Despite the absence of a nucleic acid genome, prions exist as multiple strains that can be serially propagated in laboratory animals and differentiated by the patterns of disease they produce. Because multiple strains can be maintained in inbred mice with identical PrP genes, prions cannot be encoded by differences in PrP primary structure (its amino acid sequence). Rather, it is thought that they represent structurally different PrP^{Sc} seeds that recruit host PrP^{C} into polymers of misfolded PrP. Thus, strains may be associated with biochemically distinct PrP^{Sc} types that can propagate on serial passage in susceptible hosts, including those from different species (*3*–*5*) (see the figure).

MRC Prion Unit, Institute of Neurology, University College London, London WC1N3BG, UK. E-mail: j.collinge@prion.ucl.ac.uk

PrPs have a highly conserved structure, which is presumably central to their ability to infect across species. Although differences in PrP^{C} primary structure have been considered a barrier to cross-species infection, the "strain-ness" of a prion is fundamental to its ability to infect a new species. Thus, two prion types, or strains, that propagate in one species may have different abilities to cross a transmission barrier (*6*). Under the conformational selection model (*7*), of the possible PrP^{Sc} strains that can overcome natural clearance and propagate effectively in mammals, only a subset is compatible with a given host PrP^{C} structure, and can thereby propagate in that host. Transmission barriers can be explained by the degree of overlap between strain types that are permissible in the two species concerned. Such effects may also be encountered within a species where there are PrP polymorphisms. A common human PrP polymorphism (at amino acid position 129) dramatically affects strain selection (*4*, *8*) and has a powerful effect on human susceptibility to prion disease (*9*, *10*). Important PrP polymorphisms are also seen in sheep and other species, and conformational selection occurs with yeast prions as well (*11*).

However, in some cases, prions do not maintain their identity in a new host but switch properties. Such strain "mutation" (*12*) may result from crossing between species, or intraspecies transmission due to PrP polymorphism or the effect of genetic background (*13*). The new strain generated may be more or less pathogenic in a second species than its progenitor, so mutation has potential public and animal health implications.

Although is has been argued that prion strains may be cloned (*12*), such material

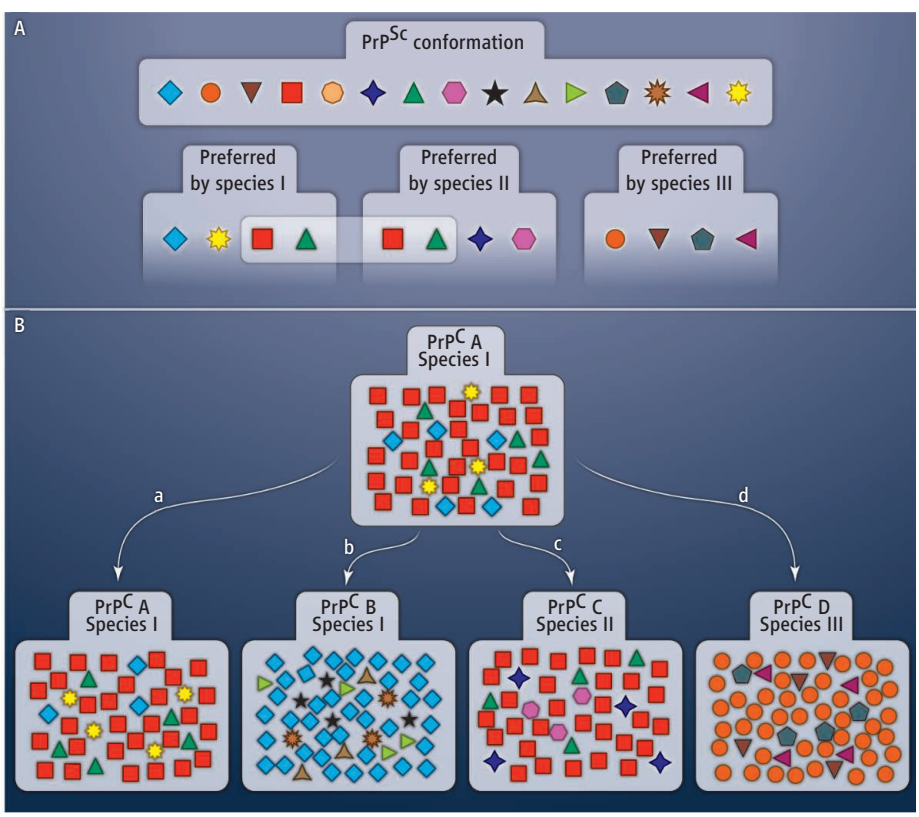

Prion propagation. (**A**) A limited set of mammalian PrP^{Sc} conformations can propagate as prions using the PrP^{C} present in susceptible host species. Prions transmit readily between hosts that express the same PrP^{C}, and may do so in those with different PrP^{C} if there is substantial overlap of permissible conformations (species I and II). If there is little or no overlap (species I and III), a major transmission barrier occurs. (**B**) A prion strain may be a molecular ensemble maintained under host selection. (a) A strain can propagate in the same species expressing identical PrP^{C}; (b) strain mutation may occur when prions colonize the same species with a different PrP^{C}, or (c) may propagate in a different species with compatible PrP^{C}; (d) if not compatible in a new species, mutation may occur.

CREDIT: Y. GREENMAN/*SCIENCE*

Published by AAAS

is heterogeneous when assessed by physical and biochemical methods. It may be that prion strains represent an ensemble of molecular species maintained under host selection (*14*). Such a quasispecies would have a dominant component with recognizable biochemical and biological properties, but also have lower-abundance subspecies. The preferential selection of the latter in an alternate host that is unable to propagate the dominant species could explain strain mutation (*14*), as observed in prion-infected cell cultures (*15*).

CWD is prevalent in wild cervids (deer and elk) in several U.S. states and has been recognized in Canada and South Korea. It spreads readily between wild animals, and urine, feces, and saliva are infectious (*16*). The occurrence of multiple strains of CWD is likely, given that multiple cervid species and different PrP^C structures (including within-species PrP polymorphism) are involved, and the existence of at least two CWD strains (CWD 1 and 2) has now been demonstrated by Angers *et al*. The authors show that CWD prion strain selection and mutation are influenced by the amino acid at position 226 in PrP (*4*, *8*), which differs between deer and elk. Although CWD 1 and 2 can be distinguished by biological strain typing methods, their biochemical characteristics are similar by the molecular strain typing methods used. Assuming that the "protein-only" model of replication is correct, such differences in disease-associated PrP must exist. However, these differences may reside in protease-sensitive forms of abnormal PrP, which are important components of prion isolates.

What is the importance of the findings of Angers *et al*. for public health? One method to model human susceptibility, as done with BSE in the 1990s (*2*), is to determine the susceptibility of transgenic mice expressing human PrP^C to CWD prion infection in comparison to susceptibility in human and other animal strains. Studies so far show that such mice are resistant (*17*, *18*). However, it is necessary to repeat these studies with all CWD strains identified and to take account of permutations of PrP polymorphisms in CWD-affected animals and humans. This further evidence for the role of PrP polymorphism on strain selection and mutation should highlight the potential for a new zoonotic prion strain to emerge from prion evolution in animal reservoirs, notably in worldwide endemic scrapie of sheep and goats as well as CWD in deer and elk.

Prion-like mechanisms may be relevant in common human neurodegenerative diseases such as Alzheimer's and Parkinson's diseases. Accumulation of misfolded host proteins occurs in these diseases, and seeded protein aggregation may be relevant to the etiology and spread of pathology (*14*). It will be of great interest to see if the phenomena of conformational and kinetic selection of strains and their mechanisms of neurotoxicity are also important in these and other diseases of protein misfolding.

References

1. R. C. Angers *et al*., *Science* **328**, 1154 (2010).
2. J. Collinge, *Annu. Rev. Neurosci.* **24**, 519 (2001).
3. R. A. Bessen, R. F. Marsh, *J. Virol.* **68**, 7859 (1994).
4. J. Collinge *et al*., *Nature* **383**, 685 (1996).
5. G. C. Telling *et al*., *Science* **274**, 2079 (1996).
6. A. F. Hill *et al*., *Nature* **389**, 448, 526 (1997).
7. J. Collinge, *Lancet* **354**, 317 (1999).
8. J. D. Wadsworth *et al*., *Science* **306**, 1793 (2004).
9. M. S. Palmer *et al*., *Nature* **352**, 340 (1991).
10. S. Mead *et al*., *Science* **300**, 640 (2003).
11. R. B. Wickner *et al*., *Annu. Rev. Genet.* **38**, 681 (2004).
12. M. E. Bruce, A. G. Dickinson, *J. Gen. Virol.* **68**, 79 (1987).
13. S. E. Lloyd *et al*., *J. Gen. Virol.* **85**, 2471 (2004).
14. J. Collinge, A. R. Clarke, *Science* **318**, 930 (2007).
15. J. Li *et al*., *Science* **327**, 869 (2010).
16. C. K. Mathiason *et al*., *PLoS ONE* **4**, e5916 (2009).
17. G. Tamguney *et al*., *J. Virol.* **80**, 9104 (2006).
18. Q. Kong *et al*., *J. Neurosci.* **25**, 7944 (2005).

10.1126/science.1190815

PLANETARY SCIENCE

Nitrogen in the Solar System

Nitrogen isotopic compositions can serve as useful tracers to understand the input materials and processes during formation and evolution of the solar system.

Kurt Marti and John Kerridge

Nitrogen within the solar system is not isotopically uniform: $^{15}N/^{14}N$ ratios in planetary objects such as Earth, Mars, and Jupiter range from 1.9 to 5.9×10^{-3} (*1*), some meteoritic materials exhibit ratios as high as 22×10^{-3} (*2*), and samples from the lunar surface reveal an unexplained variability between 2.8 and 4.3×10^{-3} (*3*). These variations are best explained by mixing of isotopically distinct components which could have been carried to the lunar surface by the solar wind or originated from some unknown source. Identifying the compositions and sources of those components will clarify fundamental issues such as how planets accreted and how their atmospheres subsequently evolved.

In situ measurements of solar-wind N implanted in collectors carried by NASA's Genesis spacecraft yielded a value of 2×10^{-3} for $^{15}N/^{14}N$ (*4*, *5*), close to the N isotope ratios in NH_3 in the jovian atmosphere [1.9 to 2.3×10^{-3} (*1*, *6*)]. This agreement indicates that the N isotopic ratio in the protosolar nebula was similar to that in the contemporary galactic disk (*7*) but lower than in Earth and inner planets where the ratio is ~3.7×10^{-3}.

Important insights into possibly variable environments may be found in the powdery surface layer on the Moon—the lunar regolith—where several billion years of history within the heliosphere are recorded, and in which soils and breccias contain well-documented records of highly variable nitrogen components (*3*), including, in addition to solar wind, non–solar-wind N, of unknown origin, that is isotopically much heavier than the solar wind.

Nonsolar N in the lunar regolith [and in surfaces of rocks (*8*)] is an order of magnitude more abundant (and much heavier) than solar-wind N (*9*). It is implanted into the surface together with the solar wind, although resolution of a two-component mixture indicates somewhat shallower implantation depths (*10*).

Shooting for the Moon. Comparing the nitrogen isotopic ratios from lunar-surface samples implanted at known times in the past may help provide a picture of the processes that shaped our solar system.

CREDIT: JUPITERIMAGES

Department of Chemistry and Biochemistry, University of California San Diego, La Jolla, CA 92093, USA. E-mail: jkerridg@ucsd.edu

Published by AAAS

The abundance of nonsolar N in the regolith increases with duration of surface exposure. Based on results from Apollo samples, the carbon/nitrogen (C/N) ratio of the nonsolar component is estimated to be less than half of the solar contribution (*11*).

Heavy N was apparently added to the regolith up to recent times, as observed in surfaces of ejecta from 2-million-year-old South Ray Crater (*8*). In a suite of 24 regolith samples obtained by Apollo 16, the $^{15}N/^{14}N$ ratios of nonsolar N vary by 15%, with young soils from 50-million-year-old North Ray Crater averaging $^{15}N/^{14}N = 4.14 \times 10^{-3}$, while older material averages $^{15}N/^{14}N = 3.92 \times 10^{-3}$ (*12*).

The source of nonsolar N is delivered at 30 μg N/cm^2 per million years to the lunar surface as ions coupled to the solar wind, either in the heliosphere or in temporary lunar atmospheres. Furthermore, the observed low C/N ratio may serve as a useful tracer of origin, although possible C/N fractionation during photoionization or loss mechanisms from the lunar surface needs to be further studied. The observations do not favor a meteoritic origin for nonsolar N but may indicate reservoirs enriched in NH_3 (*13*, *14*).

The source of the nonsolar N must be either isotopically variable or comprise multiple, isotopically distinct components whose mixing ratio can vary. The Apollo 16 data suggest either that the North Ray impact event supplied heavy N, which was photoionized and reimplanted from the temporary atmosphere, or that the average nonsolar N component implanted in the past 50 million years was heavier.

Continuing isotopic studies of selected materials from the lunar regolith and other solar system objects will help to elucidate the quantitative range and possible spatial, and even temporal, distribution of $^{15}N/^{14}N$ variations in the solar system. High-resolution molecular-spectroscopic observations and theoretical modeling will shed light on the existence of, and possible isotopic fractionation mechanisms within, potential reservoirs that could have contributed N to the nascent solar system. It is also important to investigate possible mechanisms whereby non–solar-wind N could be transported to, and implanted within, the lunar surface. Finally, much more information is needed regarding N-containing molecules and elemental/isotopic tracers that will assist in discriminating among potential heavy-N reservoirs, including components with different nucleosynthetic histories.

Non–solar-wind N in the lunar and other solar-system regoliths provides a promising pathway to identifying the source and composition of isotopically heavy N components in the solar system. Disentangling those distinct components will aid our understanding of evolutionary histories of inner-solar-system objects, including planets and the Moon.

References and Notes

1. T. Owen *et al.*, *Astrophys. J.* **553**, L77 (2001).
2. G. Briani *et al.*, *Proc. Natl. Acad. Sci. U.S.A.* **106**, 10522 (2009).
3. J. F. Kerridge, *Rev. Geophys.* **31**, 423 (1993).
4. A. P. A. Kallio *et al.*, abstract 2481, *41st Lunar and Planetary Science Conference*, The Woodlands, TX, 1 to 5 March 2010.
5. B. Marty *et al.*, *Geochim. Cosmochim. Acta* **74**, 340 (2010).
6. M. A. Abbas *et al.*, *Astrophys. J.* **602**, 1063 (2004).
7. M. Gerin *et al.*, *Astron. Astrophys.* **498**, L9 (2009).
8. J. S. Kim *et al.*, *Nature* **375**, 383 (1995).
9. R. Wieler *et al.*, *Earth Planet. Sci. Lett.* **167**, 47 (1999).
10. K. J. Mathew *et al.*, *Geophys. Res. Lett.* **25**, 4293 (1998).
11. The abundance of solar-wind N in any regolith sample can be calculated using the measured ^{36}Ar content and the solar $N/^{36}Ar$ ratio, with the assumption that both species are implanted quantitatively in the lunar surface. Similarly, the C/N ratio of the nonsolar component can be calculated from bulk values by difference, using the solar C/N ratio.
12. Using the solar $^{15}N/^{14}N$ ratio from (*4*) and the solar N content from (*11*), the abundance and $^{15}N/^{14}N$ ratio of nonsolar N can be calculated from bulk analyses by difference.
13. S. B. Charnley, S. D. Rodgers, *Astrophys. J.* **569**, L133 (2002).
14. L. Bizzocchi *et al.*, *Astron. Astrophys.* **510**, L5 (2010).

15. We thank K. D. McKeegan, A. P. A. Kallio, and V. S. Heber for helpful discussion.

10.1126/science.1189836

MEDICINE

Beige Can Be Slimming

Prostaglandins promote the development of thermogenic beige fat in mice and may be a therapeutic approach to treat obesity.

Jeff Ishibashi and Patrick Seale

How can we decrease the body's energy efficiency? The answer to this could be used to fight the exploding obesity crisis. Our ability to accumulate and retain energy reserves once provided a survival advantage. However, these ingrained energy-conservation pathways are now driving unprecedented weight gain in modern societies where calorie-dense food pervades. Burning off excess fuel (analogous to heating a house in winter with the windows open) may be an effective therapeutic avenue to reduce obesity when diet and exercise are not enough. On page 1158 in this issue, Vegiopoulos *et al.* demonstrate that the fatty acid derivatives called prostaglandins encourage adipocytes (fat cells) to do exactly this—waste energy through increased heat production (*1*).

Institute for Diabetes, Obesity and Metabolism and the Department of Cell and Developmental Biology, University of Pennsylvania School of Medicine, Philadelphia, PA 19104, USA. E-mail: sealep@upenn.edu

In contrast to the familiar white adipocytes that specialize in lipid storage, brown adipocytes burn fat to produce heat (thermogenesis). Infants have prominent depots of brown fat that regulate body temperature. Although these "newborn" depots regress during childhood, appreciable amounts of brown fat persist in adults and correlate with adult leanness (*2*–*5*). Similarly, brown fat counteracts obesity and metabolic disease in rodents (*6*) Therefore, enhancing brown fat thermogenesis is an attractive target for anti-obesity therapy. Vegiopoulos *et al.* show that white fat can be induced to form intermediate "beige" adipocytes with many of the properties of brown adipocytes, but having completely independent developmental origins (*7*) (see the figure).

The thermogenic activity of fat tissue is controlled by the sympathetic nervous system. Cold exposure in rodents and humans causes sympathetic nerve fibers to release norepinephrine in fat tissues (*6*). Norepinephrine then activates β_3-adrenergic receptors on brown fat cells to stimulate lipolysis and heat production. In white fat depots, prolonged exposure to cold or β_3-adrenergic agonists causes tissue transdifferentiation from white to beige (*6*). Unfortunately, β_3-adrenergic agonists have not reached successful clinical application for weight loss because of technical, efficacy and safety issues (*8*).

Vegiopoulos *et al.* have now discovered an alternative—prostaglandins drive beige fat development in white fat. This signaling pathway may lead to new therapies for obesity. Specifically, the authors found that white fat cells in mice increase expression of the enzyme cyclooxygenase-2 (COX-2) in response to cold or β_3-adrenergic agonists, which consequently produces prostaglandins. Prostaglandins then act locally, triggering brown fat–specific gene expression in white fat cells. In mice engineered to express

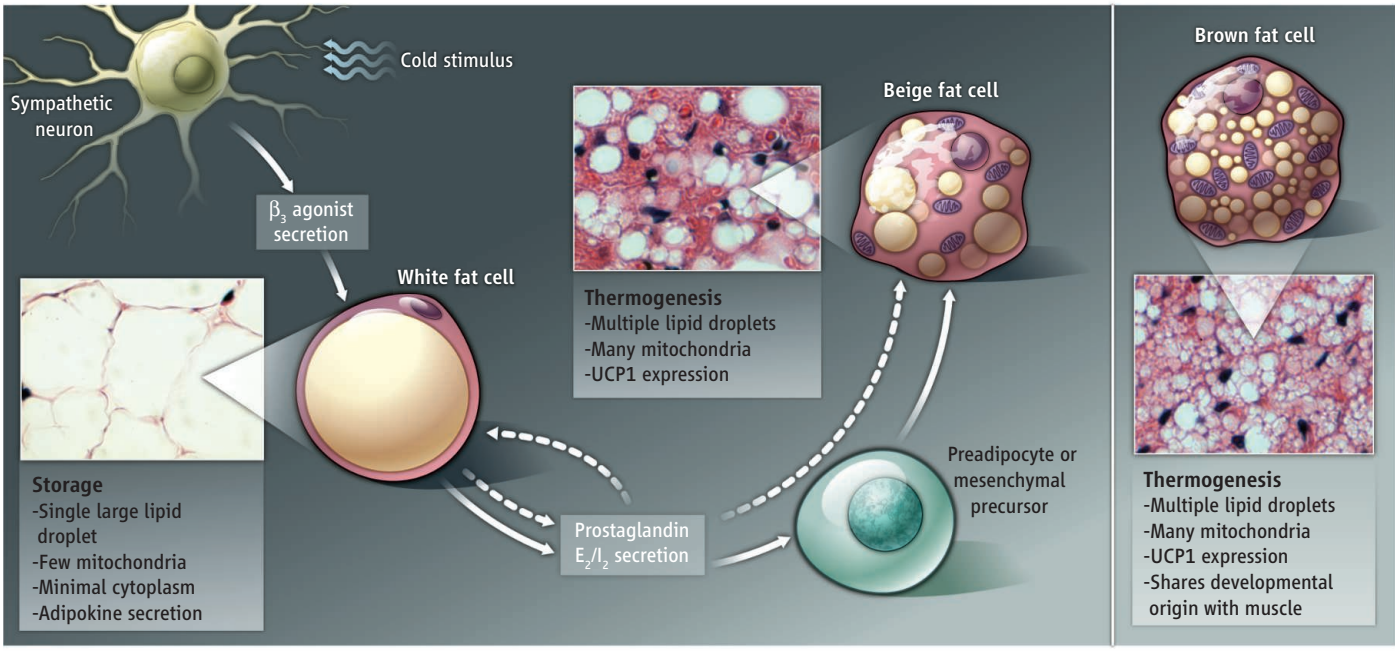

White to beige. Fat cells can be classified as white storage cells, brown thermogenic cells, or intermediate beige cells. Prostaglandins produced by white fat cells (in response to β_3-awdrenergic agonists released by sympathetic neurons) or from the circulation stimulate the formation of thermogenic beige cells in white fat. It is not clear if beige cells are derived from a precursor cell, arise by transdifferentiation of white fat cells, or by both mechanisms. UCP1, uncoupling protein 1.

COX-2 in the skin, a systemic increase of two prostaglandins (PGE_2 and PGI_2) caused white fat pads to become beige. By contrast, brown fat depots were unresponsive to increased prostaglandin synthesis. Whether housed in cool or warm conditions, the transgenic animals ate more than their wild-type counterparts and remained lean, even when fed a high-fat diet. The lean phenotype was due to elevated energy expenditure and increased body temperature, similar to findings in rats given PGE_2 (*9*). Although many factors suppress beige fat development, prostaglandin is the first positive acting signal that is both necessary and sufficient to promote thermogenesis selectively in the white fat compartment.

The relative roles of PGE_2 and PGI_2 in beige fat development remain to be determined. Genetic deletion of the PGI_2 receptor reduces the expression of brown fat–specific genes in subcutaneous but not in visceral fat. The "browning" effect of β_3-adrenergic agonists is most prominent in subcutaneous fat. Thus, differential activity of the PGI_2 receptor may underlie fat depot–selective metabolic effects of β_3-adrenergic agonists.

Prostaglandins have a broad array of functions in numerous tissues, with PGE_2 acting through four different receptors (EP1-4), and PGI_2 acting through the prostacyclin (IP) receptor (*10*). The complexities of prostaglandin-receptor signaling make therapeutic side effects a concern. For example, prostaglandins powerfully induce the inflammatory response through various combinations of ligand-receptor interactions (*11*). However, Vegiopoulos *et al*. did not observe increased systemic inflammation in the transgenic mice that overexpress COX-2. Regardless, unraveling the molecular mechanism of prostaglandin action in white fat may reveal more selective methods to promote beige fat development and avoid undesirable and unpredictable side effects. Conceivably, systemic delivery of a highly specific prostaglandin or a synthetic analog could treat obesity

Prostaglandins appear to act directly on fat cells, because treatment of isolated white fat precursors with PGI_2 stimulated the expression of brown fat-related genes. PGI_2 treatment also amplified this effect in response to norepinephrine. Thus, prostaglandins likely potentiate the response of fat cells to sympathetic nerve activity in tissues. Consistent with this, inhibition of COX-2 suppressed the emergence of beige fat in white fat depots of cold-exposed or β_3-adrenergic agonist–treated mice. The intracellular signaling pathways stimulated by norepinephrine involve adenylate cyclase and production of adenosine 3′,5′-monophosphate (cyclic AMP). Prostaglandin receptors also converge on adenylate cyclase (*12*) and thus may promote the production of beige fat by further activating a common signaling cascade.

The question of where beige cells come from remains unanswered. The study by Vegiopoulos *et al*. suggests that progenitor cells are pushed to develop into beige fat by prostaglandins. Alternatively (or additionally), white fat cells could directly convert into beige cells. Regardless of how they arise, the development of beige adipocytes in white fat correlates extremely well with protection against obesity and associated disease.

Nonsurgical therapies for obesity are desperately needed. Healthy diet and exercise are accessible and affordable treatments, with broad health benefits beyond weight reduction. However, behavioral modifications are often insufficient. Stimulating white to beige fat conversion through prostaglandin signaling can hopefully be translated into an effective standalone or adjunct therapy to raise energy expenditure and promote weight loss.

References and Notes

1. A. Vegiopoulos *et al*., *Science* **328**, 1158 (2010); published online 6 May 2010 (10.1126/science.1186034).
2. W. D. van Marken Lichtenbelt *et al*., *N. Engl. J. Med.* **360**, 1500 (2009).
3. K. A. Virtanen *et al*., *N. Engl. J. Med.* **360**, 1518 (2009).
4. A. M. Cypess *et al*., *N. Engl. J. Med.* **360**, 1509 (2009).
5. M. Saito *et al*., *Diabetes* **58**, 1526 (2009).
6. P. Seale *et al*., *Genes Dev.* **23**, 788 (2009).
7. P. Seale *et al*., *Nature* **454**, 961 (2008).
8. J. R. Arch, *Eur. J. Pharmacol.* **440**, 99 (2002).
9. N. C. Long *et al*., *J. Physiol.* **444**, 363 (1991).
10. Y. Sugimoto, S. Narumiya, *J. Biol. Chem.* **282**, 11613 (2007).
11. S. L. Tilley *et al*., *J. Clin. Invest.* **108**, 15 (2001).
12. R. Reimer, H. K. Heim, K. F. Sewing, R. Muallem, H. S. Odes, *Prostaglandins* **44**, 485 (1992).
13. Our work on this topic is supported by NIH grant DK081605 (to P.S.) and by the Institute for Diabetes and Metabolism at the University of Pennsylvania School of Medicine.

Published online 6 May 2010;
Include this information when citing this paper.

10.1126/science.1190816

CHEMISTRY

Harmony of the Self-Assembled Spheres

Slight changes in the shape of organic molecules can dramatically alter the size of hollow spheres that form spontaneously upon addition of palladium ions.

Artur R. Stefankiewicz and Jeremy K. M. Sanders

Chemists conventionally assemble molecules stepwise in the laboratory, but nature often relies on self-assembly, especially when it comes to combining smaller subunits into amazingly complex architectures on the nanoscale. Tobacco mosaic virus is an inspiring example of self-assembly: 2130 identical protein subunits self-organize around a single strand of RNA to form the final helical structure of the virus (*1*). Weak but numerous noncovalent interactions direct assembly between individual subunits. These processes can be dynamic; in such cases, assembly is accompanied by disassembly and occurs at or near equilibrium. In general, these processes are not only rapid but are intrinsically self-correcting (*2*). On page 1144 of this issue, Sun *et al*. (*3*) report a step forward toward synthetic analogs of large-scale self-assembly in which metal ions and organic ligands self-assemble into giant coordination spheres with intriguing thermodynamic behavior and astonishing precision.

The structural complexity characteristic of biology has until recently been considered irrelevant in coordination chemistry, in which metal centers form bonds to both organic and inorganic ligands, or even to other metals. In most coordination compounds, only a few metal centers might be joined by bridging organic ligands. However, Lehn and Stoddart separately suggested more than a decade ago that coordination bonds, which can also assemble reversibly, could be viewed in the same light as the weak inter- or intramolecular interactions formed during biological self-assembly (*4*, *5*).

Metal-assisted self-assembly has recently given access to a wide range of supramolecular entities of truly impressive architectural complexity (*6*). The final shape of the self-assembled entity is defined not only through the metal coordination geometry, but also through the size and shape of the ligand, which can determine the orientation of its interaction sites with the metal ions. Because the generation of well-defined metallosupramolecular architecture generally proceeds under thermodynamic equilibrium, it allows the desired product to be obtained with an accuracy similar to that achieved in conventional stepwise molecular synthesis. The dynamic nature of the assembly process also allows modification through the exchange of components added into solution at a later point (*7*).

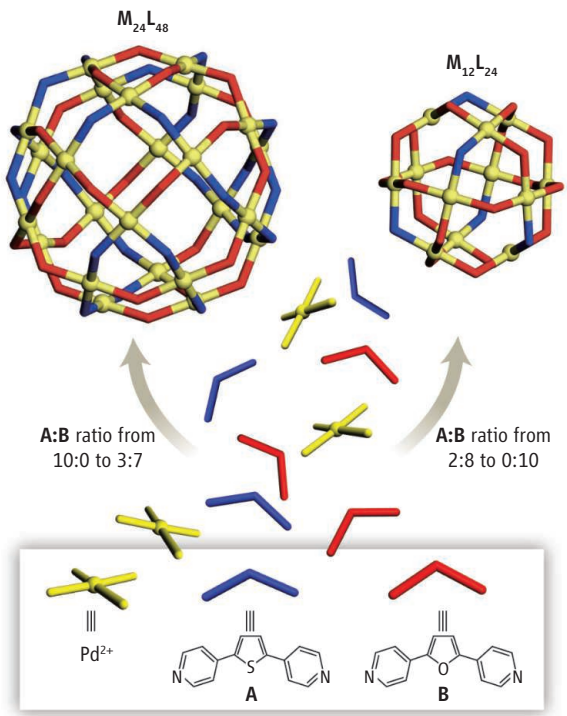

Spheres are subtly influenced. Sun *et al*. have shown that slight changes in ligand shape (molecules **A** and **B** differ in bend angle) change the outcome of self-assembly with Pd ions dramatically. Only one type of sphere forms even when a mixture of ligands is used, and the size of sphere formed exhibits a threshold at a particular ratio of ligand concentrations. Such crossover behavior is an example of self-organized criticality.

This principle has been realized by recently developed syntheses beyond assembly around a few metal centers (*8*, *9*). In particular, coordination chemistry has been successfully used to construct such discrete structures as helices, grids, cages, and spheres, the last being particularly interesting because of their potential application as synthetic receptors and nanoreactors. Fujita and co-workers had already shown that simple banana-shaped organic molecules and palladium(II) ions self-organize into finite, spherical coordination networks with diameters of up to 5 nm (*10*). These impressive superstructures consist of 36 components (12 equivalent metal centers and 24 equivalent ligands) that self-organize into a well-defined object of cuboctahedral symmetry (ligand **B** in the figure, leading to $M_{12}L_{24}$).

It is synthetically easy to introduce a variety of new substituents and form multifunctional nanoscale architectures with specific physicochemical properties. Porphyrins and C_{60} have been attached to the outside of the spheres to generate a highly decorated surface. Alternatively, perfluoroalkyl groups were attached and a spherical complex formed with an interior filled with 24 perfluoroalkyl chains. The interior of the sphere can be regarded as a fluorous phase (one that can selectively dissolve fluorocarbons) while the surrounding solution cannot. Even more remarkably, photoisomerization of a chromophore functionality attached to the internal site of the ligand components gives access to a variety of photoresponsive "molecular nanoparticles" whose interior environments can be dramatically changed by light (*11*).

Sun *et al*. now describe an elegant and synthetically simple strategy for creating a massive spherical framework of 72 components that spontaneously self-assemble in solution. Building on their earlier experience, they obtained this new molecule by opening up the bend angle from 127° to 149° between the two metal-binding sites of the ligand to give **A**. Separately, these ligands, when combined with palladium ions, form spheres consisting of 72 and 36 components for **A** and **B**, respectively (see the figure). The authors then mixed the two ligands **A** and **B** in different ratios. At every ligand ratio from 9:1 to 1:9, there was no indication of forming a mix of different compounds. Only pure complexes of either $M_{12}L_{24}$ or $M_{24}L_{48}$ were

University Chemical Laboratory, Lensfield Road, Cambridge CB2 1EW, UK. E-mail: jkms@cam.ac.uk; as2044@cam.ac.uk

Published by AAAS

observed. $M_{24}L_{48}$ was exclusively assembled until the ratio of **A**:**B** was 2:8, whereupon the outcome was $M_{12}L_{24}$.

This result is surprising. Even if the sphere constructed from **A** is enthalpically favored in $M_{24}L_{48}$ (that is, it has lower internal energy than structures made from **B**), the entropic cost of creating such a large ordered object might be expected to be prohibitive. Perhaps the stability of the bigger nanosphere results from its relatively huge internal volume. The solvent and counterions might be less ordered and more liquid-like than in the smaller sphere, thus shifting the equilibrium toward the bigger structure.

Whatever the explanation at the molecular or thermodynamic level, we are observing emergent behavior in this chemical system, in which small differences in geometry are effectively amplified into the production of the preferred sphere. The work of Sun *et al*. is an impressive demonstration of artificial multicomponent self-assembly similar to that observed in the assembly of biological structures. The success of this approach suggests that supramolecular nanoreactors with high stability could be made through relatively simple synthetic routes.

References

1. A. Klug, *Angew. Chem. Int. Ed. Engl.* **22**, 565 (1983).
2. J.-M. Lehn, *Science* **295**, 2400 (2002).
3. Q.-F. Sun *et al*., *Science* **328**, 1158 (2010); published online 29 April 2010 (10.1126/science.1188605).
4. B. Hasenknopf *et al*., *J. Am. Chem. Soc.* **119**, 10956 (1997).
5. M. C. T. Fyfe, J. F. Stoddart, *Acc. Chem. Res.* **30**, 393 (1997).
6. G. F. Swiegers, T. J. Malefetse, *Chem. Rev.* **100**, 3483 (2000).
7. E. Stulz *et al*., *Chemistry* **9**, 6039 (2003).
8. D. N. Reinhoudt, M. Crego-Calama, *Science* **295**, 2403 (2002).
9. G. Alcaraz *et al*., *Acc. Chem. Res.* **42**, 1640 (2009).
10. M. Tominaga *et al*., *Angew. Chem. Int. Ed.* **43**, 5621 (2004).
11. T. Murase *et al*., *Angew. Chem. Int. Ed.* **46**, 5133 (2007).

10.1126/science.1190821

IMMUNOLOGY

The Origin of T_H2 Responses

The adaptive immune response to helminth infection and allergens is stimulated by cytokines secreted by innate immune cells.

Robert L. Coffman

Helper T lymphocytes (T_H cells) have multiple functions during human immune responses, including stimulating B cells, the "help" needed to spur antibody production. Naïve T_H precursor cells give rise to four functionally distinct subsets that can be further divided into subtypes or regulated states. Once the first two T_H subsets were recognized—T_H1 and T_H2 cells (*1*)—the obvious question became: How does the immune system decide which response to make? Recent reports present an important advance in understanding the origins of T_H2 responses and mechanisms of immune recognition of two medically important classes of antigens: helminth parasites and allergens.

T_H1 cells produce proinflammatory cytokines, such as interferon-γ (IFN-γ), that trigger responses against intracellular pathogens. By contrast, T_H2 cells make cytokines such as interleukin (IL)–4, IL-5, and IL-13, which activate responses to allergens and parasitic helminths, such as increased eosinophil and mast cell production and immunoglobulin E (IgE) antibody responses (*2*). The essential features of T_H1 cell induction—including the key roles of IFN-γ, IFN-α, and IL-12—have long been understood (*3*). However, our understanding of T_H2 cell origins has been elusive. IL-4 itself turns out to be a key factor for the development of IL-4–producing T_H2 cells. Candidate sources of this initial IL-4 have been identified, but their link to recognition of allergens or helminths by the innate immune system (the less specific and more immediate arm of defense against infection) has been difficult to establish. Furthermore, it was gradually realized that T_H2 cell responses to some helminths did not require IL-4. Three cytokines—IL-25, IL-33, and thymic stromal lymphopoietin—have emerged as candidates for the link between the innate immune system's recognition of the pathogen and T_H2 cell action, the ultimate, adaptive immune system response (*4*).

IL-25 was identified a decade ago as the "odd" member of the IL-17 cytokine family. Although it stimulates many of the hallmark

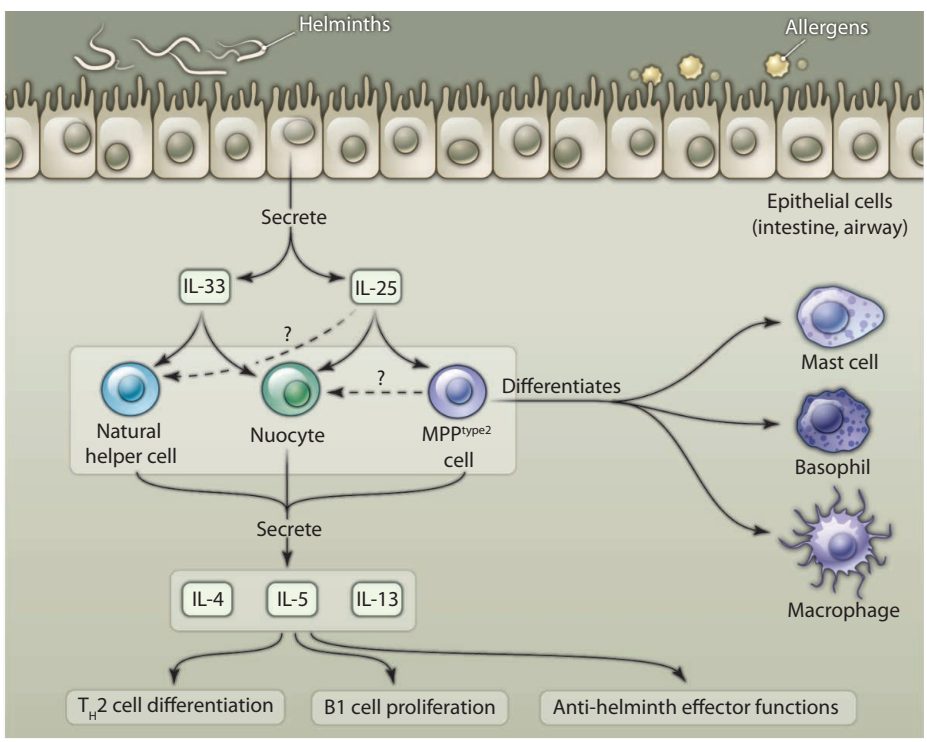

Path to T_H2 responses. Parasitic helminths or allergens induce epithelial cells to produce cytokines that stimulate three populations of cells to produce other cytokines. This cytokine combination promotes differentiation of T_H2 and B1 cells and stimulates effector functions, leading to parasite expulsion. MPP^{type2} cells can give rise to multiple cell types, including basophils, which can bias toward T_H2 differentiation. It is not clear whether natural helper, nuocyte, and MPP^{type2} cells are different, or the same cell type viewed differently.

CREDIT: Y. GREENMAN/*SCIENCE*

Dynavax Technologies Corporation, 2929 Seventh Street, Suite 100, Berkeley, CA 94710, USA. E-mail: RCoffman@dynavax.com

Published by AAAS

features of the immune response mediated by T_H2 cells—rapid and substantial production of IL-4, IL-5, IL-13, eosinophils, and IgE—it does so even in the absence of T cells (*5*). IL-33 is a member of a very different cytokine (IL-1) family, yet evokes T_H2-like immune responses similar to those of IL-25 (*6*). The importance of IL-25 for T_H2 responses has been demonstrated, but the identity of the cell making the large, rapid T_H2-like response to either IL-25 or IL-33 has remained a mystery—defined more by what it is not than by what it is. Three reports (*7*–*9*) provide the clearest view yet of this cell (or cells), though from different perspectives.

Saenz *et al*. show that injection of IL-25 into mice leads to the expansion of cells that produce IL-4 in gut-associated lymphoid tissue (*7*). These cells express the cell surface proteins Sca-1 and cKit, a phenotype that suggests a relationship to hematopoietic stem cells or multipotential precursors (MPPs). Likewise, Neill *et al*. report that injection of mice with either IL-25 or IL-33 generates an expansion of cells with a similar cell surface phenotype that produce IL-13 in the gut-associated lymphoid tissue, mesenteric lymph nodes, and spleen (*8*). And Moro *et al*. identified an IL-33–responsive cell type with a lymphoid morphology and similar cell surface protein expression in fat-associated lymphoid clusters in the mesenteric tissue of mice (*9*). By comparing cell surface markers and gene expression profiles, as well as their presence in mice deficient in known cell types, the three studies make a convincing case that the cells represent one or more previously undefined cell types (see the figure). These IL-25 and/or IL-33–responsive cells proliferate and produce large amounts of IL-5 and IL-13 (with lesser amounts of IL-4) in response to helminth parasite infection as well. This response to helminths is blocked by an antibody to IL-25, impaired in mice lacking the IL-25 or IL-33 receptor, and largely absent in mice lacking both cytokine receptors. Moreover, this "T_H2-like" response does not require T cells at all—it is unimpaired in mice devoid of T and B cells.

There is less agreement on what the IL-25 and IL-33–responsive cells do, with each group bestowing a name that reflects a different view of their function. The IL-25–responsive cells of Saenz *et al*. are actually heterogeneous (*7*). Cells expressing cKit that produce IL-4 differentiate into mast cells, whereas cells expressing cKit but not IL-4 develop into basophils and macrophages. In addition, this heterogeneous cell population promotes the development of T_H2 cells from naïve T cells, suggesting the name multipotent progenitor type 2 (MPP^{type2}) cells. Moro *et al*. also view their cells as important regulatory cells promoting T_H2 responses and the proliferation and activation of B1 cells (a B cell subset in the gut-associated lymphoid tissue), and thus have named them natural helper cells (*9*). Neill *et al*. have called the IL-25 and IL-33–inducible, IL-13–expressing cells "nuocytes," nu being the 13th letter of the Greek alphabet. The authors show that nuocytes can serve as the sole source of IL-13 necessary for the expulsion of intestinal helminths, demonstrating a direct role as effector cells (*8*). Their prominence in the gut-associated lymphoid tissue suggests a central role in responding to intestinal pathogens. Yet they do not respond directly to parasites; rather, they are intermediates, responding to IL-25 and/or IL-33 produced by epithelial and possibly other nonhematopoietic cell types (*10*).

Despite striking similarities, it is not clear whether MPP^{type2} cells, natural helper cells, and nuocytes represent the same discrete cell type or several—probably related—cell types. Some of the apparent differences may be explained by different techniques, but some may be more telling. T1/ST2, a polypeptide chain of the IL-33 receptor, is expressed by natural helper cells and nuocytes but not by MPP^{type2} cells, the latter of which, unlike the others, is not induced by IL-33. It is possible that MPP^{type2} cells are actually progenitors of natural helper cells and nuocytes.

References

1. T. R. Mosmann, R. L. Coffman, *Annu. Rev. Immunol.* **7**, 145 (1989).
2. R. M. Locksley, *Cell* **140**, 777 (2010).
3. A. K. Abbas *et al*., *Nature* **383**, 787 (1996).
4. W. E. Paul, J. Zhu, *Nat. Rev. Immunol.* **10**, 225 (2010).
5. S. D. Hurst *et al*., *J. Immunol.* **169**, 443 (2002).
6. J. Schmitz *et al*., *Immunity* **23**, 479 (2005).
7. S. A. Saenz *et al*., *Nature* **464**, 1362 (2010).
8. D. R. Neill *et al*., *Nature* **464**, 1367 (2010).
9. K. Moro *et al*., *Nature* **463**, 540 (2010).
10. S. A. Saenz *et al*., *Immunol. Rev.* **226**, 172 (2008).

10.1126/science.1192009

PALEOCLIMATE

Uncorking the Southern Ocean's Vintage CO_2

New radiocarbon evidence suggests that the Southern Ocean released CO_2 into the atmosphere at the end of the last ice age. Two scenarios could explain how and why.

Robert F. Anderson[1] and Mary-Elena Carr[2]

Antarctic ice cores provide a well-documented link between Earth's climate and the CO_2 content of the atmosphere over the past 800,000 years (*1*). Many hypotheses to explain this relationship envision releases of CO_2 to the atmosphere from the deep waters of the Southern Ocean around Antarctica (*2*), but there has been limited evidence. On page 1147 of this issue, Skinner *et al*. (*3*) use the radiocarbon (^{14}C) content in the shells of surface- and bottom-dwelling organisms (foraminifera) recovered from the Southern Ocean to track how CO_2 moved from the deep sea to the atmosphere during the warming transition out of the last ice age (deglaciation). First, bottom-dwelling foraminifera record the buildup of ^{14}C-depleted CO_2 in the deep ocean during the last glacial period, more than 21,000 years ago. Second, the shells of surface dwellers record the transfer of ^{14}C-depleted CO_2 to the surface between ~17,000 and 21,000 years ago.

CO_2 records from ice cores (*4*) and ^{14}C records from marine archives (*5*) reveal that the ^{14}C content of atmospheric CO_2 ($\Delta^{14}C_{atm}$) declined as CO_2 rose during the last deglaciation (*3*). This relationship supports hypotheses that attribute the rise in CO_2 to the release of ^{14}C-depleted CO_2 from a reservoir long isolated from the atmosphere.

The deep ocean (below ~2000 m) is thought to provide such a reservoir. Respiratory CO_2 can build up in the deep sea during glacial periods, when masses of relatively cold, dense water are trapped deep in the ocean and there is reduced exchange with surface waters. Because ^{14}C is produced by cosmic rays in the atmosphere, CO_2 isolated in deep waters loses its ^{14}C content through radioactive decay. During deglaciation, increased exchange with surface waters then raises the CO_2 content of the

[1]Lamont-Doherty Earth Observatory of Columbia University, Palisades, NY 10964, USA. [2]Columbia Climate Center, Columbia University, New York, NY 10025, USA. E-mail: boba@ldeo.columbia.edu

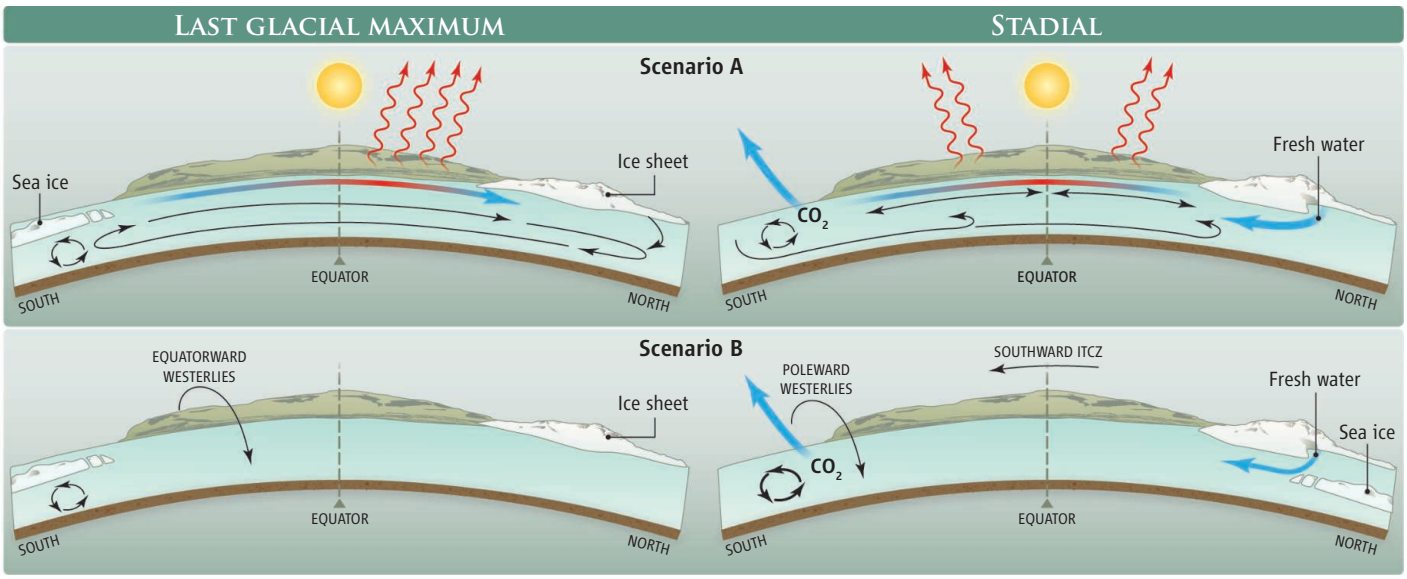

Currents and winds. Two scenarios that could account for the rise in atmospheric CO_2 at the end of the last ice age. Changes in the ocean play the more important role in Scenario A (**top**), while the atmosphere is more important in Scenario B (**bottom**). Each panel presents a section of the Atlantic Ocean viewed from the east. Scenario A, left panel: Expanding sea ice around Antarctica during glacial periods lowers the transfer of momentum from winds to the ocean, reducing exchange between deep and surface waters (*3*), and perhaps acting as a physical barrier to the release of CO_2 from upwelled deep water (*14*). Formation of (NADW) transports heat northward in the Atlantic Ocean. During stadials (right panel), injection of fresh water (FW) from northern ice sheets reduces the formation of NADW and allows more heat to remain in the Southern Hemisphere, melting back sea ice and allowing more efficient ventilation of CO_2 from deep water. Scenario B, left panel: An equatorward position of the Southern Westerlies (relative to today) (*15*) allows sea ice to expand over the Southern Ocean while reducing the wind-driven ventilation of deep water. During stadials (right panel), expanding winter sea ice in the North Atlantic following FW influx and reduced NADW formation induces a global reorganization of atmospheric circulation, including a southward displacement (or intensification) of the Southern Westerlies. Reorganization of the winds increases the exchange between surface and deep waters, releasing CO_2 into the atmosphere.

atmosphere while lowering $\Delta^{14}C_{atm}$ by dilution with deepwater CO_2 (*6*).

The ^{14}C contents of contemporary surface- and deep-dwelling marine organisms do not always support this hypothesis. Although studies in the Atlantic Ocean consistently show that the difference between ^{14}C levels for deep water and the atmosphere was much greater during the last glacial period than it is currently (*7*, *8*), results from the Pacific Ocean are equivocal (*9*, *10*). In particular, Broecker *et al*. (*10*) found no significant difference between the Last Glacial Maximum and today when comparing the ^{14}C of foraminifera from the surface and those from a depth of 2.8 km in the western equatorial Pacific. Broecker *et al.*'s results present a serious challenge to any hypothesis that invokes storage of ^{14}C-depleted CO_2 in the deep ocean during the last glacial period because nearly 70% of the ocean lies above a depth of 2.8 km. If not in the deep Pacific, then where? The new ^{14}C results from Skinner *et al*. (*3*) suggest that a ^{14}C-depleted reservoir in the deep Southern Ocean may account for at least half the observed drop in $\Delta^{14}C_{atm}$ during deglaciation.

Increased exchange between the Southern Ocean's surface and deep waters during deglaciation accounts for the "where" and "when" of the processes responsible for the rise in atmospheric CO_2, but key questions concerning "how" and "why" remain. Two different (but not mutually exclusive) scenarios leading to a deglacial CO_2 rise are illustrated in the figure. One ascribes a leading role to changes in the ocean (Scenario A). Skinner *et al*. invoke a change in ocean circulation during deglaciation known as the bipolar seesaw (*11*, *12*). During cold intervals known as stadials [e.g., Heinrich Stadial 1 and the Younger Dryas Stadial (*3*)], the introduction of fresh water to the North Atlantic Ocean reduces the northward heat transport associated with North Atlantic Deep Water (NADW) formation. Heat retained in the Southern Hemisphere melts back sea ice, allowing the winds to drive more effectively the exchange between surface and deep waters in the Southern Ocean and to enhance the release of CO_2 to the atmosphere.

An alternative scenario (B), while retaining basic features of the bipolar seesaw, ascribes a greater role to atmospheric processes. During stadials, the expansion of winter sea ice on the North Atlantic Ocean forces a reorganization of atmospheric circulation. Stadial conditions, known to induce a southward shift in the Intertropical Convergence Zone (ITCZ) (*13*), are thought to strengthen the Southern Westerlies and/or displace them southward (*6*). This change in the winds enhances the exchange between surface and deep water in the Southern Ocean and the corresponding release of CO_2.

Each scenario is triggered by an injection of fresh water into the North Atlantic. The processes that transmit the signal from north to south, however, differ fundamentally. Since these processes are inherent in Earth's climate variability, sorting out the relative roles for oceanic and atmospheric changes is critical. Research on the reorganization of atmospheric circulation during periods of abrupt climate change should be carried out in tandem with studies of NADW formation.

References

1. D. Lüthi *et al*., *Nature* **453**, 379 (2008).
2. D. M. Sigman, E. A. Boyle, *Nature* **407**, 859 (2000).
3. L. C. Skinner *et al*., *Science* **328**, 1147 (2010).
4. E. Monnin *et al*., *Science* **291**, 112 (2001).
5. K. Hughen *et al*., *Quat. Sci. Rev.* **25**, 3216 (2006).
6. R. F. Anderson *et al*., *Science* **323**, 1443 (2009).
7. L. F. Robinson *et al*., *Science* **310**, 1469 (2005).
8. L. C. Skinner, N. J. Shackleton, *Paleoceanography* **19**, PA2005, 10.1029/2003PA000983 (2004).
9. E. D. Galbraith *et al*., *Nature* **449**, 890 (2007).
10. W. Broecker *et al*., *Earth Planet. Sci. Lett.* **274**, 322 (2008).
11. W. S. Broecker, *Paleoceanography* **13**, 119 (1998).
12. T. F. Stocker, S. J. Johnsen, *Paleoceanography* **18**, 1087 (2003).
13. J. C. H. Chiang, *Annu. Rev. Earth Planet. Sci.* **37**, 263 (2009).
14. B. B. Stephens, R. F. Keeling, *Nature* **404**, 171 (2000).
15. J. R. Toggweiler, J. Russell, *Nature* **451**, 286 (2008).

10.1126/science.1190765

Published by AAAS

SCIENCE POLICY

On Capitol Hill, Researchers Offer Data to Answer Climate Skeptics

When a panel of influential scientists visited Capitol Hill this month to talk about climate change, they offered none of the barbed words or emotional confrontation that have been the lingua franca of recent political discourse.

Instead, at a briefing organized by AAAS, they answered climate change skeptics as they've been trained to do: with extensive data, and with a reminder that the scientific process, though imperfect, remains the best available tool for understanding the complex workings of the natural world.

"Skepticism is an integral part of the progress of science, and it helps keep the science on the correct path," said veteran climate researcher Warren Washington, former chairman of the U.S. National Science Board. "However, skepticism without specifics, alternate hypotheses, and facts is worthless. It does not advance the science."

But Washington and others acknowledged that the reputation of climate scientists has been tarnished by the perception that they are hostile to those who reject the scientific consensus. The panelists urged their colleagues to listen carefully to skeptics and to publish their research when it meets scientific standards.

The 11 May briefing attracted more than 100 staffers from congressional offices and foreign embassies, along with representatives of the U.S. State Department, the Congressional Budget Office, research universities, and nongovernmental organizations. It was sponsored by 13 mainstream American science organizations representing fields ranging from chemistry and meteorology to statistics and agriculture.

AAAS's Center for Science, Technology, and Congress was the lead organizer, with U.S. Senator Mark Udall (D–CO) serving as honorary host.

The briefing was the science community's latest effort to answer sustained attacks based on a handful of errors discovered in the massive 4th Assessment Report of the Intergovernmental Panel on Climate Change and by e-mails apparently hacked from the Climate Research Unit at the University of East Anglia in the U.K. It came just a day before U.S. Senators Joseph Lieberman (I–CT) and John Kerry (D–MA) introduced a broad energy and climate bill.

Such context made the event "tremendously important," said moderator Alan I. Leshner, chief executive officer of AAAS. "We all have come to believe that the issue of climate change and what we do about it—particularly as it relates to the issue of energy—is among the most pressing and important issues facing not only American society, but global society as well."

In addition to Leshner, who also serves as executive publisher of *Science*, and Washington, who formerly headed the Climate Change Research Section at the National Center for Atmospheric Research, the panel included two extensively published climate researchers: Richard Alley, the Evan Pugh Professor of Geosciences at Pennsylvania State University, and Richard Smith, the Mark L. Reed III Distinguished Professor in the departments of statistics and biostatistics at the University of North Carolina at Chapel Hill.

The 90-min session served as a short course on what is known, and not known, about the changing climate.

Washington listed arguments commonly offered by skeptics—there is no global warming, or humans are not causing it, or temperature records are inaccurate. Smith and Alley deconstructed those arguments, concluding that they are largely in error.

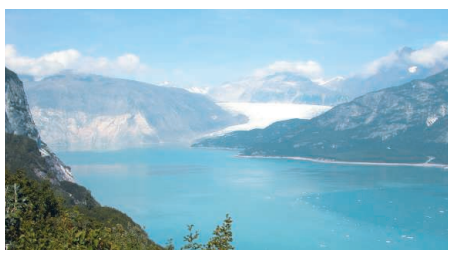

The impact of warming. Muir and Riggs glaciers in southeastern Alaska receded dramatically from 1941 (**top**) to 2004 (**bottom**).

Warming, Alley said, is a matter of basic physics: Increase the concentration of carbon dioxide, methane, and other greenhouse gases in the atmosphere, and the atmosphere will hold in more heat.

Analysis of the atmospheric gases shows that steadily rising CO_2 concentrations come not from volcanoes, he said, but from the burning of organic matter, especially fossil fuels. Thousands of scientists at research centers in many countries have taken thermometer readings on land, at sea, in the atmosphere, and by satellite, and others have documented shrinking glaciers. The inescapable conclusion: The world is getting warmer.

"A lot of what of what they [skeptics] say, at first sight it might appear that they're making reasonable points," Smith said. And yet, he added, "a lot of what they say doesn't stand up to scrutiny."

Said Alley: "The whole climate community has spent 30 years trying to find a way out of this. Could the Sun be doing it? Could the volcanoes be doing it?... [But] we can't explain what has happened recently without us—it has our fingerprints."

Even so, the panelists agreed, data alone won't build support for climate science.

"We have to continue to improve our methods and the accuracy of scientific information that's given to policy-makers," Washington said. "Skeptics must be encouraged and allowed to publish their research results in the scientific literature if the science is sound … because that would be better for science."

COMMUNICATION

Screeners Needed for Journalism Awards

Volunteer scientists are needed to review entries in the prestigious AAAS Kavli Science Journalism Awards program. Scientists residing in the Washington, D.C., area, or who will be in the area in mid-August to mid-September, are invited to help screen print, online, radio, and television reports for scientific accuracy. If interested, please contact Angela Bradley (202-326-6408; abradley@aaas.org) in the AAAS Office of Public Programs.

CREDITS: U.S. GEOLOGICAL SURVEY. (TOP PANEL) W.O. FIELD; (BOTTOM PANEL) B.F. MOLNIA

Published by AAAS

INTERNATIONAL

AAAS Group Visits Myanmar for Talks on Health, Forestry, and Science

A six-member delegation led by Nobel laureate Peter Agre, chairman of the AAAS Board of Directors, made a rare visit to Myanmar for high-level discussions on forestry, health, and other science-related issues with science and academic leaders in Naypyitaw and Yangon.

Though few Americans have visited the country in recent years, AAAS officials described the talks as cordial and constructive. They were impressed by Myanmar's interest in protecting forests and animal habitats and cooperatively addressing malaria and other infectious diseases.

"Myanmar is making an effort to educate its young scientists, which is complicated by limited resources and equipment along with a lack of networks of peers, especially in the West," said Agre, who shared the 2003 Nobel Prize in chemistry. "This trip may be an important initial step towards connecting their scientific community with their American counterparts in a way that advances science."

Thet Win, a member of the U.S. delegation and founder of the U.S. Collection Humanitarian and Research Corps, said the visit sent an important message to the people of Myanmar.

"We are compelled by compassion to help those suffering from poverty, disease, and environmental and ecological destruction," he said. "Ultimately, only science and education can contribute to the solutions and remedies for these ills.… My impression is that Myanmar scientists and educators are interested in engagement with AAAS and welcome the fact that a well-known U.S. organization is looking for mutually beneficial ways to interact."

The delegation was in Myanmar, formerly known as Burma, from 6 to 10 April. Among those who welcomed the Americans were the forestry minister, Brigadier-General Thein Aung; Dr. Mya Oo, the deputy health minister; Ko Ko Oo, director-general of the Ministry of Science and Technology; Mya Mya Oo, rector of Yangon Technological University and of Mandalay Technological University; and the pro-rectors of Yangon University.

The AAAS delegation also included Norman P. Neureiter, a former science adviser to the U.S. secretary of state and currently senior adviser to the AAAS Center for Science Diplomacy; Robert J. Swap, a research associate professor in environmental sciences at the University of Virginia; Tom Wang, deputy director of the AAAS Center for Science Diplomacy; and center Director Vaughan Turekian, who also serves as AAAS chief international officer.

A hopeful visit. AAAS Board Chairman Peter Agre with young Buddhist nuns at the Shwedagon Pagoda in Yangon, Myanmar.

PHOTO BY VAUGHAN TUREKIAN

Most people in Myanmar live at the subsistence level, and conditions declined further after Cyclone Nargis killed more than 130,000 people and caused an estimated $10 billion in damage in May 2008.

Ties between Myanmar and the United States and much of the West have been profoundly strained since a popular uprising in 1988 and subsequent suppression of democracy movements. Recent visits by U.S. officials have signaled possible interest in renewed engagement.

Since their return, delegation members have briefed members of Congress and the U.S. State Department. They also were featured in a public forum at the Center for Strategic & International Studies.

SCIENCE & SECURITY

Researchers, Regulators Share Biosecurity Risks

Research institutions should take the lead in securing their labs against biological threats, but they would benefit from biosecurity guidelines coordinated across federal agencies, says a new report from AAAS.

More than 400 American laboratories work with biological agents that have the potential to cause serious harm in a bioterror attack or accidental dispersal, but the same laboratory materials are also used in valuable disease, agricultural, and energy research. Several bills pending in the U.S. Senate and House of Representatives would consolidate the list of dangerous pathogens, expand federal oversight of these labs, and establish new security standards for the agents that pose the greatest risk.

As Congress considers this wide-ranging legislation, the AAAS report urges better communication between scientists and security specialists to promote flexible security programs that will be effective as new risks evolve and new technologies emerge.

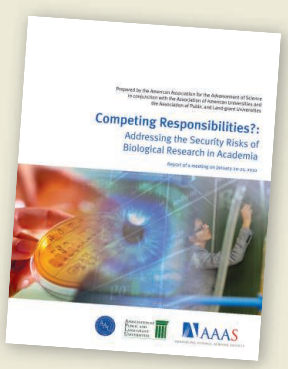

To achieve this goal, the report suggests that the federal government develop a common regulatory system for chemical, radiation, and biological agents. Academic institutions have limited administrative and financial resources with regard to regulation, it notes, and the current system of separate requirements often supports a "culture of compliance" rather than a culture of security.

At the same time, the report said, universities need to do a better job of explaining the role of their safety committees and institutional review boards to reassure regulators and the public that adequate programs are in place to address biosecurity issues.

The report, "Competing Responsibilities?: Addressing the Security Risks of Biological Research in Academia," summarizes a meeting sponsored earlier this year by AAAS, the Association of American Universities, and the Association of Public and Land-grant Universities. The 20 to 21 January event included university leaders, scientists, and representatives of the national security community.

The AAAS report is available at www.aaas.org/go/aaas_aau_2010/.

–Earl Lane and Becky Ham

Published by AAAS

Spatial and Temporal Variations of Groundwater Arsenic in South and Southeast Asia

Scott Fendorf,[1]* Holly A. Michael,[2]* Alexander van Geen[3]*

Over the past few decades, groundwater wells installed in rural areas throughout the major river basins draining the Himalayas have become the main source of drinking water for tens of millions of people. Groundwater in this region is much less likely to contain microbial pathogens than surface water but often contains hazardous amounts of arsenic—a known carcinogen. Arsenic enters groundwater naturally from rocks and sediment by coupled biogeochemical and hydrologic processes, some of which are presently affected by human activity. Mitigation of the resulting health crisis in South and Southeast Asia requires an understanding of the transport of arsenic and key reactants such as organic carbon that could trigger release in zones with presently low groundwater arsenic levels.

"The largest poisoning of a population in history" is how Smith *et al.* (*1*) described the health impact of elevated groundwater arsenic (As) concentrations in many parts of Bangladesh. Estimates of the rural population exposed to unsafe As levels by drinking untreated groundwater in India, China, Myanmar, Pakistan, Vietnam, Nepal, and Cambodia have grown to over 100 million (*2*). Widespread symptoms of disease in people drinking groundwater high in As in some of these countries and epidemiological studies conducted elsewhere lead to predictions of a doubling of the lifetime mortality risk caused by cancers of the liver, bladder, and lung (*3*, *4*). Groundwater containing As also causes cardiovascular disease and inhibits the mental development of children (*5*, *6*).

The affected areas of South and Southeast Asia are low-lying, topographically flat floodplains of rivers that drain the Himalayas (Fig. 1A) (*7*). Unconsolidated sands underlying these floodplains host increasing numbers of inexpensive wells made of polyvinyl chloride pipe with a cast-iron handpump mounted on top (tubewells) that are installed to avoid drinking surface water contaminated with microbial pathogens. Extensive, although by no means sufficient, testing of tubewell water for As has been carried out in most of the countries that are at risk, with Myanmar the glaring exception.

Within the arsenic-affected areas of South and Southeast Asia there is extensive variation in the depth distribution of wells (Fig. 1B). In Bangladesh and the bordering state of West Bengal, India, tubewells extend to depths of ~350 m compared to a maximum of ~100 m in Nepal, Cambodia, and Vietnam, owing to difference in the thickness of unconsolidated sand deposits (*8*). More than half the wells in at least one depth interval in each of the five affected countries do not meet the World Health Organization (WHO) guideline of 10 μg/liter As in drinking water (Fig. 1B). There are also numerous wells containing <10 μg/liter As at all depths. The extensive spatial variability of As concentrations at shallow depths (*9*–*11*), even within a single village, hinders comparisons among field sites and the recognition of presumably common biogeochemical-hydrological processes that regulate As levels in groundwater. The source of As is not a mystery, however; what is less clear is how the current distribution of dissolved As in the subsurface reached its current state. This review focuses on what has been learned from a decade of field research conducted in South and Southeast Asia about the processes that resulted in the current distribution of As in groundwater and the key factors that will control changes in the distribution of As over time.

CREDIT: SCOTT FENDORF

[1]Department of Earth System Sciences, Stanford University, Stanford, CA 94305, USA. [2]Department of Geological Sciences, University of Delaware, Newark, DE 19716, USA. [3]Lamont-Doherty Earth Observatory of Columbia University, Palisades, NY 10964, USA.

*To whom correspondence should be addressed. E-mail: fendorf@stanford.edu (S.F); hmichael@udel.edu (H.A.M.); avangeen@ldeo.columbia.edu (A.v.G.)

What Drives the Release of Arsenic to Groundwater?

Weathering of Himalayan-derived sediment during erosion and transport leads to downstream deposition of As. The primary sources of As within the Himalayas are thought to be eroding coal seams and rocks containing sulfide minerals (*12*). Exposed to the atmosphere, the minerals contained within these deposits are oxidized, and much of their As content is transferred to secondary phases including iron (Fe) hydroxides, oxyhydroxides, and oxides, collectively referred to as Fe oxides hereafter (*13*, *14*). There is indeed a positive relation between As and Fe extracted from hundreds of sediment samples from the Ganges-Brahmaputra-Meghna, Mekong, and Red River basins (Fig. 2) (*15*–*18*). Grain-size separation of river-borne and aquifer sediments has shown that the fine-grained, high–surface area fraction (<10 μm) contains five times as much As as bulk sediments or mica separates (*9*, *19*–*21*). Destabilizing As on these Fe oxides is now recognized as a key step in the widespread contamination of groundwater, with other phases possibly playing a subordinate role (*14*, *22*, *23*).

Arsenic is released from Fe oxides into groundwater as a result of two potentially concurrent processes under the anoxic conditions that prevail in the subsurface. First, field and laboratory evidence suggest that microbial reduction of Fe(III) oxides liberates As into the dissolved phase (*23*, *24*). Reduction of As(V) to more labile As(III) probably contributes to this release but is hard to distinguish from the reduction of Fe oxides under natural conditions given the rates of groundwater flow. Second, dissolution of Fe oxides is accompanied by the release of other ligands such as phosphate that compete with As for adsorption on the remaining Fe oxide surface sites (*9*).

The restriction of high dissolved As concentrations to aquifers composed of gray-colored sands, indicative of coatings of reduced or mixed-valence Fe(II+III) oxides, and the absence of elevated concentrations from aquifers containing orange sands coated with Fe(III) oxides (Box 1) suggest that Fe (III) reduction is a primary factor contributing to high As concentrations in groundwater (*9*, *24*–*28*). A systematic analysis of the composition of hundreds of groundwater samples from the Bengal, Mekong, and Red River basins has shown that high concentrations of As in groundwater prevail under advanced stages of reduction rather than the onset of Fe oxide reduction (*29*).

Microbial Fe(III) and As(V) reduction both require a supply of labile organic carbon. When the biological oxygen demand from the decom-

position of organic carbon exceeds the rate of oxygen infusion, anaerobic metabolism prevails and, following nitrate and manganese reduction, causes microbially mediated reduction of Fe(III) to Fe(II), as well as As(V) to As(III). Elevated groundwater As concentrations that broadly correspond with increased levels of metabolic by-products in groundwater including inorganic carbon, ammonium, and methane, in addition to dissolved Fe(II), are consistent with the central role of organic-matter metabolism (*18*, *19*, *28*–*30*).

Where Does Arsenic Release to Groundwater Occur?

There are three environmental requirements for groundwater As concentrations to increase: water saturation (which limits diffusion of atmospheric oxygen), a limited supply of sulfur, and a source of organic carbon to drive microbial dissolution of Fe oxides. The height of the water table, typically within 5 m of the surface, indicates where oxygen supply is limited and reductive dissolution can potentially be initiated (Fig. 3B). The domain within which As can be released to groundwater is restricted in some shallow (<20 m) aquifers where sulfate supplied by recharge has not been depleted. This is because sulfate reduction promoted by organic carbon produces sulfide that can bind As, forming sparingly soluble sulfides mineral that effectively remove As from groundwater (*13*, *29*). Marine-influenced areas also show inhibition of As release by sulfate reduction along the coasts of Bangladesh (*9*) and Vietnam (*31*).

The availability of labile organic carbon as a driver of microbial reduction is possibly the most prominent outstanding issue limiting our ability to predict the distribution of As in groundwater. Organic carbon necessary to drive reduction of Fe(III) and As(V) can be supplied through various pathways. One is co-deposition of plant material with sediments over geologic time, also referred to as an autochthonous source of carbon (*9*). Dissolved organic carbon (DOC), produced by recent degradation of plants in modern soils or in buried peat layers and transported to a different location by groundwater flow, could be an alternative allochtonous supply (*26*, *28*). The reactivity of organic matter needs to be considered as well (*32*, *33*), as indicated by dissolved inorganic carbon typically being younger than DOC (*14*, *28*) and by assays of microbial decomposition (*34*). The relative importance of different sources of organic carbon remains undetermined and even controversial (*32*–*34*).

In principle, where As is released from aquifer sediment and in what quantity will depend on the amount of reactive organic carbon and availability of As in the sediment. Sediment with recalcitrant organic carbon and/or As-bearing Fe oxides is expected to release As slowly. In contrast, highly reactive forms of both organic carbon and labile sediment-bound As should result in the strongest release. Field evidence from Nepal, West Bengal, Bangladesh, Cambodia, and Vietnam suggests both rapid, shallow release of As as well as more gradual release at depth (*9*, *17*, *18*, *25*, *28*, *35*, *36*). The available data show that the geological setting likely plays an important role, but there

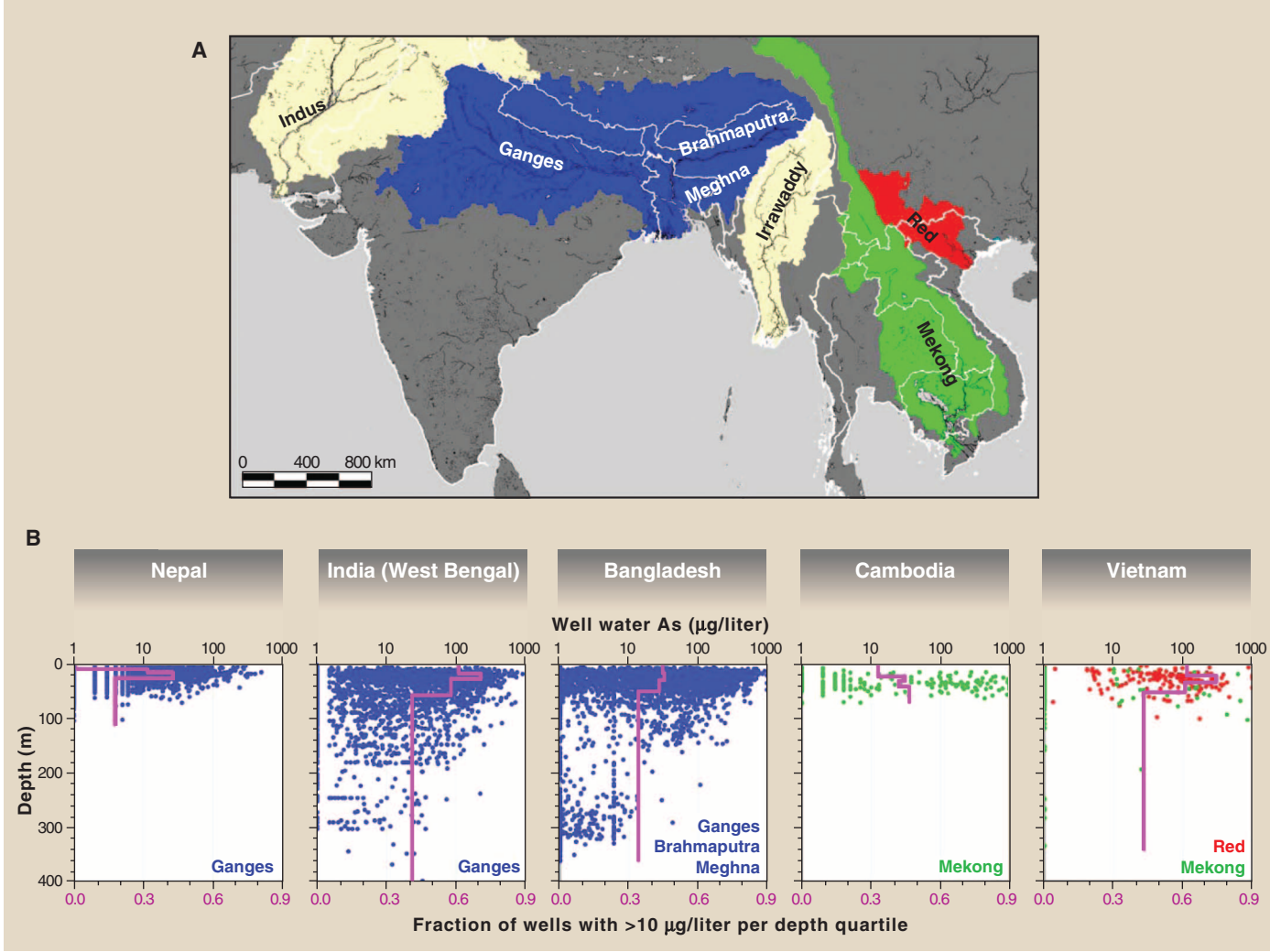

Fig. 1. Distribution of arsenic in groundwater of South and Southeast Asia. (**A**) Map of four major river basins draining the Himalayas. (**B**) Depth distribution of As in groundwater determined for five affected countries. Concentrations of As are shown on a logarithmic scale. Symbols are color-coded according to the major river basins shown in (A). The pink line depicts the fraction of wells that exceed the WHO As guideline of 10 µg/liter for each depth quartile of the available data (*54*).

remain notable uncertainties regarding rates of carbon metabolism coupled to As release.

The pool of labile As within an interval of an aquifer sediment is finite and can become depleted despite continued reduction of Fe oxides. Such a situation has been documented for deeper aquifers of Bangladesh where dissolved As levels are low despite elevated Fe(II) concentrations in groundwater (*16*). In other situations, the available pool of labile organic carbon has been depleted although some labile As is still bound to sediment particles. Sediments deposited prior to about 20,000 years ago and that were well drained because of incision during the last glacial sea-level low stand, for instance, contain limited reactive organic matter. The orange color of these oxidized deposits indicates that they were deposited with a low concentration of organic carbon or that their initial organic carbon was oxidized during the low stand (*9*, *15*, *16*, *25*, *26*).

After the initial biogeochemical transformations that result in As release from the sediment, adsorption on residual or newly formed aquifer solids will control dissolved As concentrations. Weaker surface complexes of As(III) and the degradation of Fe oxides (*9*) mean that adsorption is less pronounced than for As(V) in oxidized surface environments (*37*). Nevertheless, adsorption of As(III) does occur within reduced aquifers, as indicated by a fairly systematic relation between dissolved and adsorbed As across a broad range of conditions in Bangladesh (*38*). This implies that As transport is substantially retarded relative to groundwater flow, even if adsorption sites may be saturated in aquifer sands under certain conditions (*9*, *28*).

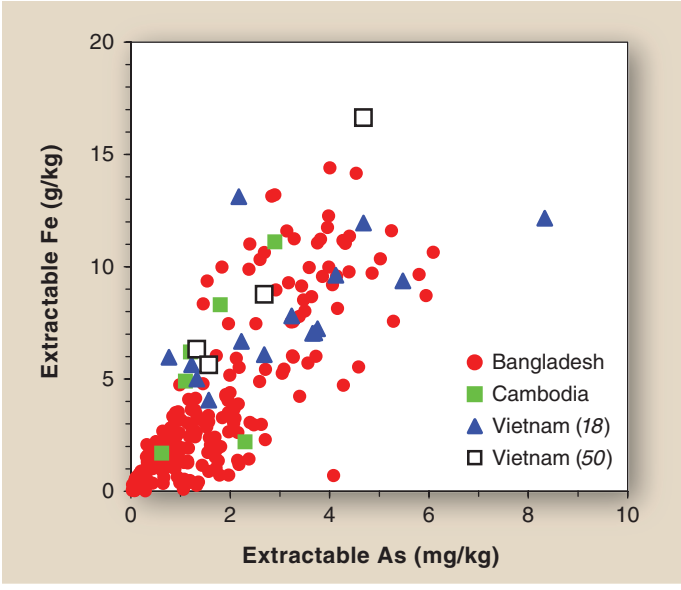

Fig. 2. Relation between As and Fe concentrations for a suite of sediment samples from three countries based on different extraction methods (*9*, *14*, *18*, *50*).

How Does Groundwater Flow Affect the Distribution of Arsenic?

Groundwater flow transports dissolved As as well as DOC, oxygen, sulfate, and competing adsorbates, all of which influence As concentrations. When the system is not in a steady state, either hydrologically or biogeochemically, As concentrations can be expected to change over time. Groundwater flow therefore plays a key role in the current distribution of groundwater As and its evolution.

The main river basins affected by As (Fig. 1A) share similar hydrogeologic features, most notably a monsoonal climate and rapid sediment accumulation. Groundwater flow systems range in scale from the local (tens of meters) to the regional (hundreds of kilometers). Studies of local-scale flow systems (*39*–*42*), which are most relevant to the distribution of As in shallow aquifers, illustrate the complex, site-specific, and transient nature of natural patterns of recharge and discharge (Fig. 3B). Further, abundant surface water bodies such as rivers, ponds, and wetlands interact with the groundwater systems. Monsoonal rains and dry-season irrigation pumping cause reversals in hydraulic gradients that can transform a water body from a source to a sink of groundwater and back over a year (*39*–*42*). Constructed ponds, for instance, are numerous in the Bengal Basin and vary in their contribution to aquifer recharge (*34*, *39*, *43*), depending on the accumulation of fine-grained bottom sediment. Such seasonally and spatially variable forcing can result in highly complex groundwater flowpaths connecting recharge and discharge areas.

High groundwater pumping can substantially alter natural flow patterns. In Bangladesh, the rate of groundwater pumping for irrigation is at least an order of magnitude higher than integrated flow from hand pumps (*16*, *39*, *44*). Irrigation pumping and return flow through fields rearrange recharge and discharge areas, increase recharge rates, and modify regional and local flow patterns (*34*, *39*, *44*–*46*). Groundwater use for irrigation is greatest in the Bengal Basin and the Terai Basin along the southern border of Nepal, less in the Red River Basin (*17*), and least in the Mekong River Basin (*41*). Because elevated As concentrations are observed in all these areas (Fig. 1B), processes associated with irrigation pumping, though potentially important, cannot be the only trigger of As release to groundwater.

The time since recharge, or groundwater age, is also an important factor that influences groundwater As concentrations. Groundwater age, measured by two different radioactive clocks, ranges from less than 1 year to a few decades in shallow (<20 m deep) aquifers in Bangladesh and Vietnam and from centuries to thousands of years in deeper strata of Bangladesh (50 to 400 m deep) (Fig. 3A). The vertical gradient in groundwater ages reflects regional flow systems and flowpaths that link distant recharge and discharge areas beneath more vigorous shallow and local groundwater circulation (Fig. 3B). Irrigation water is typically drawn from shallow (<100 m) depths and may be partly responsible for the pronounced difference in age between shallow and deeper aquifers (*39*, *45*).

Box 1: The color of aquifer sands is a useful visual indicator of the redox state of an aquifer. (Bottom) Orange sands from Vietnam indicate the presence of Fe(III) oxides that are consistently associated with low-As water, whereas gray sands with reduced or mixed-valence Fe(II+III) oxides (top) are often, though not always, associated with higher dissolved As. Sand color has been used by drillers to target low-As groundwater in spatially heterogeneous aquifers. [Photo courtesy of Benjamin Bostick]

Within the river basins considered here, the highly variable As concentrations in young groundwater in shallow strata may be due to differences in topography on multiple scales. Slightly elevated, often coarse, sandy deposits appear to be associated with lower As concentrations in Bangladesh and Cambodia (*47*–*49*). Such observations suggest that rapid recharge through these deposits locally inhibits the release of As, possibly by supplying oxygen, nitrate, or sulfate as alternatives to Fe oxides for oxidizing organic carbon (*34*, *48*). Similar processes prevent release of arsenic in water recharged through rice field bunds (*34*). In contrast, low-lying areas in the river basins are typically covered with finer-grained sediment, frequently flooded, and associated with high dissolved As concentrations at shallow depths. Rapid release of As under these conditions is attributed to co-deposition of labile carbon and As-bearing Fe oxides in the seasonally saturated surface sediments (*18*, *30*), infiltration of recharge with abundant DOC (*17*, *39*), or simply slow flow of water through As-releasing sediment (*48*).

Along the pathway of groundwater flow, changes in As concentration will depend on local partitioning (adsorption/desorption) with the sediment as well as reductive release. Arsenic can be released from the sediment and eventually flushed from the aquifer in areas where the concentration of As in inflowing water is below that dictated by partitioning, even within reduced gray sands depleted in Fe(III) (*38*). Along anaerobic, shallow flowpaths containing organic carbon, As concentrations typically increase. This is consistent with a correlation between As and groundwater age or flow rate within shallow aquifers (*21*, *40*), and with As plumes that originate from natural wetlands high in organic carbon (*18*, *30*) or constructed ponds (*34*). The subsurface maximum in groundwater As frequently observed within shallow gray reduced aquifers is likely the result of layering of groundwater flow having different evolutionary histories. High-As groundwater indicates a plume evolved from active Fe/As reductive dissolution/desorption; low-As water can reflect flowpaths that lack Fe/As reduction, secondary As-sulfide precipitation, various extents of sediment flushing, or mixing near irrigation well intakes (*16*, *28*, *34*, *38*, *45*).

How Vulnerable Are Low-Arsenic Zones?

Low-As zones within the aquifer systems of the affected basins are rarely distinct aquifers and can be associated with reduced gray [Fe(II) dominated] or oxidized orange [Fe(III) dominated] sands (*16*). Zones of low dissolved As occur in gray sands where As is removed by sulfide (*13*) and along flowpaths where adsorbed As has been flushed by sustained recharge or has never been released (*16*, *38*). Low-As zones associated with oxidized orange sands are often deeper (>100 m) but, depending on the local geology, are occasionally preserved at shallower depths (*9*, *10*, *50*). Groundwater is typically anoxic throughout the affected region, even within orange sand deposits. The vulnerability of shallower and deeper low-As zones to human perturbation must be understood because millions of households in Bangladesh have switched their consumption to a nearby low-As well identified by testing in the field (*51*).

Low-As zones can be protected against intrusion of high-As groundwater by favorable hydraulics or geochemical processes. Hydraulic protection occurs where the source area that contributes water to a particular zone is not high in dissolved As or solutes that can mobilize As. Geochemical protection occurs because of As adsorption or precipitation (e.g., As-bearing sulfides). Experiments and modeling indicate that breakthrough of As through 10 m of orange sands may lag groundwater flow by hundreds of years because of adsorption (*37*).

Shallow low-As zones are particularly vulnerable to As invasion owing to complex and rapid flow combined with the patchy distribution of dissolved and solid-phase As (Fig. 3B). The adsorption capacity of gray sands that prevail at shallow depths is lower than that of orange sands and further contributes to the vulnerability of shallow low-As zones. A primary threat is advective transport from adjacent high-As zones because groundwater flows much more easily laterally than vertically through stratified sediments.

Deeper groundwater (>100m deep) is more uniformly low in As (Fig. 1B) and already a

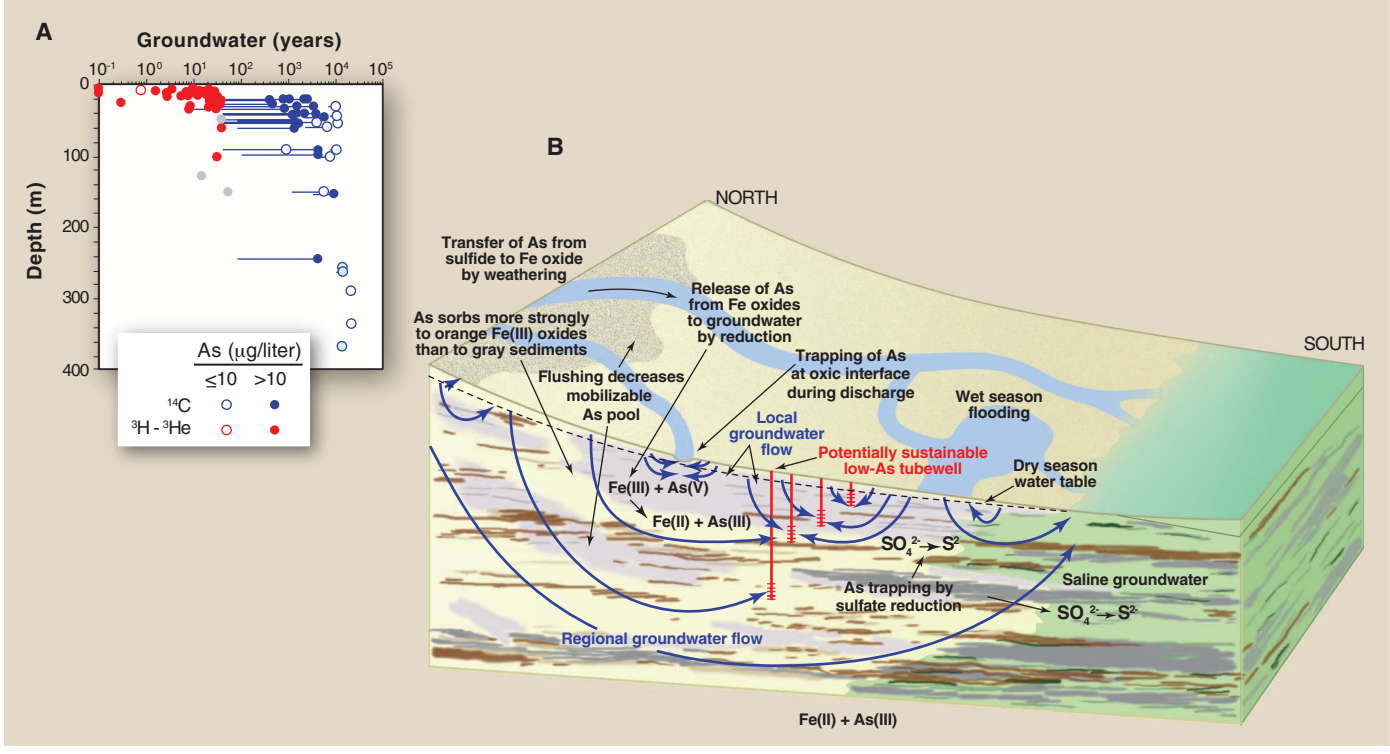

Fig. 3. (**A**) Depth distribution of groundwater ages in Bangladesh determined by either the ^{3}H-^{3}He method (red symbols) or radiocarbon in those cases where ^{3}H was measured and not detected (blue symbols) (*54*). Concentrations of As were not reported for three deep samples shown as light blue circles but are likely to be low; the age of samples shown as gray circles is uncertain owing to their low ^{3}He content. (**B**) Conceptual diagram modified from (*9*) showing the key processes affecting the distribution of As in groundwater.

widely used and potentially sustainable source of safe water in certain portions of the Bengal Basin. Hydraulic protection of deep groundwater requires geologic separation of high- and low-As strata or a regional flow system in which the recharge location is low in As. Deep, regional systems likely occur in much of the Bengal Basin despite low regional hydraulic gradients because of its large extent, depth, and extreme vertical heterogeneity (*44*, *52*). Hydraulic gradients in the Mekong (*41*), Red River (*42*), and Terai basins are similarly low, but the basins are smaller and shallower, and thus may have more limited regional flow. Numerical modeling of groundwater flow in the Bengal Basin (*44*) has shown that hydraulic protection may last for at least 1000 years in much of the As-affected area if wells are deeper than 150 m and pumping rates from deep aquifers are limited to domestic supply. In contrast, deep pumping for irrigation occurs at order-of-magnitude higher rates compared to hand pumps and could induce much earlier and larger-scale downward migration of As (*44*).

Human-induced changes have and will continue to threaten low-As zones. Whereas hydraulic heads and flow velocities respond quickly to changes in physical forcing, solute concentrations require a period at least equivalent to the groundwater residence time to reach a new equilibrium. This applies in particular to shallow aquifers where the duration of human-induced change, such as irrigation pumping or the digging of ponds, has been approximately equivalent to the residence time of groundwater (*39*). Raising villages above flood level using low-permeability clay also creates a cap that inhibits recharge and could lead to a buildup of As in shallow aquifers previously suitable for drinking (*49*). Transport of reactive DOC by irrigation pumping into a zone of either gray or orange sands that currently lacks a source of organic matter could also lead to the onset of reductive dissolution and As release into groundwater (*28*, *34*).

Where hydraulic protection does not exist, in shallower strata or where pumping rates are high, a zone may remain low in As for extended periods because of retardation by adsorption (*37*). The delay in the appearance of elevated levels of As should decrease with increasing velocity and increase with flow distance, particularly through orange sands. The lower rate at which water is drawn from a community hand pump is therefore preferable to a mechanized pump connected to a piped-water supply system. Where feasible, wells should extend as deep as possible into deep orange sands rather than into gray sands or shallow orange sands. These recommendations are consistent with the outcome of monitoring a set of hand-pumped community wells in Bangladesh during which a few increases in As concentrations were recorded during the initial years (mostly in wells <60 m deep) and none since (*53*).

Priorities for the Future

The laterally and vertically heterogeneous distribution of As has one advantage—many villagers in the affected regions live within walking distance of a well that is low in As or within drilling distance of such a zone. Governments and international organizations should therefore reinvigorate moribund well-testing campaigns and encourage periodic monitoring of wells using field kits. Better use should also be made of existing geological data and compiling test results to target those zones that are low in As for the installation of community wells. Even if wells tapping deeper strata are more likely to be hydraulically and chemically protected, tens of thousands of deep wells installed throughout Bangladesh (*51*) should be retested, which currently happens rarely.

As outlined in this review, the downside of patchiness is poor predictability and potential sensitivity of those aquifers that are low in As to changes in flow and/or related biogeochemical reactions. At a limited number of judiciously selected locations, analysis of organic matter and As reactivity should therefore be coupled with more detailed evaluation of the local hydrology. Another topic that deserves closer study is the viability of rural piped-water supply systems, currently favored by some governments and international organizations, as opposed to community hand pumps. Mechanized pumps concentrate deep pumping and are more likely to draw in high-As water from shallower aquifers.

Every effort should be made to prevent irrigation by pumping from deeper aquifers that are low in As. The accumulation of As in paddy soil and rice grains is a source of concern, but deep aquifers should not be compromised by abstraction for irrigation. This precious resource must be preserved for drinking—the most direct and efficient route of exposure to As.

References and Notes

1. A. H. Smith, E. O. Lingas, *Bull. World Health Organ.* **78**, 1093 (2000).
2. P. Ravenscroft, H. Brammer, K. Richards, *Arsenic Pollution: A Global Synthesis* (RGS-IBG Book Series, Wiley-Blackwell, Chichester, UK, 2009).
3. U. K. Chowdhury *et al.*, *Environ. Health Perspect.* **108**, 393 (2000).
4. Y. Chen, H. Ahsan, *Am. J. Public Health* **94**, 741 (2004).
5. C. J. Chen, H. Y. Chiou, M. H. Chiang, L. J. Lin, T. Y. Tai, *Arterioscler. Thromb. Vasc. Biol.* **16**, 504 (1996).
6. G. A. Wasserman *et al.*, *Environ. Health Perspect.* **112**, 1329 (2004).
7. L. Winkel, M. Berg, M. Amini, S. J. Hug, C. Annette Johnson, *Nat. Geosci.* **1**, 536 (2008).
8. S. L. Goodbred Jr., S. A. Kuehl, *Sediment. Geol.* **133**, 227 (2000).
9. D. G. Kinniburgh, P. L. Smedley, Eds., *Arsenic Contamination of Ground Water in Bangladesh, Final Report* (BGS Technical Report WC/00/19, British Geological Survey, Keyworth, UK, 2001), vol. 2.
10. A. van Geen *et al.*, *Water Resour. Res.* **39**, 1140 (2003).
11. R. Nickson *et al.*, *J. Environ. Sci. Health Part A Tox. Hazard. Subst. Environ. Eng.* **42**, 1707 (2007).
12. S. K. Acharyya *et al.*, *Nature* **401**, 545, discussion 546 (1999).
13. H. A. Lowers *et al.*, *Geochim. Cosmochim. Acta* **71**, 2699 (2007).
14. B. D. Kocar *et al.*, *Appl. Geochem.* **23**, 3059 (2008).
15. C. H. Swartz *et al.*, *Geochim. Cosmochim. Acta* **68**, 4539 (2004).
16. Y. Zheng *et al.*, *Geochim. Cosmochim. Acta* **69**, 5203 (2005).
17. M. Berg *et al.*, *Chem. Geol.* **249**, 91 (2008).
18. D. Postma *et al.*, *Geochim. Cosmochim. Acta* **71**, 5054 (2007).
19. C. B. Dowling *et al.*, *Water Resour. Res.* **38**, 1173 (2002).
20. A. A. Seddique *et al.*, *Appl. Geochem.* **23**, 2236 (2008).
21. B. Nath *et al.*, *J. Hydrol. (Amst.)* **364**, 236 (2009).
22. B. J. Mailloux *et al.*, *Appl. Environ. Microbiol.* **75**, 2558 (2009).
23. F. S. Islam *et al.*, *Nature* **430**, 68 (2004).
24. K. J. Tufano, C. Reyes, C. W. Saltikov, S. Fendorf, *Environ. Sci. Technol.* **42**, 8283 (2008).
25. A. Horneman *et al.*, *Geochim. Cosmochim. Acta* **68**, 3459 (2004).
26. J. M. McArthur *et al.*, *Water Resour. Res.* **44**, W11411 (2008).
27. M. von Brömssen *et al.*, *Sci. Total Environ.* **379**, 121 (2007).
28. C. F. Harvey *et al.*, *Science* **298**, 1602 (2002).
29. J. Buschmann, M. Berg, *Appl. Geochem.* **24**, 1278 (2009).
30. M. L. Polizzotto, B. D. Kocar, S. G. Benner, M. Sampson, S. Fendorf, *Nature* **454**, 505 (2008).
31. S. Jessen *et al.*, *Appl. Geochem.* **23**, 3116 (2008).
32. H. A. L. Rowland *et al.*, *Geobiology* **5**, 281 (2007).
33. N. Mladenov *et al.*, *Environ. Sci. Technol.* **44**, 123 (2009).
34. R. B. Neumann *et al.*, *Nat. Geosci.* **3**, 46 (2010).
35. J. Gurung, H. Ishiga, M. S. Khadka, *Environ. Geol.* **49**, 98 (2005).
36. N. C. Papacostas, B. C. Bostick, A. N. Quicksall, J. D. Landis, M. Sampson, *Geology* **36**, 891 (2008).
37. K. G. Stollenwerk *et al.*, *Sci. Total Environ.* **379**, 133 (2007).
38. A. van Geen *et al.*, *Environ. Sci. Technol.* **42**, 2283 (2008).
39. C. F. Harvey *et al.*, *Chem. Geol.* **228**, 112 (2006).
40. M. Stute *et al.*, *Water Resour. Res.* **43**, W09417 (2007).
41. S. G. Benner *et al.*, *Appl. Geochem.* **23**, 3072 (2008).
42. F. Larsen *et al.*, *Appl. Geochem.* **23**, 3099 (2008).
43. S. Sengupta *et al.*, *Environ. Sci. Technol.* **42**, 5156 (2008).
44. H. A. Michael, C. I. Voss, *Proc. Natl. Acad. Sci. U.S.A.* **105**, 8531 (2008).
45. S. Klump *et al.*, *Environ. Sci. Technol.* **40**, 243 (2006).
46. A. Mukherjee, A. E. Fryar, P. D. Howell, *Hydrogeol. J.* **15**, 1397 (2007).
47. J. Buschmann, M. Berg, C. Stengel, M. L. Sampson, *Environ. Sci. Technol.* **41**, 2146 (2007).
48. Z. Aziz *et al.*, *Water Resour. Res.* **44**, W07416 (2008).
49. B. Weinman *et al.*, *Geol. Soc. Am. Bull.* **120**, 1567 (2008).
50. E. Eiche *et al.*, *Appl. Geochem.* **23**, 3143 (2008).
51. M. F. Ahmed *et al.*, *Science* **314**, 1687 (2006).
52. P. Ravenscroft, W. G. Burgess, K. M. Ahmed, M. Burren, J. Perrin, *Hydrogeology J.* **13**, 727 (2005).
53. A. van Geen *et al.*, *J. Environ. Sci. Health Part A Tox. Hazard. Subst. Environ. Eng.* **42**, 1729 (2007).
54. Data sources and methods are available on *Science* Online.

55. We thank J. W. Rosenboom of Water Supply Program/World Bank and M. A. Sampson, founder and director of RDI International, Cambodia (deceased 19 March 2009), for help in organizing the AGU Chapman conference held in Siem Reap, Cambodia, in March 2009 that resulted in this review. Travel support for the conference was contributed by the Woods Institute for the Environment at Stanford University and the European Union Asia-Link CALIBRE Project. We also acknowledge research funding by the Environmental Venture Projects program of Stanford's Woods Institute for the Environment and the Stanford NSF Environmental Molecular Science Institute (NSF-CHE-0431425) (S.E.F.), the U.S. Geological Survey, the U.S. Agency for International Development, the British Department for International Development, and UNICEF (H.A.M.), National Institute of Environmental Health Sciences SRP grant 1 P42 ES10349, NIH FIC grant 5 D43 TW05724, and NSF grant EAR 0345688 (AvG). We thank R. Beckie, G. Breit, C. Harvey, J. Lloyd, and an anonymous reviewer for helpful comments. This is Lamont-Doherty Earth Observatory contribution no. 7355.

10.1126/science.1172974

cidence angle. The calculated scattering spectra of a heptamer for different polarization angles are shown in Fig. 3C, where the cluster geometry is identical to that used in Fig. 3A. These spectra display Fano minima at 1450 nm, with asymmetric line shapes that match the experimental spectra. The nanoshell separation modeled here is smaller than that used for the trimer calculations to account for the strongly red-shifted Fano minimum. This red shift is probably due to a combination of at least three factors: (i) smaller nanoshell separation due to inhomogeneous self-assembled monolayer coverage, (ii) a higher–refractive-index environment near the cluster due to excess polymer deposition, and (iii) increased capacitive coupling between the nanoparticles due to nanoshell faceting.

This cluster concept can be generalized to other functional 2D and 3D structures. One example is the tetrahedral cluster, which supports isotropic electric and magnetic resonances in three dimensions (*28*) and can be used as a building block for isotropic metamaterials. Symmetry breaking can be applied to engineer other types of optical modes: Trimers comprising three different particle types support magnetoelectric modes, and tetrahedral clusters comprising four different particle types are chiral. Nonspherical plasmonic particles can be used to construct more elaborate structures, provided that their orientations can be controlled during assembly. In all of these structures, resonances can be tuned by varying individual particle geometries, interparticle separation, and the dielectric environment of the cluster. The assembly of clusters from solution is highly versatile: It can lead to liquid metamaterials or "metafluids" (*28*), be integrated into soft materials such as gels, or be encapsulated and dried onto surfaces of arbitrary curvature or patterning. Future work will focus on these applications and on achieving higher cluster yields comparable to those attained with lithographically defined patterns (*29*), emulsion droplets (*30*), and DNA linking (*31*).

References and Notes

1. W. L. Barnes, A. Dereux, T. W. Ebbesen, *Nature* **424**, 824 (2003).
2. V. M. Shalaev, *Nat. Photonics* **1**, 41 (2007).
3. V. M. Shalaev *et al.*, *Opt. Lett.* **30**, 3356 (2005).
4. J. B. Pendry, D. Schurig, D. R. Smith, *Science* **312**, 1780 (2006); published online 25 May 2006 (10.1126/science.1125907).
5. M. W. Klein, C. Enkrich, M. Wegener, S. Linden, *Science* **313**, 502 (2006).
6. D. J. Bergman, M. I. Stockman, *Phys. Rev. Lett.* **90**, 027402 (2003).
7. N. Engheta, *Science* **317**, 1698 (2007).
8. S. A. Maier *et al.*, *Adv. Mater.* **13**, 1501 (2001).
9. L. J. Sherry *et al.*, *Nano Lett.* **5**, 2034 (2005).
10. J. B. Pendry, A. J. Holden, D. J. Robbins, W. J. Stewart, *IEEE Trans. Microwave Theory Tech.* **47**, 2075 (1999).
11. T. J. Yen *et al.*, *Science* **303**, 1494 (2004).
12. N. Verellen *et al.*, *Nano Lett.* **9**, 1663 (2009).
13. N. Liu *et al.*, *Nat. Mater.* **8**, 758 (2009).
14. K. J. Stebe, E. Lewandowski, M. Ghosh, *Science* **325**, 159 (2009).
15. T. Ming *et al.*, *Angew. Chem. Int. Ed.* **47**, 9685 (2008).
16. J. H. Lee, Q. Wu, W. Park, *Opt. Lett.* **34**, 443 (2009).
17. M. S. Wheeler, J. S. Aitchison, J. I. L. Chen, G. A. Ozin, M. Mojahedi, *Phys. Rev. B* **79**, 073103 (2009).
18. E. Prodan, C. Radloff, N. J. Halas, P. Nordlander, *Science* **302**, 419 (2003).
19. S. J. Oldenburg, R. D. Averitt, S. L. Westcott, N. J. Halas, *Chem. Phys. Lett.* **288**, 243 (1998).
20. J. C. Love, L. A. Estroff, J. K. Kriebel, R. G. Nuzzo, G. M. Whitesides, *Chem. Rev.* **105**, 1103 (2005).
21. J. J. Mock, M. Barbic, D. R. Smith, D. A. Schultz, S. Schultz, *J. Chem. Phys.* **116**, 6755 (2002).
22. C. Enkrich *et al.*, *Phys. Rev. Lett.* **95**, 203901 (2005).
23. Y. A. Urzhumov, G. Shvets, *Solid State Commun.* **146**, 208 (2008).
24. D. W. Brandl, N. A. Mirin, P. Nordlander, *J. Phys. Chem. B* **110**, 12302 (2006).
25. E. Plum *et al.*, *Phys. Rev. Lett.* **102**, 113902 (2009).
26. Random symmetry breaking can be experimentally addressed by using smoother thick-shelled nanoparticles, assembling nanoparticles with atomically smooth facets such as crystalline nanocubes, or assembling clusters with larger gap sizes, which would effectively reduce gap geometry variation (but at the expense of total mode strength).
27. N. A. Mirin, K. Bao, P. Nordlander, *J. Phys. Chem. A* **113**, 4028 (2009).
28. Y. A. Urzhumov *et al.*, *Opt. Express* **15**, 14129 (2007).
29. Y. D. Yin, Y. Lu, B. Gates, Y. N. Xia, *J. Am. Chem. Soc.* **123**, 8718 (2001).
30. V. N. Manoharan, M. T. Elsesser, D. J. Pine, *Science* **301**, 483 (2003).
31. C. J. Loweth, W. B. Caldwell, X. G. Peng, A. P. Alivisatos, P. G. Schultz, *Angew. Chem. Int. Ed.* **38**, 1808 (1999).

32. J.A.F., F.C., C.W., and G.S. acknowledge funding by the NSF Nanoscale Interdisciplinary Research Team under grant no. ECCS-0709323; G.S. and C.W. acknowledge funding by Air Force Office of Scientific Research (AFOSR) Multidisciplinary University Research Initiative grants FA9550-06-1-0279 and FA9550-08-1-0394; R.B, N.J.H., and P.N. acknowledge support from the U.S. Department of Defense National Security Science and Engineering Faculty Fellowship program, the Robert A. Welch Foundation (C-1220 and C-1222), AFOSR grant F49620-03-C-0068, the SUG@R (Shared University Grid at Rice) team, and the Center for Advanced Solar Photophysics, a U.S. Department of Energy Energy Frontier Research Center. Electron microscopy was performed at the Center for Nanoscale Science at Harvard University, a member of the National Nanotechnology Infrastructure Network. J.A.F. acknowledges R. Guerra for helpful discussions and D. Bell for EM support.

Supporting Online Material

www.sciencemag.org/cgi/content/full/328/5982/1135/DC1
Materials and Methods
SOM Text
Figs. S1 to S6
References

4 February 2010; accepted 22 April 2010
10.1126/science.1187949

How Grain Growth Stops: A Mechanism for Grain-Growth Stagnation in Pure Materials

Elizabeth A. Holm* and Stephen M. Foiles

The thermodynamic equilibrium state of crystalline materials is a single crystal; however, polycrystalline grain growth almost always stops before this state is reached. Although typically attributed to solute drag, grain-growth stagnation occurs, even in high-purity materials. Recent studies indicate that grain boundaries undergo thermal roughening associated with an abrupt mobility change, so that at typical annealing temperatures, polycrystals will contain both smooth (slow) and rough (fast) boundaries. Mesoscale grain-growth models, validated by large-scale polycrystalline molecular dynamics simulations, show that even small fractions of smooth, slow boundaries can stop grain growth. We conclude that grain-boundary roughening provides an alternate stagnation mechanism that applies even to high-purity materials.

Most metals and ceramics are polycrystalline: They are made up of many individual crystallites, called grains, separated by internal interfaces or grain boundaries. When polycrystalline materials are annealed at sufficiently high temperatures, grain boundaries move and rearrange so as to increase the average grain size and decrease the grain-boundary area per unit volume. However, even at very high temperatures, grain growth only rarely proceeds to the equilibrium single-crystal state. Instead, grain growth usually stops, though substantial internal interface remains. In fact, grain stagnation is so pervasive that most grain-growth models presume a finite maximum grain size based purely on empirical observations (*1*).

Understanding and controlling grain growth is important to nearly every engineered material. For materials that rely on strength, toughness or formability, including most nanocrystalline materials, a stable, fine grain size is desirable. However, there are also important systems, such as superalloy turbine blades and silicon photovoltaics, in which a large (or even single-crystal) grain size is preferred.

There have been many grain-growth stagnation mechanisms proposed, each valid in certain regimes. Well-known processes that reduce the driving force for grain growth sufficiently to

Computational Materials Science and Engineering Department, Sandia National Laboratories, Albuquerque, NM 87185–1411, USA.

*To whom correspondence should be addressed. E-mail: eaholm@sandia.gov

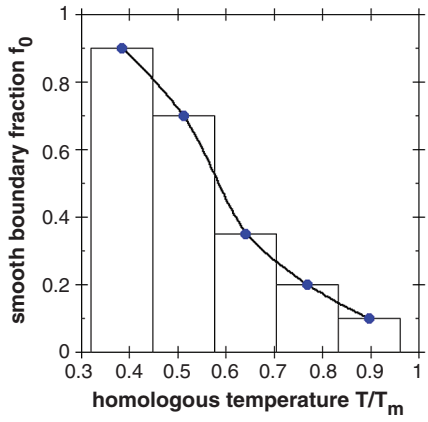

Fig. 1. Distribution of grain-boundary roughening-transition temperatures for several hundred grain boundaries in Ni calculated by MD simulations (*17*). The width of the bars corresponds to the temperature bin width; data points are located at the mean temperature of each bin. The solid line is a guide for the eye.

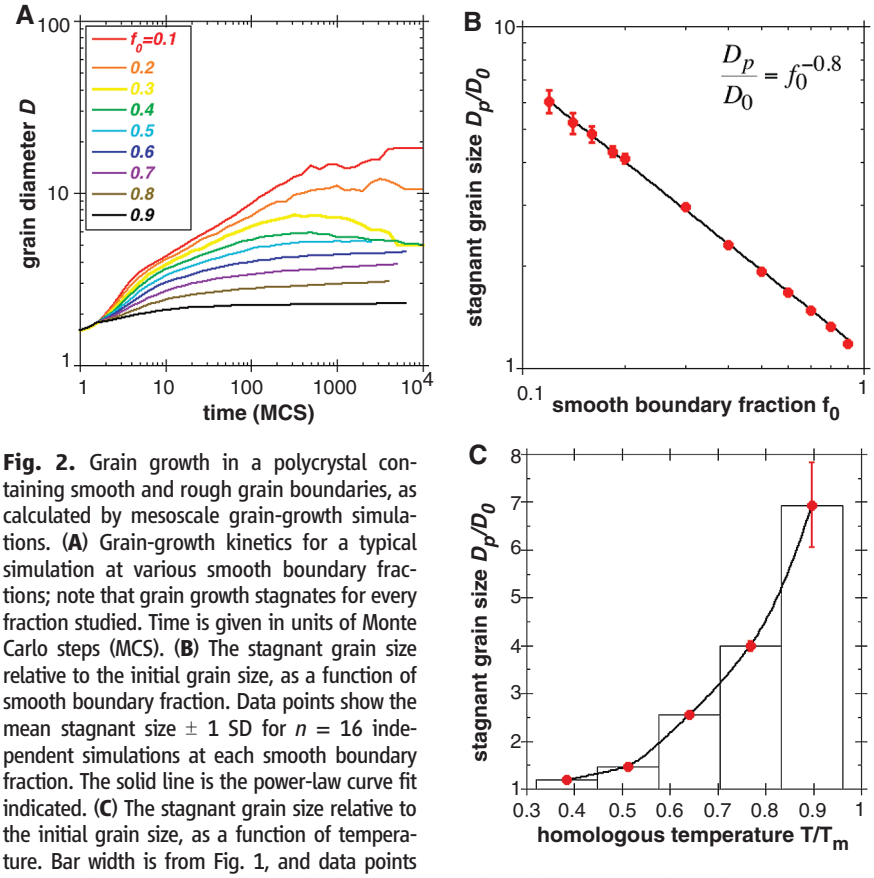

Fig. 2. Grain growth in a polycrystal containing smooth and rough grain boundaries, as calculated by mesoscale grain-growth simulations. (**A**) Grain-growth kinetics for a typical simulation at various smooth boundary fractions; note that grain growth stagnates for every fraction studied. Time is given in units of Monte Carlo steps (MCS). (**B**) The stagnant grain size relative to the initial grain size, as a function of smooth boundary fraction. Data points show the mean stagnant size ± 1 SD for n = 16 independent simulations at each smooth boundary fraction. The solid line is the power-law curve fit indicated. (**C**) The stagnant grain size relative to the initial grain size, as a function of temperature. Bar width is from Fig. 1, and data points and error bars are extracted from the data in Fig. 2B. The solid line is a guide for the eye.

produce a metastable polycrystal include pinning by dispersed particles (*2*), pinning by thermal grooves (*3*), and the film-thickness effect (*4*). These occur only in films or in systems containing an immobile second phase. In other materials, grain-growth stagnation is often attributed to the segregation of solute species to the grain boundary. Solutes inhibit grain growth by requiring the boundary to move in concert with its solute cloud (*5*–*9*) or by directly changing boundary-migration mechanisms (*10*, *11*). For most solutes and temperatures of interest, this substantially slows grain-boundary motion and, hence, also slows grain growth. However, grain-growth stagnation is also observed in systems in which solutes should not limit growth, including high-purity materials (*12*, *13*), nanocrystalline materials that should be in the solute breakaway regime (*14*, *15*), and materials at high homologous temperatures where solute diffusivity should be high (*15*). It is reasonable to suppose that there might be another active grain-growth stagnation mechanism in these systems.

We recently calculated grain-boundary mobility, which scales how fast a boundary can move in response to a driving force, for a catalog of 388 grain boundaries in Ni using a synthetic–driving force molecular dynamics (MD) method (*16*, *17*). At a given temperature, mobility falls into two ranges: (i) high-mobility (fast) boundaries and (ii) low-mobility (slow) boundaries, whose mobility is too small for us to measure via MD. Typical high-mobility boundaries move continuously with well-defined activation energies and atomically rough-boundary structures. On the other hand, low-mobility boundaries move in a jerky, stepwise manner with different activation energies and atomically smooth boundary structures (*18*). The boundary structure changes from smooth/low-mobility to rough/high-mobility at a characteristic temperature, T_r (the roughening temperature), which can vary by hundreds of degrees from boundary to boundary, as discussed by Olmsted *et al.* (*17*). Figure 1 shows the distribution of roughening temperatures for our catalog of Ni boundaries: At low temperature, most boundaries are smooth and slow, but even at 0.9 T_m (where T_m is the melting temperature), ~10% of the boundaries remain smooth and slow.

It is important to note that the roughening transition is not related to faceting, in which certain crystallographically favored grain boundaries decompose into flat facets that lie along low-energy inclinations (*19*–*21*). Because faceting results in both high and low grain-boundary mobilities (*22*, *23*), it is not generally implicated in grain-growth stagnation (*24*). In contrast, the roughening transition occurs in all boundaries, not just those that are thermodynamically inclined to facet, and the structure of smooth boundaries does not include crystallographic facets (*18*). Smooth boundaries generally have very low mobility, which could inhibit grain growth. Because faceting and roughening are distinct phenomena, it is possible that a single grain boundary could undergo both transitions at different temperatures; however, this report concerns only the microstructural effects of grain-boundary roughening and its associated mobility transition.

To determine the effect of boundary roughening on grain growth in a polycrystal, we incorporate the boundary mobility and roughening data in Fig. 1 into a mesoscale simulation of polycrystalline microstructural evolution (*25*–*28*). When all boundaries are rough/high-mobility, we find that grain growth proceeds to the equilibrium single-crystal state. In contrast, in simulations that include smooth/low-mobility boundaries, grain growth slows dramatically at a finite grain size that decreases as the fraction of smooth boundaries, f_0, increases, as shown in Fig. 2A. It is not surprising that immobile boundaries can slow or stop grain growth; however, it is unexpected that the grain structure stagnates at such small smooth boundary fractions, because the motion of mobile boundaries can sweep out immobile boundaries. Our results show that in a polycrystal, grain boundaries form an interconnected network that may be pinned, even when many individual boundaries remain unpinned. This observation applies, not only to pinning by smooth boundaries, but also to other stagnation mechanisms. For example, particle pinning theories disagree on whether all or merely a fraction of boundaries must be pinned by intersecting particles for the grain structure to be stabilized (*29*, *30*). The present results indicate that pinning a fraction of boundaries is sufficient.

The stagnant grain size relative to the initial grain size (that is, D_p/D_0) decreases as a power law in f_0, as shown in Fig. 2B. By combining Fig. 1 and Fig. 2B, we can determine the stagnant grain size as a function of temperature, as shown

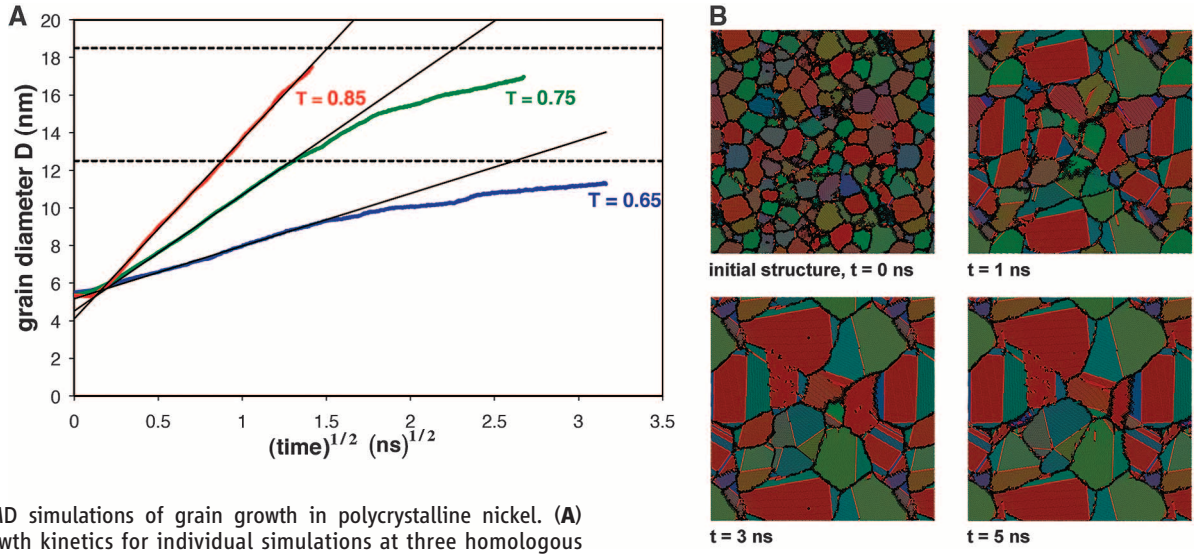

Fig. 3. MD simulations of grain growth in polycrystalline nickel. (**A**) Grain-growth kinetics for individual simulations at three homologous temperatures. Solid black lines show normal growth kinetics with grain diameter proportional to the square root of time; dashed lines indicate the stagnant grain size predicted by mesoscale simulations. (**B**) Time evolution of a slice through the 3D system at $T = 0.75\ T_m$ at 0, 1, 3, and 5 ns. The atomic color scheme reflects local lattice orientation: Red atoms are hexagonal close-packed coordinated (i.e., dislocations, twins); black atoms are of unknown coordination (i.e., grain boundaries).

in Fig. 2C. At low temperatures, very little grain growth can occur due to a large fraction of smooth/low-mobility boundaries. Even at 0.9 T_m, which is higher than many industrial-annealing temperatures, the grain size can increase only by one order of magnitude before being pinned by smooth boundaries. Within our mesoscale simulations, smooth boundaries can provide an effective grain-growth pinning mechanism, but are they likely to be a factor in real materials?

Although we observed grain-boundary roughening in flat grain boundaries (*18*), boundaries in real polycrystals are curved. It seems reasonable to wonder whether the geometric constraints imposed by boundary curvature might prevent the realization of a smooth/low-mobility boundary structure. The obvious solution is to measure the atomic roughness of curved boundaries directly, but this poses a challenge for boundaries of unknown shape. Furthermore, geometric roughness is an inherently noisy measurement, and for small boundaries, the noise often obscures the signal of the roughening transition (*18*). Mobility is a reliable indicator of boundary roughness, but it is not feasible to measure the mobility of boundaries in a polycrystal, in which the driving force is poorly characterized and continually changing. Although we do not yet have a robust metric to probe boundary roughness in a polycrystal, we can look for the effects of smooth boundaries indirectly via atomic-scale grain-growth simulations.

We begin by building realistic, three-dimensional (3D) nickel polycrystals. Grains are randomly oriented, and grain boundaries assume the structure, crystallography, energy, and mobility naturally imposed by the orientations of the two neighboring grains. We used MD to evolve these structures at various temperatures (*28*, *31*, *32*). Figure 3A shows the evolution of grain size with time. After an initial transient, the average grain radius increases with the square root of time, as expected for normal grain growth (*4*). Some investigators have suggested that, in nanocrystals, grain growth should be governed by triple junction mobility and should follow a linear growth law (*33*), and a previous polycrystal MD simulation seemed to support this (*34*). However, those simulations examined only the first 500 ps of growth. Our results show that, after a short initial transient, nanocrystalline grain growth follows the same $t^{1/2}$ kinetics (where t is time) observed in microcrystalline materials.

After a period of normal grain growth, Fig. 3A shows that grain growth slows dramatically at the two lower temperatures that we studied. Earlier simulations of grain growth in a perfectly pure metal were not able to access the system size or time scale necessary to reach the grain size where slowing occurs (*34*). A cross section of a stagnant polycrystal is shown in Fig. 3B; there are no apparent microstructural features that distinguish this stagnant microstructure from a freely evolving one.

The mesoscale grain-growth simulation data in Fig. 2C suggest that smooth grain boundaries should pin grain growth at a relative grain size $D_p/D_0 = 2.5$ (12.5 nm) at $T = 0.65\ T_m$ (where T is temperature) and at $D_p/D_0 = 3.7$ (18.5 nm) at $T = 0.75\ T_m$. [At $T = 0.85\ T_m$, the pinned relative grain size $D_p/D_0 = 5.6$ (28 nm) is beyond the limitations of the MD system size.] These pinned grain sizes are shown as dotted lines in Fig. 3A. The stagnant grain sizes predicted by the mesoscale grain-growth model are in agreement with the stagnant grain sizes observed in the MD simulations. Although this is not conclusive proof that smooth boundaries are a mechanism of grain-growth stagnation in pure polycrystals, it is highly suggestive.

Controlling grain size to optimize properties is a fundamental problem in materials science. One aspect of this is understanding how grain growth stops. A number of mechanisms have been proposed to explain various instances of grain-growth stagnation. Smooth-boundary pinning offers a mechanism for how grain growth stops in perfectly pure materials, even at high homologous temperatures.

References and Notes

1. J. E. Burke, *AIME Trans.* **180**, 73 (1949).
2. C. S. Smith, *AIME Trans.* **175**, 15 (1948).
3. W. Mullins, *Acta Metall.* **6**, 414 (1958).
4. J. E. Burke, D. Turnbull, *Prog. Met. Phys.* **3**, 220 (1952).
5. J. W. Cahn, *Acta Metall.* **10**, 789 (1962).
6. K. Lucke, K. Detert, *Acta Metall.* **5**, 628 (1957).
7. K. Lucke, H. Stuwe, in *Recovery and Recrystallization of Metals*, L. Himmel, Ed. (Interscience Publications, New York, 1963), p. 131.
8. F. Liu, G. Yang, H. Wang, Z. Chen, Y. Zhou, *Thermochim. Acta* **443**, 212 (2006).
9. E. Rabkin, *Scr. Mater.* **42**, 1199 (2000).
10. G. Gottstein, D. A. Molodov, L. S. Shvindlerman, *Interface Sci.* **6**, 7 (1998).
11. S. Dillon, S. Behera, M. Harmer, *Acta Mater.* **56**, 1374 (2008).
12. G. F. Bolling, W. C. Winegard, *Acta Metall.* **6**, 283 (1958).
13. H. Hu, *Can. Metall. Quart.* **13**, 275 (1974).
14. T. Malow, C. Koch, *Acta Mater.* **45**, 2177 (1997).
15. T. Kizuka, H. Ichinose, Y. Ishida, *J. Mater. Sci.* **32**, 1501 (1997).
16. K. G. F. Janssens *et al.*, *Nat. Mater.* **5**, 124 (2006).
17. D. Olmsted, E. Holm, S. Foiles, *Acta Mater.* **57**, 3704 (2009).
18. D. L. Olmsted, S. M. Foiles, E. A. Holm, *Scr. Mater.* **57**, 1161 (2007).
19. D. Y. Yoon, Y. K. Cho, *J. Mater. Sci.* **40**, 861 (2005).
20. Z. X. Wu, Y. W. Zhang, D. J. Srolovitz, *Acta Mater.* **57**, 4278 (2009).
21. C. Rottman, *Scr. Metall.* **23**, 1037 (1989).
22. S. J. Dillon, M. P. Harmer, *J. Am. Ceram. Soc.* **90**, 2291 (2007).
23. V. G. Sursaeva, B. B. Straumal, A. S. Gornakova, L. S. Shvindlerman, G. Gottstein, *Acta Mater.* **56**, 2728 (2008).

24. E. Rabkin, *J. Mater. Sci.* **40**, 875 (2005).
25. M. Anderson, G. Grest, D. Srolovitz, *Philos. Mag. B* **59**, 293 (1989).
26. M. Anderson, D. Srolovitz, G. Grest, P. Sahni, *Acta Metall.* **32**, 783 (1984).
27. G. N. Hassold, E. Holm, *Comput. Phys.* **7**, 97 (1993).
28. Materials and methods are available as supporting material on *Science* Online.
29. M. Hillert, *Acta Metall.* **36**, 3177 (1988).
30. P. Hazzledine, R. Oldershaw, *Philos. Mag. A* **61**, 579 (1990).
31. S. M. Foiles, J. J. Hoyt, *Acta Mater.* **54**, 3351 (2006).
32. S. J. Plimpton, LAMMPS Molecular Dynamics Simulator (Sandia National Laboratories, Albuquerque, NM, 2007), http://lammps.sandia.gov.
33. A. Galina, V. Fradkov, L. Schvindlerman, *Fiz. Met. Metalloved.* **63**, 1220 (1987).
34. D. Farkas, S. Mohanty, J. Monk, *Phys. Rev. Lett.* **98**, 165502 (2007).
35. Our initial work on grain growth with frozen boundaries, which informed this study, was performed in collaboration with G. Hassold. Support for this work was provided by the U.S. Department of Energy (DOE), Office of Basic Energy Sciences, and by the Laboratory Directed Research and Development program at Sandia National Laboratories. Sandia National Laboratories is a multiprogram laboratory operated by Sandia Corporation, a wholly owned subsidiary of Lockheed Martin company, for the DOE's National Nuclear Security Administration under contract DE-AC04-94AL85000.

Supporting Online Material

www.sciencemag.org/cgi/content/full/328/5982/1138/DC1
Materials and Methods
References and Notes

2 February 2010; accepted 19 April 2010
10.1126/science.1187833

Interface-Confined Ferrous Centers for Catalytic Oxidation

Qiang Fu,[1]* Wei-Xue Li,[1,2]* Yunxi Yao,[1] Hongyang Liu,[1] Hai-Yan Su,[1,2] Ding Ma,[1] Xiang-Kui Gu,[1,2] Limin Chen,[1] Zhen Wang,[1] Hui Zhang,[3] Bing Wang,[3] Xinhe Bao[1]†

Coordinatively unsaturated ferrous (CUF) sites confined in nanosized matrices are active centers in a wide range of enzyme and homogeneous catalytic reactions. Preparation of the analogous active sites at supported catalysts is of great importance in heterogeneous catalysis but remains a challenge. On the basis of surface science measurements and density functional calculations, we show that the interface confinement effect can be used to stabilize the CUF sites by taking advantage of strong adhesion between ferrous oxides and metal substrates. The interface-confined CUF sites together with the metal supports are active for dioxygen activation, producing reactive dissociated oxygen atoms. We show that the structural ensemble was highly efficient for carbon monoxide oxidation at low temperature under typical operating conditions of a proton-exchange membrane fuel cell.

In many catalytic processes, the size of metal-containing catalysts falls typically in the range of 1 to 10 nm. The catalytically active sites in these catalysts are often coordinatively unsaturated metal cations that are able to undergo facile electron transfer and promote catalytic reactions, as has been studied in (*1*–*5*). In oxygen-carrying hemoglobin, the iron (II) ion constrained in a planar porphyrin ring could transport O_2 via facile interconversion between Fe^{2+} and Fe^{3+} states (*6*). Homogeneous catalysis in aqueous solutions uses Fenton's reagent, being a mixture of Fe^{2+} ions and H_2O_2, to produce hydrated ferryl ions $[(H_2O)_5Fe^{IV}O]^{2+}$, which act as the active intermediates to oxidize various organic compounds, such as methane (*7*). However, for heterogeneous catalysis with nanopore environments the active species in Fe-ZSM-5 and Fe-silicalite zeolites are also coordinatively unsaturated Fe^{2+} grafted to the zeolite crystalline matrix. The dissociation of N_2O at the Fe sites leads to formation of "α-oxygen" species, which are active in the selective oxidation of benzene to phenol at mild conditions (*8*). These characteristic coordinatively unsaturated ferrous (CUF) sites are confined by various ensembles such as proteins, ligands, and nanopore matrix, which are essential for their high reactivity and stability in the catalytic oxidation reactions mentioned above (*9*).

Preparation of an analogous ensemble at supported heterogeneous catalysts, which account for 80% of the catalytic processes in industrial chemistry, is of great importance. This, however, remains a challenge because of their high structural complexity and flexibility under operating conditions. On the basis of surface science measurements, density functional calculations, and catalytic reactions under realistic conditions, we describe here a strategy to achieve this goal that takes advantage of the confinement effect at interfaces between nanostructured ferrous oxides (FeO) and metal (Pt) substrates. The interface-confined CUF sites and neighboring Pt atoms are identified conclusively as the active centers to activate O_2. The dissociated atomic oxygen atoms therein present modest adsorption energy and thus are highly reactive. Catalytic reaction experiments on the supported Pt-Fe catalysts prepared by a dedicated and reproducible synthesis method show that the identified ensemble is highly active, selective, and robust for CO oxidation, even under operating conditions of a proton-exchange membrane fuel cell (PEMFC).

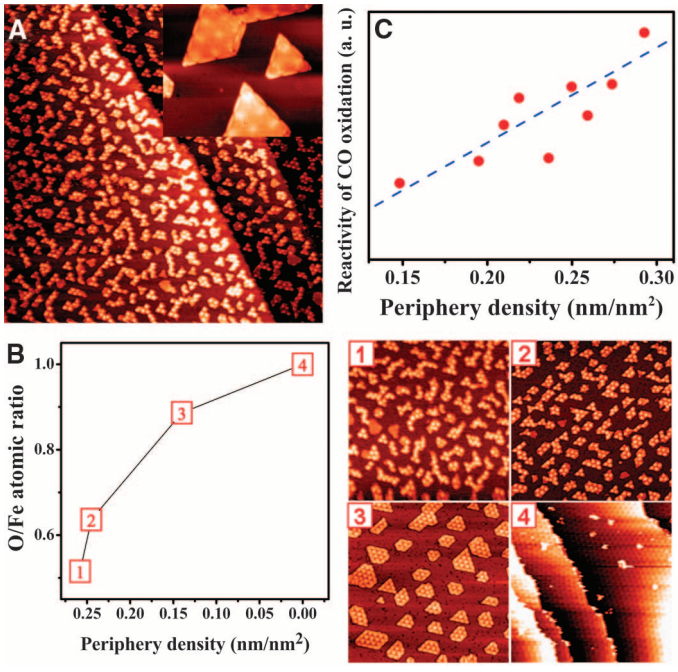

Fig. 1. (**A**) STM image (200 nm × 200 nm) from the 0.25-ML FeO_{1-x}/Pt(111) surface. (Inset) An atomic-resolution STM image of FeO monolayer nanoislands (25 nm × 20.8 nm) recorded at liquid N_2 temperature. (**B**) Ratios of XPS O 1*s* to Fe $2p_{3/2}$ peak intensity from FeO_{1-x}/Pt(111) surfaces with different periphery density of FeO nanoisland. Samples 1 to 3 are 0.25-ML FeO nanoislands prepared at 1.3 × 10^{-6} mbar O_2 and annealed in UHV at 473, 573, and 673 K, respectively. Sample 4 is the full-monolayer FeO film on Pt(111). The STM images are all 100 nm by 100 nm. (**C**) Dependence of reactivity of CO oxidation on the periphery density at 0.25-ML FeO_{1-x}/Pt(111) surfaces.

[1]State Key Laboratory of Catalysis, Dalian Institute of Chemical Physics, Chinese Academy of Sciences, Dalian 116023, China. [2]Center for Theoretical and Computational Chemistry, Dalian Institute of Chemical Physics, Chinese Academy of Sciences, Dalian 116023, China. [3]Hefei National Laboratory for Physical Sciences at the Microscale, University of Science and Technology of China, Hefei 230026, China.

*These authors contributed equally to this work.
†To whom correspondence should be addressed. E-mail: xhbao@dicp.ac.cn

Construction of FeO nanoislands on the metal support was done by depositing Fe on Pt(111) under oxidizing conditions and characterized by an ultra-high vacuum (UHV) multi-probe surface system (*10*). Figure 1A shows a typical scanning tunneling microscopy (STM) image taken from Pt(111) with 0.25-monolayer (ML) Fe deposited at 150 K in the presence of 1.3×10^{-7} mbar O_2, followed by annealing up to 473 K in UHV. The FeO nanoislands formed are monolayer-dispersed. The Moiré patterns and surface atomic structures of the nanoislands are the same as those of a monolayer FeO film grown on Pt(111), comprising one layer of Fe above Pt substrates and one layer of O on top of the Fe layer (*11*). The presence of ferrous species was further verified by the characteristic x-ray photoelectron spectra (XPS) Fe $2p_{3/2}$ peak at binding energy (BE) of 709.3 eV, in comparison with the BEs of 707.3 eV from a metallic Fe film grown on Pt(111) and 711.0 eV in ferric oxide deposited on highly oriented pyrolytic graphite (fig. S1).

At the periphery of the two-dimensional (2D) FeO nanoislands, there are a number of CUF sites indicated by the decreased ratio of the measured O 1s and Fe $2p_{3/2}$ peak heights as compared with that of the monolayer FeO films grown on Pt(111). To more easily identify the changes, we deposited a fixed amount of Fe (0.25 ML) but annealed at various temperatures. In this way, the corresponding dispersion of FeO nanoislands prepared could be changed gradually. To quantify the dispersion, we defined the specific periphery density (SPD) as the length of the periphery of FeO nanoislands per unit area of the Pt substrate. As shown in Fig. 1B, the ratios of O/Fe XPS signals measured from 0.25 ML FeO nanoislands with different dispersions are all less than that of the monolayer stoichiometric FeO film on Pt(111). This shows that the FeO nanoislands are oxygen-deficient. Moreover, the ratio of O/Fe XPS signals decreases monotonically as the SPD increases. This means that the oxygen deficiency mainly occurs at the peripheries of FeO nanoislands, and the corresponding ferrous Fe atoms there are coordinatively unsaturated (denoted as FeO_{1-x}/Pt(111), $x < 1$).

XPS and ultraviolet photoelectron spectroscopy (UPS) were used to study CO oxidation on the 0.25 ML FeO_{1-x}/Pt(111) surfaces. Because of the strong bonding of CO on Pt (*12*), the exposed Pt(111) surface would be saturated by CO even at room temperature (RT). In contrast, the FeO surface is inert for CO adsorption at RT (*13*). This can be seen from fig. S2, in which the O 1s peak from the adsorbed CO decreases linearly with the coverage of the FeO nanoislands. To investigate the reactivity of the FeO_{1-x}/Pt(111) surfaces, we first presaturated the samples with CO. Afterward, a steady-state flux of O_2 at nominally 5.2×10^{-8} mbar was leaked into the chamber at RT. The removal of CO was studied by monitoring the variation of the characteristic in situ UPS peaks at a BE of 9.4 eV from 5σ and 1π states of adsorbed CO (*14*). On the FeO_{1-x}/Pt(111) surfaces, the adsorbed CO was found to react off by O_2 exposure within 5 min, whereas Pt(111) shows negligible activity under the same conditions. The reaction rate was determined on the basis of the UPS intensity versus the reaction time plots (fig. S3). In Fig. 1C, the rate of CO removal is plotted as a function of the SPD of the FeO nanoislands, and a linear correlation between the rate and SPD can be seen. This shows unambiguously that the CUF sites at the peripheries of the FeO nanoislands on Pt(111) are the active sites for CO oxidation.

If the prepared 2D FeO nanoislands were oxidized further (to 1.3×10^{-6} mbar O_2, 673 K) to 3D ferric oxide nanoislands [denoted as FeO_{1+x}/Pt(111)], the corresponding reactivity was remarkably lower at RT (fig. S4). Considerable reactivity could only be found when the temperature was higher than 400 K (*15*). The reactivities of metallic Fe overlayers grown on Pt(111) and Pt(111) with subsurface Fe were lowered too (fig. S4). Among various model systems considered, the FeO_{1-x}/Pt(111) surface presents the highest reactivity because of the presence of the CUF sites.

Density functional theory (DFT) calculations were performed in order to reveal the origin of the high reactivity of the FeO_{1-x}/Pt(111) surfaces (*10*). First, calculated adsorption energies for CO and O_2 on Pt(111) (0.25 ML) are –1.64 eV per CO molecule and –0.71 eV per O_2 molecule (Fig. 2A). The substantially larger adsorption energy of CO than O_2 by about one eV indicates that Pt(111) tends to be covered by CO, which would block the sites for O_2 adsorption and activation. Thus, CO oxidation on Pt(111) would be hindered by adsorbed CO at modest temperatures despite that the calculated reaction barrier (0.85 eV) between CO and dissociated O is not high, which agrees well with previous experiments (*16*).

In contrast, FeO_{1-x}/Pt(111) shows a much higher reactivity for O_2 activation (fig. S5). Depending on the CUF sites, O_2 may either dissociate directly to atomic O without barrier, or adsorb molecularly first with a binding energy of about –1.51 eV per O_2 (Fig. 2A) and afterward dissociate to atomic O with a barrier of 0.42 eV [the corresponding transition state (TS) shown in Fig. 2B]. On the other hand, we find that CO adsorption at the CUF sites is unstable. The preferential adsorption and activation of O_2 over the CUF sites on the FeO_{1-x}/Pt(111) surfaces are the main reason why these surfaces do not become CO poisoned. Adsorption energy for the dissociated O atoms at the CUF sites is –1.10 eV/O. Compared with oxygen atoms adsorbed on metallic Fe or inside a 2D FeO overlayer with energy of –3.0 eV, which was too strong to be reactive, the bonding strength for

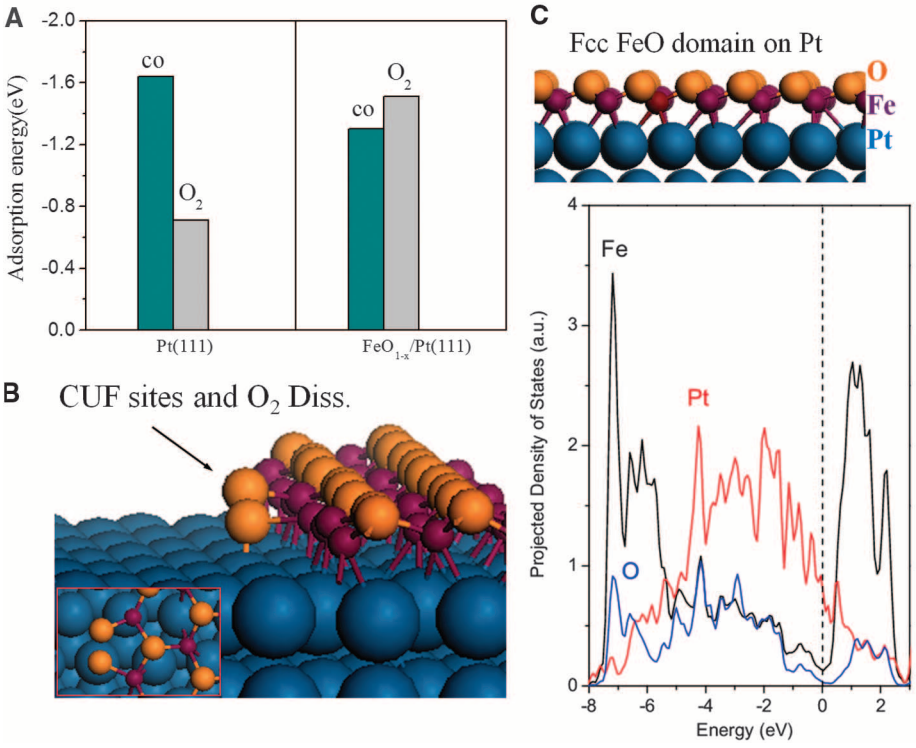

Fig. 2. (**A**) Calculated adsorption energy (in eV) for CO and O_2 molecules on Pt(111) and FeO_{1-x}/Pt(111) surfaces. (**B**) Schematic structure of the CUF sites and calculated transition states of O_2 dissociation (the inset shows the top view) at the boundary between FeO and Pt(111). (**C**) Projected density of states for interfacial Fe, O, and Pt atoms at FCC domains of FeO overalyer on Pt(111) using $(\sqrt{84} \times \sqrt{84})R10.9^0$–FeO/Pt(111) supercell. Pt, Fe, C, and O atoms are indicated by blue, purple, gray, and brown balls, respectively. For details, see figs. S5, S6, and S7 and (*10*).

O atoms at the CUF sites is optimum and would make these sites active. Indeed, the reaction barrier between O at the CUF sites and CO adsorbed on neighboring Pt atoms is only 0.63 eV (the corresponding TS is shown in fig. S6). After removal of atomic O by CO, Fe atoms at the boundary resume the coordinatively unsaturated state and get ready for O_2 adsorption and dissociation to close the cycle. In this catalytic cycle, the boundary between the FeO nanoisland and Pt provides multiple sites (CUF and Pt atoms) for O_2 activation and CO adsorption, and the CO oxidation occurs according to the bifunctional mechanism (*17*, *18*).

The formation of the CUF sites at the peripheries of the FeO nanoislands is due to the stabilization of interface confinement between the oxide overlayers and the metal supports. To verify this, we studied the interfacial interaction between FeO overlayer and Pt(111) substrate using a model of $(\sqrt{84} \times \sqrt{84})R10.9^0$ – FeO/Pt(111), and the calculated interfacial adhesion energy is 1.40 eV per FeO formula (fig. S7). The interfacial adhesion comes from the strong interaction between interfacial Fe and Pt atoms, as seen clearly from their extensive orbital hybridizations (Fig. 2C). The strong adhesion between FeO overlayers and Pt substrates stabilizes the monolayer ferrous oxide against further oxidation into ferric oxide (*19*, *20*). CO oxidation on FeO_{1-x}/Pt(111) might maintain its activity even in the presence of H_2 because dissociative adsorption of H_2 on Pt suffers from CO poisoning. Indeed, our calculations show that on 0.67-ML CO precovered Pt(111), dissociative adsorption of H_2 becomes endothermic. Meanwhile, dissociative adsorption of H_2 on FeO at RT is difficult, too (*21*, *22*). This is desirable for the preferential oxidation of CO in excess of H_2 (PROX) (*18*, *23*, *24*).

Guided by these insights, we prepared Pt-Fe [4 weight percent (wt %) Pt, 0.5 wt % Fe] nanoparticles (NPs) and Pt (4 wt %) NPs supported on nanosized silica spheres. To realize the main structural features shown above, we developed a dedicated preparation process with proper reduction at 473 K for 2 hours in H_2 (*10*). The treatment with H_2 reduces the as-prepared samples to metallic states. Transmission electron microscopy (TEM) analysis found that the metal NPs in the Pt/SiO_2 (Fig. 3A) and Pt-Fe/SiO_2 (Fig. 3B) samples are anchored evenly over the silica hosts and have a narrow distribution in average size of 2 to 3 nm and 2 to 4 nm, respectively. High-resolution TEM (HRTEM) images (Fig. 3, A and B, insets) show that NPs over both Pt/SiO_2 and Pt-Fe/SiO_2 samples present the same face-centered cubic (FCC) Pt lattice with a Pt(111) interlayer spacing of 0.23 nm. This means that the cores of the Pt-Fe NPs are still dominated by Pt. This was further corroborated through x-ray diffraction (XRD) measurements. There is no shift of 2θ value for the Pt-Fe NPs compared to the Pt/SiO_2 sample observed (fig. S8), and the formation of PtFe bulk alloy in the Pt-Fe NPs is excluded. We performed an energy-dispersive x-ray spectroscopic (EDX) mapping and point analysis over dozens of the Pt-Fe NPs, and found that Fe signal is accompanied exclusively with Pt signal (fig. S9). These show that Fe species are present mainly on the outer layers of the Pt-Fe NPs. However, Fe does not completely cover Pt-Fe NPs because there is a considerable amount of CO adsorbed on Pt-Fe/SiO_2 samples, as seen from temperature-programmed desorption (TPD) experiments (fig. S10). Correspondingly, the structure of the prepared Pt-Fe NPs consists of the Pt NPs with Fe patches on the surfaces.

CO PROX reactions under stoichiometric condition (1% CO and 0.5% O_2, 98.5% H_2, 0.1 M Pa, 36000 ml g^{-1} h^{-1}) are conducted on the Pt-Fe/SiO_2 and Pt/SiO_2 catalysts. The corresponding activity and selectivity were measured from the temperature-dependent reaction profiles (Fig. 3, C and D). For the Pt/SiO_2 catalysts, CO conversion is negligible below RT, but increases slowly with temperature. At 473 K, only 70% CO was reacted off. In contrast, the Pt-Fe/SiO_2 catalysts show a high activity, with almost 100% CO conversion and 100% CO selectivity at RT. At 353 K, the catalysts have 95% CO conversion and 95% selectivity, which remain high. Even at 200 K, the Pt-Fe/SiO_2 catalysts maintain 20% CO conversion and 100% CO selectivity. We measured the oxidation state of the Fe species under reaction conditions using in situ x-ray adsorption spectroscopy (XAFS) performed in the beamline of BL14W1 in the Shanghai Synchrotron Radiation Facility (SSRF) (fig. S11). Compared with the Fe K-edge XAFS spectra from the reduced and fully oxidized Pt-Fe catalysts, the pre-edge feature from the Pt-Fe NPs under the reaction conditions was located in the middle. This shows the presence of ferrous species under the operating conditions. Thus, the highly active Pt-Fe NPs in the CO PROX reaction should comprise Pt-rich core and ferrous species on the surfaces, restoring the characteristics of the FeO_{1-x}/Pt(111) model system described in the above model system.

The Pt-Fe catalysts prepared are very stable, and no deterioration of their performance was found after 40 hours at RT (fig. S12). Under PEMFC working conditions operated typically at 353 to 373 K, there are considerable amounts of water and CO_2 present. We tested the Pt-Fe catalysts under the realistic PEMFC conditions. As plotted in fig. S13, the catalysts were stable and showed good performances, with 92% CO selectivity/conversion at 353 K. By using slight excess of O_2, CO can be removed to a level lower than 1 part per million (fig S14). We also assembled the Pt-Fe nanocatalysts into a 1-kW PEMFC working system. We found that the cell performance stays quite stable after a 930-hour test but deactivates quickly after a 30-min test without using the Pt-Fe catalyst (fig. S15). Extraordinary activity and stability of the Pt-Fe catalysts under the operating conditions suggests that the Pt-Fe nanocatalysts prepared are eligible for industrial applications.

We demonstrated a strategy of preparing coordinatively unsaturated metal sites with lower valent states on metal substrates by taking advantage of the confinement effects at interfaces between nanostructured oxides and metal substrates. The confined CUF sites and neighboring metal atoms show a high activity and stability in CO oxidation under realistic conditions. The concept of interface confinement and fabrication of coordinately unsaturated low-valent cations

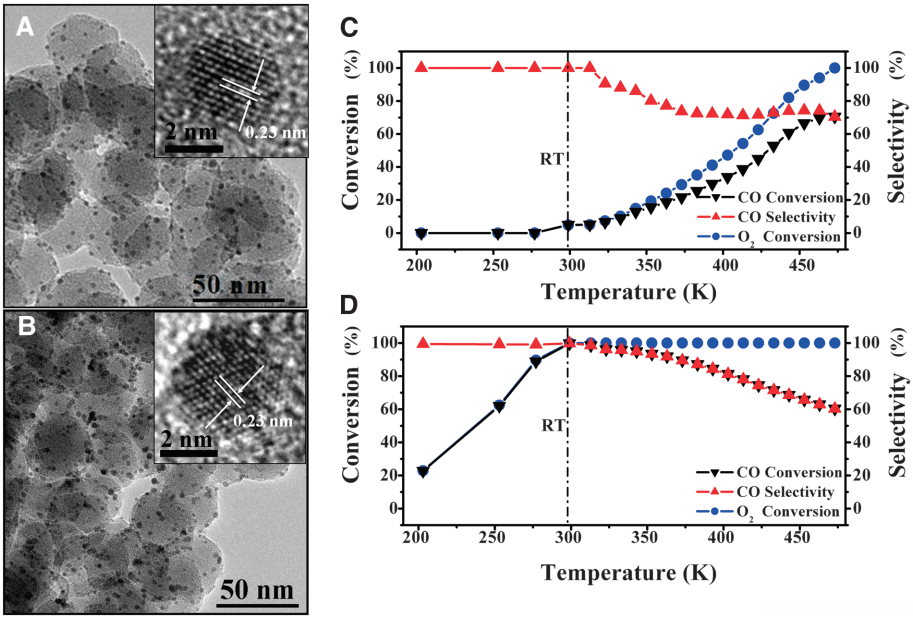

Fig. 3. TEM images of the (**A**) Pt/SiO_2 and (**B**) Pt-Fe/SiO_2 catalysts pretreated with H_2 at 473 K for 2 hours. Insets show HRTEM images. (**C** and **D**) PROX reaction of the (C) Pt/SiO_2 and (D) Pt-Fe/SiO_2 catalysts under the conditions 1% CO, 0.5% O_2, and 98.5% H_2. Space velocity is 36000 ml $g^{-1}h^{-1}$; pressure = 0.1 MPa.

could be widely applied in various heterogeneous oxides-metals catalytic systems and illustrates a promising and efficient way to design active sites for nanocatalysts.

References and Notes

1. G. A. Somorjai, J. Y. Park, *Angew. Chem. Int. Ed.* **47**, 9212 (2008).
2. K. Honkala *et al.*, *Science* **307**, 555 (2005).
3. J. H. Kwak *et al.*, *Science* **325**, 1670 (2009).
4. J. M. Thomas, *J. Chem. Phys.* **128**, 182502 (2008).
5. T. F. Jaramillo *et al.*, *Science* **317**, 100 (2007).
6. T. K. Das, M. Couture, Y. Ouellet, M. Guertin, D. L. Rousseau, *Proc. Natl. Acad. Sci. U.S.A.* **98**, 479 (2001).
7. B. Ensing, F. Buda, M. C. M. Gribnau, E. J. Baerends, *J. Am. Chem. Soc.* **126**, 4355 (2004).
8. G. I. Panov, A. K. Uriarte, M. A. Rodkin, V. I. Sobolev, *Catal. Today* **41**, 365 (1998).
9. A. Zecchina, M. Rivallan, G. Berlier, C. Lamberti, G. Ricchiardi, *Phys. Chem. Chem. Phys.* **9**, 3483 (2007).
10. Materials and methods are available as supporting material on *Science* Online.
11. W. Weiss, W. Ranke, *Prog. Surf. Sci.* **70**, 1 (2002).
12. Y. Y. Yeo, L. Vattuone, D. A. King, *J. Chem. Phys.* **106**, 392 (1997).
13. R. Meyer *et al.*, *Surf. Sci.* **586**, 174 (2005).
14. T. Ma *et al.*, *ChemPhysChem* **10**, 1013 (2009).
15. Y. N. Sun *et al.*, *J. Catal.* **266**, 359 (2009).
16. C. Campbell, G. Ertl, H. Kuipers, J. Segner, *J. Chem. Phys.* **73**, 5862 (1980).
17. J. A. Rodriguez *et al.*, *Science* **318**, 1757 (2007).
18. M. Kotobuki, A. Watanabe, H. Uchida, H. Yamashita, M. Watanabe, *J. Catal.* **236**, 262 (2005).
19. Q. Fu, T. Wagner, *Surf. Sci. Rep.* **62**, 431 (2007).
20. F. P. Netzer, *Surf. Rev. Lett.* **9**, 1553 (2002).
21. L. R. Merte *et al.*, *Surf. Sci.* **603**, L15 (2009).
22. W. X. Huang, W. Ranke, *Surf. Sci.* **600**, 793 (2006).
23. X. S. Liu, O. Korotkikh, R. Farrauto, *Appl. Catal. A Gen.* **226**, 293 (2002).
24. S. Alayoglu, A. U. Nilekar, M. Mavrikakis, B. Eichhorn, *Nat. Mater.* **7**, 333 (2008).

25. We gratefully acknowledge the Natural Science Foundation of China, Chinese Academy of Sciences, and Ministry of Science and Technology of China for the support of this work. We thank the SSRF and Sunrise Power Co. for the beamline and assistance with the PEMFC test.

Supporting Online Material

www.sciencemag.org/cgi/content/full/328/5982/1141/DC1
Materials and Methods
Figs. S1 to S15
References

12 February 2010; accepted 19 April 2010
10.1126/science.1188267

Self-Assembled $M_{24}L_{48}$ Polyhedra and Their Sharp Structural Switch upon Subtle Ligand Variation

Qing-Fu Sun,[1] Junji Iwasa,[1] Daichi Ogawa,[1] Yoshitaka Ishido,[1] Sota Sato,[1] Tomoji Ozeki,[2] Yoshihisa Sei,[3] Kentaro Yamaguchi,[3] Makoto Fujita[1]*

Self-assembly is a powerful technique for the bottom-up construction of discrete, well-defined nanoscale structures. Large multicomponent systems (with more than 50 components) offer mechanistic insights into biological assembly but present daunting synthetic challenges. Here we report the self-assembly of giant $M_{24}L_{48}$ coordination spheres from 24 palladium ions (M) and 48 curved bridging ligands (L). The structure of this multicomponent system is highly sensitive to the geometry of the bent ligands. Even a slight change in the ligand bend angle critically switches the final structure observed across the entire ensemble of building blocks between $M_{24}L_{48}$ and $M_{12}L_{24}$ coordination spheres. The amplification of this small initial difference into an incommensurable difference in the resultant structures is a key mark of emergent behavior.

Chemists are often inspired by the spontaneous and precise assembly of multiple protein subunits into giant, well-defined, functional superstructures (*1*, *2*). Spherical virus capsids, consisting of hundreds to thousands of identical protein subunits, are simple and accessible examples of biological self-assembly and have been extensively studied (*3*, *4*) and mimicked on a much smaller scale. Most virus capsids are polyhedra assembled from 60*T* subunits, where *T* is a mathematically defined triangulation number, and *T* = 1, 3, 4, 7, 13, and 16 are naturally occurring values (*5*, *6*). As a result, the possible final capsid polyhedral structures are limited by simple geometrical constraints.

Similar geometrical constraints have often been used in artificial multicomponent self-assembly (*7*–*26*). The formation of roughly spherical polyhedra with a general formula of M_nL_{2n} is predicted when metal ions with square planar coordination sphere (M) and rigid bent ligands (L) are mapped onto the vertices and edges, respectively, of the polyhedra. For entropically favored regular or semiregular polyhedra, *n* is limited by geometrical constraints to be 6, 12, 24, 30, or 60 (Fig. 1A) (*27*), and spherical coordination assemblies have been reported for *n* = 6 (*25*) and 12 (*10*, *26*) but not for larger *n* values. Here we report the self-assembly of the giant, 5-nm-diameter $M_{24}L_{48}$ spherical framework **2** (where *n* = 24) from square planar Pd^{2+} ions and bent dipyridylthiophene ligand **1** (Fig. 1B). The formation of this 72-component system is highly sensitive to the ligand geometry. We previously reported that the smaller 36-component $M_{12}L_{24}$ coordination sphere **4** (*n* = 12) forms when the analogous dipyridylfuran ligand **3** is used (Fig. 1C) (*10*). Systematically varying the mean ligand angle by mixing **1** and **3** in various ratios revealed that even a slight change in the mean ligand bend angle critically switches the final structure between $M_{24}L_{48}$ and $M_{12}L_{24}$ coordination spheres. The amplification of a small initial difference into an incommensurable difference in the resultant structures is a key mark of emergent behavior. Emergent phenomena are attracting considerable current interest (*28*–*30*) and usually refer to the emergence of macroscopic differences based on microscopic differences. We believe that our results are a good example of chemical emergence because an incommensurable difference is observed at a molecular level. By demonstrating, in an artificial system, emergent behavior on similar scale to that observed in the assembly of biological structures, we provide a synthetically simple system for the mechanistic scrutiny of massive multicomponent self-assembly. In addition, we extend the scale and the practical feasibility of using self-assembly as a powerful bottom-up technology for the construction of discrete nanoscale systems.

Ligands **1a** to **1c** were synthesized in a single step from 4-pyridyl pinacol boronate ester and the corresponding 2,5-dihalothiophenes in reasonable yields by using the Suzuki-Miyaura procedure (*31*). When ligand **1a** (10 μmol) and $Pd(NO_3)_2$ (5.0 μmol) were heated in dimethyl sulfoxide-d_6 (DMSO-d_6) (0.7 ml) at 70°C for 17 hours, two broad peaks were observed in the ^{1}H nuclear magnetic resonance (NMR) spectrum (Fig. 2B). The peak at 9.2 parts per million (ppm) was assigned to PyH_α (Py = pyridyl) and the peak at 8.0 ppm was assigned to the superimposed PyH_β and thiophene protons, where α and β indicate the two positions on the pyridinyl group. The broad ^{1}H and ^{13}C signals are indicative of a very large complex, the tumbling motion of which is slow on the NMR time scale. Diffusion-ordered NMR spectroscopy (DOSY) evinced a single product with a single band at diffusion coefficient $D = 3.3 \times 10^{-11}$ m^2•s^{-1} (log$D$ = –10.49) (Fig. 2C), which is indicative of a much larger structure than $M_{12}L_{24}$ coordination sphere **4**, which has a log$D$ value of –10.3. A quantitative yield was confirmed by ^{1}H (one-dimensional and DOSY) and ^{13}C NMR spectra and mass spectrometry (MS). The coordination of ligands **1b** and **1c** with

[1]Department of Applied Chemistry, School of Engineering, The University of Tokyo and Core Research for Evolutional Science and Technology (CREST), Japan Science and Technology Corporation (JST), 7-3-1 Hongo, Bunkyo-ku, Tokyo 113-8656, Japan. [2]Department of Chemistry and Materials Science, Tokyo Institute of Technology, 2-12-1 O-okayama, Meguro-ku, Tokyo 152-8551, Japan. [3]Faculty of Pharmaceutical Sciences at Kagawa Campus, Tokushima Bunri University, 1314-1 Shido, Sanuki, Kagawa 769-2193, Japan.

*To whom correspondence should be addressed. E-mail: mfujita@appchem.t.u-tokyo.ac.jp

$Pd(NO_3)_2$ gave similar spectra, and the ^1H NMR spectra of **2c** resolved into two sets of signals, in a 1:1 ratio, consistent with two inequivalent ligands in the $M_{24}L_{48}$ rhombicuboctahedral structure of **2c** (Fig. 3 and figs. S10 to S16).

The $M_{24}L_{48}$ composition of **2b** was first established by ultrahigh-resolution cold-spray ionization time-of-flight mass spectrometry (CSI-TOF-MS) (*32*). The molecular weight of sphere **2b** $\{[Pd_{24}(C_{14}H_9BrN_2S)_{48}]^{48+}\bullet 48(BF_4^-)\}$ was calculated to be 21,946.73 daltons, confirming the $M_{24}L_{48}$ composition, from the series of prominent peaks for $[\mathbf{2b} - (BF_4^-)_m]^{m+}$ (m = 28 to ~15) (Fig. 2D). The resolution of each peak was quite high [>45,000 based on full width at half maximum (*33*) (table S2)] and the isotope distribution closely matched the simulated spectrum (error = <3.5 ppm) (Fig. 2E). Similar CSI-TOF-MS spectra were observed for $M_{24}L_{48}$ structures **2a** and **2c** (*31*).

Structural confirmation of the $M_{24}L_{48}$ coordination geometry was provided by x-ray crystallographic analysis. X-ray–quality single crystals were obtained by the slow diffusion of ethyl acetate vapor into a DMSO:CH_3CN (1:1) solution of **2c** (PF_6^- salt). The sheer number of disordered, amorphous solvent molecules and counter ions that were expected for the expansive hollow framework of **2c** required that synchrotron x-ray radiation was used to collect high-quality data (*34*).

Mapping the 48 ligands to edges and 24 metal ions to vertices, the framework $M_{24}L_{48}$ **2c** forms a rhombicuboctahedron, which is an Archimedean solid with eight triangular and 18 rectangular faces (26 in total), with one triangle and three rectangles meeting at each vertex. The rhombicuboctahedral structure of **2c** is highly spherical with the 5.0-nm-diameter circumscribed and 3.6-nm-diameter inscribed spheres defining the molecular shell. The distance between antipodal palladium atoms is 4.0 nm, much longer than that in the smaller $M_{12}L_{24}$ sphere **4** (2.6 nm) (*10*). The spherical $M_{24}L_{48}$ framework demarcates a huge void space, and the framework occupies less than 20% of the total cell volume; disordered solvent molecules and counter ions occupied the remaining 80%. Despite many trials for collecting better diffraction data, we were unable to refine the solvents within the sphere **2c** because of their severe disorder. Given the giant, hollow structure of **2c**, the modest residual index based on the observed structure factor F_0 (R_1) value (22%) is quite reasonable.

Bipyridyl ligands **1** and **3** are isomorphic, differing by the substitution of a single sulfur atom for oxygen, and yet they combine with palladium ions to give coordination spheres of different scale (5 nm versus 3.5 nm) and disparate composition ($M_{24}L_{48}$ versus $M_{12}L_{24}$). The difference in the final polyhedral structure presumably arises from the slight difference in ligand bend angle [149° in **1** and 127° in **3**, based on a density functional theory (DFT) calculation at B3LYP/631-G+ level] stemming from the longer

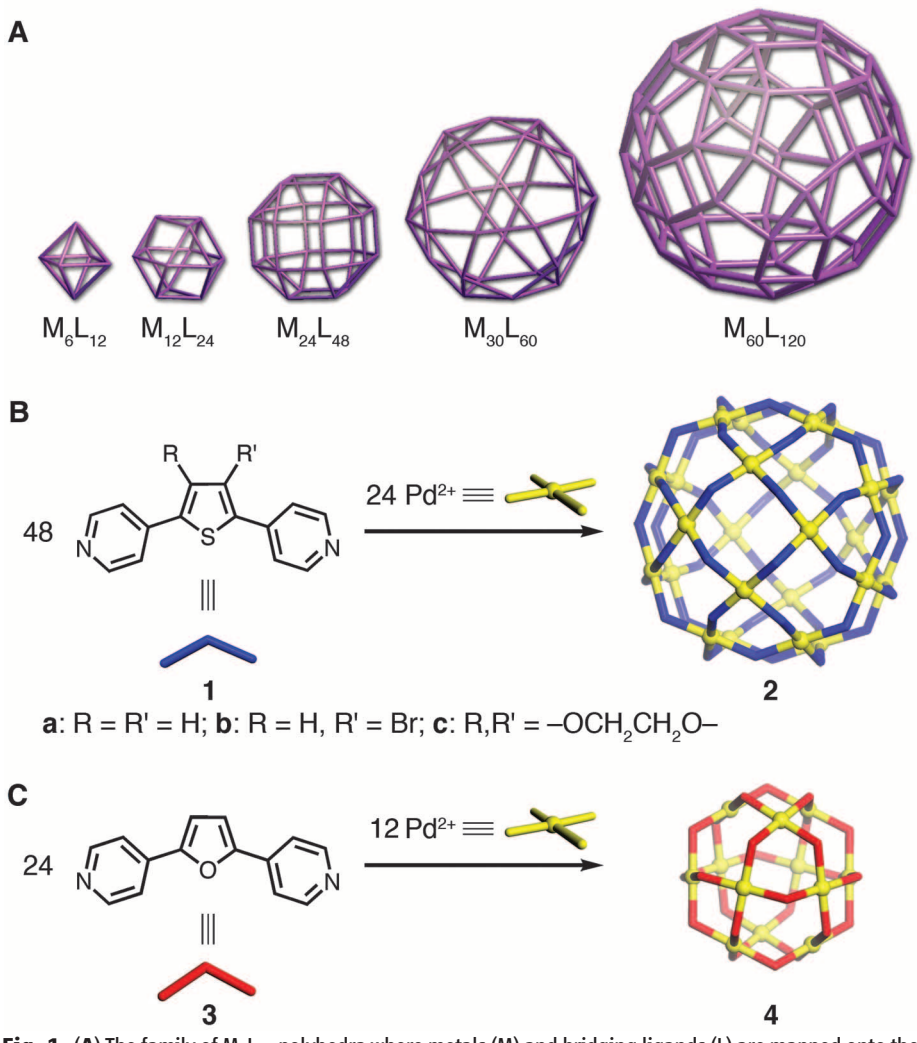

Fig. 1. (**A**) The family of M_nL_{2n} polyhedra where metals (M) and bridging ligands (L) are mapped onto the vertices and edges, respectively, of the polyhedra. (**B**) Self-assembly of $M_{24}L_{48}$ spheres **2**. (**C**) Self-assembly of $M_{12}L_{24}$ sphere **4**.

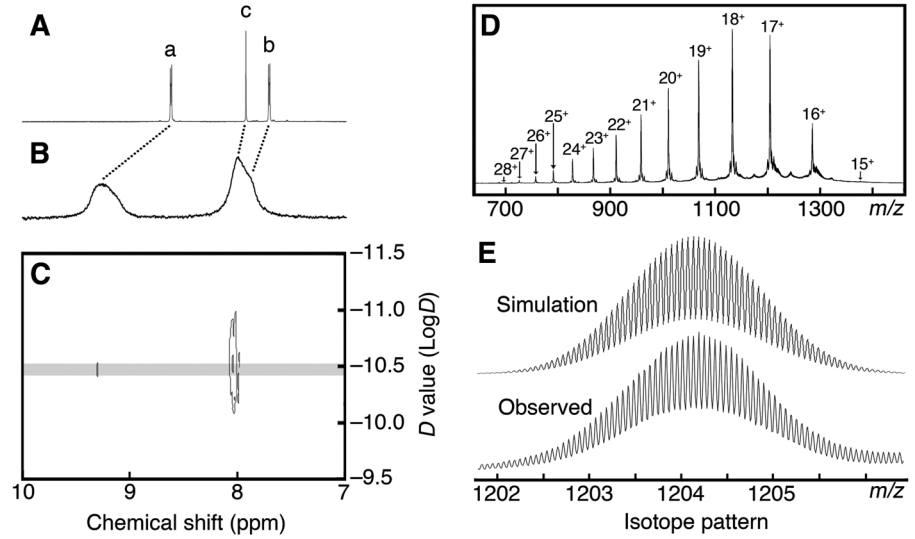

Fig. 2. ^1H NMR spectra (500 MHz, DMSO-d_6, 300 K) of (**A**) ligand **1a** and (**B**) sphere **2a** (NO_3^- salt). Signals a, b, and c in (A) denote PyH_α, PyH_β, and thiophene protons, respectively. (**C**) ^1H DOSY spectrum of **2a** (500 MHz, DMSO-d_6, 300 K). (**D**) CSI-TOF mass spectrum recorded on maXis spectrometer of sphere **2b** (BF_4^- salt). (**E**) Expanded spectrum of the 17^+ peak in (D) and the simulated spectrum.

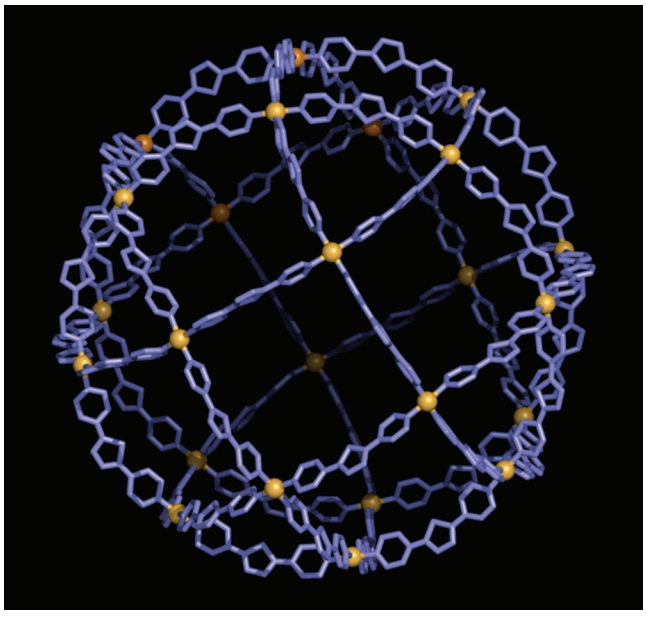

Fig. 3. The crystal structure of **2c**. Two counter ions (PF_6^-) that are present at the apical positions of each Pd^{2+} center and the $-OCH_2CH_2O-$ substituent on each thiophene ring are omitted for clarity. Crystal data: Space group $I\bar{4}$, $a = b = 47.527(1)$ Å, $c = 68.663(1)$ Å, $V = 155097(5)$ Å^3, $Z = 2$, $T = 293$ K. Numbers in parentheses indicate the estimated standard deviations. Anisotropic least-squares refinement for palladium and sulfur atoms and isotropic refinement for the other atoms on 39,679 independent merged reflections ($R_{int} = 0.0804$) converged at the residual index based on F_0^2 $wR_2 = 0.5427$ for all data; residual $R_1 = 0.2222$ for 16,668 observed data [$I > 2\sigma(I)$], and goodness of fit = 1.701.

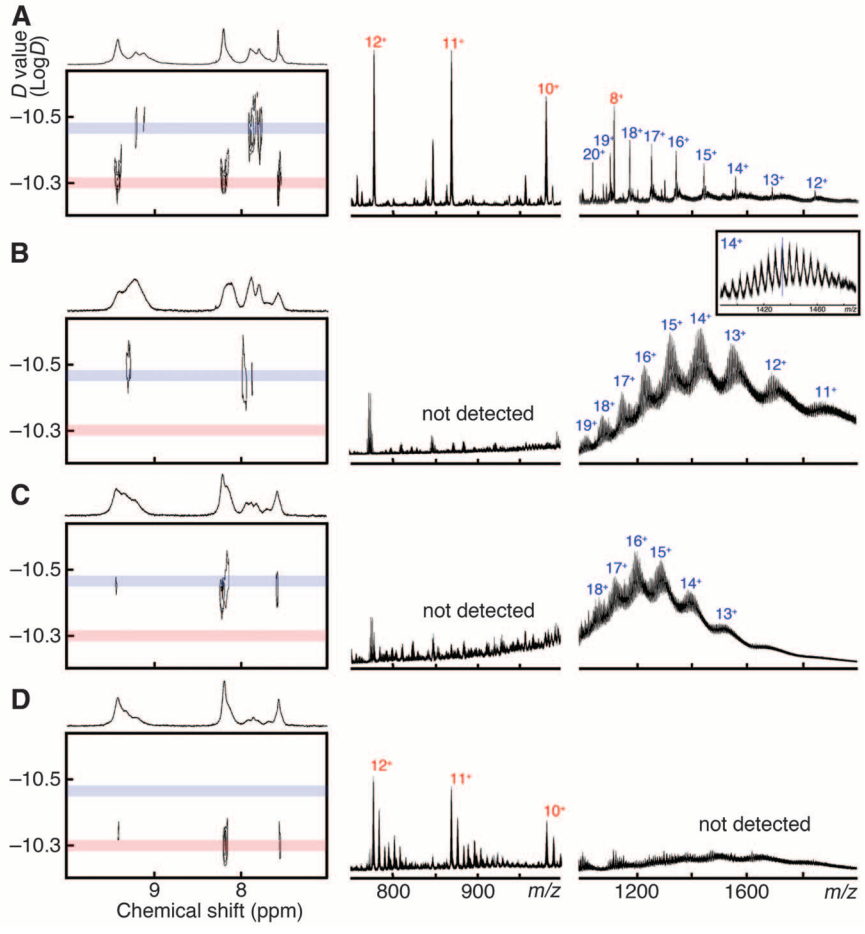

Fig. 4. The DOSY NMR spectra (500 MHz, DMSO-d_6, 300 K) and CSI-TOF mass spectra (CH_3CN:DMSO = 9:1, OTf^- salt) for (**A**) the 1:1 mixture of individually prepared **2c** and **4**, and for the reaction of (**B**) 1:1, (**C**) 3:7, and (**D**) 2:8 mixtures of ligand **1c** and ligand **3** with Pd^{2+}. $M_{12}L_{24}$ and $M_{24}L_{48}$ are indicated in blue and red, respectively, and the mass spectra excerpts show the $M_{12}L_{24}$ region on the left (mass/charge ratio $m/z = 750$ to 1000) and the $M_{24}L_{48}$ region on the right ($m/z = 1000$ to 2000). An inset in (B) is a magnified view for the 14^+ region displaying a series of $[Pd_{24}(\mathbf{1c})_m(\mathbf{3})_{48-m} - (OTf^-)_{14}]^{14+}$. The center peak marked with a blue line is assigned for $m = 24$.

C–S bond (1.80 Å) in thiophene compared with the C–O bond (1.39 Å) in furan. In an ideal rhombicuboctahedron ($M_{24}L_{48}$) or cuboctahedron ($M_{12}L_{24}$), the edges adopt angles of 135° or 120°, respectively, assuming perfectly square-planar vertices. In terms of enthalpy, ligand **1** should favor assembly into a less-distorted rhombicuboctahedron, whereas ligand **3** should lie on the midline between angles favoring a cuboctahedron versus a rhombicuboctahedron. The selective formation of $M_{12}L_{24}$ from ligand **3** is rationalized by reduced loss of entropy for $M_{12}L_{24}$ than for $M_{24}L_{48}$ (which incorporates more components). If ligand **1** were to form a $M_{12}L_{24}$ cuboctahedron, substantial pinching and distortion would offset the entropic advantage; thus the enthalpically favored $M_{24}L_{48}$ forms instead.

The question then arises, which structure forms given a mixture of ligands **1** and **3**? The ligands could exclusively self-organize into distinct $M_{12}L_{24}$ and $M_{24}L_{48}$ structures, or else assemble into a statistical mixture, wherein a varied ligand ratio could offer systematic, continuous modulation of the ligand bend angle from 127° to 149° (for example, the mean bend angle of a 1:1 mixture of **1c** and **3** is 138°). When Pd^{2+} ions were added to a 1:1 mixture of **1c**:**3** (M:L ratio = 1:2), both DOSY and CSI-TOF-MS revealed the selective formation of a $M_{24}L_{48}$ structure. In the DOSY spectrum, all signals exhibit a single diffusion coefficient ($\log D = -10.45$) that is characteristic of the $M_{24}L_{48}$ complex. Only $M_{24}L_{48}$ complexes were observed by CSI-TOF-MS; a series of prominent peaks corresponded to $[Pd_{24}(\mathbf{1c})_m(\mathbf{3})_{48-m} - (OTf^-)_n]^{n+}$ (with m values from 16 to 32 and n values from 11 to 19) and no peaks were detected in the $M_{12}L_{24}$ regions (Fig. 4B). DOSY and TOF-MS analysis of a 1:1 mixture of individually prepared spheres **2** and **4** (Fig. 4A) confirmed that the spheres **2** and **4** are distinct and distinguishable and that these methods are reliable for analyzing $M_{12}L_{24}/M_{24}L_{48}$ mixtures.

The ratio of ligand **1c** and **3** was then varied sequentially from 9:1 to 1:9, and, surprisingly, only pure $M_{12}L_{24}$ or $M_{24}L_{48}$ was observed (Table 1). Starting from 100% of ligand **1**, $M_{24}L_{48}$ assembled exclusively until the ratio of **1c**:**3** was 2:8 (Fig. 4C),

Table 1. Self-organization criticality of **1c** and **3** mixtures.

1c:3 ratio (angle)*	Product
10:0 (149.3)	$M_{24}L_{48}$ only
9:1 (147.1)	$M_{24}L_{48}$ only
8:2 (144.8)	$M_{24}L_{48}$ only
7:3 (142.6)	$M_{24}L_{48}$ only
6:4 (140.3)	$M_{24}L_{48}$ only
5:5 (138.1)	$M_{24}L_{48}$ only
4:6 (135.9)	$M_{24}L_{48}$ only
3:7 (133.6)	$M_{24}L_{48}$ only
2:8 (131.4)	$M_{12}L_{24}$ only
1:9 (129.1)	$M_{12}L_{24}$ only
0:10 (126.9)	$M_{12}L_{24}$ only

*Mean bent angle (°).

whereupon a threshold was passed and $M_{12}L_{24}$ was exclusively observed (Fig. 4D). This self-organized criticality is reminiscent of emergent behavior observed in complex systems and patterns arising from a multiplicity of simple interactions, such as the emergence of complex biological structures from simple polypeptides (*30*).

With this example, artificial multicomponent self-assembly edges yet closer to the massive scale of biological self-assembly and provides a synthetically simple system for a deeper mechanistic understanding of emergent behavior.

References and Notes

1. R. W. Horne, *Virus Structure* (Academic Press, New York, 1974).
2. S. Casjens, *Virus Structure and Assembly* (Jones and Bartlett, Boston, 1985).
3. J. M. Grimes *et al*., *Nature* **395**, 470 (1998).
4. W. R. Wikoff *et al*., *Science* **289**, 2129 (2000).
5. D. L. D. Caspar, A. Klug, *Cold Spring Harbor Symp. Quant. Biol.* **27**, 1 (1962).
6. R. Twarock, *Philos. Trans. R. Soc. London Ser. A* **364**, 3357 (2006).
7. R. W. Saalfrank, A. Stark, K. Peters, H. G. Schnering, *Angew. Chem. Int. Ed. Engl.* **27**, 851 (1988).
8. M. Fujita *et al*., *Nature* **378**, 469 (1995).
9. N. Takeda, K. Umemoto, K. Yamaguchi, M. Fujita, *Nature* **398**, 794 (1999).
10. M. Tominaga *et al*., *Angew. Chem. Int. Ed.* **43**, 5621 (2004).
11. D. L. Caulder, R. E. Powers, T. N. Parac, K. N. Raymond, *Angew. Chem. Int. Ed.* **37**, 1840 (1998).
12. D. L. Caulder, K. N. Raymond, *Acc. Chem. Res.* **32**, 975 (1999).
13. P. J. Stang, B. Olenyuk, D. C. Muddiman, R. D. Smith, *Organometallics* **16**, 3094 (1997).
14. B. Olenyuk, J. A. Whiteford, A. Fechtenkötter, P. J. Stang, *Nature* **398**, 796 (1999).
15. B. Olenyuk, M. D. Levin, J. A. Whiteford, J. E. Shield, P. J. Stang, *J. Am. Chem. Soc.* **121**, 10434 (1999).
16. S. R. Seidel, P. J. Stang, *Acc. Chem. Res.* **35**, 972 (2002).
17. B. F. Abrahams, S. J. Egan, R. Robson, *J. Am. Chem. Soc.* **121**, 3535 (1999).
18. A. Müller, P. Kögerler, A. W. M. Dress, *Coord. Chem. Rev.* **222**, 193 (2001).
19. A. Müller, S. Roy, *Coord. Chem. Rev.* **245**, 153 (2003).
20. M. Eddaoudi *et al*., *J. Am. Chem. Soc.* **123**, 4368 (2001).
21. D. J. Tranchemontagne, Z. Ni, M. O'Keeffe, O. M. Yaghi, *Angew. Chem. Int. Ed.* **47**, 5136 (2008).
22. B. Moulton, J. Lu, A. Mondal, M. J. Zaworotko, *Chem. Commun. (Camb.)* (9): 863 (2001).
23. L. R. MacGillivray, J. L. Atwood, *Nature* **389**, 469 (1997).
24. M. M. Conn, J. Rebek Jr., *Chem. Rev.* **97**, 1647 (1997).
25. K. Suzuki, M. Tominaga, M. Kawano, M. Fujita, *Chem. Commun. (Camb.)* (13): 1638 (2009).
26. S. Sato *et al*., *Science* **313**, 1273 (2006).
27. H. S. M. Coxeter, *Regular Polytopes* (Dover Publications, New York, ed. 3, 1973).
28. P. Bak, C. Tang, K. Wiesenfeld, *Phys. Rev. Lett.* **59**, 381 (1987).
29. N. Krasnogor, S. Gustafson, D. A. Pelta, J. L. Verdegay, Eds., *Systems Self-Assembly: Multidisciplinary Snapshots*, vol. 5 of *Studies in Multidisciplinary Series* (Elsevier, Amsterdam, 2008).
30. H. J. Jensen, *Self-Organized Criticality: Emergent Complex Behavior in Physical and Biological Systems*, Cambridge Lecture Notes in Physics (Cambridge Univ. Press, Cambridge, 2003).
31. Materials, methods, and additional figures are available as supporting material on *Science* Online.
32. K. Yamaguchi, *J. Mass Spectrom.* **38**, 473 (2003).
33. P. Price, *J. Am. Soc. Mass Spectrom.* **2**, 336 (1991).
34. The *Cambridge Crystallographic Data Centre* (CCDC) entry 765717 contains the supplementary crystallographic data for this paper. These data can be obtained free of charge via www.ccdc.cam.ac.uk/conts/retrieving.html (or from the Cambridge Crystallographic Data Centre, 12 Union Road, Cambridge CB2 1EZ, UK; fax: (+44) 1223-336-033; or e-mail: deposit@ccdc.cam.ac.uk).

35. This work was supported by the Japanese Ministry of Education, Culture, Sports, Science and Technology (MEXT) via Grant-in-Aids for Scientific Research on Innovative Areas "Emergence in Chemistry" (20111007) and for Young Scientists (A) (21685007). The experiments of synchrotron x-ray crystallography were performed at the BL38B1 in the SPring-8 with the approval of the Japan Synchrotron Radiation Research Institute (JASRI) (proposal number 2009B1967) and at the NW2A beamline in the advanced ring for pulse x-rays (PF-AR) with the approval of the High Energy Accelerator Research Organization (KEK) (proposal number 2009G502). We thank N. Iwasaki and M. Pelzing (Bruker Daltonics) for the support of CSI-TOF-MS measurements and K. Miura (JASRI) for the support of synchrotron x-ray measurements.

Supporting Online Material

www.sciencemag.org/cgi/content/full/science.1188605/DC1
Materials and Methods
Figs. S1 to S31
Tables S1 to S4
References

22 February 2010; accepted 13 April 2010
Published online 29 April 2010;
10.1126/science.1188605
Include this information when citing this paper.

Ventilation of the Deep Southern Ocean and Deglacial CO_2 Rise

L. C. Skinner,[1]* S. Fallon,[2] C. Waelbroeck,[3] E. Michel,[3] S. Barker[4]

Past glacial-interglacial increases in the concentration of atmospheric carbon dioxide (CO_2) are thought to arise from the rapid release of CO_2 sequestered in the deep sea, primarily via the Southern Ocean. Here, we present radiocarbon evidence from the Atlantic sector of the Southern Ocean that strongly supports this hypothesis. We show that during the last glacial period, deep water circulating around Antarctica was more than two times older than today relative to the atmosphere. During deglaciation, the dissipation of this old and presumably CO_2-enriched deep water played an important role in the pulsed rise of atmospheric CO_2 through its variable influence on the upwelling branch of the Antarctic overturning circulation.

There is a broad consensus that glacial-interglacial atmospheric carbon dioxide (CO_2) change depends primarily on marine processes operating in the Southern Ocean (*1*–*3*). The special importance of this region is suggested by the observed link between atmospheric CO_2 and Antarctic temperature change on both orbital and millennial time scales (*4*, *5*). However, the expectation of a Southern Ocean role in past CO_2 variability is also based on strong conceptual grounds because this is the region of the global ocean where most deep water makes its first contact with the sea surface (*6*), and consequently where CO_2 that has accumulated in the deep sea can be released to the atmosphere.

One important clue regarding the ocean's potential role in atmospheric CO_2 variability comes from the record of atmospheric radiocarbon activity ($\Delta^{14}C_{atm}$), which reveals an apparent "excess" of atmospheric ^{14}C during the last glacial period relative to the present and relative to concurrent ^{14}C production rates (*7*). This apparent $\Delta^{14}C_{atm}$ excess was eliminated across the last deglaciation in two steps (*8*, *9*), each of which coincided with a sharp rise in atmospheric CO_2 (*10*) (Fig. 1, vertical lines). The widely held expectation is therefore that lowered glacial CO_2 and the rapid deglacial CO_2 rise were made possible by the sequestration of an aged, carbon-rich deep-water mass that was mixed with the atmosphere in two pulses across the deglaciation.

Although this expectation, referred to here as the "deep re-coupling hypothesis," is compelling and circumstantially supported (*2*, *11*), it has yet to be confirmed directly through marine ^{14}C ventilation reconstructions. For example, available ^{14}C evidence from the deep Pacific appears to restrict the putative aged carbon reservoir to depths of >2.8 km in this basin (*8*, *12*). Other marine ^{14}C evidence from the North Pacific and North Atlantic suggests at the very least the existence of strong ^{14}C activity gradients within the glacial ocean (*9*, *11*, *13*, *14*). The oldest water body thus identified was more than 3000 years offset from the atmosphere (*11*), although its existence and extent during the glacial before ~18 thousand years before the present (ky B.P.) remains unconfirmed. Indeed, none of the available marine ^{14}C reconstructions reveal the occurrence of a relatively aged and widely exported deep-water mass before the initiation of the so-

[1]Godwin Laboratory for Palaeoclimate Research, Department of Earth Sciences, University of Cambridge, Downing Street, Cambridge CB2 3EQ, UK. [2]Research School of Earth Sciences, Australian National University (ANU), Canberra ACT 0200, Australia. [3]Laboratoire des Sciences du Climat et l'Environnement/Institut Pierre-Simon Laplace, Laboratoire CNRS-CEA-UVSQ, Bâtiment 12, Avenue de la Terrasse, F-91198, Gif-sur-Yvette Cedex, France. [4]School of Earth and Ocean Sciences, Cardiff University, Cardiff CF10 3YE, UK.

*To whom correspondence should be addressed. E-mail: lcs32@esc.cam.ac.uk

called "mystery interval" [approximately equivalent to Heinrich Stadial 1 (HS1)] at ~17.9 ky B.P., when atmospheric CO_2 began to rise and $\Delta^{14}C_{atm}$ began to drop sharply (*8*). Here, we bridge precisely this gap by demonstrating the existence during the last glaciation of a poorly ventilated carbon pool deep in the Atlantic sector of the Southern Ocean that dissipated in two pulses across the deglaciation.

Radiocarbon analyses were performed on paired samples of (monospecific) planktonic and (mixed) benthic foraminifera from core MD07-3076 CQ (44° 4.46'S, 14°12.47'W, 3770 m). All ^{14}C samples were subjected to a rigorous cleaning procedure so as to eliminate all adhering phases other than primary carbonate (*15*). Auxiliary Mg/Ca analyses were performed on samples of the planktonic foraminifer species *Globigerina bulloides* and *Neogloboquadrina pachyderma* (left coiling) from the same core (*15*).

The site of MD07-3076 (fig. S1) currently lies on the locus of water that is spread throughout the ocean via upper-ocean and abyssal circulation limbs (*15*). It is expected that this site experienced less North Atlantic Deep Water (NADW) influence during the last glaciation, such as in the deep Cape Basin (*16*), while nevertheless remaining on the deep-water "umbilicus" that links the Atlantic with the immense Indo-Pacific.

The chronology for core MD07-3076 is based on 59 monospecific planktonic foraminifer accelerator mass spectrometry (AMS) ^{14}C dates that have been corrected for variable reservoir age effects. We applied two independent methods to constrain local reservoir age variability. First, Antarctic ice-core ages obtained via correlation of Antarctic and local sea-surface temperature trends (fig. S3) were used to derive reservoir age ranges at stratigraphic tie-points (*15*). These estimates were verified against surface reservoir ages that were inferred independently from the published chronology for core TNO57-21 (Cape Basin) (*3*). Both methods yield strikingly similar histories of reservoir age variability at the site of MD07-3076, with a large increase in surface reservoir ages occurring during HS1 in particular. Reservoir ages at the more southerly site of MD07-3076 exceed those in the Cape Basin by ~2000 years, suggesting the northward migration of the sub-Antarctic Front (and divergence) to a position between the two cores. We derived age-depth models for multiple reservoir age scenarios using the Bayesian calibration and age-modeling program *Bchron* (*17*), providing a bounded "best estimate" reservoir age scenario and chronology that uses all available chronostratigraphic constraints (ice core and marine). The resulting chronology possesses quantifiable uncertainties and is in good agreement with two independent age scales (fig. S8).

The reconstructed deep-water ventilation/reservoir age history from core MD07-3076 is illustrated in Fig. 2D [benthic-planktonic age offsets (B-P)] and Fig. 2E [benthic-atmospheric age offsets (B-Atm)]. As shown in Fig. 2, D and E, deep water in the Atlantic sector of the Southern Ocean was poorly ventilated during the last glacial period, before HS1, reaching on average ~1630 years older than the local sea surface (B-P) and 2000 to 3750 years older than the atmosphere (B-Atm). This represents an increase of between 1.6 and 3 times relative to the modern ventilation ages (modern B-P is ~550 years, and modern B-Atm is ~1250 years) (Fig. 2, D and E). During the last glacial period, and at the Last Glacial Maximum (LGM) in particular, the time scale of carbon exchange between the atmosphere and the deep Southern Ocean therefore appears to have exceeded that of the most poorly ventilated regions of the modern deep North Pacific. All else being equal, this increase in the ventilation time scale of the deep sea would have enhanced the carbon sequestration capacity of the deep ocean during the last glacial period, thus helping to reduce atmospheric CO_2.

Across the deglaciation, between the LGM and the end of the Pre-Boreal/Younger Dryas (PB-YD), the influence of exceptionally aged deep water gradually decreased at the location of MD07-3076 (Fig. 2E). This long-term trend toward better-ventilated deep water occurred in parallel with a general trend toward increased atmospheric CO_2 (Fig. 2A), a gradual reduction in Antarctic sea-ice production (Fig. 2B), and generally more negative but increasing atmospheric $\partial^{13}CO_2$ (Fig. 2C) (*18*). This time interval also coincides with a broad $\partial^{13}C$ "minimum" recorded by planktonic foraminifera in the Eastern Equatorial Pacific (EEP), which has been interpreted to reflect a combination of increased upwelling at low latitudes and increased remineralized nutrient export from the Southern Ocean (*19*, *20*). All of these records are consistent, with a "mode shift" in the exchange of CO_2 between the ocean interior and the atmosphere across the last deglaciation, resulting in a tendency for greater exchange between the atmosphere and a marine carbon pool (*18*) that was especially depleted in $\partial^{13}C$ (*19*, *21*) and $\Delta^{14}C$ (Figs. 1A and 2D).

However, closer inspection of Fig. 2 also reveals that the deglacial trends in CO_2, Antarctic

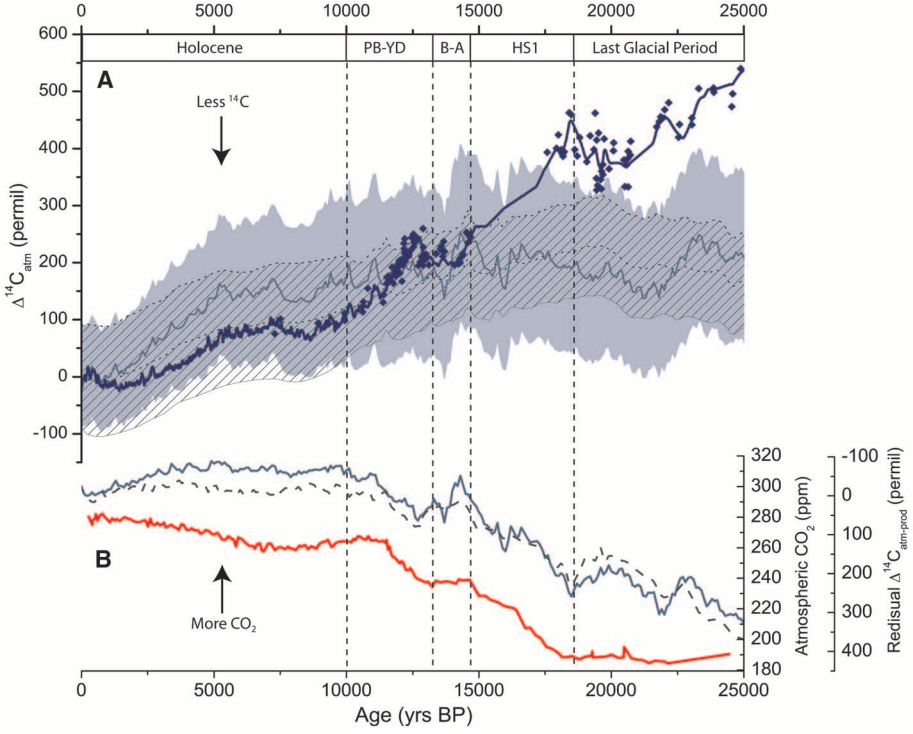

Fig. 1. Atmospheric CO_2 and radiocarbon activity ($\Delta^{14}C$) changes across the last deglaciation. (**A**) Reconstructed atmospheric $\Delta^{14}C$ [blue diamonds indicate coral data (*22*), and the blue line is the INTCAL04 calibration curve (*23*)], compared with the expected atmospheric $\Delta^{14}C$ record based only on ^{14}C-production changes, derived using the BICYCLE model (*24*) with constant modern carbon cycling, and upper and lower ^{14}C production limits from Greenland ice-core ^{10}Be fluxes (shaded area) (*25*) and global paleomagnetic field intensity (hatched area) (*26*). (**B**) Atmospheric CO_2 concentrations from the European Project for Ice Coring in Antarctica (EPICA) Dome C (EDC) ice core (red line) (*10*), including one CO_2 measurement at 24.4 ky B.P. from the Taylor Dome ice core (*27*). The CO_2 data are shown here on EDML-GICC05 equivalent ages (*15*). The gray and blue lines in (B) indicate the difference between the reconstructed $\Delta^{14}C_{atm}$ record and the median simulated production histories from paleomagnetic intensity (dashed gray line) and ^{10}Be fluxes (solid blue line). These lines indicate atmospheric $\Delta^{14}C$ changes that may be attributed to carbon cycle changes (indicated with the inverted *y* axis). Vertical lines bound two rapid drops in atmospheric $\Delta^{14}C$, which do not coincide with similar changes in ^{14}C-production but do coincide with rapid jumps in CO_2. These intervals are roughly coincident with HS1 and the YD, as indicated by the chronostratigraphic labels at the top of the graph. BA, Bølling-Allerød.

sea ice, atmospheric $\partial^{13}CO_2$, and deep-water ventilation were not monotonic. During the Antarctic Cold Reversal (ACR)/Bølling-Allerød, CO_2 (Fig. 2A) and $\partial^{13}CO_2$ (Fig. 2C) reversed their increasing trends, whereas $\Delta^{14}C_{atm}$ paused in its rapid decline (Fig. 1). In order to explain why these changes may have occurred, we identify three sets of conditions: (i) LGM, maximally extended Antarctic sea ice in conjunction with exceptionally aged circumpolar deep water (CDW) and stable but low CO_2; (ii) HS1 and YD, receding Antarctic sea ice in conjunction with relatively aged CDW and rising CO_2; and (iii) ACR/Bølling-Allerød, reduced but expanding Antarctic sea ice in conjunction with very young CDW and more elevated but approximately stable CO_2.

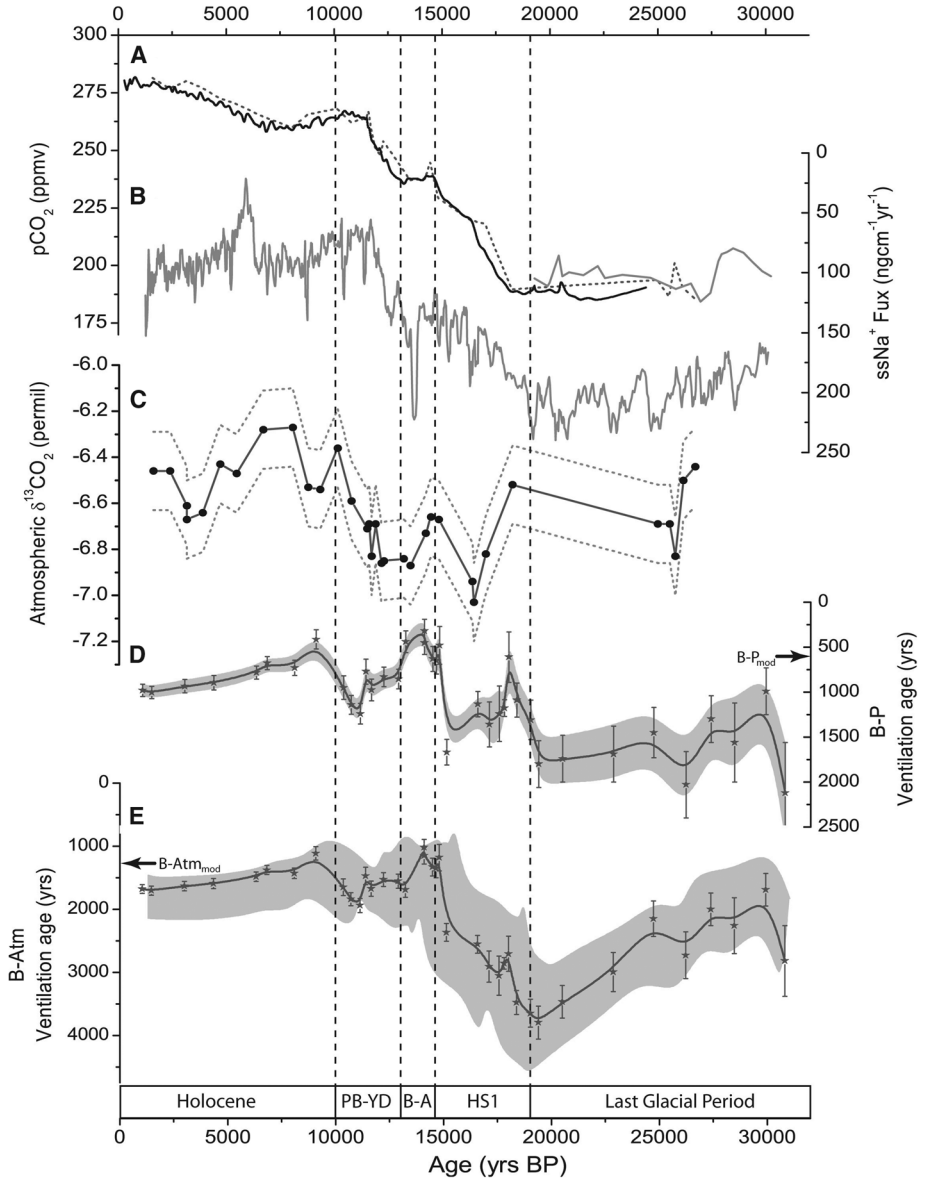

Fig. 2. Deep-water ventilation changes in the Atlantic sector of the Southern Ocean. (**A**) Atmospheric CO_2 from the EDC (*10*), Taylor Dome (*18*), and Byrd (*5*) ice cores, shown by solid dark gray, dashed, and light gray lines, respectively, and placed on the age scale of (*28*). (**B**) Sea salt–derived sodium fluxes from the EPICA Dronning Maud Land (EDML) ice core (*29*), as a regional sea-ice proxy, also on the NGRIP-GICC05 age scale. Although this is only an indirect sea ice proxy, it shows a deglacial pattern that is qualitatively similar to other marine proxy–based reconstructions. (**C**) $\partial^{13}CO_2$ measurements from the Taylor Dome Antarctic ice core (*18*), placed on the NGRIP-GICC05 age scale by alignment of CH_4 trends (*15*). Dotted lines indicate 2σ uncertainty range. (**D**) Benthic-planktonic ^{14}C age offsets in core MD07-3076 (error bars represent combined 1σ error in ^{14}C dates; shaded area indicates b-spline smoothed upper/lower limits of B-P defined by the 1σ error bars). (**E**) Apparent deep-water ventilation in core MD07-3076 (B-Atm). Heavy gray line (b-spline smoothed) and stars indicate the best estimate ventilation history and associated chronology. Vertical error ranges show the magnitude of combined planktonic/benthic ^{14}C date uncertainties (1σ). The shaded area shows the range of ventilation histories (b-spline smoothed) that could be supported by alternative surface reservoir age scenarios. Labels at the base indicate approximate timing of North Atlantic event-stratigraphy chronozones.

The associations identified above are consistent with the idea that the retraction of Antarctic sea ice from its maximal LGM extent may have increased the latitude band over which westerly winds could "stir up" CDW along steepened isopycnals, which would now outcrop increasingly to the south. This process may have been exacerbated during North Atlantic stadials (HS1 and the YD) because of an increase in the southward heat transport of the South Atlantic gyre via the "bipolar seesaw" mechanism (*2*, *3*). Although the CDW being brought to the surface in this way remained under the influence of an exceptionally aged and presumably high-potential partial pressure of CO_2 (PCO_2) abyssal reservoir (water that would have high PCO_2 when brought to the sea surface), the rate of CO_2 release from the Southern Ocean would have been enhanced (such as during HS1 and the YD) (Fig. 2, D and E). On the other hand, when the CDW that was being brought to the surface came under the influence of much better ventilated and presumably lower potential PCO_2 deep water, as it did during the ACR/Bølling-Allerød (Fig. 2, D and E), the release of CO_2 from the Southern Ocean would have been much reduced.

The drop in ventilation ages observed in MD07-3076 approximately in time with the ACR/Bølling-Allerød (Fig. 2E) is coherent with similar features observed in the Pacific (*11*, *14*) and North Atlantic (*9*, *13*). This is shown in Fig. 3, which compares the evolution of atmospheric $\Delta^{14}C_{atm}$ with ventilation changes reconstructed for the deep Southern Ocean [MD07-3076 (this study)], the shallow east Pacific [GCMV99-GC31/PC08 (*11*)], and the deep Northeast Atlantic [MD99-2334K (*13*), supplemented here with three additional benthic ^{14}C dates (*15*)]. This comparison suggests that the exceptionally aged deep water that is thought to have escaped into the shallow Pacific via Antarctic Intermediate Water (AAIW) during HS1 and the YD (*11*), and that is also inferred to have been mixed into the North Atlantic at these times (*9*, *13*), was previously restricted to the deep Southern Ocean where it increasingly influenced the site of MD07-3076 as the LGM approached. It would also appear that despite its proximity to this exceptionally aged water mass, the site of MD07-3076 apparently was not (or did not remain) at its core. This is implied by the increase in ventilation ages in MD07-3076 toward the LGM and by the much higher ventilation ages observed at the shallow Pacific site between the middle of HS1 and the end of the YD (~16 to 10 ky B.P., Fig. 3B). Assuming that the shallow Pacific site is indeed representative of southern sourced water, the reversal in ventilation gradient between the two marine sites could suggest that the aged abyssal reservoir remained partially intact somewhere in the abyss until the end of the YD, despite having substantially withdrawn from the Atlantic sector of the deep Southern Ocean by this time (Fig. 2E).

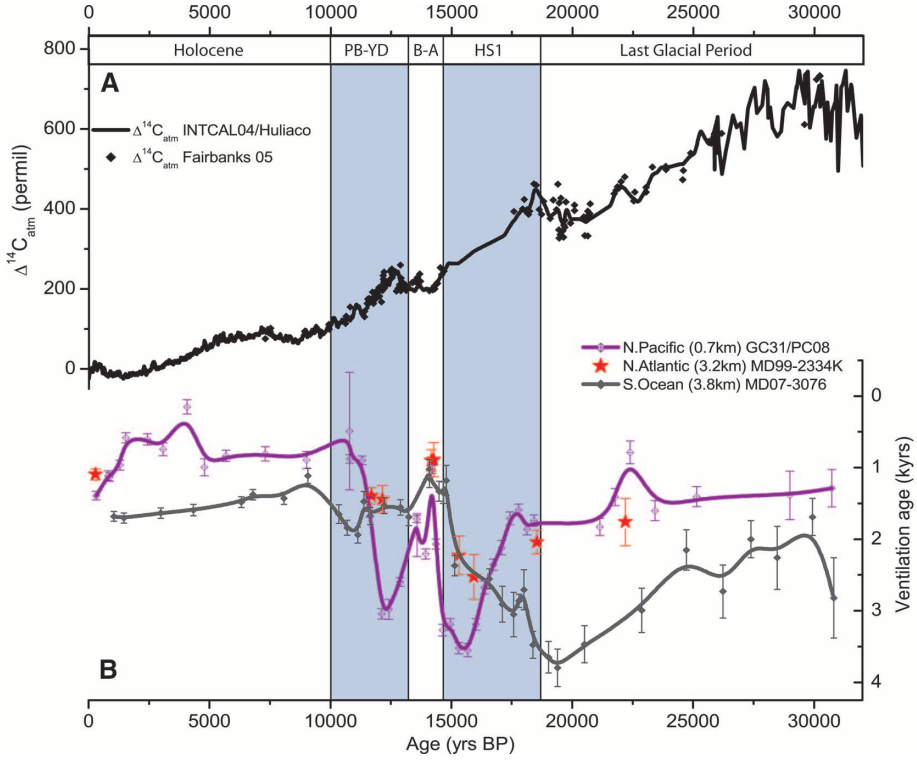

Fig. 3. Atmospheric $\Delta^{14}C$ change and deep-water reservoir age variability in the shallow Pacific, deep North Atlantic (*13*, *15*), and the deep Southern Ocean (this study). (**A**) Atmospheric $\Delta^{14}C$ [black diamonds, coral data (*22*); black line, INTCAL04 calibration curve (*23*) spliced with the Cariaco data set from 26 ky B.P. (*7*)]. (**B**) Deep water reservoir ages, derived from the offset between benthic- and atmospheric-^{14}C ages (reversed *y* axis). Solid red stars indicate MD99-2334K from the deep Northeast Atlantic (*13*), purple crossed diamonds and b-spline smoothed line indicate GCMV99-GC31/PC08 from the shallow Pacific (*11*), and gray diamonds and b-spline smoothed indicate MD07-3076 from the Southern Ocean (this study). Error ranges for MD99-2334K and MD07-3076 indicate combined planktic and benthic ^{14}C age uncertainties (1σ), whereas those for GCMV99-GC31/PC08 are 2σ uncertainties in benthic ^{14}C ages alone (Fig. 2E). Shaded vertical bars highlight the coincidence of rapid changes in deep water ventilation with marked changes in $\Delta^{14}C_{atm}$ and major North Atlantic chronozones.

One important question that arises concerns the extent to which the changes in deep-water ventilation recorded in MD07-3076 help to explain the apparent glacial $\Delta^{14}C_{atm}$ excess and the rapid 190 per mil (‰) drop in $\Delta^{14}C_{atm}$ during HS1 (*8*) (Fig. 1). Answering this question accurately would require knowledge of the exact volume of deep water that was affected by the ventilation changes recorded at the site of MD07-3076. Without this knowledge, we can only say that if the ~2000-year reduction in B-Atm recorded across HS1 in MD07-3076 (Fig. 2E) was experienced by ~30% of the ocean [all water deeper than the next deepest ^{14}C constraint from the glacial Pacific (*12*)], this could explain just over half of the 190‰ drop in atmospheric $\Delta^{14}C$ across the mystery interval (*15*). At the very least, this provides cause for optimism regarding the eventual reconciliation of the deglacial "radiocarbon mystery" (*8*), though it also underlines the need for a wider array of deep-ocean ^{14}C data with precise calendar chronologies.

The cause of the transient increase in ventilation recorded during the ACR/Bølling-Allerød in MD07-3076 [and in other records from the Atlantic and Pacific (Fig. 3B)] is also difficult to assess accurately without knowledge of the changing "end-member" composition and mixing ratio of local deep water. Neodymium isotope data from core RC11-83 in the deep Cape Basin (*16*) suggests a variable but generally increased influence of northern-sourced deep water during the ACR/Bølling-Allerød relative to the LGM, but crucially not relative to the late Holocene. If this record is taken as representative of end-member mixing ratio changes at our more open Atlantic site, it follows that mixing ratio changes alone might

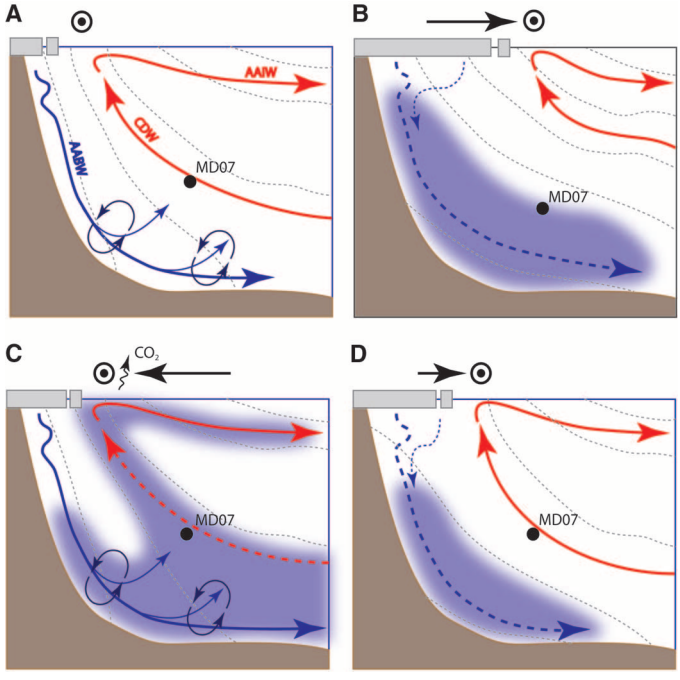

Fig. 4. Schematic illustration of hypothesized changes in Southern Ocean overturning across the last deglaciation (with south at left). (**A**) The modern overturning. Red arrows indicate the "upper overturning limb," which here includes CDW upwelling in the Southern Ocean at the ACC divergence and AAIW flowing northwards at shallow depths. Upper and lower CDW, which may include North Atlantic– and Antarctic-sourced water in variable proportions, have been combined for simplicity. Blue arrows indicate the "lower overturning limb," which consists of Antarctic Bottom Water (AABW) and its derivatives. Gray dashed lines indicate hypothetical isopycnals. Dark blue circular arrows indicate intense diapycnal mixing around topography in the Southern Ocean, which permits effective lower-limb overturning and the incorporation of AABW into CDW (*15*). Sea ice is represented by the gray boxes (top left), and the westerly wind position is indicated by the dotted circle (top). The solid circle marks the approximate position of core MD07-3076. (**B**) LGM overturning. The North Atlantic (salt) contribution to the upper-limb circulation is subdued relative to the present; Antarctic sea ice and the effective westerly wind stress in the Southern Ocean (driving isopycnal outcropping) are pushed far northward (black arrow). Flattened and widely spaced isopycnals south of the main outcropping area cause the ^{14}C-depleted lower overturning limb to expand without substantial diapycnal mixing into CDW. The shaded area indicates a ^{14}C-depleted, high potential Pco_2 deep-water mass. (**C**) HS1/YD overturning. The supply of North Atlantic deep water to CDW is severely reduced, the Southern Ocean warms in part because of the bipolar seesaw, Antarctic sea ice retracts substantially from its maximum glacial extent, and the main isopycnal outcrop area shifts southward. Poorly ventilated (high potential Pco_2) AABW is drawn upward along steepened isopycnals and mixed to a greater extent into CDW, which releases ^{14}C-depleted CO_2 to the atmosphere when brought to the surface. (**D**) Bølling-Allerød overturning. The Southern Ocean cools because of the bipolar seesaw, and sea ice reverses its retreat. Mixing of AABW into upward-flowing CDW is impeded once again, and the release of ^{14}C-depleted CO_2 pauses as a result.

not account for near modern deep-water ventilation ages observed during the ACR/Bølling-Allerød (Fig. 2E). This would suggest that either the export rate or ocean-atmosphere equilibration of one or both of the main Atlantic deep-water end-members (North Atlantic and/or Antarctic) increased during the ACR/Bølling-Allerød.

Our results demonstrate the existence before HS1 of an exceptionally aged abyssal carbon reservoir that could have substantially contributed to the sequestration of CO_2 in the deep sea during the last glacial period. These results also underline the potential importance of the combined effects of changing Antarctic sea ice, wind forcing, and abyssal stratification on the deglacial rise of CO_2. As illustrated schematically in Fig. 4, we envisage that although the meridional extent of Antarctic sea ice should influence the efficacy of the westerly wind stress that can effectively be applied to the Antarctic Circumpolar Current (ACC) to drive the upwelling of the densest classes of CDW in the Southern Ocean, the impact of upwelling on atmospheric CO_2 ($\Delta^{14}C_{atm}$ and $\partial^{13}CO_2$) might ultimately be determined by changes in the potential Pco_2 and sequestration age of the CDW that is brought to the surface. Thus, the deglacial trends in atmospheric CO_2, $\partial^{13}CO_2$, and $\Delta^{14}C_{atm}$ may have been interrupted during the ACR/Bølling-Allerød at least partly as a result of a pronounced increase in the ventilation of CDW brought to the surface Southern Ocean at this time (Figs. 2D and 4D). In contrast, with the preponderance of exceptionally aged CDW during HS1 and the YD [and with Antarctic sea ice already pulled back from its maximal meridional extent (Fig. 4C)], high potential Pco_2 water would be brought to the surface Southern Ocean instead. The result would have been to greatly enhance the release of ^{14}C-depleted CO_2 to the atmosphere, as well as the export of ^{14}C-depleted water from the ACC to the Atlantic and Pacific at these times.

References and Notes

1. W. Broecker, G. M. Henderson, *Paleoceanography* **13**, 352 (1998).
2. R. F. Anderson *et al.*, *Science* **323**, 1443 (2009).
3. S. Barker *et al.*, *Nature* **457**, 1097 (2009).
4. U. Siegenthaler *et al.*, *Science* **310**, 1313 (2005).
5. J. Ahn, E. J. Brook, *Science* **322**, 83 (2008).
6. F. Primeau, *J. Phys. Oceanogr.* **35**, 545 (2005).
7. K. Hughen, J. Southon, S. Lehman, C. Bertrand, J. Turnbull, *Quat. Sci. Rev.* **25**, 3216 (2006).
8. W. Broecker, S. Barker, *Earth Planet. Sci. Lett.* **256**, 90 (2007).
9. L. F. Robinson *et al.*, *Science* **310**, 1469 (2005).
10. E. Monnin *et al.*, *Science* **291**, 112 (2001).
11. T. M. Marchitto, S. J. Lehman, J. D. Ortiz, J. Flückiger, A. van Geen, *Science* **316**, 1456 (2007).
12. W. Broecker, E. Clark, S. Barker, *Earth Planet. Sci. Lett.* **274**, 322 (2008).
13. L. C. Skinner, N. J. Shackleton, *Paleoceanography* **19**, PA2005 (2004).
14. E. D. Galbraith *et al.*, *Nature* **449**, 890 (2007).
15. Materials and methods are available as supporting material on *Science* Online.
16. A. M. Piotrowski, S. L. Goldstein, S. R. Hemming, R. G. Fairbanks, *Earth Planet. Sci. Lett.* **225**, 205 (2004).
17. A. C. Parnell, J. Haslett, J. R. M. Allen, C. E. Buck, B. Huntley, *Quat. Sci. Rev.* **27**, 1872 (2008).
18. H. J. Smith, H. Fischer, M. Wahlen, D. Mastroianni, B. Deck, *Nature* **400**, 248 (1999).
19. H. J. Spero, D. W. Lea, *Science* **296**, 522 (2002).
20. L. Pena, I. Cacho, P. Ferretti, M. A. Hall, *Paleoceanography* **23**, PA3101 (2008).
21. P. Kohler, H. Fischer, G. Munhoven, R. E. Zeebe, *Global Biogeochem. Cycles* **19**, GB4020 (2005).
22. R. G. Fairbanks *et al.*, *Quat. Sci. Rev.* **24**, 1781 (2005).
23. P. J. Reimer *et al.*, *Radiocarbon* **46**, 1029 (2004).
24. P. Kohler, R. Muscheler, H. Fischer, *Geochem. Geophys. Geosyst.* **7**, Q11N06 (2006).
25. R. Muscheler, J. Beer, P. W. Kubik, H.-A. Synal, *Quat. Sci. Rev.* **24**, 1849 (2005).
26. C. Laj, C. Kissel, J. Beer, in *Timescales of the Paleomagnetic Field*. (American Geophysical Union, 2004), vol. 145, pp. 255–265.
27. A. Indermuhle, E. Monnin, B. Stauffer, T. F. Stocker, M. Wahlen, *Geophys. Res. Lett.* **27**, 735 (2000).
28. B. Lemieux-Dudon *et al.*, *Quat. Sci. Rev.* **29**, 8 (2010).
29. H. Fischer *et al.*, *Earth Planet. Sci. Lett.* **260**, 340 (2007).

30. We are grateful to N. Caillon, F. Dewilde, G. Isguder, H. Rebaubier, L. Booth, P. Ljubic, and K. James for technical assistance. A. Parnell provided generous and invaluable help with *Bchron*, and P. Köhler very kindly provided unpublished $\Delta^{14}C_{atm}$ simulations. We thank R. Gersonde and A. Mackensen for sharing their South Atlantic expertise, and we acknowledge the crew of the R/V Marion Dufresne and the Paul Emile Victor Institute (IPEV) who collected core MD07-3076CQ. This work was funded by the Royal Society, by Natural Environment Research Council Radiocarbon grant 1245.1007, and via a University Fellowship held by L.C.S. This work was facilitated by a visiting fellowship held by L.C.S. at ANU and by travel grants from the Royal Society and Christ's College. C.W. and E.M. are supported financially by Centre National de la Recherche Scientifique, Institut National des Sciences de l'Univers, and Commissariat à l'Energie Atomique. This is Laboratoire des Sciences du Climat et l'Environnement contribution 4188.

Supporting Online Material

www.sciencemag.org/cgi/content/full/328/5982/1147/DC1
Materials and Methods
Figs. S1 to S8
Tables S1 to S3
References

20 October 2009; accepted 8 April 2010
10.1126/science.1183627

Mirid Bug Outbreaks in Multiple Crops Correlated with Wide-Scale Adoption of Bt Cotton in China

Yanhui Lu,[1] Kongming Wu,[1]* Yuying Jiang,[2] Bing Xia,[2] Ping Li,[2] Hongqiang Feng,[1] Kris A. G. Wyckhuys,[1]† Yuyuan Guo[1]

Long-term ecological effects of transgenic *Bacillus thuringiensis* (Bt) crops on nontarget pests have received limited attention, more so in diverse small holder–based cropping systems of the developing world. Field trials conducted over 10 years in northern China show that mirid bugs (Heteroptera: Miridae) have progressively increased population sizes and acquired pest status in cotton and multiple other crops, in association with a regional increase in Bt cotton adoption. More specifically, our analyses show that Bt cotton has become a source of mirid bugs and that their population increases are related to drops in insecticide use in this crop. Hence, alterations of pest management regimes in Bt cotton could be responsible for the appearance and subsequent spread of nontarget pests at an agro-landscape level.

Genetically engineered crops that express δ-endotoxins (Cry proteins) from *Bacillus thuringiensis* (Bt) can successfully control several insect pests. The adoption of Bt crops increases yield and causes vast reductions in insecticide use (*1*–*5*). With Bt crops presently adopted in over 20 countries (*6*), the ecological risks of their commercial cultivation have received considerable scientific scrutiny (*7*–*11*). In China, Bt cotton was approved in 1997 for commercial use to control cotton bollworm, *Helicoverpa armigera*, and has steadily been adopted by the bulk of Chinese cotton growers (i.e., presently 95% adoption in northern China). Bt cotton controls *H. armigera* larvae very effectively and acts as a dead-end trap crop for regional populations of this pest in local agricultural landscapes (*12*); that is, a large percentage of the pest moths lay their eggs in cotton, where the hatching larvae are killed and do not subsequently infest other crops as adults. Hence, Bt cotton controls a key target pest not only within cotton fields but also on multiple other non-Bt host crops (i.e., corn, peanuts, soybeans, and vegetables), reducing the overall need for insecticide sprays (*3*, *12*). Nevertheless, long-term impacts of Bt cotton on nontarget arthropods, such as polyphagous insect pests, in local agro-ecosystems remain to be quantified (*13*–*15*).

Mirid bugs (Heteroptera: Miridae) are herbivores in a broad range of cultivated plants, including

[1]State Key Laboratory for Biology of Plant Diseases and Insect Pests, Institute of Plant Protection, Chinese Academy of Agricultural Sciences, Beijing 100193, People's Republic of China. [2]National Agro-Technical Extension and Service Center, Beijing 100026, People's Republic of China.

*To whom correspondence should be addressed. E-mail: kmwu@ippcaas.cn

†Present address: Horticulture Research Center, Universidad Jorge Tadeo Lozano, Chia (Cundinamarca), Colombia.

cotton, cereals, vegetables, and fruit crops. In China, mirid bugs have historically been considered occasional or minor pests in most crops, occurring at relatively low population densities and only sporadically requiring pest management intervention (*16*). Nevertheless, mirid bugs can easily attain outbreak densities, switch host crops, or experience geographic spread because of their environmental adaptability (*16*–*18*), high population growth rate (*16*, *17*), and strong dispersal capacity (*19*, *20*). In this study, we determined whether mirid bug outbreaks are more likely to occur in Bt cotton than in conventional cotton and to what extent these insects could cause unintended ecological impacts in the broader agro-ecosystem (*21*). Research was conducted in six major cotton-growing provinces (i.e., Henan, Hebei, Jiangsu, Anhui, Shandong, and Shanxi) of northern China (Fig. 1), where 3 million ha of cotton and 26 million ha of alternative crops, potentially susceptible to mirid bug attack, are cultivated annually by >10 million small-scale farmers.

Mirid bugs were sampled from 1998–2009 in Bt and non-Bt cotton plots at the Langfang Experiment Station in Heibei province (*21*). Mirid bug abundance did not differ between cotton varieties with similar management regimes ($P > 0.05$), and calendar-based insecticide sprays for *H. armigera* control in non-Bt cotton significantly lowered mirid bug infestation densities ($P < 0.05$) (Fig. 2 and table S3). Hence, Bt cotton per se does not affect mirid bug infestation densities, and mirid bug populations prove susceptible to broad-spectrum insecticides for *H. armigera*.

We simultaneously monitored mirid bug abundance and insecticide use in cotton at 38 locations throughout the study region during 1997–2008 and 1992–2008, respectively (*21*). Mirid bug population levels gradually increased over time and were significantly related to Bt cotton planting proportion ($P < 0.05$) (Fig. 3). Insecticide use patterns also changed with Bt cotton adoption (fig. S1). After introduction of Bt cotton, the number of insecticide sprays against *H. armigera* and all insect pests was evidently lower than during 1992–1996. On the other hand, the number of sprays against mirid bugs increased over time, in line with Bt cotton planting proportion (fig. S1). Meanwhile, *H. armigera* insecticide use was a highly explanatory variable for annual mirid bug population levels and insecticide use for mirid bug control ($P < 0.05$) (Table 1).

Additionally, mirid bug infestations were recorded in alternative host crops: Chinese date, grapes, apple, peach, and pear (*21*). Mirid bug infestation severity increased in alternative host crops, and respective infestation severities were significantly correlated with regional proportion of Bt cotton planted ($P < 0.05$) (Fig. 4).

Over the study period, mirid bugs gradually increased population densities and damage in cotton and multiple other crops. Mirid bug attraction to flowering plants and associated seasonal host alternation partially explains the observed pattern

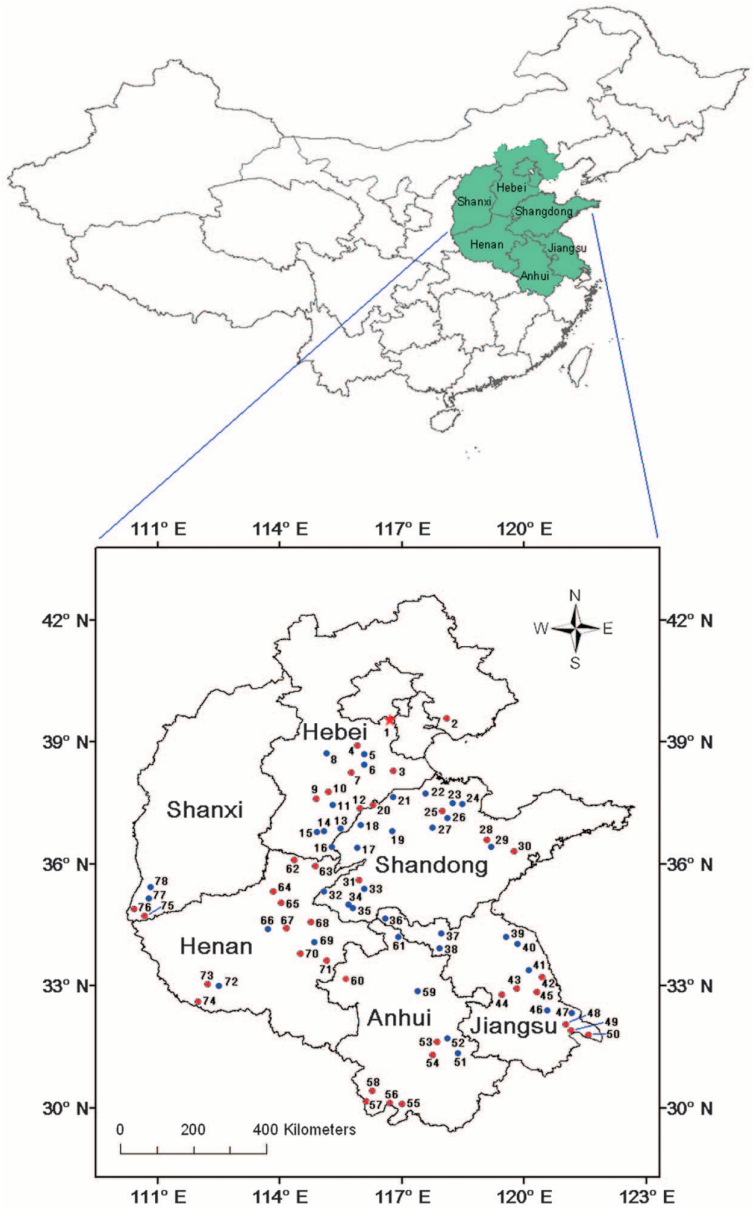

Fig. 1. Survey locations in northern China. Mirid bug population dynamics on Bt and non-Bt cotton were monitored at Langfang site (star). Population densities were surveyed on cotton at 38 sites (red), and infestation densities were determined on other host crops at 77 sites (red and blue).

Fig. 2. Mirid bug population dynamics in Bt and non-Bt cotton with different management regimes from 2002–2009. Bt and Non-Bt indicate Bt cotton and non-Bt cotton, respectively, without insecticide sprays, whereas Non-Bt-CC represents non-Bt cotton with *H. armigera* insecticide sprays.

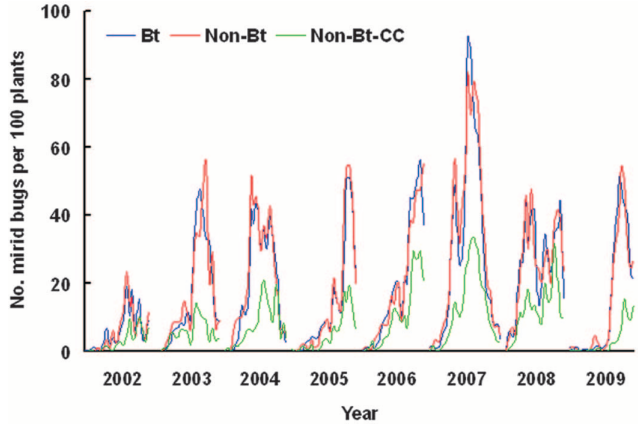

(*16*, *22*). In mid- to late June, mirid bugs largely move from early-season host plants to crop fields, where they build up their initial populations. Results of 2006–2009 field-plot trials indicate that mirid bugs greatly prefer cotton over other major host crops in mid- to late June (fig. S2), because cotton is locally one of few flowering host crops during this time period. Before Bt cotton adoption, broad-spectrum *H. armigera* insecticide use reduced early mirid bug populations, with cotton acting as a dead-end trap crop. Current absence of insecticide sprays in Bt cotton permits unrestrained mirid bug population buildup and subsequent (active) spread or (passive) spillover to a multitude of other (flowering) crops. Hence, a reduction in insecticide use for *H. armigera* control in Bt cotton correlates with mirid bug outbreaks in cotton and various fruit crops in the broader agro-landscape.

Most polyphagous insects exhibit clear preferences for one or few host plants and may seasonally concentrate in patches of these plants. Consequently, management actions in these patches can greatly determine population dynamics of such insects at the landscape level (*23*). Our work shows that a drop in insecticide use in Bt cotton fields leads to a reversal of the ecological role of cotton: from being a sink for mirid bugs in conventional systems to being an actual source for these pests in Bt cotton–growing systems. This perspective should be instrumental in developing regionwide management strategies for these polyphagous pests in northern China and elsewhere in the world.

Pest resurgence and replacement are usually ascribed to alterations in pest management re-

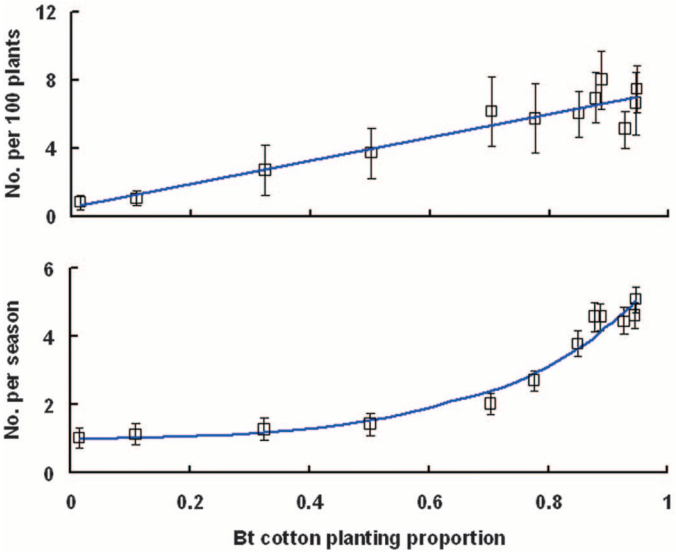

Fig. 3. Association between mirid bug population density (**top**) or number of mirid bug insecticide sprays (**bottom**) and Bt cotton planting proportion in northern China during 1997–2008. Linear model for population density: $y = 6.81x + 0.54$, $F_{1,10} = 88.65$, $P < 0.0001$, coefficient of determination (R^2) = 0.90. Nonlinear model for number of mirid bug insecticide sprays: $y = 0.89 + 0.08*\exp(4.21x)$, $F_{2,9} = 126.46$, $P < 0.0001$, $R^2 = 0.97$.

Table 1. Multivariate assessment of determinants of mirid bug population density and insecticide spray frequency in northern China during 1997–2008. For stepwise regression, only variables with significance $P < 0.05$ were entered into the analysis. "Other insecticide sprays" target insect pests different from *H. armigera* or mirid bugs. *r*, regression coefficient. R^2, coefficient of determination. A slash indicates no analysis.

Parameters	Mirid bug population density						Number of mirid bug insecticide sprays					
	Single regression			Stepwise regression			Single regression			Stepwise regression		
	r	R^2	*P*	*r*	R^2	*P*	*r*	R^2	*P*	*r*	R^2	*P*
Total number of insecticide sprays	–0.2093	0.51	0.0095				/		/	/		/
Number of *H. armigera* insecticide sprays	–0.1079	0.87	<0.0001	–0.1079	0.87	<0.0001	–0.7214	0.84	<0.0001	–0.7214	0.84	<0.0001
Number of other insecticide sprays	+0.1361	0.01	0.7131				–1.8505	0.06	0.4570			
Temperature	–0.0921	0.04	0.5242				–0.4116	0.02	0.6773			
Rainfall	–0.0001	<0.01	0.8956				–0.0005	<0.01	0.9487			

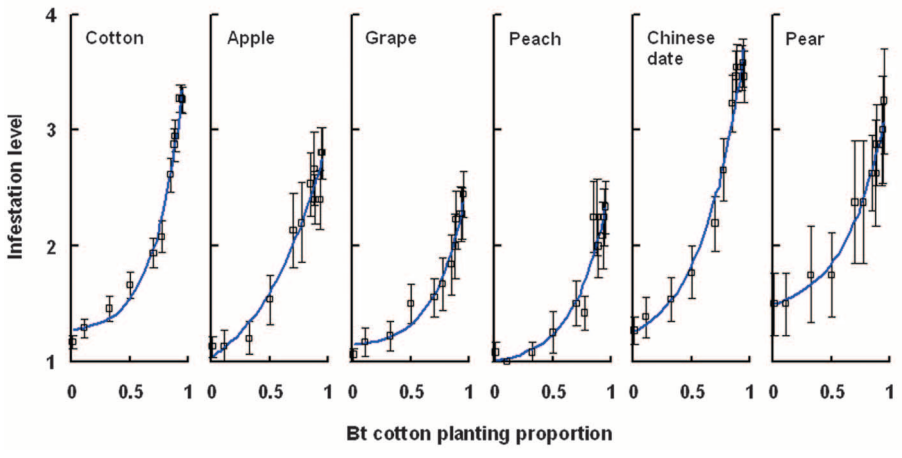

Fig. 4. Association between mirid bug infestation severity in either cotton or key fruit crops and Bt cotton planting proportion. The measure of mirid bug infestation was assigned a score ranging from 1 (no infestation) to 5 (extreme infestation). Nonlinear model for cotton, $y = 1.23 + 0.04*\exp(4.24x)$ ($F_{2,9} = 346.40$, $R^2 = 0.99$, $P < 0.0001$); apple, $y = 0.64 + 0.40*\exp(1.76x)$ ($F_{2,9} = 107.77$, $R^2 = 0.96$, $P < 0.0001$); grape, $y = 1.12 + 0.02*\exp(4.15x)$ ($F_{2,9} = 118.05$, $R^2 = 0.96$, $P < 0.0001$); peach, $y = 0.97 + 0.04*\exp(3.61x)$ ($F_{2,9} = 46.07$, $R^2 = 0.91$, $P < 0.0001$); Chinese date, $y = 1.06 + 0.20*\exp(2.74x)$ ($F_{2,9} = 166.88$, $R^2 = 0.97$, $P < 0.0001$); and pear, $y = 1.39 + 0.11*\exp(2.88x)$ ($F_{2,9} = 153.39$, $R^2 = 0.97$, $P < 0.0001$).

gimes (*24*). For example, cotton aphid, *Aphis gossypii*, evolved as a primary pest of cotton in the mid-1970s because of intensive insecticide use for *H. armigera* control (*25*, *26*) but currently occurs at low population densities in Bt cotton (*27*). In a similar fashion, mirid bugs were previously suppressed by *H. armigera* insecticide use and only acquired pest status in cotton and other crops after Bt cotton adoption. Hence, areawide cultivation of transgenic crops may bring various (direct and indirect) effects on ecological status of different organisms, which should be assessed or anticipated in a comprehensive fashion.

In many parts of the world, transgenic crops such as Bt crops have come to dominate agricultural landscapes, and their landscape-level impact has been quantified on target pests (*12*, *28*), nontarget organisms such as natural enemies (*7*, *29*, *30*), or charismatic species such as the monarch butterfly *Danaus plexippus* (*31*). However, few studies have described the impact of transgenic crops on nontarget insect pests (*2*, *13*) or, more specifically, assessed their landscape-level effects (*15*, *32*, *33*). This study confirms reports of a landscape-level emergence of nontarget pests with the adoption of Bt crops resulting from reductions in insecticide applications. Our work highlights a critical need to predict landscape-level impacts of transgenic crops on (potentially) pestiferous organisms in future ecological agricultural risk assessment. Such more-comprehensive risk management may be crucial to help advance integrated pest management and ensure sustainability of transgenic technologies.

References and Notes

1. A. M. Shelton, J. Z. Zhao, R. T. Roush, *Annu. Rev. Entomol.* **47**, 845 (2002).
2. M. G. Cattaneo *et al.*, *Proc. Natl. Acad. Sci. U.S.A.* **103**, 7571 (2006).
3. J. Huang, S. Rozelle, C. Pray, Q. Wang, *Science* **295**, 674 (2002).
4. M. Qaim, D. Zilberman, *Science* **299**, 900 (2003).
5. G. P. Fitt, in *Integration of Insect-Resistant Genetically Modified Crops Within IPM Programs*, J. Romeis, A. M. Shelton, G. G. Kennedy, Eds. (Springer, Dordrecht, Netherlands, 2008), pp. 303–328.
6. C. James, "Global status of commercialized biotech/GM crops: 2009" (ISAAA Brief No. 41, International Service for the Acquisition of Agri-Biotech Applications, Ithaca, NY, 2009).
7. J. Romeis *et al.*, *Nat. Biotechnol.* **26**, 203 (2008).
8. J. E. Losey, L. S. Rayor, M. E. Carter, *Nature* **399**, 214 (1999).
9. L. L. Wolfenbarger, P. R. Phifer, *Science* **290**, 2088 (2000).
10. P. J. Dale, B. Clarke, E. M. G. Fontes, *Nat. Biotechnol.* **20**, 567 (2002).
11. D. A. Andow, C. Zwahlen, *Ecol. Lett.* **9**, 196 (2006).
12. K.-M. Wu, Y.-H. Lu, H.-Q. Feng, Y.-Y. Jiang, J.-Z. Zhao, *Science* **321**, 1676 (2008).
13. M. Marvier, C. McCreedy, J. Regetz, P. Kareiva, *Science* **316**, 1475 (2007).
14. K. M. Wu, *Chin. J. Agric. Biotechnol.* **4**, 93 (2007).
15. S. E. Naranjo, J. R. Ruberson, H. C. Sharma, L. Wilson, K. Wu, in *Integration of Insect-Resistant Genetically Modified Crops Within IPM Programs*, J. Romeis, A. M. Shelton, G. G. Kennedy, Eds. (Springer, Dordrecht, Netherlands, 2008), pp. 159–194.
16. Y. H. Lu, K. M. Wu, *Biology and Control of Cotton Mirids* (Golden Shield, Beijing, 2008).
17. Y. Q. Ting, *Acta Phytophylacica Sin.* **2**, 285 (1963).
18. Y. Q. Ting, *Acta Entomol. Sin.* **13**, 298 (1964).
19. Y. H. Lu, K. M. Wu, Y. Y. Guo, *Environ. Entomol.* **36**, 1007 (2007).
20. Y. H. Lu, K. M. Wu, K. A. G. Wyckhuys, Y. Y. Guo, *Bull. Entomol. Res.* **99**, 543 (2009).
21. Materials and methods are available as supporting material on *Science* Online.
22. H. F. Chu, H. L. Meng, *Acta Entomol. Sin.* **8**, 97 (1958).
23. G. G. Kennedy, N. P. Storer, *Annu. Rev. Entomol.* **45**, 467 (2000).
24. J. D. Dutcher, in *General Concepts in Integrated Pest and Disease Management*, A. Ciancio, K. G. Mukerji, Eds. (Springer, Dordrecht, Netherlands, 2007), pp. 27–43.
25. K. M. Wu, Y. Y. Guo, *Annu. Rev. Entomol.* **50**, 31 (2005).
26. K. Wu, Q. Liu, *Acta Ecol. Sin.* **12**, 341 (1992).
27. K. Wu, Y. Guo, *Environ. Entomol.* **32**, 312 (2003).
28. Y. Carrière *et al.*, *Proc. Natl. Acad. Sci. U.S.A.* **100**, 1519 (2003).
29. S. E. Naranjo, *Environ. Entomol.* **34**, 1193 (2005).
30. J. Romeis, M. Meissle, F. Bigler, *Nat. Biotechnol.* **24**, 63 (2006).
31. M. K. Sears *et al.*, *Proc. Natl. Acad. Sci. U.S.A.* **98**, 11937 (2001).
32. M. R. Williams, in *Proceedings of the Beltwide Cotton Conferences* (National Cotton Council of America, Memphis, TN, 2006), pp. 1151–1204.
33. N. P. Storer, G. P. Dively, R. A. Herman, in *Integration of Insect-Resistant Genetically Modified Crops Within IPM Programs*, J. Romeis, A. M. Shelton, G. G. Kennedy, Eds. (Springer, Dordrecht, Netherlands, 2008), pp. 273–302.

34. This work was supported by the National Key Basic Research Program (2006CB102004), the National Natural Science Foundation of China (30625028), the Key Project for Breeding Genetically Modified Organisms (2008ZX08012-004), and the Commonwealth Agricultural Scientific Research Project (200803011). We thank two anonymous reviewers for helpful comments and suggestions.

Supporting Online Material

www.sciencemag.org/cgi/content/full/science.1187881/DC1
Materials and Methods
Figs. S1 and S2
Tables S1 to S3
References

3 February 2010; accepted 22 April 2010
Published online 13 May 2010;
10.1126/science.1187881
Include this information when citing this paper.

Prion Strain Mutation Determined by Prion Protein Conformational Compatibility and Primary Structure

Rachel C. Angers,[1]* Hae-Eun Kang,[2] Dana Napier,[2] Shawn Browning,[1]† Tanya Seward,[2] Candace Mathiason,[4] Aru Balachandran,[5] Debbie McKenzie,[6] Joaquín Castilla,[7] Claudio Soto,[8] Jean Jewell,[9] Catherine Graham,[10] Edward A. Hoover,[4] Glenn C. Telling[1,2,3]‡

Prions are infectious proteins composed of the abnormal disease-causing isoform PrP^{Sc}, which induces conformational conversion of the host-encoded normal cellular prion protein PrP^{C} to additional PrP^{Sc}. The mechanism underlying prion strain mutation in the absence of nucleic acids remains unresolved. Additionally, the frequency of strains causing chronic wasting disease (CWD), a burgeoning prion epidemic of cervids, is unknown. Using susceptible transgenic mice, we identified two prevalent CWD strains with divergent biological properties but composed of PrP^{Sc} with indistinguishable biochemical characteristics. Although CWD transmissions indicated stable, independent strain propagation by elk PrP^{C}, strain coexistence in the brains of deer and transgenic mice demonstrated unstable strain propagation by deer PrP^{C}. The primary structures of deer and elk prion proteins differ at residue 226, which, in concert with PrP^{Sc} conformational compatibility, determines prion strain mutation in these cervids.

Prions are protein-based transmissible agents causing lethal, incurable neurodegenerative diseases of mammals, including sheep scrapie, bovine spongiform encephalopathy, human Creutzfeldt-Jakob disease, and chronic wasting disease (CWD), a contagious prion disorder of cervids (a family of hoofed mammals, including deer and elk). During propagation, PrP^{Sc}, the β-sheet–rich disease-associated conformer of the prion protein (PrP), coerces the physiological form, PrP^{C}, to adopt the PrP^{Sc} conformation. Prions share with nucleic acid–based pathogens the ability to propagate strain information. Although distinct conformers of PrP^{Sc} appear to encipher the characteristics of certain strains (*1*–*5*), it is unclear how prions mutate and adapt in the absence of nucleic acids. Strain mutation has been reported after interspecies prion transmission—for example, scrapie transmission to rodents (*6*). Prion mutation may result in increased host range (*7*), a factor that complicates risk assessments for new hosts.

Although strain diversity has been recorded for sheep, human, and bovine prions, the existence of strains in CWD is unclear (*8*–*10*). Polymorphic residue 129 of human PrP and the corresponding elk PrP residue influence prion susceptibility at the level of strain selection (*11*, *12*). PrP primary structures of CWD-susceptible species differ at residue 226, which is glutamic acid (E) in Rocky Mountain elk and glutamine (Q) in other susceptible cervids. To determine CWD strain prevalence and to assess the influence of

References and Notes

1. R. A. Bessen, R. F. Marsh, *J. Virol.* **68**, 7859 (1994).
2. G. C. Telling *et al.*, *Science* **274**, 2079 (1996).
3. J. Collinge, K. C. L. Sidle, J. Meads, J. Ironside, A. F. Hill, *Nature* **383**, 685 (1996).
4. D. Peretz *et al.*, *Protein Sci.* **10**, 854 (2001).
5. K. M. Green *et al.*, *PLoS Pathog.* **4**, e1000139 (2008).
6. M. E. Bruce, A. G. Dickinson, *J. Gen. Virol.* **68**, 79 (1987).
7. J. C. Bartz, R. F. Marsh, D. I. McKenzie, J. M. Aiken, *Virology* **251**, 297 (1998).
8. S. R. Browning *et al.*, *J. Virol.* **78**, 13345 (2004).
9. G. LaFauci *et al.*, *J. Gen. Virol.* **87**, 3773 (2006).
10. G. Tamgüney *et al.*, *J. Virol.* **80**, 9104 (2006).
11. J. D. F. Wadsworth *et al.*, *Science* **306**, 1793 (2004); published online 11 November 2004 (10.1126/science.1103932).
12. K. M. Green *et al.*, *J. Gen. Virol.* **89**, 598 (2008).
13. R. C. Angers *et al.*, *Science* **311**, 1117 (2006); published online 26 January 2006 (10.1126/science.1122864).
14. R. C. Angers *et al.*, *Emerg. Infect. Dis.* **15**, 696 (2009).
15. A. G. Dickinson, V. M. H. Meikle, *Mol. Gen. Genet.* **112**, 73 (1971).
16. M. E. Bruce, A. G. Dickinson, in *Slow Transmissible Diseases of the Nervous System*, *Vol. 2*, S. B. Prusiner, W. J. Hadlow, Eds. (Academic Press, New York, 1979), pp. 71–86.
17. M. E. Bruce, P. A. McBride, C. F. Farquhar, *Neurosci. Lett.* **102**, 1 (1989).
18. Materials and methods are available as supporting material on *Science* Online.
19. H. Fraser, A. G. Dickinson, *J. Comp. Pathol.* **78**, 301 (1968).
20. A. Taraboulos *et al.*, *Proc. Natl. Acad. Sci. U.S.A.* **89**, 7620 (1992).
21. M. E. Bruce, H. Fraser, *Acta Neuropathol.* **58**, 133 (1982).
22. J. Castilla, P. Saá, C. Hetz, C. Soto, *Cell* **121**, 195 (2005).
23. J. Li, S. Browning, S. P. Mahal, A. M. Oelschlegel, C. Weissmann, *Science* **327**, 869 (2010); published online 31 December 2009 (10.1126/science.1183218).
24. G. Legname *et al.*, *Proc. Natl. Acad. Sci. U.S.A.* **103**, 19105 (2006).
25. M. Polymenidou *et al.*, *Lancet Neurol.* **4**, 805 (2005).
26. J. Collinge, *Lancet* **354**, 317 (1999).
27. J. Collinge, A. R. Clarke, *Science* **318**, 930 (2007).
28. C. J. Sigurdson *et al.*, *J. Virol.* **80**, 12303 (2006).
29. G. J. Raymond *et al.*, *J. Virol.* **81**, 4305 (2007).
30. C. Johnson *et al.*, *J. Gen. Virol.* **87**, 2109 (2006).
31. Q. Kong *et al.*, *J. Neurosci.* **25**, 7944 (2005).

32. We thank Prionics for mAb 6H4, V. Saylor for technical help, A. Aguzzi for mAb POM2, P. Nelson for neuropathological expertise, R. Kryscio and J. Marcum for biostatistical advice, and C. Ryou for reading the manuscript. C.S. is currently Founder and Chief Scientific Officer of Amprion Inc., a privately held company focusing on exploiting PMCA for sensitive detection of prions and early disease diagnosis. These studies were supported by grant 2RO1 NS040334-04 from the National Institute of Neurological Disorders and Stroke, grants N01-AI-25491 and 1P01AI077774-01 from the National Institute of Allergy and Infectious Diseases, and grant V180003 from the U.S. Department of Defense. R.C.A. and S.B. were supported by T32 DA022738 and T32 AI49795 Training Programs from the National Institute on Drug Abuse and the National Institute of Allergy and Infectious Diseases, respectively.

Supporting Online Material

www.sciencemag.org/cgi/content/full/science.1187107/DC1
Materials and Methods
Table S1
References

14 January 2010; accepted 1 April 2010
Published online 13 May 2010;
10.1126/science.1187107
Include this information when citing this paper.

Cyclooxygenase-2 Controls Energy Homeostasis in Mice by de Novo Recruitment of Brown Adipocytes

Alexandros Vegiopoulos,[1]* Karin Müller-Decker,[2]* Daniela Strzoda,[1] Iris Schmitt,[1] Evgeny Chichelnitskiy,[1] Anke Ostertag,[1] Mauricio Berriel Diaz,[1] Jan Rozman,[3] Martin Hrabe de Angelis,[3] Rolf M. Nüsing,[4] Carola W. Meyer,[5] Walter Wahli,[6] Martin Klingenspor,[7] Stephan Herzig[1]†

Obesity results from chronic energy surplus and excess lipid storage in white adipose tissue (WAT). In contrast, brown adipose tissue (BAT) efficiently burns lipids through adaptive thermogenesis. Studying mouse models, we show that cyclooxygenase (COX)–2, a rate-limiting enzyme in prostaglandin (PG) synthesis, is a downstream effector of β-adrenergic signaling in WAT and is required for the induction of BAT in WAT depots. PG shifted the differentiation of defined mesenchymal progenitors toward a brown adipocyte phenotype. Overexpression of COX-2 in WAT induced de novo BAT recruitment in WAT, increased systemic energy expenditure, and protected mice against high-fat diet–induced obesity. Thus, COX-2 appears integral to de novo BAT recruitment, which suggests that the PG pathway regulates systemic energy homeostasis.

Obesity arises from chronic energy surplus and excess lipid storage in white adipose tissue (WAT). In contrast to WAT, brown adipose tissue (BAT) burns lipid to generate heat. Until recently, BAT was thought to function primarily in rodents and in newborn babies as a mechanism that facilitates adaptation to cold. However, recent studies have revealed that adult humans also have functional BAT (*1*–*4*), a finding that has fueled speculation that pharmacologic enhancement of BAT development and activity might be a useful strategy to counteract obesity.

In this study, we have explored whether cyclooxygenase-2 (COX-2), a rate-limiting enzyme in prostaglandin (PG) synthesis, contributes to BAT development in mice. Previous work by others had implicated COX-2 in the control of whole-body energy homeostasis and adipose tissue metabolism; for example, selective inhibition of COX-2 was shown to attenuate weight loss and energy expenditure in cancer patients and tumor-bearing mice (*5*, *6*), and genetically manipulated mice that express only one wild-type allele of COX-2 were shown to exhibit fat accumulation (*7*).

These findings prompted us to screen for differential COX-2 expression in WAT obtained from various mouse models of altered energy homeostasis (*8*). No clear differences in COX-2 mRNA expression were detected in mice with genetic or diet-induced obesity or in cachectic mice. However, an increase by a factor of two in COX-2 mRNA was observed in intra-abdominal WAT after 4 weeks of cold exposure (Fig. 1A). This was accompanied by up-regulation of uncoupling protein 1 (UCP1), the major determinant of mitochondrial thermogenesis (Fig. 1B). In the cold, thermogenic inducible BAT (indBAT) is readily engaged in WAT depots upon sympathetic activation of β-adrenergic receptor signaling by norepinephrine (NE) (*9*, *10*). To recapitulate cold exposure, we treated mice with the β_3-adrenoreceptor agonist CL316243 (CL) (*10*). Acute stimulation with CL resulted in a marked induction of COX-2 but not COX-1 mRNA in intra-abdominal WAT (Fig. 1C) and enhanced the release of the major WAT-derived PG (*11*), PGE_2 and PGI_2, from WAT explants (fig. S2). Notably, COX-2 mRNA levels were also induced upon ex vivo stimulation of mature adipocytes with NE, but only marginally in the stromal-vascular cell fraction (SVF) (fig. S3).

We next investigated the effect of prolonged β_3-adrenergic stimulation in wild-type and COX-2–deficient mice (*12*) and in wild-type mice fed a control diet or a diet containing celecoxib (cx), a selective COX-2 inhibitor (*13*). CL treatment resulted in induction of COX-2 protein expression along with a pronounced BAT-like phenotype in WAT of wild-type mice fed control diet, as judged by the predominance of smaller cells with rich cytoplasmic staining, multilocular lipid droplets, and UCP1 expression (Fig. 1, D to F, and fig. S4). BAT characteristics were substantially diminished in WAT of CL-treated animals on a celecoxib diet

[1]Emmy Noether and Marie Curie Research Group Molecular Metabolic Control, German Cancer Research Center (DKFZ) Heidelberg, 69120 Heidelberg, Germany. [2]Core Facility Tumor Models, DKFZ-ZMBH Alliance, German Cancer Research Center (DKFZ) Heidelberg, 69120 Heidelberg, Germany. [3]Institute of Experimental Genetics, Helmholtz Center Munich, 85764 Neuherberg, Germany. [4]Institute of Clinical Pharmacology, Johann Wolfgang Goethe-University, 60590 Frankfurt, Germany. [5]Department of Animal Physiology, Philipps University Marburg, 35043 Marburg, Germany. [6]Center for Integrative Genomics, National Research Center Frontiers in Genetics, University of Lausanne, 1015 Lausanne, Switzerland. [7]Molecular Nutritional Medicine, Else-Kröner Fresenius Center, Technische Universität München, 85350 Freising-Weihenstephan, Germany.

*These authors contributed equally to this work.
†To whom correspondence should be addressed. E-mail: s.herzig@dkfz.de

as well as in COX-2$^{-/-}$ mice (Fig. 1, E and F, and fig. S5). Also, in comparison with vehicle control, CL caused a strong reduction of fat accumulation under control diet, whereas the effect of CL under celecoxib diet and COX-2 deficiency was attenuated (fig. S6). These results suggested that de novo indBAT recruitment and the systemic thermogenic response to β-adrenergic stimulation depend on COX-2 activity. Consistent with this interpretation, CL-mediated induction of genes that are critical for cellular thermogenesis (UCP1, CIDEA, CPT1B, and DIO2) (*9*), for brown adipocyte differentiation (CEBPB), or for the genetic activation of thermogenesis (PGC1A and PPARA) (*9*, *14*) was markedly blunted upon pharmacologic or genetic COX-2 inhibition (Fig. 1G and figs. S7 and S8). In contrast, CL-stimulated thermogenic mRNA expression in interscapular BAT, a constitutive BAT (conBAT) depot in mice (*9*), was not influenced by celecoxib (fig. S9).

To explore whether increased COX-2 activity is also sufficient for indBAT recruitment under conditions of steady-state β-adrenergic stimulation, we studied transgenic mice overexpressing the COX-2 gene under the control of the promoter for the keratin 5 gene (K5COX2) (*15*). In the absence of systemic inflammation (fig. S10), the K5COX2 model mimicked the CL-induced elevation of WAT PG levels (fig. S11) and of COX-2 expression in multilocular adipocytes within intra-

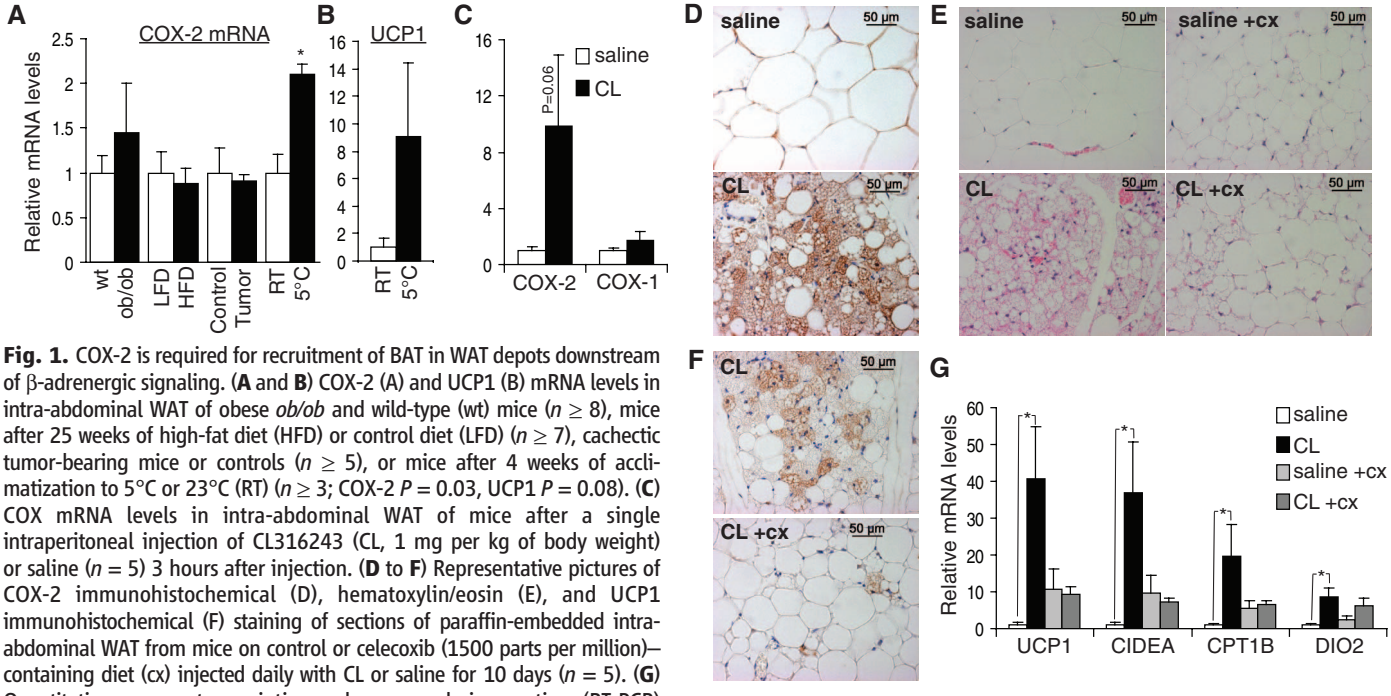

Fig. 1. COX-2 is required for recruitment of BAT in WAT depots downstream of β-adrenergic signaling. (**A** and **B**) COX-2 (A) and UCP1 (B) mRNA levels in intra-abdominal WAT of obese *ob/ob* and wild-type (wt) mice ($n \geq 8$), mice after 25 weeks of high-fat diet (HFD) or control diet (LFD) ($n \geq 7$), cachectic tumor-bearing mice or controls ($n \geq 5$), or mice after 4 weeks of acclimatization to 5°C or 23°C (RT) ($n \geq 3$; COX-2 $P = 0.03$, UCP1 $P = 0.08$). (**C**) COX mRNA levels in intra-abdominal WAT of mice after a single intraperitoneal injection of CL316243 (CL, 1 mg per kg of body weight) or saline ($n = 5$) 3 hours after injection. (**D** to **F**) Representative pictures of COX-2 immunohistochemical (D), hematoxylin/eosin (E), and UCP1 immunohistochemical (F) staining of sections of paraffin-embedded intra-abdominal WAT from mice on control or celecoxib (1500 parts per million)–containing diet (cx) injected daily with CL or saline for 10 days ($n = 5$). (**G**) Quantitative reverse transcription polymerase chain reaction (RT-PCR) mRNA analysis of intra-abdominal WAT from same mice as in (D) to (F) [$n \geq 4$; analysis of variance (ANOVA) post tests, $^*P < 0.05$]. Means ± SEM.

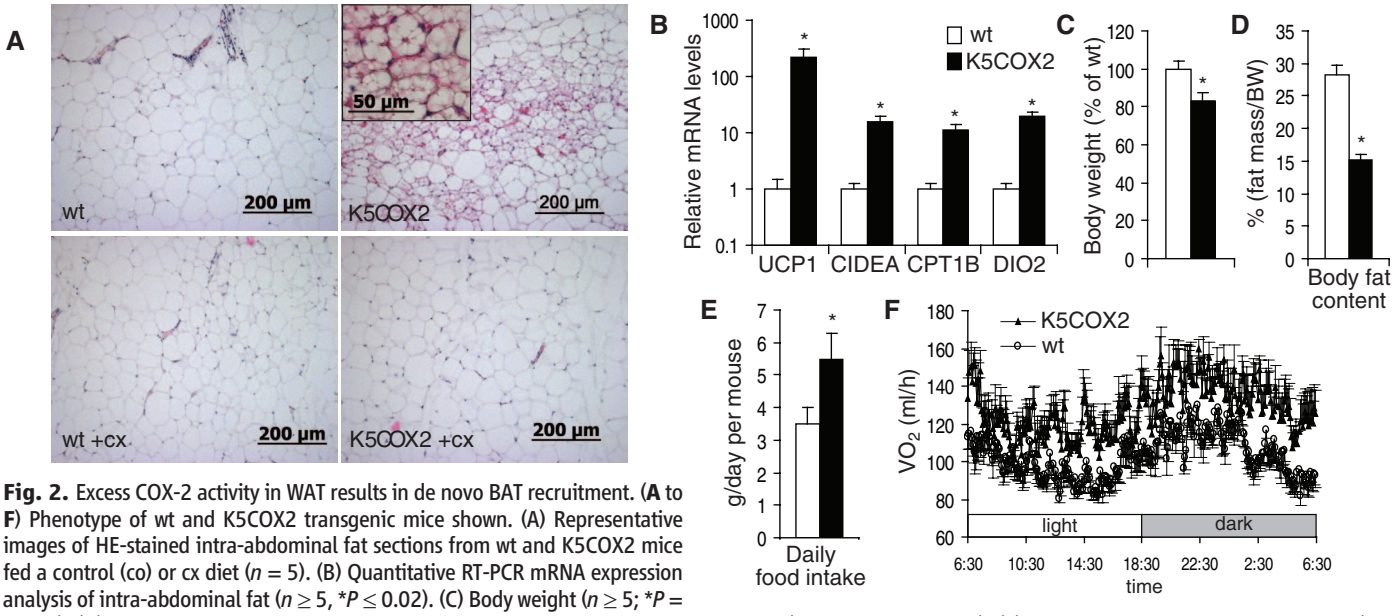

Fig. 2. Excess COX-2 activity in WAT results in de novo BAT recruitment. (**A** to **F**) Phenotype of wt and K5COX2 transgenic mice shown. (A) Representative images of HE-stained intra-abdominal fat sections from wt and K5COX2 mice fed a control (co) or cx diet ($n = 5$). (B) Quantitative RT-PCR mRNA expression analysis of intra-abdominal fat ($n \geq 5$, $^*P \leq 0.02$). (C) Body weight ($n \geq 5$; $^*P = 0.015$). (D) Body fat content determined by nuclear magnetic resonance quantitation ($n = 17$; $^*P < 0.0001$). (E) Daily chow consumption per mouse ($n \geq 6$; $P = 0.04$). (F) Oxygen consumption rate of individual mice determined during a 24-hour period ($n \geq 6$; $P = 0.002$ for wt versus K5COX2 area under the curve). Means ± SEM.

abdominal WAT (fig. S12), which could be attributed to a positive feedback loop of PG on local COX-2 expression (figs. S1 and S11 to S14). Clusters of BAT-like cells were detectable within WAT in intra-abdominal fat sections from K5COX2 mice (Fig. 2A). Correlating with loss of COX-2 expression in WAT and normalized plasma PG levels (figs. S12 and S13), BAT-like cells were absent in intra-abominal fat upon "therapeutic" celecoxib exposure (Fig. 2A). Consistently, mRNA expression analysis showed a marked induction of the thermogenic gene expression program in K5COX2 mice (Fig. 2B and fig. S15), which suggests that local COX-2 overexpression in WAT is sufficient for ectopic indBAT development.

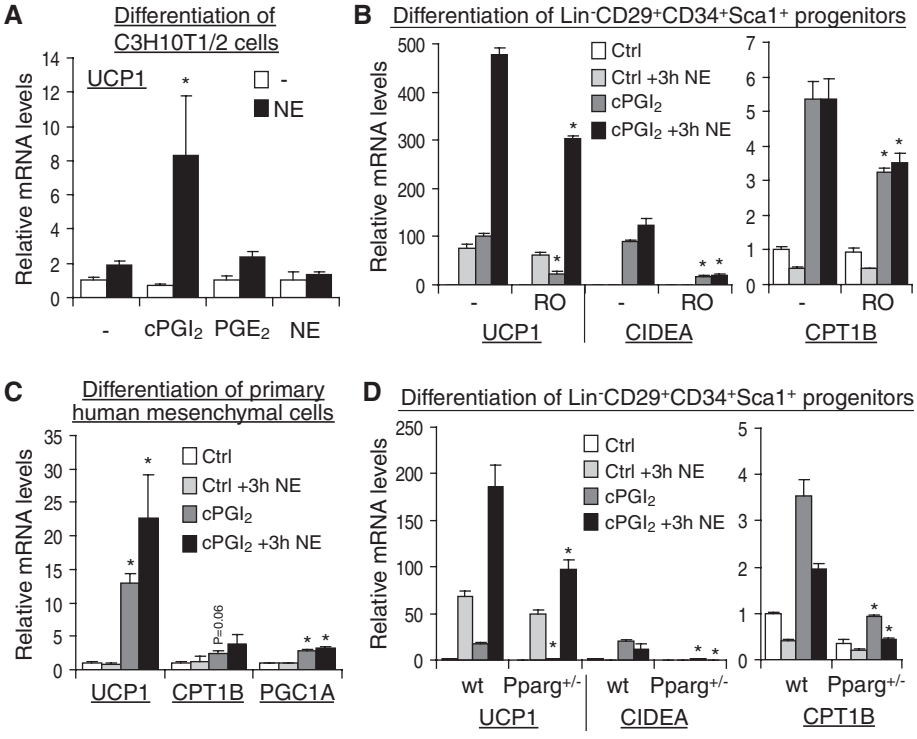

Fig. 3. Carbaprostacyclin ($cPGI_2$) shifts the differentiation of WAT mesenchymal progenitors toward a brown adipocyte phenotype. (**A** to **D**) Quantitative RT-PCR mRNA expression analysis. (A) C3H10T1/2 cells were induced to differentiate with adipogenic medium for 12 days in the presence of 1 μM of the indicated substance. Three hours before harvest, cells were acutely stimulated with 1 μM NE or vehicle in the absence of PG ($n = 3$; ANOVA interaction: UCP1 $P = 0.002$, PGC1A $P = 0.002$; *, post tests – versus $cPGI_2$: UCP1 $P < 0.01$, PGC1A $P < 0.05$). (B) Mouse $Lin^-CD29^+CD34^+Sca1^+$ mesenchymal progenitor cells were sorted from WAT-derived SVF and induced to differentiate as in (A) +/– 1 μM Ptgir antagonist RO1138452 (RO) ($n = 3$; *, $cPGI_2$-treated – versus RO $P < 0.03$). (C) Human enriched adipose tissue mesenchymal cells were treated as in (A) ($n = 3$; ANOVA interaction: $P > 0.05$; *, post tests Ctrl versus $cPGI_2$: $P < 0.001$). (D) $Lin^-CD29^+CD34^+Sca1^+$ cells from wt and $Pparg^{+/-}$ WAT were treated as in (A) ($n = 3$; *, $cPGI_2$-treated wt versus $Pparg^{+/-}$ $P < 0.015$). Means ± SEM.

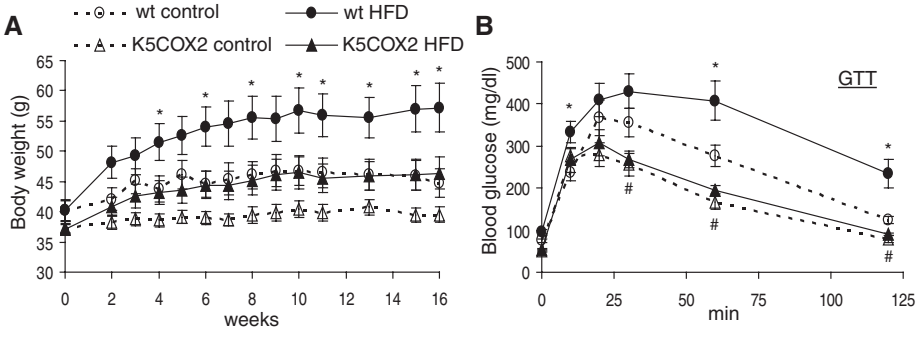

Fig. 4. Chronic COX-2 excess in WAT protects mice from diet-induced obesity and dysregulated glucose homeostasis. (**A**) Body weight time course of 7-month-old wt and K5COX2 mice fed a HFD or a control diet (60% and 10% calories from fat, respectively) for 16 weeks ($n \geq 9$, ANOVA post tests, *$P < 0.05$). (**B**) Intraperitoneal glucose tolerance test (GTT) in same mice as in (A) [$n = 7$; ANOVA post tests, wt: control versus HFD $P < 0.05$ (*); control diet: wt versus K5COX2 $P < 0.05$ (#)]. Means ± SEM.

K5COX2 mice displayed a 20% reduction in body weight, correlating with a severe reduction in body fat content but not muscle mass or bone length (Fig. 2, C and D, and fig. S16), which was reversed in animals on a celecoxib diet (fig. S17). The reduced adiposity of K5COX2 mice could not be explained by decreased food intake (Fig. 2E), increased activity of thermogenic and/or futile cycles in skeletal muscle (fig. S18), enhanced conBAT activity (fig. S19), or compromised skin insulation (figs. S18 to S22), but was associated with increased energy expenditure. Oxygen consumption was increased in K5COX2 mice compared with controls (Fig. 2F), which, along with an increase in body temperature (fig. S22), reflected a significant elevation of the resting metabolic rate (fig. S22). Consistent with increased substrate use, plasma free fatty acid and glycerol levels were lower in K5COX2 mice as compared with controls (fig. S23). Taken together, these results indicate that COX-2 has a critical role in indBAT development and function in WAT depots and that the COX-2-PG pathway contributes to adaptive thermogenesis and energy homeostasis.

Because the cellular origin of indBAT is currently a matter of dispute (*9*, *16*), we sought to determine the cell type responding to PG downstream of COX-2. Whereas NE treatment resulted in moderate but significant increases in UCP1, PGC1A, and PPARA mRNA expression, neither PGE_2 nor carbaprostacyclin ($cPGI_2$), a stable analog of PGI_2, induced these genes in mature adipocytes (fig. S24). In contrast to conBAT cells, induced brown adipocytes in WAT depots do not originate from common BAT/myogenic progenitors during cold exposure (*16*, *17*). Indeed, markers of conBAT progenitors, MYF5 and LHX8, were not enriched in indBAT of CL-treated or K5COX2 mice (fig. S25), substantiating the hypothesis that indBAT cells derive from unique mesenchymal progenitors residing in the SVF of WAT depots (*9*). As a model for multipotent mesenchymal progenitors, we first studied C3H10T1/2 cells (*16*, *18*) and treated them with PG or NE during adipogenic differentiation. Differentiation of these progenitors in the presence of $cPGI_2$ generated lipid-containing adipocytes with enhanced bona fide brown adipocyte capacities, as shown by a substantially increased response of thermogenic gene expression to postdifferentiation acute NE stimulation (Fig. 3A and fig. S26) (*19*). Additionally, acute treatment of primary SVF cells from WAT with PGE_2 or $cPGI_2$ led to a significant increase in UCP1 and PGC1A mRNA expression to an extent comparable to or greater than that induced by NE (fig. S27), supporting the notion that (progenitor) cells within the SVF are PG-responsive and in principle capable of upregulating BAT-specific genes.

We next isolated primary $Lin^-CD29^+CD34^+Sca1^+$ progenitor cells from WAT-derived SVF. These cells have the potential to differentiate along several mesenchymal lineages, including the lineage leading to white adipocytes (*20*) (fig. S28). Treatment with $cPGI_2$ or coculture with

CL-treated WAT explants induced the expression of UCP1 mRNA in these undifferentiated progenitor cells (figs. S29 and S30). Exposure of the $Lin^-CD29^+CD34^+Sca1^+$ cells to $cPGI_2$ during adipogenic differentiation potently elevated BAT marker gene expression and enhanced the post-differentiation responsiveness to NE (Fig. 3B and fig. S31). Similar results were also obtained with primary mesenchymal progenitors obtained from human WAT (Fig. 3C). The $cPGI_2$ effects in $Lin^-CD29^+CD34^+Sca1^+$ progenitors were blocked by loss-of-function of cellular PGI_2 receptors, Ptgir (7-transmembrane receptor) (*21*) or nuclear receptor PPARγ (*22*) (Fig. 3, B and D, and figs. S31 and S32) but were unaffected by PPARα/PPARβ/δ double knockout (fig. S33). Consistently, CL-induced indBAT recruitment was impaired in $Ptgir^{-/-}$ mice (figs. S34 to S36). Likewise, CL-induced indBAT recruitment was partially inhibited in $PPARγ^{+/-}$ animals (figs. S37 and S38) (*23*) but not in $PPARα^{-/-}$ or $β/δ^{-/-}$ mice (figs. S39 and S40), although the effect of PPARγ heterozygosity on UCP1 expression was compensated in the context of the intact tissue in vivo. These results demonstrate that COX-2 triggers recruitment of indBAT in WAT through a conserved PG-mediated differentiation shift of WAT mesenchymal progenitors toward the brown adipocyte phenotype using both membrane (Ptgir) and nuclear (PPARγ) receptor pathways.

Lastly, the critical role of COX-2 in the de novo recruitment of indBAT prompted us to assess the potential of this pathway to counteract adiposity and its pathophysiological consequences. Wild-type mice on a high-fat diet (HFD) showed a marked body weight gain throughout a 16-week feeding period (Fig. 4A). In contrast, weight gain was not significant in K5COX2 mice after 16 weeks on HFD; these mice reached body weight levels of wild-type mice on control diet (Fig. 4A). Moreover, K5COX2 mice were protected against HFD-induced fasting hyperglycemia (fig. S41), hyperinsulinemia (fig. S41), and glucose intolerance (Fig. 4B), suggesting that the stimulation of indBAT recruitment and energy expenditure through the COX-2-PG pathway confers protection against several adverse metabolic consequences of diet-induced obesity.

In conclusion, our data are consistent with a model in which NE released from sympathetic nerves induces COX-2 activity in WAT. We propose that downstream $PG(I_2)$/Ptgir/PPARγ signaling then shift(s) the differentiation of mesenchymal progenitors toward a brown phenotype with increased sensitivity to NE (fig. S1). This feed-forward mechanism results in the recruitment of indBAT in WAT depots, contributing to thermogenesis and systemic energy expenditure. Currently, there are no drugs available that induce BAT. β-adrenergic agonists that increase thermogenesis have been tested in humans as antiobesity drugs, but with limited success (*24*, *25*). Manipulation of COX-2/PG signaling in defined indBAT progenitors represents an alternative strategy for enhancing BAT activity that could help protect against energy surplus and body weight gain.

References and Notes

1. F. S. Celi, *N. Engl. J. Med.* **360**, 1553 (2009).
2. A. M. Cypess *et al.*, *N. Engl. J. Med.* **360**, 1509 (2009).
3. W. D. van Marken Lichtenbelt *et al.*, *N. Engl. J. Med.* **360**, 1500 (2009).
4. K. A. Virtanen *et al.*, *N. Engl. J. Med.* **360**, 1518 (2009).
5. T. W. Davis *et al.*, *J. Pharmacol. Exp. Ther.* **308**, 929 (2004).
6. K. Lundholm, P. Daneryd, U. Körner, A. Hyltander, I. Bosaeus, *Int. J. Oncol.* **24**, 505 (2004).
7. J. N. Fain, L. R. Ballou, S. W. Bahouth, *Prostaglandins Other Lipid Mediat.* **65**, 199 (2001).
8. Materials and methods are available as supporting material on *Science* Online.
9. S. Gesta, Y. H. Tseng, C. R. Kahn, *Cell* **131**, 242 (2007).
10. C. Guerra, R. A. Koza, H. Yamashita, K. Walsh, L. P. Kozak, *J. Clin. Invest.* **102**, 412 (1998).
11. B. Richelsen, *Biochem. J.* **247**, 389 (1987).
12. J. K. Akunda *et al.*, *Mol. Carcinog.* **46**, 354 (2007).
13. T. D. Penning *et al.*, *J. Med. Chem.* **40**, 1347 (1997).
14. P. Seale *et al.*, *Cell Metab.* **6**, 38 (2007).
15. G. Neufang, G. Furstenberger, M. Heidt, F. Marks, K. Müller-Decker, *Proc. Natl. Acad. Sci. U.S.A.* **98**, 7629 (2001).
16. P. Seale *et al.*, *Nature* **454**, 961 (2008).
17. J. A. Timmons *et al.*, *Proc. Natl. Acad. Sci. U.S.A.* **104**, 4401 (2007).
18. Y. H. Tseng *et al.*, *Nature* **454**, 1000 (2008).
19. B. Cannon, J. Nedergaard, *Physiol. Rev.* **84**, 277 (2004).
20. M. S. Rodeheffer, K. Birsoy, J. M. Friedman, *Cell* **135**, 240 (2008).
21. T. Murata *et al.*, *Nature* **388**, 678 (1997).
22. E. Falcetti *et al.*, *Biochem. Biophys. Res. Commun.* **360**, 821 (2007).
23. S. L. Gray *et al.*, *Endocrinology* **147**, 5708 (2006).
24. K. L. Palamara, H. R. Mogul, S. J. Peterson, W. H. Frishman, *Cardiol. Rev.* **14**, 238 (2006).
25. J. R. Arch, *Eur. J. Pharmacol.* **440**, 99 (2002).

26. We thank K. Hexel, A. Jones, D. Kucher, P. Kulozik, A. Lacher, F. Mattijssen, D. Metzger, A. Pohl-Arnold, A. Reimann, S. Schmitt, B. Steinbauer, M. Willershäuser, and A. E. Schwarz for experimental support; A. Rose for comments on the manuscript; J. Masferrer (Pfizer, St. Louis, USA) for providing celecoxib; and S. Narumiya (Kyoto, Japan) for Ptgir knockout mice. This work was supported by the German National Genome Research Network (grants 01GS0822 to M.K. and 01GS0869 to M.K. and M.H.) and by the Deutsche Forschungsgemeinschaft He3260/2-1, the Network Aging Research Heidelberg/Mannheim, and a Marie Curie Excellence Grant to S.H.

Supporting Online Material

www.sciencemag.org/cgi/content/full/science.1186034/DC1
Materials and Methods
Figs. S1 to S41
References

16 December 2009; accepted 8 April 2010
Published online 6 May 2010;
10.1126/science.1186034
Include this information when citing this paper.

Genome-Wide Kinetics of Nucleosome Turnover Determined by Metabolic Labeling of Histones

Roger B. Deal,[1] Jorja G. Henikoff,[1] Steven Henikoff[1,2]*

Nucleosome disruption and replacement are crucial activities that maintain epigenomes, but these highly dynamic processes have been difficult to study. Here, we describe a direct method for measuring nucleosome turnover dynamics genome-wide. We found that nucleosome turnover is most rapid over active gene bodies, epigenetic regulatory elements, and replication origins in *Drosophila* cells. Nucleosomes turn over faster at sites for trithorax-group than polycomb-group protein binding, suggesting that nucleosome turnover differences underlie their opposing activities and challenging models for epigenetic inheritance that rely on stability of histone marks. Our results establish a general strategy for studying nucleosome dynamics and uncover nucleosome turnover differences across the genome that are likely to have functional importance for epigenome maintenance, gene regulation, and control of DNA replication.

Nucleosome disassembly and reassembly, or turnover, is necessary for epigenome maintenance, but the mechanisms that are responsible remain unclear (*1*). One approach to this problem has been to map enrichment of the universal histone replacement variant, H3.3 (*2*–*6*), which requires complete unwrapping of DNA from around the histone core for its replication-independent deposition to occur. Genome-wide profiling of steady-state amounts of H3.3 from *Drosophila melanogaster* S2 cells indicated that nucleosome replacement occurs most prominently across transcribed regions of active genes and at promoters and binding sites of trithorax group (trxG) and polycomb group (PcG) proteins (*2*, *3*). Similar results were obtained for HeLa cells (*7*) and *Caenorhabditis elegans* embryos (*8*). A more direct approach, which can measure dynamics but is limited to yeast, is to express constitutive and inducible histone transgenes and to measure the relative incorporation of their encoded tagged histones (*9*–*11*). These studies indicated that turnover rates were high at promoters and chromatin boundary

[1]Basic Sciences Division, Fred Hutchinson Cancer Research Center, Seattle, WA 98109, USA. [2]Howard Hughes Medical Institute, Seattle, WA 98109, USA.

*To whom correspondence should be addressed. E-mail: steveh@fhcrc.org

elements but low within transcribed regions. Both approaches are limited by the requirement for transgenes and tags and by the time lag during induction.

We have developed a general method for directly measuring the kinetics of nucleosome turnover that overcomes these limitations (*12*). Our strategy uses cotranslational incorporation of the methionine (Met) surrogate azidohomoalanine (Aha) into proteins and subsequent ligation of biotin to Aha-containing proteins through the [3+2] cycloaddition reaction between the azide group of Aha and an alkyne linked to biotin (*13*, *14*) (fig. S1A). To measure nucleosome turnover rates, we treated cells briefly with Aha, coupled biotin to nucleosomes containing newly incorporated histones, affinity-purified with streptavidin, washed stringently to remove nonhistone proteins, and analyzed the affinity-purified DNA by using tiling microarrays. We call this strategy CATCH-IT, for covalent attachment of tags to capture histones and identify turnover. In *Drosophila* S2 cells, Aha was incorporated into total protein, including histones, in a translation-dependent manner (fig. S1, B to D). Incorporation of Aha into newly synthesized histones increased in proportion to the length of Aha treatment for at least 3 hours.

To measure nucleosome turnover across the genome, we starved late log-phase S2 cells for methionine for 30 minutes and treated them with Aha for 3 hours, performed the biotin coupling reaction on isolated nuclei, and digested chromatin with micrococcal nuclease to yield mostly mononucleosomes. Biotin-tagged nucleosomes containing newly synthesized histones were then isolated by using streptavidin beads and washed with a urea-salt solution to remove H2A/H2B dimers and other DNA-binding proteins (fig. S2), leaving only $(H3/H4)_2$ tetramers (*15*), and the remaining DNA was labeled and hybridized to high-density tiling microarrays along with the corresponding input DNA. For comparison, we also performed streptavidin precipitations using chromatin from S2 cells expressing biotin-tagged H3.3 over a 2-day period as previously described (*2*). When array data for all genes with annotated ends were divided into quintiles by gene expression and aligned by gene ends and when $\log_2$

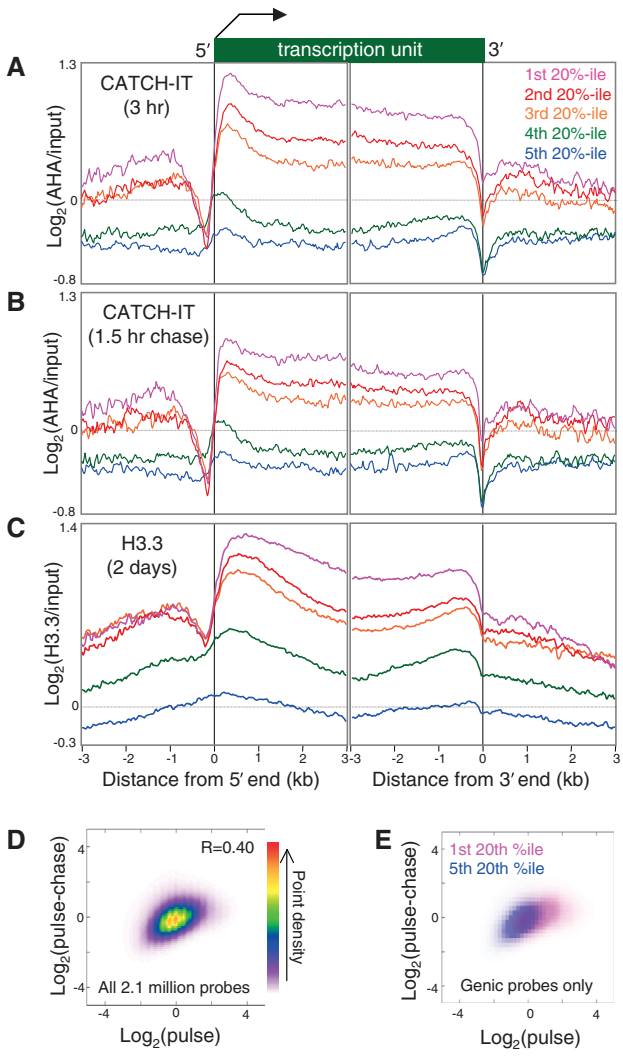

Fig. 1. CATCH-IT marks sites of histone replacement and reveals kinetics. (**A**) Gene ends analysis of a CATCH-IT experiment from a 3-hour Aha treatment (pulse). All 9820 genes from FlyBase r5.13 with annotated 5′ and 3′ ends were grouped by gene expression quintiles (top 20% to bottom 20% based on GEO GSM333845) and aligned by gene ends versus the $\log_2$ ratios of precipitated DNA/input DNA averaged across genes. (**B**) Same as in (A) but with cells treated with Aha for 3 hours (pulse) followed by a 1.5-hour Met treatment (chase). (**C**) Same as in (A) but for biotin-tagged H3.3 nucleosomes. (**D**) Scatter plot showing the correlation between the pulse and the difference between the pulse and chase with use of all 2.1 million probes on the array. (**E**) Same as in (D) but with use of only genic probes from highest and lowest gene expression quintiles.

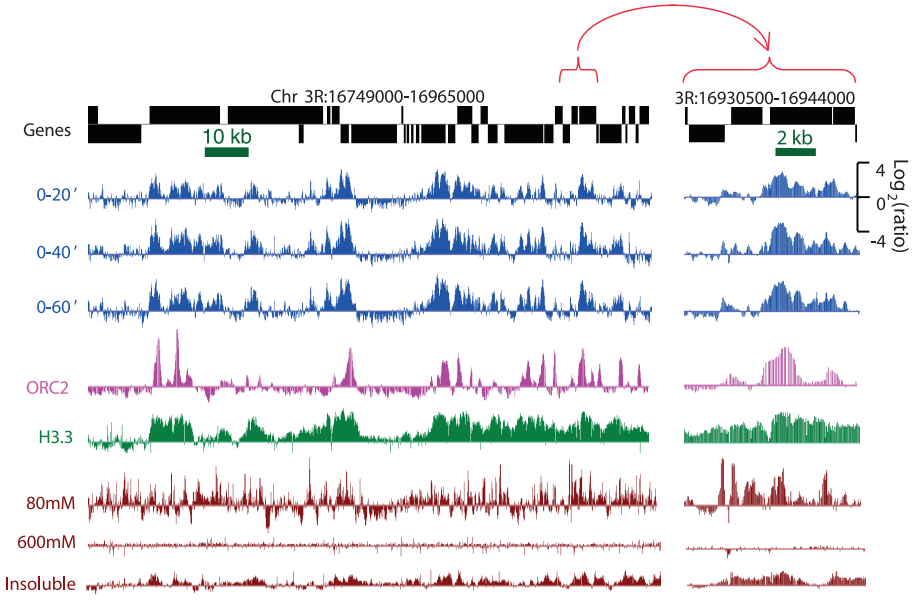

Fig. 2. Chromatin landscapes of CATCH-IT, ORC, H3.3, and salt fractions. Chromatin landscapes over a representative euchromatic region of chromosome arm 3R from a CATCH-IT time course of 20-, 40-, and 60-min Aha treatment. Also shown are ORC binding; biotinylated H3.3 nucleosomes; and successive 80 mM, 600 mM, and insoluble chromatin salt fractions (*18*). Genes are shown above chromatin tracks. Those above the line are on the top strand and those below the line are on the bottom strand. Right section shows a magnification of the indicated region of the left section.

ratios of precipitated DNA/input DNA were averaged across genes, we found that CATCH-IT and H3.3 profiles were highly similar (Fig. 1, A and C). In addition, CATCH-IT landscapes corresponded overall to steady-state H3.3 landscapes (Fig. 2, blue and green tracks), albeit with better definition of chromatin features. Such correspondence confirms that CATCH-IT depends on nucleosome dynamics, and we attribute the better resolution of CATCH-IT to its capturing turnover kinetics rather than steady-state replacement.

As a control, we also treated S2 cells with Met rather than Aha and obtained a featureless profile, confirming that the signals obtained with Aha represent newly synthesized histones (fig. S3).

We also found that independent biological replicates of the CATCH-IT procedure yielded similar results (fig. S4).

We next asked whether CATCH-IT could measure nucleosome turnover kinetics. After treating cells with a 3-hour pulse of Aha, a sample was taken, and then cells were switched back to Met-containing media for a 1.5-hour chase; both samples were processed as before. As expected, the chase resulted in an overall reduction of signal across expressed genes when compared with the pulse signal (Fig. 1, A and B). We also compared the difference between the pulse and chase signals to the pulse signal on scatter plots by using either all 2.1 million probes or only genic probes from genes in each expression quintile. As expected for kinetic measurements, nucleosomes undergoing the highest turnover also tended to show the largest decrease during the chase, and this trend depended on gene expression (Fig. 1, D and E, and fig. S5). We conclude that CATCH-IT captures the dynamics of histone replacement. In addition, these results show that turnover across gene bodies is highly dependent on expression level (Fig. 1, A and B). We suggest that the high turnover seen for gene bodies in *Drosophila* but low rate seen for yeast (*10*) reflects biological differences between the two organisms in processes that evict or retain nucleosomes during transcription.

To estimate rates of nucleosome turnover, we removed successive samples after treating with Aha for 20, 40, and 60 min. We observed that the nucleosome turnover landscapes generated at each time point were highly similar (Fig. 2, blue tracks), and this was confirmed by ends analysis (fig. S6). We also examined turnover at sites of epigenetic regulatory elements, as represented by sites of binding of the trxG proteins GAF (GAGA factor or trithorax-like) and Zeste and of the PcG proteins EZ (enhancer of zeste) and PSC (posterior sex combs) (*16*, *17*). Comparison of average turnover profiles across GAF, Zeste, and EZ+PSC sites showed that CATCH-IT identified these sites as regions of high turnover relative to surrounding regions, with higher turnover at GAF than at EZ+PSC sites (Fig. 3, A and B, and fig. S7, A and B). There was also better peak delineation with CATCH-IT than was observed for H3.3 or low salt-soluble chromatin, which represents classical "active" chromatin (*18*) (Fig. 3, A to D, and fig. S7). By using the 20-min data sets from two independent experiments to calculate turnover rates (fig. S8), we obtained mean lifetimes of ~1 hour for the peak just downstream of the transcriptional start site of active genes, ~1 hour for GAF sites, and ~1.5 hours for EZ+PSC sites (table S1). These estimates are conservative, because any delay in incorporation of Aha would lead us to overestimate mean lifetimes. Therefore, nucleosomes within active genes and at epigenetic regulatory elements turn over multiple times during each ~20-hour cell cycle.

We also compared CATCH-IT turnover landscapes to binding sites for the ORC2 subunit of the origin recognition complex (ORC), which specifies replication initiation (*19*). We observed a notable correspondence, as exemplified by visual examination of a typical gene-rich region of the *Drosophila* genome (Fig. 2, magenta tracks). Although H3.3 amounts also showed a correspondence to ORC amounts (Fig. 2, green tracks) as previously observed (*20*), the resemblance of CATCH-IT profiles to ORC profiles was far more conspicuous. To better evaluate these correspondences, we aligned CATCH-IT, H3.3, and other chromatin profiles around the 5135 ORC peaks (*20*) and divided them into quintiles on the basis of ORC binding score (Fig. 3, E to G). The nested peaks indicate a quantitative relationship

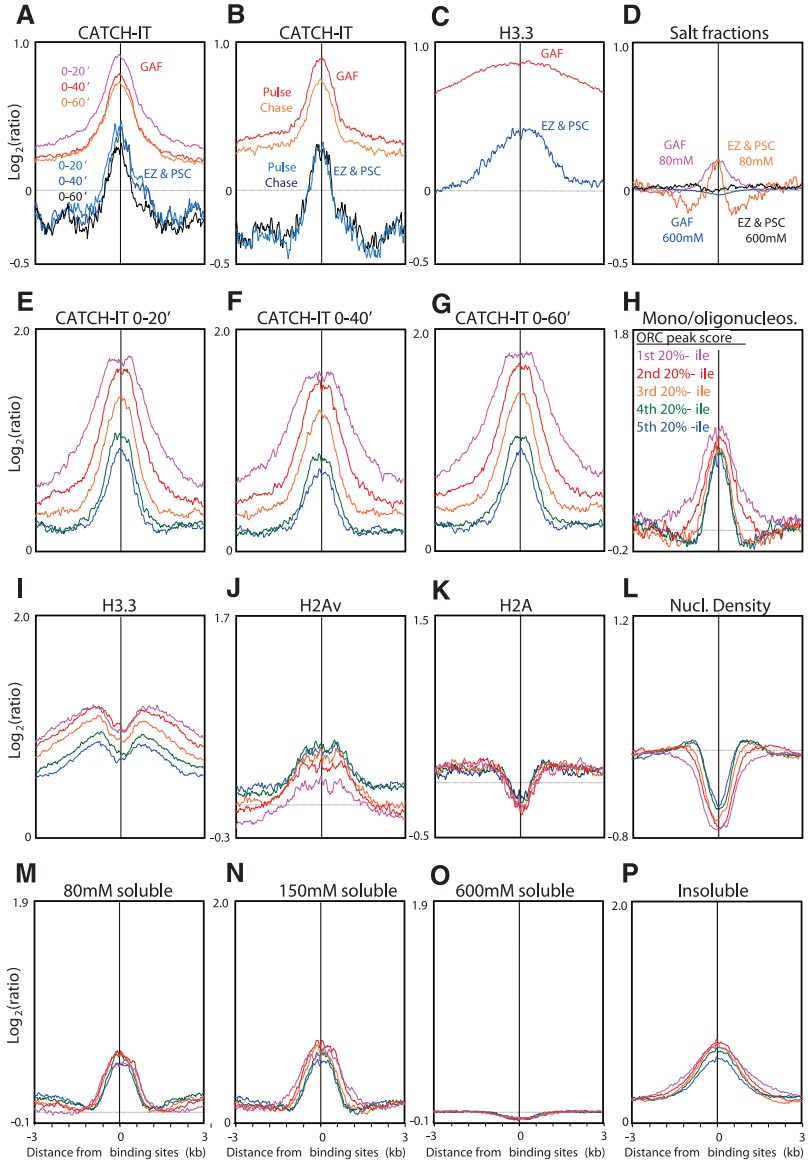

Fig. 3. Kinetics of nucleosome turnover at epigenetic regulatory elements and sites of ORC binding. (**A**) Average CATCH-IT time course signals over GAF and EZ+PSC binding sites. (**B**) Same as in (A) but for a pulse-chase experiment with a 3-hour Aha pulse and 1.5-hour Met chase. (**C**) Average biotinylated H3.3 signals over GAF and EZ+PSC binding sites. (**D**) Average signals from chromatin salt fractions over GAF and EZ+PSC binding sites. (**E** to **P**) Plots of various chromatin signals aligned at peaks of ORC binding and divided into quintiles by ORC peak score (*20*).

between ORC binding and nucleosome turnover, suggesting that turnover facilitates ORC binding. In contrast, other chromatin features that would be expected for open or dynamic chromatin, including nucleosome density, mononucleosome/oligonucleosome ratio (a measure of micrococcal nuclease accessibility), H2Av (an H2A.Z histone variant enriched in active chromatin), and salt-soluble nucleosomes, show little if any dependence on ORC abundance (Fig. 3, H to P). Our findings support the hypothesis that replication origins are determined by chromatin, not by sequence features (*20*, *21*). The better quantitative correspondence of ORC to CATCH-IT data than to other chromatin measurements implies that the ORC occupies DNA that is made accessible by nucleosome turnover. In support of this interpretation, we note that very similar correspondences are seen when CATCH-IT data are aligned with GAF sites (fig. S9) and that GAF directs nucleosome turnover in vivo (*22*, *23*).

Our direct strategy for measuring the kinetics of nucleosome turnover does not rely on transgenes or antibodies but rather uses native histones and generic reagents. Thus, CATCH-IT provides a general tool for studying activities that influence nucleosome turnover. With use of CATCH-IT, we found direct evidence that epigenetic maintenance involves nucleosome turnover, a process that erases histone modifications (*10*). The fact that EZ is responsible for di- and trimethylation of H3K27, but the nucleosomes that it modifies turn over faster than a cell cycle, argues against proposals that histone modifications required for cellular memory themselves transmit epigenetic information (*24*). Rather, by simply increasing or decreasing accessibility of DNA to sequence-specific binding proteins, regulated nucleosome turnover may perpetuate active or silent gene expression states and facilitate initiation of replication.

References and Notes

1. S. Henikoff, *Nat. Rev. Genet.* **9**, 15 (2008).
2. Y. Mito, J. G. Henikoff, S. Henikoff, *Nat. Genet.* **37**, 1090 (2005).
3. Y. Mito, J. G. Henikoff, S. Henikoff, *Science* **315**, 1408 (2007).
4. U. Braunschweig, G. J. Hogan, L. Pagie, B. van Steensel, *EMBO J.* **28**, 3635 (2009).
5. C. M. Chow *et al.*, *EMBO Rep.* **6**, 354 (2005).
6. C. Wirbelauer, O. Bell, D. Schübeler, *Genes Dev.* **19**, 1761 (2005).
7. C. Jin *et al.*, *Nat. Genet.* **41**, 941 (2009).
8. S. L. Ooi, J. G. Henikoff, S. Henikoff, *Nucleic Acids Res.* **38**, e26 (2010).
9. A. Jamai, R. M. Imoberdorf, M. Strubin, *Mol. Cell* **25**, 345 (2007).
10. M. F. Dion *et al.*, *Science* **315**, 1405 (2007).
11. A. Rufiange, P.-E. Jacques, W. Bhat, F. Robert, A. Nourani, *Mol. Cell* **27**, 393 (2007).
12. Materials and methods are available as supporting material on *Science* Online.
13. J. A. Prescher, C. R. Bertozzi, *Nat. Chem. Biol.* **1**, 13 (2005).
14. D. C. Dieterich, A. J. Link, J. Graumann, D. A. Tirrell, E. M. Schuman, *Proc. Natl. Acad. Sci. U.S.A.* **103**, 9482 (2006).
15. K. Yamasu, T. Senshu, *J. Biochem.* **107**, 15 (1990).
16. Y. B. Schwartz *et al.*, *Nat. Genet.* **38**, 700 (2006).
17. N. Nègre *et al.*, *PLoS Genet.* **6**, e1000814 (2010).
18. S. Henikoff, J. G. Henikoff, A. Sakai, G. B. Loeb, K. Ahmad, *Genome Res.* **19**, 460 (2009).
19. B. P. Duncker, I. N. Chesnokov, B. J. McConkey, *Genome Biol.* **10**, 214 (2009).
20. H. K. Macalpine, R. Gordan, S. K. Powell, A. J. Hartemink, D. M. Macalpine, *Genome Res.* **20**, 201 (2010).
21. D. M. Gilbert, *Nat. Rev. Mol. Cell Biol.* **5**, 848 (2004).
22. T. Nakayama, K. Nishioka, Y. X. Dong, T. Shimojima, S. Hirose, *Genes Dev.* **21**, 552 (2007).
23. S. J. Petesch, J. T. Lis, *Cell* **134**, 74 (2008).
24. K. H. Hansen *et al.*, *Nat. Cell Biol.* **10**, 1291 (2008).

25. We thank T. Furuyama for suggesting this approach, members of our lab for helpful discussions, and the Hutchinson Center Genomics Shared Resource for microarray processing. This work was supported by NIH grant 1R21DA025758 to S.H. and NIH Postdoctoral Fellowship 1F32GM083449 to R.B.D. All data sets can be found in GEO: GSE19788.

Supporting Online Material

www.sciencemag.org/cgi/content/full/328/5982/1161/DC1
Materials and Methods
Figs. S1 to S9
Table S1
References

7 January 2010; accepted 1 April 2010
10.1126/science.1186777

Global Biodiversity: Indicators of Recent Declines

Stuart H. M. Butchart,[1,2]* Matt Walpole,[1] Ben Collen,[3] Arco van Strien,[4] Jörn P. W. Scharlemann,[1] Rosamunde E. A. Almond,[1] Jonathan E. M. Baillie,[3] Bastian Bomhard,[1] Claire Brown,[1] John Bruno,[5] Kent E. Carpenter,[6] Geneviève M. Carr,[7]† Janice Chanson,[8] Anna M. Chenery,[1] Jorge Csirke,[9] Nick C. Davidson,[10] Frank Dentener,[11] Matt Foster,[12] Alessandro Galli,[13] James N. Galloway,[14] Piero Genovesi,[15] Richard D. Gregory,[16] Marc Hockings,[17] Valerie Kapos,[1,18] Jean-Francois Lamarque,[19] Fiona Leverington,[17] Jonathan Loh,[20] Melodie A. McGeoch,[21] Louise McRae,[3] Anahit Minasyan,[22] Monica Hernández Morcillo,[1] Thomasina E. E. Oldfield,[23] Daniel Pauly,[24] Suhel Quader,[25] Carmen Revenga,[26] John R. Sauer,[27] Benjamin Skolnik,[28] Dian Spear,[29] Damon Stanwell-Smith,[1] Simon N. Stuart,[1,12,30,31] Andy Symes,[2] Megan Tierney,[1] Tristan D. Tyrrell,[1] Jean-Christophe Vié,[32] Reg Watson[24]

In 2002, world leaders committed, through the Convention on Biological Diversity, to achieve a significant reduction in the rate of biodiversity loss by 2010. We compiled 31 indicators to report on progress toward this target. Most indicators of the state of biodiversity (covering species' population trends, extinction risk, habitat extent and condition, and community composition) showed declines, with no significant recent reductions in rate, whereas indicators of pressures on biodiversity (including resource consumption, invasive alien species, nitrogen pollution, overexploitation, and climate change impacts) showed increases. Despite some local successes and increasing responses (including extent and biodiversity coverage of protected areas, sustainable forest management, policy responses to invasive alien species, and biodiversity-related aid), the rate of biodiversity loss does not appear to be slowing.

In 2002, world leaders committed, through the Convention on Biological Diversity (CBD), "to achieve by 2010 a significant reduction of the current rate of biodiversity loss" (*1*), and this "2010 target" has been incorporated into the United Nations Millennium Development Goals in recognition of the impact of biodiversity loss on human well-being (*2*). The CBD created a framework of indicators to measure biodiversity loss at the level of genes, populations, species, and ecosystems (*3*, *4*). Although a minority have been published individually (*5*), hitherto they have not been synthesized to provide an integrated outcome. Despite suggestions that the target is unlikely to be (*6*–*8*), or has not been (*4*, *9*, *10*), met, we test this empirically using a broad suite of biodiversity indicators.

To evaluate achievement of the 2010 target, we (i) determined the trend, and timing and direction of significant inflections in trend for individual indicators (*11*) and (ii) calculated aggregated indices relating to the state of biodiversity, pressures upon it, policy and management responses, and the state of benefits (ecosystem services) that people derive from biodiversity, using the best available sources. To calculate aggregate indices, we first scaled each of 24 indicators (out of 31) with available trend information to a value of 1 in the first year with data from 1970 onward (only eight indicators had earlier trends) and calculated annual proportional change from this first year. Then we used a generalized additive modeling framework (*5*, *12*, *13*) and determined significant inflections (*12*). Although absolute values are difficult to interpret because they aggregate different elements of biodiversity, this approach permits a synthetic interpretation of rate changes across the elements measured: For example, the aggregated state index should show positive inflections if biodiversity loss has been significantly reduced.

Our analyses suggest that biodiversity has continued to decline over the past four decades, with most (8 out of 10) state indicators showing negative trends (Fig. 1 and Table 1). There have been declines in population trends of (i) vertebrates (*13*) and (ii) habitat specialist birds; (iii) shorebird populations worldwide; extent of (iv) forest (*14*, *15*); (v) mangroves; (vi) seagrass beds; and (vii) the condition of coral reefs. None show significant recent reductions in the rate of decline (Table 1), which is either fluctuating (i), stable (ii), based on too few data to test significance (iii to vi), or stable after a deceleration two decades ago (vii). Two indicators, freshwater quality and trophic integrity in the marine ecosystem, show stable and marginally improving trends, respectively, which are likely explained by geographic biases in data availability for the former and spatial expansion of fisheries for the latter (*5*). Aggregated trends across state indicators have declined, with no significant recent reduction in rate: The most recent inflection in the index (in 1972) was negative (Fig. 2). Because there were fewer indicators with trend data in the 1970s, we recalculated the index from 1980, which also showed accelerating biodiversity loss: The most recent inflection (2004) was negative. Finally, aggregated species' extinction risk (i.e., biodiversity loss at the species level) has accelerated: The International Union for Conservation of Nature (IUCN) Red List Index (RLI), measuring rate of change (*16*, *17*), shows negative trends.

The majority of indicators of pressures on biodiversity show increasing trends over recent decades (Fig. 1 and Table 1), with increases in (i) aggregate human consumption of the planet's ecological assets, (ii) deposition of reactive nitrogen, (iii) number of alien species in Europe, (iv) proportion of fish stocks overharvested, and (v) impact of climate change on European bird population trends (*18*). In no case was there a significant reduction in the rate of increase (Table 1), which was stable (i, iii, and v), fluctuating (iv), or based on too few data to test significance (ii), although growth in global nitrogen deposition may have slowed, and this may explain why the most recent inflection in aggregated trends (in 2006) was negative (Fig. 2) (*5*). Global trends for habitat fragmentation are unavailable, but it is probably increasing; for example, 80% of remaining Atlantic Forest fragments are <0.5 km^2 in size (*19*), and 59% of large river systems are moderately or strongly fragmented by dams and reservoirs (*20*).

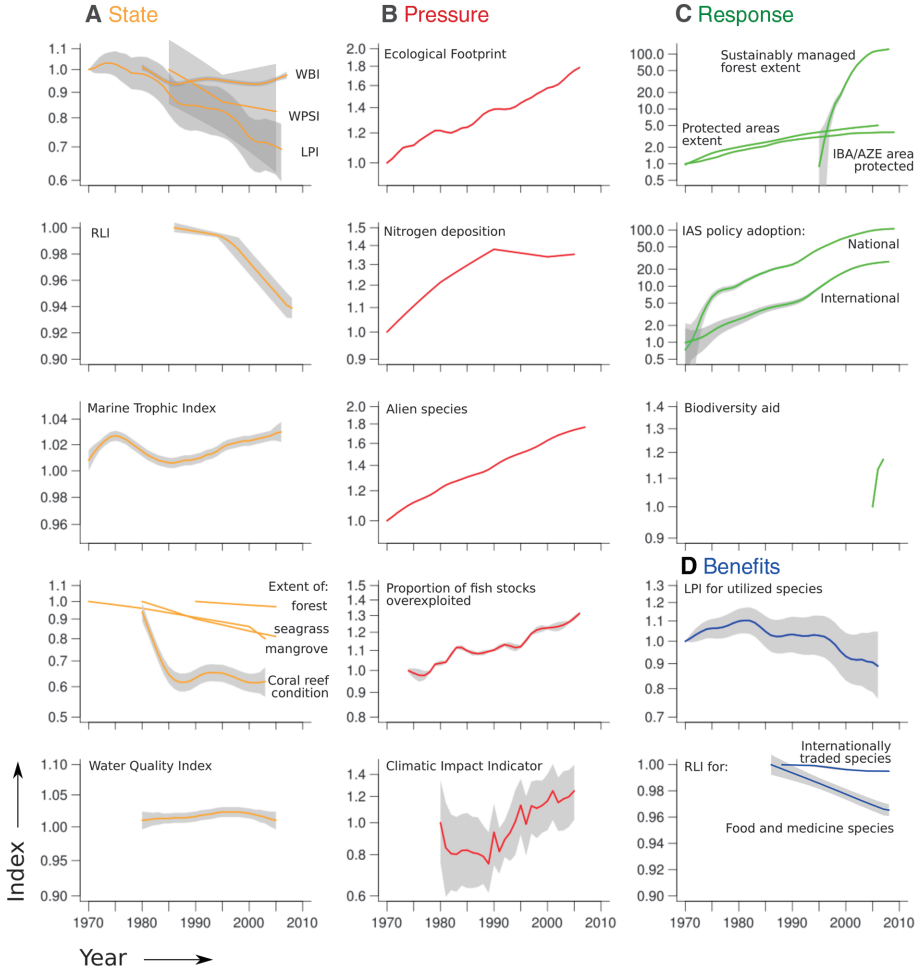

Fig. 1. Indicator trends for (**A**) the state of biodiversity, (**B**) pressures upon it, (**C**) responses to address its loss, and (**D**) the benefits humans derive from it. Data scaled to 1 in 1970 (or for first year of data if >1970), modeled (if >13 data points; see Table 1), and plotted on a logarithmic ordinate axis. Shading shows 95% confidence intervals except where unavailable (i.e., mangrove, seagrass, and forest extent, nitrogen deposition, and biodiversity aid). WBI, Wild Bird Index; WPSI, Waterbird Population Status Index; LPI, Living Planet Index; RLI, Red List Index; IBA, Important Bird Area; AZE, Alliance for Zero Extinction site; IAS, invasive alien species.

[1]United Nations Environment Programme World Conservation Monitoring Centre, 219 Huntingdon Road, Cambridge CB3 0DL, UK. [2]BirdLife International, Wellbrook Court, Cambridge CB3 0NA, UK. [3]Institute of Zoology, Zoological Society of London, Regent's Park, London NW1 4RY, UK. [4]Statistics Netherlands, Post Office Box 24500, The Hague, 2490 HA, Netherlands. [5]Department of Marine Sciences, University of North Carolina at Chapel Hill, 340 Chapman Hall, CB 3300, Chapel Hill, NC 27599, USA. [6]International Union for Conservation of Nature (IUCN) and Conservation International Global Marine Species Assessment, Biological Sciences, Old Dominion University, Norfolk, VA 23529, USA. [7]United Nations Environment Programme, Global Environment Monitoring System—Water, c/o National Water Research Institute, 867 Lakeshore Road, Burlington, Ontario L7R 4A6, Canada. [8]IUCN Species Survival Commission, Conservation International, Biodiversity Assessment Unit, c/o Center for Applied Biodiversity Science, Conservation International, 2011 Crystal Drive, Suite 500, Arlington, VA 22202, USA. [9]Fisheries and Aquaculture Management Division, Food and Agriculture Organization of the United Nations, Viale delle Terme di Caracalla 00153, Rome, Italy. [10]Secretariat of the Ramsar Convention on Wetlands, Rue Mauverney 28, 1196 Gland, Switzerland. [11]European Commission Joint Research Centre, Institute for Environment and Sustainability, TP290, Via Enrico Fermi 2749, 21027 Ispra (VA), Italy. [12]Center for Applied Biodiversity Science, Conservation International, 2011 Crystal Drive, Suite 500, Arlington, VA 22202, USA. [13]Global Footprint Network, 312 Clay Street, Suite 300, Oakland, CA 94607–3510, USA. [14]Environmental Sciences Department, University of Virginia, Charlottesville, VA 22903, USA. [15]Istituto Superiore per la Protezione e la Ricerca Ambientale, Via Curtatone 3, I-00185 Rome, Italy. [16]Royal Society for the Protection of Birds, The Lodge, Sandy SG19 2DL, UK, and European Bird Census Council. [17]School of Integrative Systems, University of Queensland, St. Lucia, Brisbane, Qld 4067, Australia. [18]Department of Zoology, University of Cambridge, Downing Street, Cambridge CB2 3EJ, UK. [19]National Center for Atmospheric Research, 3450 Mitchell Lane, Boulder, CO 80301, USA. [20]World Wildlife Fund (WWF) International, 1196 Gland, Switzerland. [21]South African National Parks, Centre for Invasion Biology and Global Invasive Species Programme, Post Office Box 216, Steenberg 7947, South Africa. [22]United Nations Educational, Scientific, and Cultural Organization, 7 place de Fontenoy, 75352 Paris, France. [23]TRAFFIC International, 219 Huntingdon Road, Cambridge CB3 0DL, UK. [24]Sea Around Us Project, Fisheries Centre, University of British Columbia, 2202 Main Mall, Vancouver, BC V6T1Z4, Canada. [25]National Centre for Biological Sciences, Tata Institute of Fundamental Research, GKVK Campus, Bellary Road, Bangalore 560 065, India. [26]The Nature Conservancy, 4245 North Fairfax Drive, Arlington, VA 22203, USA. [27]U.S. Geological Survey, Patuxent Wildlife Research Center, 12100 Beech Forest Road, Laurel, MD 20708–4039, USA. [28]American Bird Conservancy, 1731 Connecticut Avenue, N.W., 3rd Floor, Washington, DC 20009, USA. [29]Centre for Invasion Biology, Stellenbosch University, Private Bag X1, Matieland 7602, South Africa. [30]IUCN Species Survival Commission, Department of Biology and Biochemistry, University of Bath, Bath BA2 7AY, UK. [31]Al Ain Wildlife Park and Resort, Post Office Box 45553, Abu Dhabi, United Arab Emirates. [32]IUCN, Rue Mauverney 28, 1196 Gland, Switzerland.

*To whom correspondence should be addressed. E-mail: stuart.butchart@birdlife.org

†Present address: Indian and Northern Affairs Canada, 15 Eddy, Gatineau QC K1A 0H4, Canada.

Table 1. Summary of global biodiversity indicator trends.

Indicator	Data availability (years)†	% Change since 1970‡	Mean annual % change§					Trends in rate of change‖
			1970s	1980s	1990s	2000s	Since 1970	
		State						
Living Planet Index (LPI) (mean population trends of vertebrates)	1970–2006	−31*	−0.2	−1.4	−1.4	−0.9	−1.0	F
Wild Bird Index [mean population trends of habitat specialists in Europe and North America, disaggregated for terrestrial (t) and wetland (w) species]	1980–2007	−2.6* −16*(t) +40*(w)		−0.6 −1.3 +1.1	−0.2 −0.7 +1.3	+0.6 +0.3 +1.1	−0.1 −0.7 +1.2	S D 1982–2007 S
Waterbird Population Status Index (% shorebird populations increasing, stable, or decreasing)	1985–2005†	−33		−1.4	−2.0	−2.4	−2.0	A?
Red List Index (RLI) (extinction risk of mammals, birds, amphibians, and corals)	1986–2008	−6.1*		−0.1	−0.2	−0.5	−0.3	A
Marine Trophic Index (shift in fishing catch from top predators to lower trophic levels)	1950–2006	+3.0*	+0.1	−0.1	+0.1	+0.1	+0.1	S
Forest extent	1990–2005†	−3.1			−0.2	−0.2	−0.2	S?
Mangrove extent	1980–2005†	−19		−1.0	−0.7	−0.7	−0.8	S?
Seagrass extent	1930–2003†	−20	−0.4	−0.5	−0.5	−2.4	−0.7	A?
Coral reef condition (live hard coral cover)	1980–2004	−38*		−3.9	−0.3	+0.2	−1.8	D 1985–1988
Water Quality Index (physical/chemical quality of freshwater)	1980–2005	0		+0.1	+0.0	−0.2	+0	S
Number of state indicators declining			**2/3**	**8/9**	**8/10**	**7/10**	**8/10**	
		Pressures						
Ecological footprint (humanity's aggregate resource-consumption)	1961–2006	+78*	+2.0	+1.3	+1.3	+2.1	+1.6	S
Nitrogen deposition rate (annual reactive N deposited)	1850–2005†	+35	+2.0	+1.3	−0.3	+0.2	+0.9	D?
No. alien species in Europe (Mediterranean marine, mammal, and freshwater)	1970–2007	+76*	+2.0	+1.4	+1.6	+1.1	+1.5	S
Exploitation of fish stocks (% overexploited, fully exploited, or depleted)	1974–2006	+31*	+0.6	+0.6	+1.1	+1.2	+0.9	F
Climatic Impact Indicator (degree to which European bird population trends have responded in the direction expected from climate change)	1980–2005	+23*		−0.8	+3.2	+1.2	+1.2	S
Number of pressure indicators increasing			**4/4**	**4/5**	**4/5**	**5/5**	**5/5**	
		Responses						
Extent of Protected Areas (PAs)	1888–2006	+400*	+7.6	+4.5	+3.4	+2.4	+4.7	S
Coverage by PAs of Important Bird Areas and Alliance for Zero Extinction sites	1888–2009	+360*	+5.6	+4.6	+2.6	+0.8	+3.4	D 1999–2008
Area of forest under sustainable management (FSC certified)	1995–2008	+12,000*			+100	+20	+46	D 2006
International IAS policy adoption (no. signatories to conventions with provision for tackling IAS)	1952–2008	+2700*	+10	+6.9	+14	+5.1	+9.1	S
National IAS policy adoption (% countries with relevant legislation)	1964–2009	+10,000*	+30	+8.7	+12	+4.1	+13	D 2004–2009
Official development assistance (US$ per year provided in support of CBD)	2005–2007†	+17				+8.4	+8.3	D?
Number of response indicators increasing			**4/4**	**4/4**	**5/5**	**6/6**	**6/6**	
		Benefits						
LPI for utilized vertebrate populations	1970–2006	−15*	+1.0	−0.3	−1.3	−1.7	−0.4	A 1972–2006
RLI for species used for food and medicine	1986–2008	−3.5*		−0.2	−0.2	−0.2	−0.2	A
RLI for bird species in international trade	1988–2008	−0.5*		−0.01	−0.03	−0.02	−0.03	A
Number of benefits indicators declining			**0/1**	**3/3**	**3/3**	**3/3**	**3/3**	

*Significant trends ($P < 0.05$). †Identifies indicators with insufficient data to test significance of post-1970 trends, usually because annual estimates are unavailable. ‡Since earliest date with data if this is post-1970. §Because the indicators measure different parameters, some comparisons of mean annual % change between indicators are less meaningful than comparisons between decades for the same indicator. ‖Rate of change decelerating (D), accelerating (A), stable (S, i.e., no years with significant changes), fluctuating (F, i.e., a sequence of significant positive and negative changes), or with too few data points to test significance (?); years indicate periods in which second derivatives differed significantly from zero ($P < 0.05$).

All indicators of policy and management responses show increasing trends (Fig. 1 and Table 1), with increases in (i) extent of protected areas (PAs) (Table 2); (ii) coverage by PAs of two subsets of Key Biodiversity Areas (*21*) [39% of the area of 10,993 Important Bird Areas and 42% of the area of 561 Alliance for Zero Extinction sites (*22*) by 2009]; (iii) area of sustainably managed forests [1.6 million km^2 under Forest Stewardship Council (FSC) certification by 2007]; (iv) proportion of eligible countries signing international agreements relevant to tackling invasive alien species (IAS) [reaching 82% by 2008 (*23*)]; (v) proportion of countries with national legislation to control and/or limit the spread and impact of IAS [reaching 55% by 2009 (*23*)]; and (vi) biodiversity-related aid (reaching US$3.13 billion in 2007). The rate of increase was stable (i and iv), slowing (ii, iii, and v), or based on too few data to test significance (vi) (Table 1). The last three inflections in aggregated trends (2002, 2004, and 2008) were all negative (Fig. 2), indicating that the rate of improvement has slowed. Two other indicators have only baseline estimates: Management effectiveness was "sound" for 22% of PAs ("basic" for 65% and "clearly inadequate" for 13%), and the proportion of genetic diversity for 200 to 300 important crop species conserved ex situ in gene banks was estimated to be 70% (*24*).

Only three indicators address trends in the benefits humans derive from biodiversity (Fig. 1 and Table 1): (i) population trends of utilized vertebrates have declined by 15% since 1970, and aggregate species' extinction risk has increased

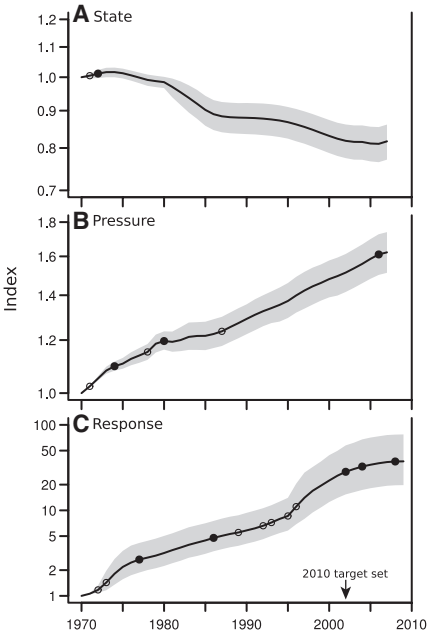

Fig. 2. Aggregated indices of (**A**) the state of biodiversity based on nine indicators of species' population trends, habitat extent and condition, and community composition; (**B**) pressures on biodiversity based on five indicators of ecological footprint, nitrogen deposition, numbers of alien species, overexploitation, and climatic impacts; and (**C**) responses for biodiversity based on six indicators of protected area extent and biodiversity coverage, policy responses to invasive alien species, sustainable forest management, and biodiversity-related aid. Values in 1970 set to 1. Shading shows 95% confidence intervals derived from 1000 bootstraps. Significant positive/upward (open circles) and negative/downward (filled circles) inflections are indicated.

Table 2. Examples of successes and positive trends relevant to the 2010 target (*5*).

Indicator	Successes and positive trends
	State
Living Planet Index of Palearctic vertebrate populations	Increased by 43% since 1970 (e.g., Eurasian beaver and common buzzard)
Waterbird populations in North America and Europe	Increased by 44% since 1980 owing to wetland protection and sustainable management (but populations remain below historic levels).
Species downlisted on the IUCN Red List	Species qualifying for downlisting to lower categories of extinction risk owing to successful conservation action include 33 birds since 1988 (e.g., Lear's macaw), 25 mammals since 1996 (e.g., European bison), and 5 amphibians since 1980 (e.g., Mallorcan midwife toad).
Wild Bird Index and Red List Index for species listed on the European Union Birds Directive	Annex 1–listed species' population trends have improved in EU countries (*27*) and extinction risk reduced (RLI increased 0.46% during 1994–2004) owing to designation of Special Protected Areas and implementation of Species Action Plans under the directive (e.g., white-tailed eagle).
Extinctions prevented	At least 16 bird species extinctions were prevented by conservation actions during 1994–2004, e.g., black stilt (*28*).
Water Quality Index in Asia	Improved by 7.4% since 1970.
	Pressures
Deforestation in Amazonian Brazil	Slowed from 2.8 million ha in 2003–2004 to 1.3 million ha in 2007–2008, but it is uncertain to what extent this was driven by improved enforcement of legislation versus reduced demand owing to economic slowdown.
	Responses
National biodiversity strategies and action plans (NBSAPs)	87% of countries have now developed NBSAPs and therefore have outlined coherent plans for tackling biodiversity loss at the national scale.
Protected areas (PAs)	Nearly 133,000 PAs designated, now covering 25.8 million km^2: 12% of the terrestrial surface (but only 0.5% of oceans and 5.9% of territorial seas), e.g., Juruena National Park, Brazil, designated in 2006, covering 19,700 km^2 of Amazon/cerrado habitat.
Invasive alien species (IAS) policy, eradication, and control	82% of eligible countries have signed international agreements relevant to preventing the spread and promoting the control/eradication of IAS. Successful eradications/control of IAS include pigs on Clipperton Atoll, France (benefiting seabirds and land crabs), cats, goats and sheep on Natividad, Mexico (benefiting black-vented shearwater), and red fox in southwest Australia (benefiting western brush wallaby).
Official development assistance for biodiversity	Increased to at least US$3.13 billion in 2007.

at an accelerating rate (as shown by the RLI) for (ii) mammals, birds, and amphibian species used for food and medicine (with 23 to 36% of such species threatened with extinction) and (iii) birds that are internationally traded (principally for the pet trade; 8% threatened). Trends are not yet available for plants and other important utilized animal groups. Three other indicators, which lack trend data, show (iv) 21% of domesticated animal breeds are at risk of extinction (and 9% are already extinct); (v) languages spoken by fewer than 1000 people (22% of the current 6900 languages) have lost speakers over the past 40 years and are in danger of disappearing within this century (loss of linguistic diversity being a proxy for loss of indigenous biodiversity knowledge); and (vi) more than 100 million poor people live in remote areas within threatened ecoregions and are therefore likely to be particularly dependent upon biodiversity and the ecosystem services it provides.

Indicator development has progressed substantially since the 2010 target was set. However, there are considerable gaps and heterogeneity in geographic, taxonomic, and temporal coverage of existing indicators, with fewer data for developing countries, for nonvertebrates, and from before 1980 and after 2005 (*4*, *5*, *25*). Interlinkages between indicators and the degree to which they are representative are incompletely understood. In addition, there are gaps for several key aspects of state, pressures, responses, and especially benefits (*4*, *5*, *7*, *26*).

Despite these challenges, there are sufficient data on key dimensions of biodiversity to conclude that at the global scale it is highly unlikely that the 2010 target has been met. Neither individual nor aggregated indicators of the state of biodiversity showed significant reductions in their rates of decline, apart from coral reef condition, for which there has been no further deceleration in decline since the mid-1980s. Furthermore, all pressure indicators showed increasing trends, with none significantly decelerating. Some local system-specific exceptions with positive trends for particular populations, taxa, and habitats (Table 2) suggest that, with political will and adequate resources, biodiversity loss can be reduced or reversed. More generally, individual and aggregated response indicators showed increasing trends, albeit at a decelerating rate (and with little direct information on whether such actions are effective). Overall, efforts to stem biodiversity loss have clearly been inadequate, with a growing mismatch between increasing pressures and slowing responses.

Our results show that, despite a few encouraging achievements, efforts to address the loss of biodiversity need to be substantially strengthened by reversing detrimental policies, fully integrating biodiversity into broad-scale land-use planning, incorporating its economic value adequately into decision making, and sufficiently targeting, funding and implementing policies that tackle biodiversity loss, among other measures. Sustained investment in coherent global biodiversity monitoring and indicators is essential to track and improve the effectiveness of these responses.

References and Notes

1. Secretariat of the Convention on Biological Diversity, *Handbook of the Convention on Biological Diversity* (Earthscan, London, 2003).
2. United Nations, Millennium Development Goals Indicators (http://unstats.un.org/unsd/mdg/Host.aspx?Content=Indicators/OfficialList.htm, 2008).
3. Convention on Biological Diversity, Framework for monitoring implementation of the achievement of the 2010 target and integration of targets into the thematic programmes of work, COP 8 Decision VIII/15 (www.cbd.int/decisions, 2006).
4. M. Walpole *et al*., *Science* **325**, 1503 (2009).
5. Further information is available as supporting material on *Science* Online.
6. H. M. Pereira, H. David Cooper, *Trends Ecol. Evol.* **21**, 123 (2006).
7. G. M. Mace, J. E. M. Baillie, *Conserv. Biol.* **21**, 1406 (2007).
8. J. D. Sachs *et al*., *Science* **325**, 1502 (2009).
9. N. Gilbert, *Nature* **462**, 263 (2009).
10. H. Mooney, G. Mace, *Science* **325**, 1474 (2009).
11. L. Soldaat, H. Visser, M. van Roomen, A. van Strien, *J. Ornithol.* **148**, (S2), 351 (2007).
12. R. M. Fewster, S. T. Buckland, G. M. Siriwardena, S. R. Baillie, J. D. Wilson, *Ecology* **81**, 1970 (2000).
13. B. Collen *et al*., *Conserv. Biol.* **23**, 317 (2009).
14. Food and Agriculture Organization, *Global Forest Resources Assessment* 2005 (FAO, Rome, 2006).
15. M. C. Hansen *et al*., *Proc. Natl. Acad. Sci. U.S.A.* **105**, 9439 (2008).
16. S. H. M. Butchart *et al*., *PLoS ONE* **2**, e140 (2007).
17. J. C. Vié, C. Hilton-Taylor, S. N. Stuart, Eds., *Wildlife in a Changing World* (IUCN, Gland, Switzerland, 2008).
18. R. D. Gregory *et al*., *PLoS ONE* **4**, e4678 (2009).
19. M. C. Ribeiro, J. P. Metzger, A. C. Martensen, F. Ponzoni, M. Hirota, *Biol. Conserv.* **142**, 1141 (2009).
20. C. Nilsson, C. A. Reidy, M. Dynesius, C. Revenga, *Science* **308**, 405 (2005).
21. G. Eken *et al*., *Bioscience* **54**, 1110 (2004).
22. T. H. Ricketts *et al*., *Proc. Natl. Acad. Sci. U.S.A.* **102**, 18497 (2005).
23. M. A. McGeoch *et al*., *Divers. Distrib.* **16**, 95 (2010).
24. SCBD, *The Convention on Biological Diversity Plant Conservation Reports* (SCBD, Montreal, 2009).
25. B. Collen, M. Ram, T. Zamin, L. McRae, *Trop. Conserv. Sci.* **1**, 75 (2008).
26. A. Balmford, P. Crane, A. Dobson, R. E. Green, G. M. Mace, *Philos. Trans. R. Soc. London Ser. B* **360**, 221 (2005).
27. P. F. Donald *et al*., *Science* **317**, 810 (2007).
28. S. H. M. Butchart, A. J. Stattersfield, N. J. Collar, *Oryx* **40**, 266 (2006).

29. We are grateful for comments, data, or help from R. Akçakaya, L. Alvarez-Filip, A. Angulo, L. Bennun, L. Coad, N. Cox, M. Dubé, C. Estreguil, M. Evans, B. Galil, V. Gaveau, F. Gherardi, S. Goldfinger, R. Green, A. Grigg, P. Herkenrath, C. Hilton-Taylor, M. Hoffmann, E. Kleynhans, J. Lamoreux, S. Livingstone, E. Marais, P. Martin, I. May, A. Milam, K. Noonan-Mooney, H. Pavese, B. Polidoro, C. Pollock, D. Pritchard, J. Schipper, F. Schutyser, V. Shutte, S. Simons, J. Škorpilová, A. Stattersfield, P. Voříšek, R. Wright, M. Wackernagel, and M. Waycott. We acknowledge support from the Global Environment Facility to the 2010 Biodiversity Indicators Partnership; Shell Foundation; European Commission; the Sea Around Us Project (University of British Columbia/Pew Environment Group) to D.P. and R.W.; World Wildlife Fund, The Nature Conservancy, and the University of Queensland to M.H. and F.L.; T. Haas and the New Hampshire Charitable Foundation to K.E.C.; and the National Science Foundation (NSF) to J.-F.L. Opinions and findings expressed here do not necessarily reflect the views of the NSF or other funding bodies.

Supporting Online Material

www.sciencemag.org/cgi/content/full/science.1187512/DC1
Methods
SOM Text
Figs. S1 and S2
Tables S1 to S4
References
Data File 1

26 January 2010; accepted 8 April 2010
Published online 29 April 2010;
10.1126/science.1187512
Include this information when citing this paper.

Plectasin, a Fungal Defensin, Targets the Bacterial Cell Wall Precursor Lipid II

Tanja Schneider,[1] Thomas Kruse,[2] Reinhard Wimmer,[3] Imke Wiedemann,[1] Vera Sass,[1] Ulrike Pag,[1] Andrea Jansen,[1] Allan K. Nielsen,[4] Per H. Mygind,[4] Dorotea S. Raventós,[4] Søren Neve,[4] Birthe Ravn,[4] Alexandre M. J. J. Bonvin,[5] Leonardo De Maria,[4] Anders S. Andersen,[2,4] Lora K. Gammelgaard,[4] Hans-Georg Sahl,[1] Hans-Henrik Kristensen[4]*

Host defense peptides such as defensins are components of innate immunity and have retained antibiotic activity throughout evolution. Their activity is thought to be due to amphipathic structures, which enable binding and disruption of microbial cytoplasmic membranes. Contrary to this, we show that plectasin, a fungal defensin, acts by directly binding the bacterial cell-wall precursor Lipid II. A wide range of genetic and biochemical approaches identify cell-wall biosynthesis as the pathway targeted by plectasin. In vitro assays for cell-wall synthesis identified Lipid II as the specific cellular target. Consistently, binding studies confirmed the formation of an equimolar stoichiometric complex between Lipid II and plectasin. Furthermore, key residues in plectasin involved in complex formation were identified using nuclear magnetic resonance spectroscopy and computational modeling.

Plectasin is a 40–amino acid residue fungal defensin produced by the saprophytic ascomycete *Pseudoplectania nigrella* (*1*). Plectasin shares primary structural features with defensins from spiders, scorpions, dragonflies and mussels and folds into a cystine-stabilized alpha-

beta structure (CSαβ). In vitro and in animal models of infection, plectasin is potently active against drug-resistant Gram-positive bacteria such as streptococci, whereas the antibacterial spectrum of an improved derivative, NZ2114 (*2*), also includes staphylococci such as methicillin-resistant *Staphylococcus aureus* (MRSA).

We set out to determine the molecular target and specific mechanism by which plectasin kills bacteria. Although many host defense peptides (HDPs) act on and disintegrate the bacterial membrane, several observations suggested that this is not the case for plectasin.

Growth kinetic measurements of the Gram-positive bacterium *Bacillus subtilis* exposed to plectasin clearly demonstrated that plectasin exhibited kinetic behavior similar to cell wall–interfering agents (such as vancomycin, penicillin, and bacitracin) and not to the rapidly lytic membrane-active agents (such as polymyxin and novispirin) or non-lytic antibiotics with replication (ciprofloxacin), transcription (rifampicin), or protein translation (kanamycin, tetracycline) as their primary target (Fig. 1A) (*3*). Consistently with this, killing kinetics indicated that over a period of approximately one generation time (0.5 hours) treated cells were unable to multiply, but remained viable (Fig. 1B inset), before the number of colony-forming units decreased (Fig. 1B).

Next, the effect of plectasin on macromolecular biosynthesis pathways was investigated. The incorporation of radiolabeled isoleucine into protein and of thymidine into nucleic acids was not affected, whereas glucosamine—an essential precursor of bacterial peptidoglycan—was no longer incorporated (Fig. 1C). Lastly, treatment of *B. subtilis* with plectasin induced severe cell-shape deformations as visualized through phase-contrast microscopy (fig. S1). These characteristics are all typical for compounds interfering with cell-wall biosynthesis rather than for membrane disintegration (*4*, *5*). Consistently, neither pore formation as measured by K^+ efflux (Fig. 1E), nor changes in membrane potential by use of TPP^+ or $DiBAC_4$ (fig. S2, A and B), nor carboxy-fluorescein efflux from liposomes were detected (fig. S2C). Thus, despite its amphipathic nature, plectasin does not compromise membrane integrity, reducing the risk of unspecific toxicity.

[1]Pharmaceutical Microbiology Section, Institute for Medical Microbiology, Immunology, and Parasitology, University of Bonn, D-53115 Bonn, Germany. [2]Statens Serum Institut, 2300 Copenhagen S, Denmark. [3]Department of Biotechnology, Chemistry, and Environmental Engineering, Aalborg University, DK-9000 Aalborg, Denmark. [4]Novozymes AS, DK-2880 Bagsvaerd, Denmark. [5]Department of Chemistry, Faculty of Science, Utrecht University, 3584 CH Utrecht, Netherlands.

*To whom correspondence should be addressed. E-mail: hahk@novozymes.com

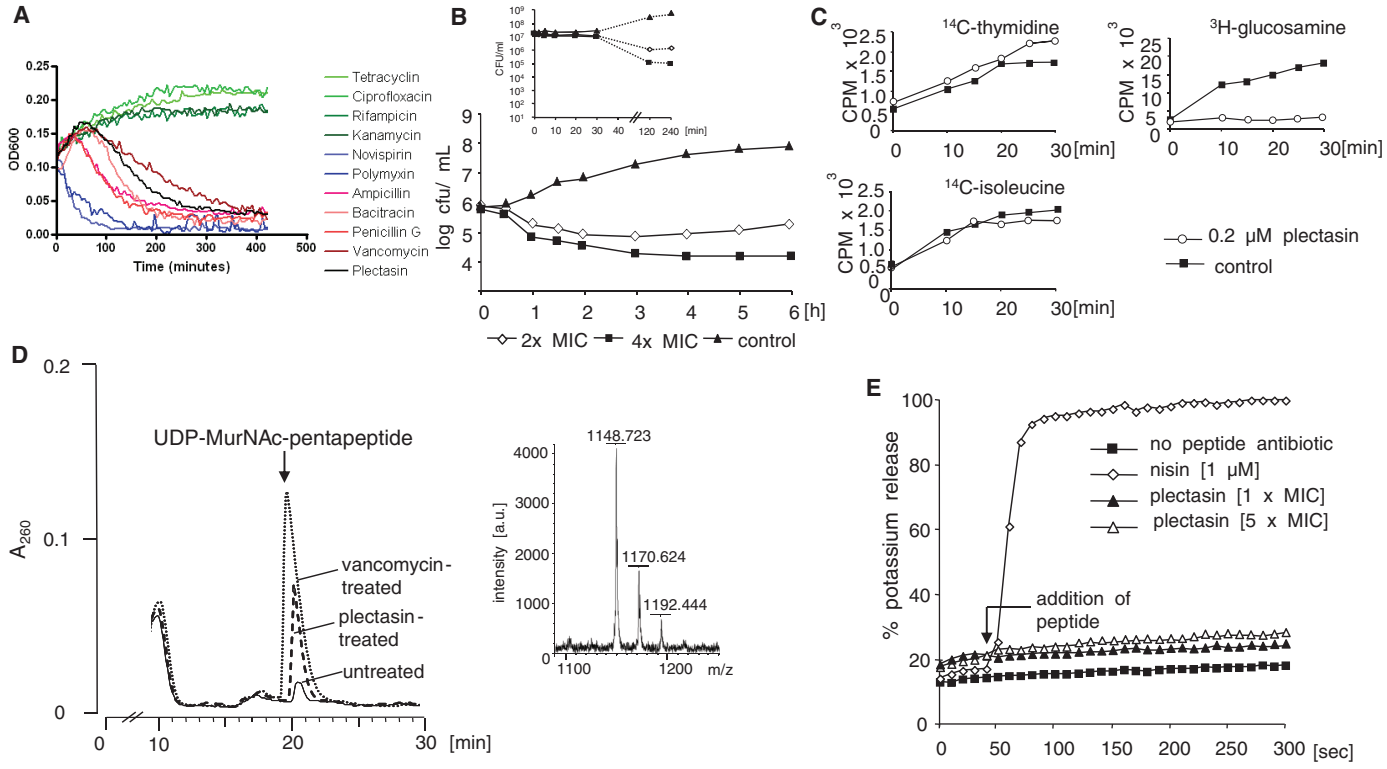

Fig. 1. Effect of plectasin on intact cells. (**A**) Classification of antimicrobial compounds by using optical density measurements. Growth kinetic measurements of *B. subtilis* exposed to plectasin or various antibiotics with known cellular targets. Two to four times the minimal inhibitory concentration (MIC) of the respective compounds were used. Plectasin (black) falls into the cluster of cell-wall biosynthesis inhibiting antibiotics (red colors). (**B**) Killing kinetics of plectasin; *Staphylococcus simulans* 22 treated with plectasin at 2 × MIC (open diamonds) and 4 × MIC (squares); control is without peptide (triangles). (Insert) A similar experiment with more time points within the first 60 min demonstrating the absence of killing in the first 30 min of treatment. (**C**) Impact of plectasin on macromolecular biosynthesis in *B. subtilis* 168. Incorporation of [^{14}C]-thymidine into nucleic acids, of L-[^{14}C]-isoleucine into protein, and of [^{3}H]–glucosamine in cell wall was measured in untreated controls (squares) and plectasin-treated cells (open circles); glucosamine incorporation into cell-wall material was selectively inhibited. (**D**) Intracellular accumulation of the ultimate soluble cell-wall precursor UDP-MurNAc-pentapeptide in vancomycin-treated (dotted line) and plectasin-treated (dashed line) cells of *S. simulans* 22. Cells were treated for 30 min with plectasin or vancomycin, which is known to form a complex with Lipid II. Treated cells were extracted with boiling water, and the intracellular nucleotide pool was analyzed by means of reverse HPLC. UDP-MurNAc-pentapeptide was identified by means of mass spectrometry using the negative mode and 1 mg/ml 6-aza-2-thiothymine [in 50% (v/v) ethanol/20 mM ammonium citrate] as matrix; the calculated monoisotopic mass is 1149.35; in addition to the singly charged ion, the mono- and disodium salts are detected. (**E**) Plectasin is unable to form pores in the cytoplasmic membrane of *S. simulans* 22. Potassium efflux from living cells was monitored with a potassium-sensitive electrode. Ion leakage is expressed relative to the total amount of potassium released after addition of 1 µM pore-forming lantibiotic nisin (100%, open diamonds). Plectasin was added at 0.2 µM (triangles) and 1 µM (open triangles); controls were without peptide antibiotics (squares).

We obtained further support for the cell wall–interfering activity using DNA microarrays to compare the transcriptional responses of plectasin-treated cells with response patterns obtained for a range of reference antibiotics. For both *B. subtilis* 168 and *S. aureus* SG511, we found that the transcriptional profiles overlapped those of established cell-wall biosynthesis inhibitors, such as vancomycin and bacitracin (*6*–*9*) (fig. S3 and tables S1 and S2).

The biosynthesis of bacterial cell walls requires a number of steps (*10*). Initially, the N-acetylmuramic acid-pentapeptide (MurNAc-pentapeptide)—a major constituent of the cell-wall building block—is produced in the cytoplasm as an uridine diphosphate (UDP)–activated precursor before it is transferred onto a membrane carrier, bactoprenolphosphate (Fig. 2B, reaction I). The resulting membrane-anchored precursor Lipid I is then further modified to the structural cell-wall subunit, Lipid II (Fig. 2B, reaction II). In some Gram-positive bacteria, Lipid II (Fig. 2A) is further decorated by an interpeptide bridge [a pentaglycine peptide in the case of *S. aureus* (*11*)] (Fig. 2B, reaction III) before it gets translocated across the cytoplasmic membrane to the outside, where it is incorporated into the peptidoglycan polymer through the activity of transglycosylases and transpeptidases (Fig. 2B, reaction IV). We analyzed the intracellular pool of cell-wall precursors by means of reverse high-performance liquid chromatography (HPLC) and mass spectrometry and found accumulation of the soluble molecule UDP-MurNAc-pentapeptide in plectasin-treated cells (Fig. 1D), suggesting that one of the later membrane-associated or extracellular processes may be targeted by plectasin.

We then analyzed the effect of plectasin on the membrane-bound steps of cell-wall biosynthesis in vitro. Cytoplasmic membranes with associated cell-wall biosynthesis apparatus were isolated and incubated with plectasin and radiolabeled substrates that are necessary for Lipid II formation. Using thin-layer chromatography and subsequent scintillation counting, we found the overall synthesis reaction to be strongly inhibited (Fig. 2C). For a more detailed analysis, we cloned the individual cell-wall biosynthesis genes from *S. aureus*, expressed them in *Escherichia coli*, and analyzed the activity of the purified enzymes in the presence of plectasin by measuring the amount of product formed. These enzymes included MraY (Fig. 2B, reaction I), MurG (Fig. 2B, reaction II), FemXAB (Fig. 2B, reaction III), and PBP2 (Fig. 2B, reaction IV). Whereas the MraY reaction was not affected

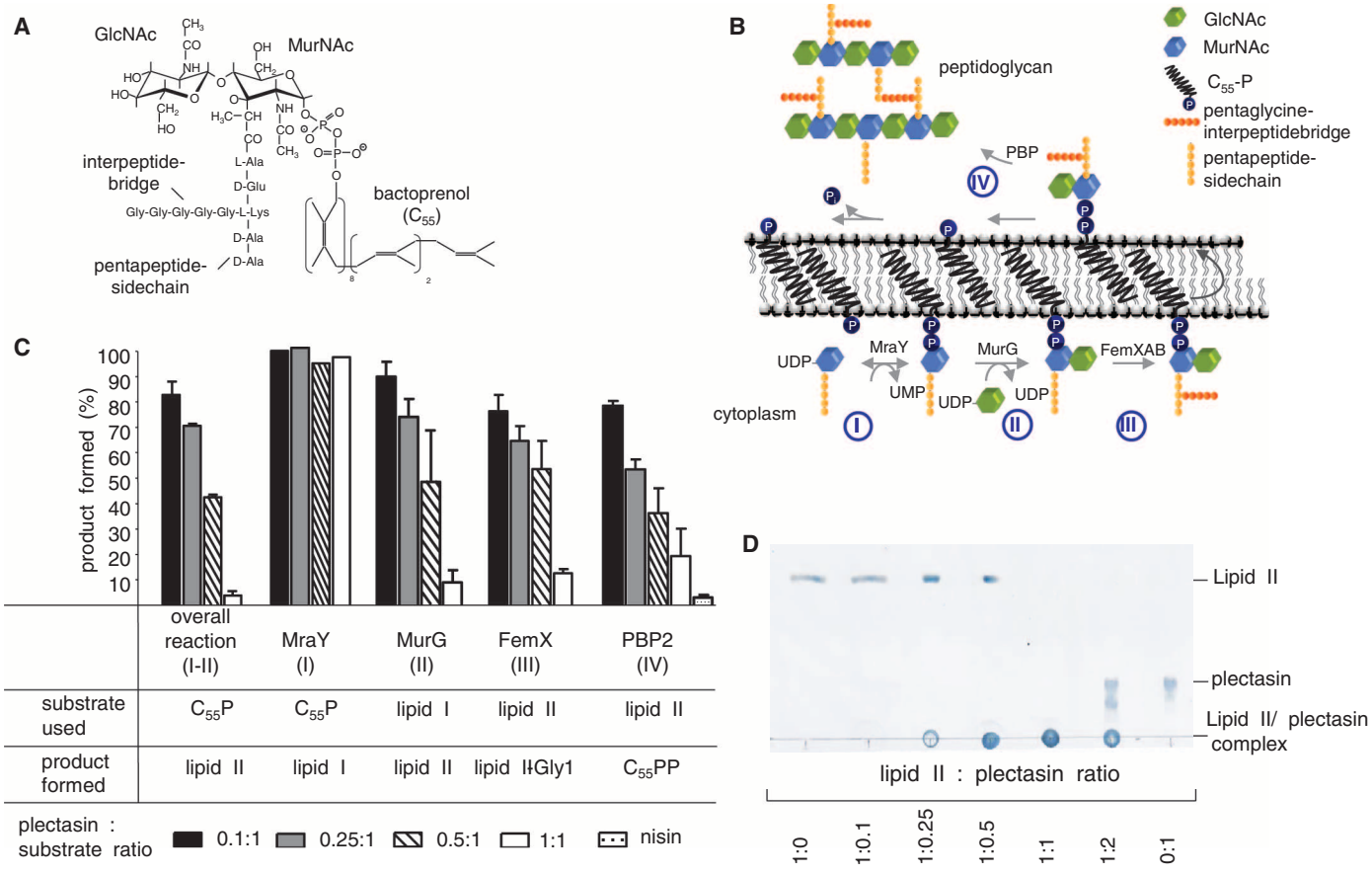

Fig. 2. Inhibition of membrane-associated cell-wall biosynthesis steps. (**A**) Structure of the cell-wall precursor Lipid II. (**B**) The membrane-bound steps of cell-wall precursor biosynthesis and bactoprenol ($C_{55}P$) carrier cycling in staphylococci. Cell-wall biosynthesis starts in the cytoplasm with the formation of the soluble precursor UDP-MurNAc-pentapeptide (UDP-MurNAc-pp). This precursor is linked to the membrane carrier bactoprenolphosphate ($C_{55}P$) by MraY yielding Lipid I (reaction I). Lipid II is formed by MurG, which adds *N*-acetyl-glucosamine (GlcNAc) (reaction II). When the interpeptide bridge, which only occurs in some Gram-positive bacteria, is accomplished (reaction III), the monomeric peptidoglycan unit is translocated across the cytoplasmic membrane to the outside and incorporated into the cell wall (reaction IV). (**C**) Inhibition of membrane-associated steps of cell-wall biosynthesis by plectasin. In all tests, plectasin was added in molar ratios of 0.1 to 1 with respect to the amount of the appropriate lipid substrate $C_{55}P$, Lipid I, or Lipid II used in the individual test system. The amount of reaction products synthesized in the absence of plectasin was taken as 100%. Product analysis was done by means of TLC and subsequent scintillation counting of stained and excised product-containing bands; radiolabeling was based on [^{3}H]-labeled $C_{55}P$ (for Lipid I), [^{14}C]-GlcNAc for Lipid II, and [^{14}C]-glycine for Lipid II-Gly1. Error bars represent ±SD, and the experiments were repeated at least three times. Technical details on the assays and the cloning and purification of the enzymes are given in (*3*). (**D**) Estimation of the stoichiometry of plectasin:Lipid II binding. Lipid II was incubated in the presence of plectasin at the molar concentration ratios indicated. The stable complex of plectasin with the Lipid II remains at the application spot, whereas both components migrate to the sites indicated. At a molar ratio of 1:1, neither free Lipid II nor free plectasin were observed.

by plectasin, we found the MurG, FemX, and PBP2 reactions to be inhibited in a dose-dependent fashion (Fig. 2C). For these three enzymes, Lipid I (MurG) or Lipid II (FemX and PBP2) are substrates, and significant inhibition of the reactions was only observed when plectasin was added in equimolar concentrations with respect to Lipid I or Lipid II (Fig. 2C). Thus, plectasin—similarly to glycopeptide antibiotics [such as vancomycin (*12*, *13*)] and lantibiotics (*14*, *15*)—may form a stoichiometric complex with the substrate rather than inhibiting the enzyme. To further validate this, we incubated either Lipid I or II with plectasin in various molar ratios and used thin-layer chromatography (TLC) to analyze the migration behavior. Free Lipid I and II as well as free peptide were found to migrate to defined positions in the chromatogram, whereas the Lipid I/II–plectasin complex remained at the start point (Fig. 2D). Free Lipid I/II and free peptide were not detectable only at an equimolar ratio, indicating the formation of a 1:1 stoichiometric complex.

We further analyzed the interaction of both Lipid I and II with plectasin using a liposome system with membranes composed of phosphatidylcholine and Lipid II [0.2 or 0.5 mole percent (mol %)] and ^{14}C-labeled plectasin. We found the maximum number of plectasin molecules that bound to liposomes to approximately match the number of Lipid II molecules available on the liposome surface (fig. S4). Using Scatchard plot analysis, we determined an equilibrium-binding constant of 1.8×10^{-7} mol for Lipid II and 1.1×10^{-6} mol for Lipid I, suggesting that the second sugar in Lipid II, the N-acetyl glucosamine, contributes to the stability of the complex.

To gain further insight into the structural nature of the plectasin/Lipid II interaction at the membrane interface, we measured chemical shift changes for ^{15}N-labeled plectasin. Heteronuclear single-quantum coherence (HSQC) nuclear magnetic resonance (NMR) spectra were measured either in solution or on binding membrane-mimicking dodecylphosphocholine (DPC) micelles (figs. S5 and S6). Fitting the binding data to a Langmuir isotherm yielded a free enthalpy of binding $\Delta G = -27 \pm 1$ kJ/mol (fig. S7). Backbone H^N and N atoms of 10 residues [G6, W8, D9, A31, K32, G33, G34, F35, V36, and C37 (*16*)], which in the tertiary structure all locate to one end of plectasin, exhibited marked changes in chemical shifts [$\Delta\delta_{obs} > 0.15$ parts per million (ppm)] (Fig. 3A, residues labeled yellow), suggesting an orientation in which one end of plectasin specifically is located in the membrane interface.

To identify the residues on plectasin that bind Lipid II, we then titrated plectasin bound to DPC with Lipid II. With increasing concentrations of Lipid II, another set of NMR signals appeared and became stronger, whereas the NMR signals of *apo*-plectasin bound to DPC micelles became weaker until they disappeared at equimolar concentrations of plectasin and Lipid II, supporting the 1:1 binding stoichiometry found by means of TLC. Addition of extra plectasin to the mixture brought the signals of *apo*-plectasin forward again, and further addition of Lipid II to equimolarity led to the disappearance of the signals again. From a three-dimensional (3D)–HNCA spectrum, we could assign backbone H^N, N, and C^α signals of the plectasin:Lipid II:DPC complex. The strongest changes in chemical shift ($\Delta\delta_{obs} > 0.22$ ppm) were obtained for amino acids F2, C4, D12, Y29, A31, G33, C37, and K38 (figs. S5 and S6). Most of these residues localize in a coherent patch in close proximity to the residues affected by binding to DPC (Fig. 3B, residues labeled magenta). A31, G33, and C37 exert chemical shift-changes both upon addition of DPC and Lipid II. To further verify this, site-saturated mutagenesis (in which a given amino acid is changed to each of the other 19 natural amino acids) was carried out at all positions in plectasin except the six cysteines. The mutant libraries were expressed in *S. cerevisiae*, and 400 to 600 transformants of each position tested for activity against *S. aureus* in a plate overlay assay. No amino acid substitutions at positions D12, Y29, or G33 resulted in activity against *S. aureus*, whereas only the very conservative mutations of A31 to G and K38 to R resulted in activity against *S. aureus*. At other amino acid positions not involved in DPC or Lipid II binding, a wide range of non-homologous amino acid substitutions gave rise to plectasin variants retaining antimicrobial activity.

To visualize the complex between Lipid II and plectasin, docking studies using the GOLD and HADDOCK programs were performed (*17*, *18*). In accordance with the NMR data, evidence in favor of a primary binding site involving the interaction of the pyrophosphate moiety of Lipid II with the amide protons F2, G3, C4, and C37 of plectasin via hydrogen bonding was obtained (Fig. 3C). Several of the other large chemical shift changes are present in residues involved in secondary structure interactions (such as the formation of beta-sheets), which most likely undergo structural changes upon binding to the target. Taken together, these data strongly support a model in which plectasin gains affinity and specificity through binding to the solvent-exposed part of Lipid II, whereas the hydrophobic part of plectasin is located in the membrane interface. Thus, plectasin shares functional features with the lantibiotic nisin in that for both peptides the pyrophosphate moiety is most relevant for binding of Lipid II, although nisin inserts deeply into the membrane bilayer, forming pores and causing major delocalization of Lipid II (*19*, *20*).

To test whether inhibition of cell-wall biosynthesis is restricted to plectasin or represents a general feature, we tested a series of defensin peptides from other fungi, mollusks, and arthropods for Lipid II binding and inhibition of the overall Lipid II synthesis and FemX reaction (fig. S8A). Two fungal defensins, oryzeasin (from *Aspergillus oryzea*) and eurocin (from *Eurotium amstelodami*), did inhibit the enzymatic reactions and bind to Lipid II in stoichiometric numbers, as did the two defensins from invertebrates, lucifensin from maggots of the blowfly *Lucilia sericata* and gallicin from the mussel *Mytilus galloprovinciali* (fig. S8, B to D). In contrast, heliomicin from the tobacco budworm *Heliothis virescens*, which shares the conserved cysteine pattern, did not show affinity for Lipid II and had no activity in these assays. These data clearly demonstrate that among the host defense peptides of eukaryotic

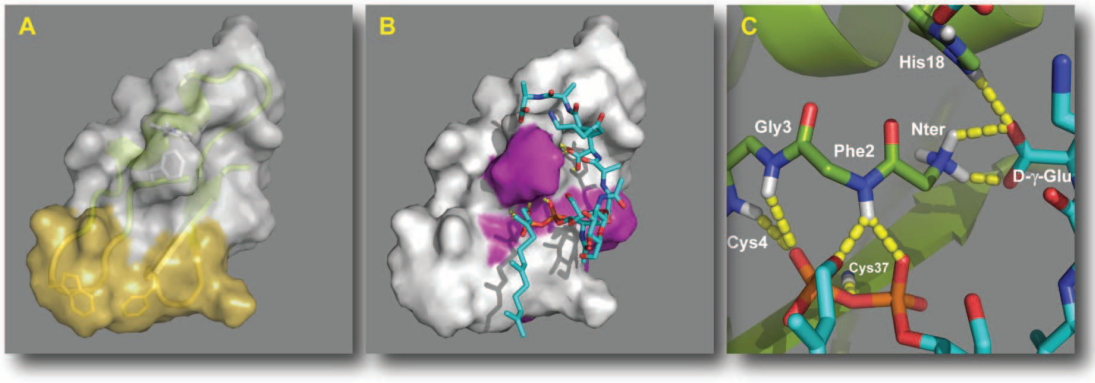

Fig. 3. NMR-based model of the plectasin/Lipid II-complex. (**A**) Surface representation of plectasin with the residues showing substantial chemical shift perturbations upon binding to DPC micelles, which are indicated in yellow. (**B**) Surface representation of plectasin with the residues showing substantial chemical shift perturbations upon Lipid II titration, which is shown in magenta. (**C**) Detailed view of the pyrophosphate-binding pocket. In this proposed HADDOCK-generated model, the pyrophosphate moiety forms hydrogen bonds to F2, G3, C4, and C27, and the D-γ-glutamate of Lipid II forms a salt bridge with the N terminus of plectasin and the side-chain of His18.

organisms, specific inhibitors of cell-wall biosynthesis can be found that directly target Lipid II, "the bacterial Achilles' heel" for antibiotic attack (*21*).

Vancomycin, one of the very few remaining drugs for the treatment of multi-resistant Gram-positive infections, has been shown to predominantly bind the D-alanyl-D-alanine (D-ala-D-ala) part of the pentapeptide in Lipid II (Fig. 2A) (*12*). However, high-level vancomycin resistance has been observed in both enterococci (VRE) and staphylococci (VRSA). There is no cross-resistance between vancomycin and plectasin, and in contrast to vancomycin, plectasin is not competitively inhibited by the presence of the D-ala-D-ala ligand (fig. S9). This further demonstrates that the primary interactions to Lipid II differ between plectasin and vancomycin, and taken together, these results suggest that future development of true cross-resistance between vancomycin and plectasin is unlikely.

Plectasin and its improved derivatives such as NZ2114 possess a range of features—such as potent activity in vitro under physiological conditions and in animal models of infection, low potential for unwanted toxicities, extended serum stability and in vivo half-life, and cost-effective large-scale manufacturing—which combined with a validated microbial target make it a promising lead for further drug development.

References and Notes

1. P. H. Mygind *et al.*, *Nature* **437**, 975 (2005).
2. D. Andes, W. Craig, L. A. Nielsen, H. H. Kristensen, *Antimicrob. Agents Chemother.* **53**, 3003 (2009).
3. Materials and methods are available as supporting material on *Science* Online.
4. M. Zasloff, *Nature* **415**, 389 (2002).
5. R. E. Hancock, H. G. Sahl, *Nat. Biotechnol.* **24**, 1551 (2006).
6. B. Hutter *et al.*, *Antimicrob. Agents Chemother.* **48**, 2838 (2004).
7. F. McAleese *et al.*, *J. Bacteriol.* **188**, 1120 (2006).
8. M. Cao, T. Wang, R. Ye, J. D. Helmann, *Mol. Microbiol.* **45**, 1267 (2002).
9. T. Mascher, N. G. Margulis, T. Wang, R. W. Ye, J. D. Helmann, *Mol. Microbiol.* **50**, 1591 (2003).
10. J. van Heijenoort, *Microbiol. Mol. Biol. Rev.* **71**, 620 (2007).
11. T. Schneider *et al.*, *Mol. Microbiol.* **53**, 675 (2004).
12. P. E. Reynolds, *Eur. J. Clin. Microbiol. Infect. Dis.* **8**, 943 (1989).
13. N. E. Allen, T. I. Nicas, *FEMS Microbiol. Rev.* **26**, 511 (2003).
14. H. Brötz *et al.*, *Mol. Microbiol.* **30**, 317 (1998).
15. J. M. Willey, W. A. van der Donk, *Annu. Rev. Microbiol.* **61**, 477 (2007).
16. Single-letter abbreviations for the amino acid residues are as follows: A, Ala; C, Cys; D, Asp; E, Glu; F, Phe; G, Gly; H, His; I, Ile; K, Lys; L, Leu; M, Met; N, Asn; P, Pro; Q, Gln; R, Arg; S, Ser; T, Thr; V, Val; W, Trp; and Y, Tyr.
17. G. Jones, P. Willett, R. C. Glen, A. R. Leach, R. Taylor, *J. Mol. Biol.* **267**, 727 (1997).
18. C. Dominguez, R. Boelens, A. M. Bonvin, *J. Am. Chem. Soc.* **125**, 1731 (2003).
19. S. T. Hsu *et al.*, *Nat. Struct. Mol. Biol.* **11**, 963 (2004).
20. H. E. Hasper *et al.*, *Science* **313**, 1636 (2006).
21. E. Breukink, B. de Kruijff, *Nat. Rev. Drug Discov.* **5**, 321 (2006).

22. We thank M. Josten, A. Hansen, and M. R. Markvardsen for expert technical assistance and acknowledge the Carlsberg Research Center for use of the 800-MHz NMR spectrometer and the Obel Foundation for supporting the NMR laboratory at Aalborg University. H.G.S. acknowledges financial support by the European Union (PIAP-GA-2008-218191), the German Research Foundation (SA 292/10-2 and SA 292/13-1), the Bundesministerium für Bildung und Forschung (SkinStaph), and by the BONFOR program of the Medical Faculty, University of Bonn. A.M.J.J.B. acknowledges financial support from the Netherlands Organization for Scientific Research (VICI grant 700.56.442). A.S.A. acknowledges financial support from the Danish Research Council for Technology and Production (274-05-0435). Novozymes AS holds a patent on plectasin (patent number WO2003/044049/044049) and has filed patent applications on improved variants of plectasin. L.D.M., A.K.N., and D.S.R. hold stock options in Novozymes AS. DNA microarray data can be accessed through ArrayExpress, accession number E-MTAB-60. NMR assignment of ^{1}H, ^{15}N, and ^{13}C atoms of plectasin have been deposited in the BioMagResBank (accession number 16739).

Supporting Online Material

www.sciencemag.org/cgi/content/full/328/5982/1168/DC1
Materials and Methods
Figs. S1 to S9
Tables S1 and S2
References

8 December 2009; accepted 5 April 2010
10.1126/science.1185723

mTORC1-Mediated Cell Proliferation, But Not Cell Growth, Controlled by the 4E-BPs

Ryan J. O. Dowling,[1]*† Ivan Topisirovic,[1]* Tommy Alain,[1] Michael Bidinosti,[1] Bruno D. Fonseca,[1] Emmanuel Petroulakis,[1] Xiaoshan Wang,[1] Ola Larsson,[1] Anand Selvaraj,[2] Yi Liu,[3] Sara C. Kozma,[2] George Thomas,[2] Nahum Sonenberg[1]‡

The mammalian target of rapamycin complex 1 (mTORC1) integrates mitogen and nutrient signals to control cell proliferation and cell size. Hence, mTORC1 is implicated in a large number of human diseases—including diabetes, obesity, heart disease, and cancer—that are characterized by aberrant cell growth and proliferation. Although eukaryotic translation initiation factor 4E–binding proteins (4E-BPs) are critical mediators of mTORC1 function, their precise contribution to mTORC1 signaling and the mechanisms by which they mediate mTORC1 function have remained unclear. We inhibited the mTORC1 pathway in cells lacking 4E-BPs and analyzed the effects on cell size, cell proliferation, and cell cycle progression. Although the 4E-BPs had no effect on cell size, they inhibited cell proliferation by selectively inhibiting the translation of messenger RNAs that encode proliferation-promoting proteins and proteins involved in cell cycle progression. Thus, control of cell size and cell cycle progression appear to be independent in mammalian cells, whereas in lower eukaryotes, 4E-BPs influence both cell growth and proliferation.

The mammalian target of rapamycin complex 1 (mTORC1) controls growth (increase in cell mass) and proliferation (increase in cell number) by modulating mRNA translation through phosphorylation of the eukaryotic translation initiation factor 4E (eIF4E)–binding proteins (4E-BP1, 2, and 3) and the ribosomal protein S6 kinases (S6K1 and 2) (*1*, *2*). 4E-BPs regulate the translation of a subset of mRNAs by competing with eIF4G for binding to eIF4E, thus preventing the assembly of the eIF4F complex, whereas the S6Ks control the phosphorylation status of a number of translational components (*1*–*3*). Rapamycin has been an important tool in understanding mTORC1 signaling; however, it inefficiently and transiently inhibits 4E-BP phosphorylation (*4*) (fig. S1A). Moreover, we found that rapamycin inhibited proliferation and G_1/S cell cycle progression of wild-type and 4E-BP double-knockout (DKO) mouse embryonic fibroblasts (MEFs) to the same extent, which suggests that its effects are not mediated by 4E-BPs (fig. S1, B to D). To directly address the role of 4E-BPs in mTORC1 signaling, we depleted raptor, a component of mTORC1 required for substrate binding (*5*), in these MEFs. 4E-BP DKO MEFs lack all three 4E-BPs, as they do not express 4E-BP3 (fig. S2A). Depletion of raptor diminished the phosphorylation of 4E-BP1 at all mTOR-sensitive sites in wild-type MEFs, and inhibited mTORC1 signaling to the same extent in wild-type and 4E-BP DKO MEFs, as illustrated by reduced phosphorylation of S6Ks and its substrates (ribosomal protein S6 and eIF4B) and increased abundance of programmed cell death protein 4 (PDCD4) (Fig. 1A). Wild-type MEFs in which raptor was depleted proliferated more slowly than control cells, whereas raptor-depleted 4E-BP DKO MEFs proliferated at a rate indistinguishable from that of control cells (Fig. 1B). Similarly, in human embryonic kidney (HEK)

[1]Department of Biochemistry and Goodman Cancer Research Centre, McGill University, Montreal, Quebec H3A 1A3, Canada. [2]Department of Cancer and Cell Biology, Metabolic Diseases Institute, University of Cincinnati, Cincinnati, OH 45237, USA. [3]Intellikine, La Jolla, CA 92037, USA.

*These authors contributed equally to this work.
†Present address: Division of Signalling Biology, Ontario Cancer Institute, University Health Network, Toronto, Ontario M5G 2M9, Canada.
‡To whom correspondence should be addressed. E-mail: nahum.sonenberg@mcgill.ca

293T cells, raptor silencing had a pronounced effect on mTORC1 signaling and proliferation (Fig. 1, C and D). The effect of raptor silencing on proliferation, but not mTOR signaling, was attenuated by co-depletion of 4E-BPs (Fig. 1D). Thus, mTORC1-dependent proliferation requires 4E-BPs.

To further assess the role of 4E-BPs in mTORC1-mediated cell proliferation, we depleted mTOR or rictor (an mTORC2-specific component) in HEK 293T cells. Depletion of mTOR resulted in decreased signaling through both mTORC1 and mTORC2, as measured by S6 Ser^{240}/Ser^{244} or Akt Ser^{473} phosphorylation (fig. S2B). In contrast, depletion of rictor abolished only mTORC2-mediated phosphorylation of Akt, which was augmented by the depletion of raptor (fig. S2B), consistent with the loss of the negative feedback loop from S6Ks to Akt (*6*). Depletion of mTOR, raptor, or rictor inhibited cell proliferation relative to control cells (fig. S2C). However, in the case of raptor or mTOR depletion, co-depletion of 4E-BPs totally or partially restored proliferation, respectively, whereas their depletion had no effect on the inhibition caused by rictor knockdown (fig. S2C). Thus, 4E-BPs mediate the effect of mTORC1, but not mTORC2, on proliferation.

mTORC1 is differentially activated by distinct stimuli, including serum growth factors and

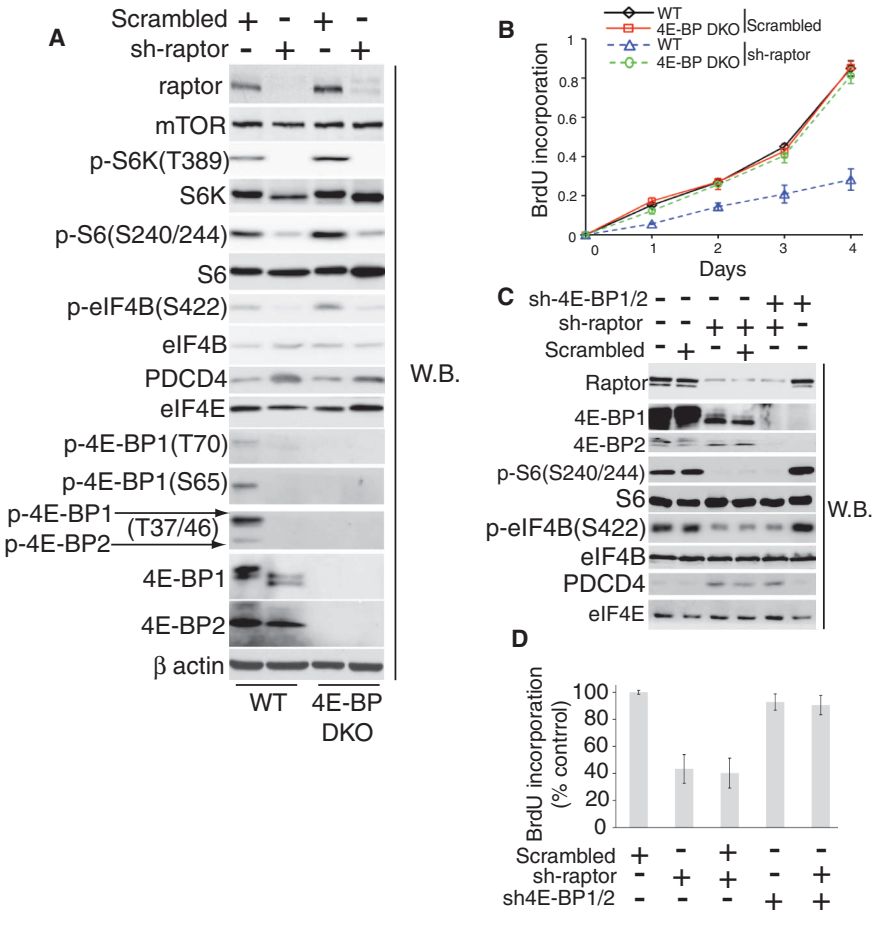

Fig. 1. 4E-BPs mediate mTORC1's effects on cell proliferation. (**A**) Levels of the indicated proteins in wild-type (WT) and 4E-BP DKO MEFs infected with a scrambled or raptor-specific shRNA (sh-raptor) were determined by Western blotting. β-actin served as a loading control. (**B**) Proliferation of MEFs from (A) was determined by 5-bromo-2′-deoxyuridine (BrdU) incorporation. Results represent means ± SD (n = 4). (**C**) Western blots of HEK 293T cells infected with raptor and 4E-BP1 and 4E-BP2 shRNA (sh-raptor; sh-4E-BP1/2) or scrambled shRNA. eIF4E served as a loading control. (**D**) Proliferation of cells from (C) was determined by BrdU incorporation. Results represent percentage of the values obtained in dimethyl sulfoxide (DMSO)–treated cells (set to 100%) ± SD (n = 4).

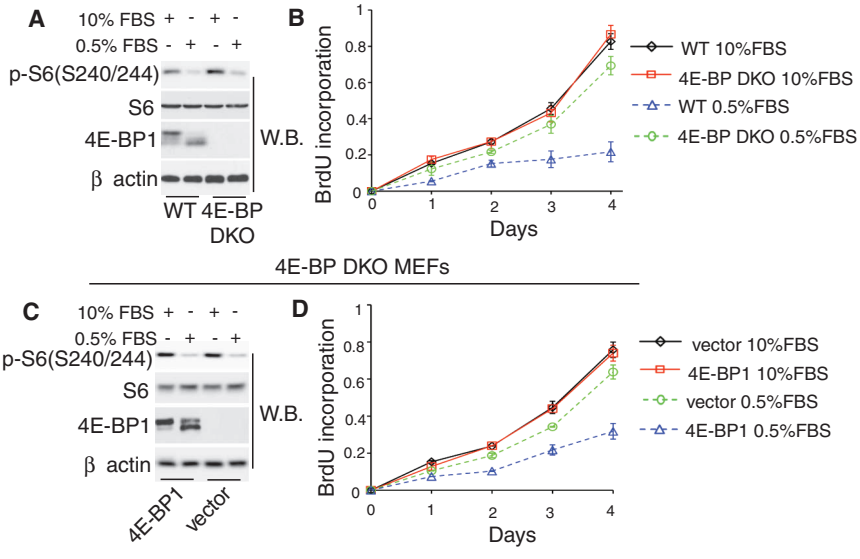

Fig. 2. 4E-BPs regulate cell proliferation in low-serum conditions. (**A** and **C**) Levels of the indicated proteins were determined by Western blotting in WT and 4E-BP DKO MEFs (A) or 4E-BP DKO MEFs infected with vector or 4E-BP1 construct (C) and maintained for 48 hours in 10% or 0.5% FBS. β-actin served as a loading control. (**B** and **D**) Proliferation of WT and 4E-BP DKO MEFs (B) or 4E-BP DKO MEFs infected with vector or 4E-BP1 construct (D) maintained in 10% or 0.5% FBS was measured by BrdU incorporation. Results represent means ± SD (n = 3).

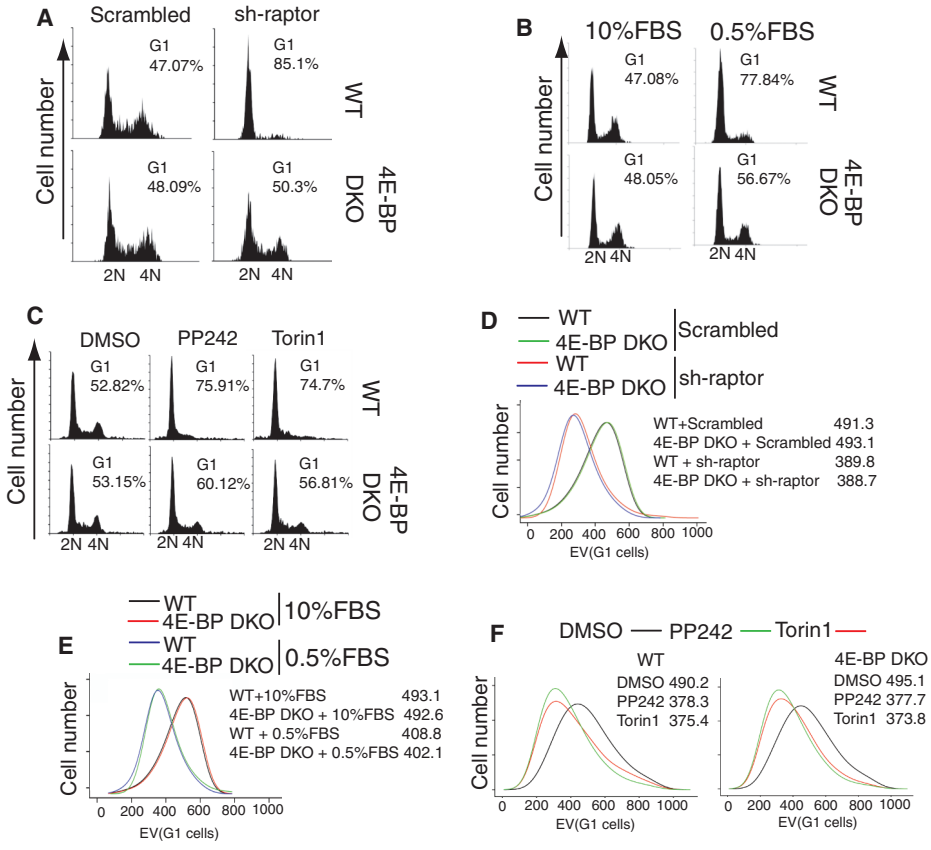

Fig. 3. 4E-BPs mediate the effects of mTORC1 signaling on cell cycle, but not on cell size. (**A** to **C**) Cell cycle distributions for WT and 4E-BP DKO MEFs infected with a control or raptor-specific (sh-raptor) shRNA (A), maintained in 10% or 0.5% FBS for 48 hours (B), or treated with 2.5 μM PP242, 250 nM Torin1, or vehicle (DMSO) for 24 hours (C) were monitored by flow cytometry. N indicates DNA content. (**D** to **F**) Cell size distributions for WT and 4E-BP DKO MEFs infected with a scrambled control or raptor-specific (sh-raptor) shRNA (D), maintained in 10% or 0.5% FBS (E), or treated as in (C) with the indicated compounds (F). The size of G_1 cells was determined by measuring electronic volume (EV) with flow cytometry; numbers represent mean EV values.

amino acids (*7*). In low (0.5%) serum, or in the absence of amino acids, mTORC1 activity was blunted, as measured by decreased 4E-BP1 and S6 phosphorylation (Fig. 2A and fig. S2D). In 10% serum or in the presence of amino acids, wild-type and 4E-BP DKO MEFs proliferated at the same rate, whereas in low serum or in the absence of amino acids, 4E-BP DKO MEFs proliferated at a faster rate than wild-type MEFs (Fig. 2B and fig. S2E). These effects were specific, as reexpression of 4E-BP1 slowed proliferation of 4E-BP DKO MEFs exposed to low serum (Fig. 2, C and D). Thus, distinct stimuli mediate proliferative responses largely through 4E-BPs.

Unlike rapamycin, active-site mTOR inhibitors (asTORi; e.g., PP242 and Torin1) suppress rapamycin-resistant phosphorylation of 4E-BPs (*8*–*10*) (fig. S1A and fig. S3, A and B). The antiproliferative effects of asTORi on wild-type MEFs were partially attenuated in 4E-BP DKO MEFs (fig. S3, C and D), most likely due the inhibition of both mTORC1 and mTORC2 (fig. S2C). The specificity of the inhibitory effects of asTORi is demonstrated by the finding that the proliferation of 4E-BP DKO MEFs, in which 4E-BP1 was reexpressed, was more strongly inhibited than in the 4E-BP DKO MEFs infected with a control virus (fig. S3E). In contrast to asTORi, U0126, a mitogen-activated protein kinase kinase (MAPKK) inhibitor (*11*), suppressed the proliferation of both MEFs to the same extent, whereas the combination of Torin1 and U0126 had an additive inhibitory effect (fig. S3F). Thus, the effects of asTORi appear to be specific for mTOR and are largely mediated by 4E-BPs. Depletion of 4E-BPs also conferred resistance of U937 (human promonocytic cell line) and Jurkat cells (human T cell leukemia cell line) to the antiproliferative effects of asTORi (fig. S3G).

Next, we investigated whether the inhibition of proliferation by 4E-BPs is associated with the attenuation of cell cycle progression, cell survival, or cell growth. Depletion of raptor by short hairpin RNA (shRNA) impaired G_1 to S phase progression of wild-type MEFs but had little effect on 4E-BP DKO MEFs (Fig. 3A). Likewise, the inhibition of wild-type cell cycle progression by serum deprivation or treatment with asTORi was largely unaffected in 4E-BP DKO MEFs (Fig. 3, B and C). Under all these conditions, there were no apparent differences in survival of wild-type and 4E-BP DKO MEFs (fig. S4, A to C). Depletion of raptor, serum deprivation, or addition of asTORi decreased cell size in wild-type and 4E-BP DKO MEFs to a similar extent (Fig. 3, D to F). Thus, mTORC1-mediated inhibition of 4E-BPs affects proliferation through the modulation of the cell cycle, rather than cell survival or cell size; this suggests that in mammalian cells, the regulation of cell size and proliferation can be uncoupled.

S6Ks play a key role in the control of cell size (*12*), and S6K DKO MEFs are smaller than their wild-type counterparts (fig. S5A). asTORi-induced reduction in cell size was abrogated in S6K DKO MEFs (fig. S5A). Reexpression of S6K1 and 2 (fig. S5G) or of a constitutively active mutant, $S6K1^{CA}$ (fig. S5H), completely restored cell size (fig. S5, A to C). asTORi decreased the size of S6K1/2-rescued MEFs as compared to S6K1/2 DKO MEFs (fig. S5B), whereas the drugs failed to reduce the size of cells expressing asTORi-insensitive $S6K1^{CA}$ (fig. S5, C and I). Thus, the inhibitory effects of asTORi on cell size appear to be mediated by the S6Ks. In contrast to cell size, asTORi induced accumulation of G_1-phase cells irrespective of their S6K status (fig. S5, D to F). Although 4E-BP DKO MEFs exhibited increased S6K activity (*13*) (Fig. 1A), these data indicate that the proliferative response is independent of S6Ks. Accordingly, the depletion of 4E-BPs rendered both wild-type and S6K DKO MEFs equally resistant to the antiproliferative effects of asTORi (fig. S6, A and B), demonstrating that 4E-BPs control proliferation downstream of mTORC1 independent of S6Ks. asTORi inhibition of cell size, cell proliferation, and cell cycle progression were all ameliorated in S6K1/4E-BP1/2 triple-knockout (TKO) MEFs (fig. S6C).

mTOR promotes cell proliferation through enhanced translation of a subset of mRNAs referred to as "eIF4E-sensitive" (*2*). Thus, the resistance of 4E-BP DKO cells to asTORi may be due to their inability to suppress the formation of eIF4F complexes, which is required for the translation of mRNAs needed for cell proliferation. We

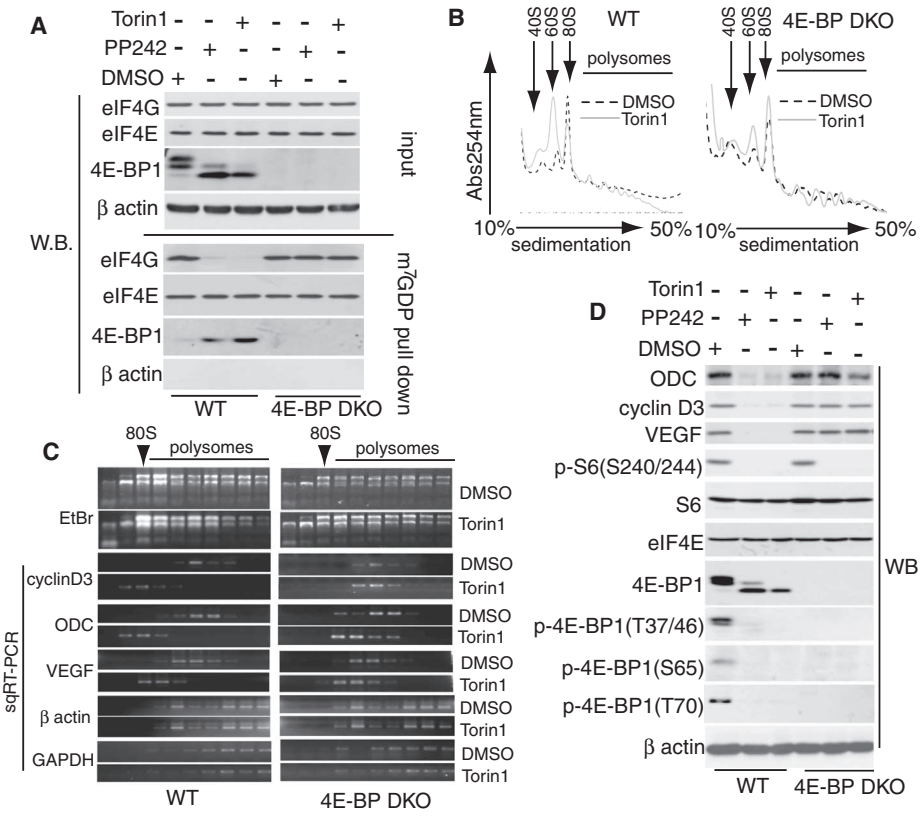

Fig. 4. asTORi inhibit translation of mRNAs encoding proliferation-promoting proteins via 4E-BPs. (**A**) WT and 4E-BP DKO MEFs treated for 24 hours with 2.5 μM PP242, 250 nM Torin1, or vehicle (DMSO) were subjected to m^7GDP pull-down. Amounts of the indicated proteins in the input (10%) or pull-down (25%) were determined by Western blotting; β-actin served as a loading control (input) and to exclude contamination (m^7GDP pull-down). (**B**) Absorption profiles of ribosomes from WT and 4E-BP DKO cells treated for 24 hours with 250 nM Torin1 or vehicle (DMSO). 40*S* and 60*S* denote the corresponding ribosomal subunits; 80*S*, monosome. (**C**) RNA was visualized by ethidium bromide (EtBr). Distribution of cyclin D3, VEGF, ODC, β-actin, and GAPDH mRNAs was determined by semiquantitative reverse transcription polymerase chain reaction (sqRT-PCR). The RT-PCR reactions were in the linear range (fig. S7I). (**D**) WT and 4E-BP DKO MEFs were treated as in (A), and the amount of the indicated proteins was determined by Western blotting. β-actin served as a loading control.

treated wild-type and 4E-BP DKO MEFs with asTORi and assessed eIF4F complex formation. Equal amounts of eIF4E were associated with N7 methyl-guanosine diphosphate (m^7GDP) in the absence or presence of asTORi (Fig. 4A). asTORi impaired eIF4F complex formation in 4E-BP wild-type MEFs, as judged by the increase in 4E-BP1 binding to m^7GDP and the corresponding decrease in eIF4G binding, but not in 4E-BP DKO MEFs (Fig. 4A); this finding demonstrated that the inhibition of eIF4F assembly by asTORi is largely mediated by 4E-BPs. Torin1 impaired translation to a greater extent in wild-type than in 4E-BP DKO MEFs, as illustrated by an increase of 40*S* and 60*S* ribosomal subunits and a decrease in polysomes (Fig. 4B), and strongly reduced polysome loading of eIF4E-sensitive ornithine decarboxylase (ODC), cyclin D3, and vascular endothelial growth factor (VEGF) mRNAs (*14*, *15*) in wild-type MEFs, but only slightly in 4E-BP DKO MEFs (Fig. 4C). Torin1 had no effect on transcription or mRNA export, as judged by the unaltered cytoplasmic levels of cyclin D3, VEGF, and ODC mRNAs (fig. S7A), and it specifically inhibited ribosome recruitment of eIF4E-sensitive mRNAs, as it had no impact on the polysome loading of eIF4E-insensitive β-actin and glyceraldehyde 3-phosphate dehydrogenase (GAPDH) mRNAs (Fig. 4C). The amounts of cyclin D3, VEGF, and ODC proteins were reduced to a greater extent by asTORi in wild-type than in 4E-BP DKO MEFs, whereas asTORi had no effect on eIF4E-insensitive S6, eIF4E, and β-actin proteins (Fig. 4D). Thus, in the absence of 4E-BPs, asTORi failed to suppress the translation of eIF4E-sensitive mRNAs required for cell proliferation.

To ascertain whether asTORi's inhibition of translation of eIF4E-sensitive mRNAs is dependent on the 4E-BP phosphorylation status, we expressed wild-type, 4Ala, or Δ4EBS 4E-BP1 (*16*, *17*) in 4E-BP DKO MEFs. 4Ala 4E-BP1 has all its mTORC1-sensitive phosphorylation sites mutated to alanines, and it constitutively binds to eIF4E (*18*). Δ4EBS 4E-BP1 does not bind to eIF4E but is phosphorylated by mTORC1, albeit to a lesser extent than wild-type 4E-BP1 (*18*, *19*) (fig. S7B). Expression of 4Ala 4E-BP1 impaired eIF4F complex formation (fig. S7C); decreased abundance of ODC, cyclin D3, and VEGF (fig. S7B); slowed proliferation rates (fig. S7D); and reduced G_1/S progression (fig. S7E). Although Torin1 completely inhibited phosphorylation of wild-type 4E-BP1 and Δ4EBS 4E-BP1, only cells expressing wild-type 4E-BP1 exhibited decreased eIF4F complex assembly (fig. S7C); lower abundance of ODC, cyclin D3, and VEGF (fig. S7B); reduced proliferation rates (fig. S7D); and slower cell cycle progression (fig. S7E). Torin1 inhibited mTORC1 signaling equally in all cell lines (fig. S7B). Expression of wild-type and 4E-BP1 mutants had no major effect on cell size or the ability of Torin1 to reduce it (fig. S7F).

Finally, it is known that mTOR signaling is frequently dysregulated in cancer (*20*, *21*) and that 4E-BPs can act as tumor suppressors (*22*, *23*). Consistent with these observations, asTORi reduced the number and size of colonies formed by E1A- and Ras-transformed wild-type MEFs, a response that was strongly attenuated in 4E-BP DKO MEFs (fig. S7, G and H). These data support the argument that the antitumorigenic effects of asTORi are in part dependent on the binding of nonphosphorylated 4E-BPs to eIF4E and suggest that malignant cells may progress through the cell cycle independently of a cell size checkpoint by inactivating 4E-BPs.

In *Drosophila*, dS6K and d4E-BP have overlapping roles, in which both proteins influence cell growth and proliferation (*24*, *25*). Our results indicate that 4E-BPs mediate mTORC1 effects to promote cell proliferation, but not growth, in mammalian cells, bolstering the theory that mammals evolved separate mechanisms to regulate cell proliferation and growth (*12*, *26*).

References and Notes

1. D. A. Guertin, D. M. Sabatini, *Cancer Cell* **12**, 9 (2007).
2. N. Hay, N. Sonenberg, *Genes Dev.* **18**, 1926 (2004).
3. A. Pause *et al.*, *Nature* **371**, 762 (1994).
4. A. Y. Choo, J. Blenis, *Cell Cycle* **8**, 567 (2009).
5. K. Hara *et al.*, *Cell* **110**, 177 (2002).
6. S. H. Um, D. D'Alessio, G. Thomas, *Cell Metab.* **3**, 393 (2006).
7. S. Wullschleger, R. Loewith, M. N. Hall, *Cell* **124**, 471 (2006).
8. M. E. Feldman *et al.*, *PLoS Biol.* **7**, e38 (2009).
9. J. M. Garcia-Martinez *et al.*, *Biochem. J.* **421**, 29 (2009).
10. C. C. Thoreen *et al.*, *J. Biol. Chem.* **284**, 8023 (2009).
11. M. F. Favata *et al.*, *J. Biol. Chem.* **273**, 18623 (1998).
12. M. Ohanna *et al.*, *Nat. Cell Biol.* **7**, 286 (2005).
13. O. Le Bacquer *et al.*, *J. Clin. Invest.* **117**, 387 (2007).
14. A. De Benedetti, J. R. Graff, *Oncogene* **23**, 3189 (2004).

15. J. R. Graff, B. W. Konicek, J. H. Carter, E. G. Marcusson, *Cancer Res.* **68**, 631 (2008).
16. A. C. Gingras *et al.*, *Genes Dev.* **13**, 1422 (1999).
17. L. Rong *et al.*, *RNA* **14**, 1318 (2008).
18. A. R. Tee, J. A. Tee, J. Blenis, *FEBS Lett.* **564**, 58 (2004).
19. X. Wang, A. Beugnet, M. Murakami, S. Yamanaka, C. G. Proud, *Mol. Cell. Biol.* **25**, 2558 (2005).
20. D. Ruggero, P. P. Pandolfi, *Nat. Rev. Cancer* **3**, 179 (2003).
21. D. M. Sabatini, *Nat. Rev. Cancer* **6**, 729 (2006).
22. E. Petroulakis *et al.*, *Cancer Cell* **16**, 439 (2009).
23. Y. Y. Kim *et al.*, *Cancer Res.* **69**, 8455 (2009).
24. M. Miron *et al.*, *Nat. Cell Biol.* **3**, 596 (2001).
25. J. Montagne *et al.*, *Science* **285**, 2126 (1999).
26. I. Conlon, M. Raff, *J. Biol.* **2**, 7 (2003).
27. Rapamycin was from LC laboratories and Calbiochem, PP242 was from Intellikine, and Torin1 was from N. Gray and D. Sabatini. Experimental procedures are described in the supplementary material. We thank M. Pende for S6K1CA construct; M. Holcik and N. Colburn for antibody to PDCD4; K. Shokat, C. Rommel, L. W. Ler, S. Fumagalli, and M. Livingstone for advice; C. Lister and P. Kirk for assistance; and M. Daston for editing. Supported by a grant from the Canadian Cancer Society and a Howard Hughes Medical Institute international research scholarship (N.S.); a Terry Fox Foundation research studentship (R.J.O.D.); NIH Mouse Models for Human Cancer Consortium grant U01 CA84292-06 (N.S., G.T., and S.C.K.); a Leukemia and Lymphoma Society special fellowship (I.T.); Canadian Institutes of Health Research and Alberta Heritage Foundation for Medical Research postdoctoral fellowships (T.A.); a Natural Sciences and Engineering Research Council of Canada predoctoral fellowship (M.B.); a CIHR consortium training fellowship award (B.D.F.); the Research Participation Program at the Air Force Research Laboratory, Human Effectiveness Directorate, Bioscience and Protection, Wright-Patterson AFB, administered by the Oak Ridge Institute for Science and Education (A.S.); NIH grants R01 DK73802 and P50 NS057531 (G.T. and S.C.K.); and the John and Gladys Strauss Chair in Cancer Research (G.T.). G.T. is a paid consultant for Novartis Oncology. There are MTAs or patents restricting use of materials listed, described as: PP242 and Torin1.

Supporting Online Material

www.sciencemag.org/cgi/content/full/328/5982/1172/DC1
Materials and Methods
Figs. S1 to S7
Table S1
References

26 January 2010; accepted 2 April 2010
10.1126/science.1187532

Fairness and the Development of Inequality Acceptance

Ingvild Almås,[1,2]*† Alexander W. Cappelen,[1]* Erik Ø. Sørensen,[1,2]* Bertil Tungodden[1,3]*

Fairness considerations fundamentally affect human behavior, but our understanding of the nature and development of people's fairness preferences is limited. The dictator game has been the standard experimental design for studying fairness preferences, but it only captures a situation where there is broad agreement that fairness requires equality. In real life, people often disagree on what is fair because they disagree on whether individual achievements, luck, and efficiency considerations of what maximizes total benefits can justify inequalities. We modified the dictator game to capture these features and studied how inequality acceptance develops in adolescence. We found that as children enter adolescence, they increasingly view inequalities reflecting differences in individual achievements, but not luck, as fair, whereas efficiency considerations mainly play a role in late adolescence.

It is well documented that adult humans are motivated by fairness considerations and are willing to sacrifice personal gains in order to eliminate inequalities they view as unfair (*1*, *2*). It is also evident from the political debate, surveys (*3*, *4*), and economic experiments (*5*–*7*) that most adults view some inequalities as fair. In particular, most adults believe that differences in individual achievements (*5*–*8*) and efficiency considerations of what maximizes total benefits (*9*–*11*) may justify an unequal distribution of income, but they disagree on whether inequalities reflecting luck are fair (*7*, *12*).

To illustrate how efficiency and individual achievements may justify an unequal distribution of resources, consider two children, Anne and Carla, who discuss how to divide a cake. Anne appeals to efficiency when she argues that total benefits are maximized by giving her the largest share because she enjoys cake the most. Carla appeals to individual achievements when she argues that she should have the largest share because her contribution to making the cake was the largest. The legitimacy of these, and other, fairness considerations has been extensively discussed in the philosophical literature (*13*–*15*), and such considerations are important for how people make decisions in a wide range of situations (*16*). For example, in the workplace, some may find it fair that a more productive colleague has a higher wage, and, in allocating public funds, some may find it fair to pay some attention to which projects produce the greatest total benefits for the population.

Disagreements over questions of fair distribution are fundamental in human life, and to get a better understanding of the sources of such disagreements, it is important to study how fairness views develop in childhood (*17*). The development of children's fairness views has been extensively studied in the psychological literature

[1]Norwegian School of Economics and Business Administration, Department of Economics, N-5045 Bergen, Norway. [2]Centre of Equality, Social Organization, and Performance (ESOP), University of Oslo, N-0317 Oslo, Norway. [3]Chr. Michelsen Institute, N-5892 Bergen, Norway.

*All authors contributed equally to this work.
†To whom correspondence should be addressed. E-mail: ingvild.almas@nhh.no

Table 1. Descriptive statistics (means ± SEM). Mean share given was calculated as the recipient's share of total income for the pair.

Share given and multiplier	Males in grade level (*n*)					Females in grade level (*n*)				
	5th (58)	7th (51)	9th (51)	11th (36)	13th (35)	5th (46)	7th (56)	9th (42)	11th (61)	13th (50)
(A) Share given in first part of experiment										
Share given	0.422	0.449	0.466	0.435	0.448	0.443	0.467	0.457	0.435	0.481
	±0.020	±0.017	±0.013	±0.027	±0.028	±0.022	±0.016	±0.014	±0.016	±0.018
(B) Share given in second part of experiment										
Share given (multiplier = 1)	0.371	0.382	0.443	0.282	0.366	0.438	0.402	0.455	0.372	0.423
	±0.031	±0.028	±0.021	±0.040	±0.038	±0.028	±0.025	±0.018	±0.024	±0.029
Share given (multiplier = 2)	0.400	0.418	0.500	0.429	0.470	0.397	0.425	0.472	0.396	0.442
	±0.035	±0.030	±0.019	±0.043	±0.033	±0.030	±0.024	±0.017	±0.025	±0.037
Share given (multiplier = 3)	0.418	0.430	0.510	0.495	0.496	0.418	0.426	0.482	0.396	0.491
	±0.037	±0.031	±0.022	±0.046	±0.047	±0.031	±0.025	±0.023	±0.032	±0.035
Share given (multiplier = 4)	0.408	0.435	0.562	0.507	0.536	0.451	0.415	0.483	0.413	0.501
	±0.037	±0.034	±0.022	±0.049	±0.046	±0.033	±0.025	±0.023	±0.032	±0.035

(*18*–*23*) and also, more recently, in the economic literature (*24*–*28*). It has been shown that, with age, young children tend to become less selfish in their reasoning (*18*, *19*, *21*, *23*) and choices (*20*, *24*, *25*, *28*), whereas the evidence for adolescents is more mixed (*23*, *25*–*27*, *29*). Furthermore, with age, children tend to move from a strict egalitarian view toward fairness views taking into account individual contributions and circumstances (*17*–*21, 30*).

There has, however, been little research on the development of two important features of adults' distributive behavior, namely that they distinguish between achievements and luck (*7*, *12*) and take efficiency considerations into account (*9*–*11*). To study the development of these features, we conducted a computer-based experiment with children in 5th grade to 13th grade (*31*), where we used two versions of the dictator game. In the dictator game, the dictator is assigned an amount of money to distribute between him or herself and another person, and the total income of the two participants is unaffected by how the money is distributed. In such a situation, there is no apparent fairness argument justifying an unequal division of the money. In the first part of the experiment, we modified this design by introducing a production phase, such that the money to be distributed was earned and depended on individual achievements and luck. In the second part of the experiment, the dictator was given a number of points to distribute, and the distribution of points determined the income for each of the two participants. To introduce efficiency considerations, we made the points most valuable for the other participant, so that the dictator could maximize the total income of the two by giving away all the points.

The framework for our analysis assumes that children make a trade-off between two motives in their distributive choices, self-interest and fairness, and that they may differ both in their level of self-interest and in what they consider fair. By observing how the children chose in a series of different situations, where different fairness views to a varying degree justified giving money to the other participant, we established the importance of each of the fairness views at the different grade levels.

Before they started the first part of the experiment, the participants were given complete information about both the production phase and the distribution phase. The production phase lasted 45 min, and the participants could move between two Web sites. At a production site, the participants could collect points by ticking off every appearance of a particular number on a sequence of screens filled with different three-digit numbers. At an entertainment site, the participants could view short videos or pictures, read cartoons, or play computer games. The participants decided how much time they wanted to spend on each of the two sites. Most participants worked all the time on the production site (average time, 42 min), but this design made salient that production was the result of individual ability and choice of effort. After the production phase, the computer calculated how many points each participant had collected. The participants were then randomly assigned either a high price per point of 0.40 NOK (U.S. ~$0.08) or a low price per point of 0.20 NOK. This design introduced a distinction between two sources of inequality in earnings: production, reflecting individual achievements, and earnings, partly reflecting luck in the random draw of prices.

In the distribution phase, the participants were randomly matched in a sequence of pairs with participants at the same grade level. For each pair, the participants were given information about the time spent on the production site, the number of points collected, the price, and the earnings, and were then asked to choose how much of the total income (the sum of individual earnings for the pair) to take for themselves. Because average production increased with age, the average income to be distributed in each pair also increased with age (table S4).

The mean share given to the other participant in the first part of the experiment was very high, close to 45% for the whole sample, and there was no statistically significant difference in mean share given between 5th grade and 13th grade [(Table 1A), *t* test, unequal variance, $P = 0.460$ (males) and $P = 0.179$ (females)]. Hence, we did not find any evidence of a change in selfishness from mid-childhood to late adolescence (*31*). Moreover, we did not find any statistically significant differences in self-interest between males and females [(Table 1A), *t* test, unequal variance, $P = 0.481$ (5th grade), $P = 0.438$ (7th grade), $P = 0.621$ (9th grade), $P = 0.996$ (11th grade), and $P = 0.330$ (13th grade)].

We did, however, observe an increase with age in the acceptance of inequalities reflecting differences in production. The coefficient for share produced by the other participant, in a regression of share given, showed that older participants were much more likely to differentiate on the basis of individual achievements (Fig. 1A). The sharpest increase in the coefficient occurred from 5th grade to 7th grade, but there was also a further increase from 7th grade to 13th grade. There was a statistically significant difference between 5th grade and all other grades in the coefficient for share produced [multiple Wald tests of equality with Bonferroni adjustments, $P = 0.001$ (7th grade), $P = 0.001$ (9th grade), $P = 0.025$ (11th grade), and $P < 0.001$ (13th grade)], and between 7th grade and 13th grade (Wald test, $P = 0.034$). We observed the same developmental pattern for

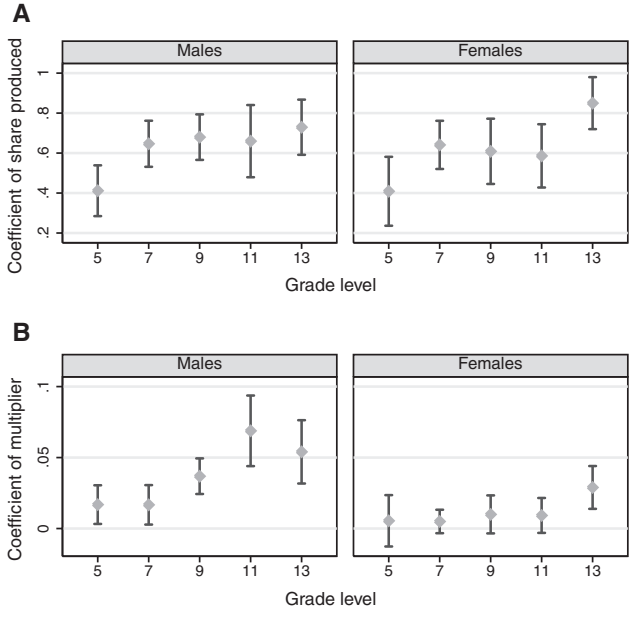

Fig. 1. (**A**) The coefficient for the share produced by the other participant in a regression of share given on share produced. (**B**) The coefficient for the multiplier in a regression of share given on the multiplier. All regressions control for personal fixed effects (*31*). Confidence intervals (95%) are indicated.

Table 2. Estimates of the choice model (estimate ± SE). The complete set of estimates is in table S3.

	Grade level					
	5th	7th	9th	11th	13th	All
Share of egalitarians	0.636	0.401	0.272	0.267	0.224	0.365
	±0.060	±0.059	±0.057	±0.056	±0.056	±0.027
Share of meritocrats	0.054	0.220	0.363	0.396	0.428	0.287
	±0.037	±0.054	±0.063	±0.069	±0.075	±0.028
Share of libertarians	0.310	0.379	0.364	0.337	0.347	0.348
	±0.057	±0.055	±0.061	±0.059	±0.069	±0.026
Log likelihood	−827.4	−881.4	−797.6	−865.0	−790.3	−4219.7

both males and females; there were no statistically significant gender differences in the coefficient for share produced [Wald test, $P = 0.980$ (5th grade), $P = 0.949$ (7th grade), $P = 0.534$ (9th grade), $P = 0.571$ (11th grade), and $P = 0.214$ (13th grade)]. The coefficient for the relative price was also statistically significantly different from zero, but stable across grade levels and gender (*31*).

To further study the importance of production and price in explaining the observed behavior, we estimated a model of individual choices that captured the basic assumptions of our theoretical framework and allowed for some randomness in the participants' choices (*31*). Specifically, for each grade level, we estimated a distribution of the weight attached to fairness and the share of participants motivated by different fairness views. Informed by normative theory and our own previous work (*7*, *12*), we assumed that there were three salient fairness views in this situation: strict egalitarianism (*13*), finding all inequalities unfair; meritocratism (*32*), justifying inequalities reflecting differences in production; and libertarianism (*14*), justifying all inequalities in earnings.

We found striking differences in the prevalence of fairness views between the grade levels (Table 2). The large majority of 5th graders were strict egalitarians, and, remarkably, there were almost no meritocrats at this grade level. In contrast, meritocratism was the dominant position in late adolescence, and the share of strict egalitarians fell dramatically. The share of libertarians was stable across grade levels. In sum, this analysis showed that, with age, individual achievements, measured by production, became increasingly important in children's fairness considerations, whereas there was no similar development in the importance of luck, measured by price.

The estimated choice model also confirmed our finding of no change in selfishness from midchildhood to late adolescence; the estimated median weight attached to self-interest was stable across grade levels (table S3). Overall, the estimated model fit the data well for all grade levels (fig. S1).

In the second part of the experiment, we studied inequality acceptance in situations involving efficiency considerations. The participants were given the task of distributing a number of points, where total benefits (in terms of income) would be maximized by giving all the points to the other participant. Specifically, the participants were informed that they would receive 1 NOK for each point kept for themselves, whereas each point given away would earn the other participant 1 NOK scaled up by a multiplier. Each participant made choices in four distributional situations, presented in random order, where the multiplier was 1 (the baseline), 2, 3, and 4, respectively (*31*). Hence, efficiency considerations did not play any role in the baseline situation, but were increasingly salient in the other three situations. In each situation, the participants were randomly paired with another participant at the same grade level. For comparability, we set the number of points to be distributed such that the average income in the baseline situation was equal to the session-specific average income in the first part of the experiment.

We observed that 5th graders and 7th graders did not assign much importance to efficiency considerations; the mean share given was only slightly higher when the points transferred were scaled up by four than in the baseline situation (Table 1B). In contrast, the effect of the multiplier was substantial for males in late adolescence and also noticeable for females in 13th grade. These patterns are reflected in the coefficient for the multiplier in a regression of share given (Fig. 1B). There was a statistically significant increase in the coefficient from 5th grade to 13th grade for both males and females [Wald test, $P = 0.003$ (males) and $P = 0.019$ (females)], which reflects that older participants were more likely to differentiate on the basis of efficiency considerations. This development, however, took place later in adolescence than the differentiation on the basis of individual achievements. Moreover, we observed a statistically significant difference between males and females from 9th grade, where efficiency considerations played a more important role for males than females [Wald test, $P = 0.316$ (5th grade), $P = 0.152$ (7th grade), $P = 0.005$ (9th grade), $P < 0.001$ (11th grade), and $P = 0.060$ (13th grade)].

Our analysis showed that children's level of self-interest was stable across adolescence, whereas their fairness views changed fundamentally in the same period. In particular, we found increased importance of the meritocratic fairness view, which requires a distinction between different sources of inequality. We did not, however, observe a uniform move away from the two less complex fairness views. Although there was a sharp decrease in the importance of the strict egalitarian fairness view, the prevalence of the libertarian fairness view was stable throughout adolescence. These findings shed some light on the role of both cognitive maturation and social experiences in shaping children's fairness preferences. The meritocratic fairness view presupposes the ability to distinguish between relevant and irrelevant information, a cognitive ability that matures during adolescence (*33*), which may partly explain why we observed increased prevalence of this view. The strict egalitarian and libertarian fairness views, however, are straightforward to implement, and thus, the different development for these two fairness views is hard to explain by cognitive maturation. This suggests that social experiences also play a role in shaping children's fairness preferences.

References and Notes

1. E. Fehr, A. Falk, *Eur. Econ. Rev.* **46**, 687 (2002).
2. C. F. Camerer, *Behavioral Game Theory: Experiments in Strategic Interaction* (Princeton Univ. Press, Princeton, NJ, 2003).
3. E. Schokkaert, K. Devooght, *Soc. Choice Welfare* **21**, 207 (2003).
4. W. Gaertner, L. Schwettmann, *Economica* **74**, 627 (2007).
5. J. Konow, *Am. Econ. Rev.* **90**, 1072 (2000).
6. N. Frohlich, J. Oppenheimer, A. Kurki, *Public Choice* **119**, 91 (2004).
7. A. W. Cappelen, A. D. Hole, E. Ø. Sørensen, B. Tungodden, *Am. Econ. Rev.* **97**, 818 (2007).
8. T. L. Cherry, P. Frykblom, J. F. Shogren, *Am. Econ. Rev.* **92**, 1218 (2002).
9. P. A. M. Van Lange, *J. Pers. Soc. Psychol.* **77**, 337 (1999).
10. J. Andreoni, J. Miller, *Econometrica* **70**, 737 (2002).
11. R. J. Fisman, S. Kariv, D. Markovits, *Am. Econ. Rev.* **97**, 1858 (2007).
12. A. W. Cappelen, E. Ø. Sørensen, B. Tungodden, *Eur. Econ. Rev.* **54**, 429 (2010).
13. J. Rawls, *A Theory of Justice* (Harvard Univ. Press, Cambridge, MA, 1971).
14. R. Nozick, *Anarchy, State, and Utopia* (Basic Books, New York, 1974).
15. A. Sen, *The Idea of Justice* (Harvard Univ. Press, Cambridge, MA, 2009).
16. L. Montada, *The Justice Motive in Everyday Life* (Cambridge Univ. Press, Cambridge, 2002).
17. C. F. Moore, S. E. Hembree, R. D. Enright, *Psychological Perspectives on Justice*, B. A. Mellers, J. Baron, Eds. (Cambridge Univ. Press, Cambridge, 1993), chap. 9, pp. 183–204.
18. J. Piaget, *The Moral Judgement of the Child* (Free Press, New York, 1965).
19. W. Damon, *The Social World of the Child* (Jossey-Bass, San Francisco, 1977).
20. J. G. Hook, T. D. Cook, *Psychol. Bull.* **86**, 429 (1979).
21. L. Kohlberg, *Essays in Moral Development.* vol. II: *The Psychology of Moral Development* (Harper and Row, San Francisco, 1984).
22. C. Gilligan, *In a Different Voice* (Harvard Univ. Press, Cambridge, MA, 1982).
23. N. Eisenberg, G. Carlo, B. Murphy, P. Van Court, *Child Dev.* **66**, 1179 (1995).
24. J. F. Benenson, J. Pascoe, N. Radmore, *Evol. Hum. Behav.* **28**, 168 (2007).
25. W. T. Harbaugh, K. Krause, L. Vesterlund, *J. Econ. Psychol.* **28**, 127 (2007).
26. M. Sutter, M. G. Kocher, *Games Econ. Behav.* **59**, 364 (2007).
27. M. Sutter, *J. Econ. Psychol.* **28**, 69 (2007).
28. E. Fehr, H. Bernhard, B. Rockenbach, *Nature* **454**, 1079 (2008).
29. M. Gummerum, M. Keller, M. Takezawa, J. Mata, *Child Dev.* **79**, 562 (2008).
30. G. Mikula, *Z. Entwicklungspsychol. Padagog. Psychol.* **4**, 151 (1972).
31. Materials and methods, as well as supporting text, are available as supporting material on *Science* Online.
32. K. Arrow, S. Bowles, S. Durlauf, Eds., *Meritocracy and Economic Inequality* (Princeton Univ. Press, Princeton, NJ, 2000).
33. L. Steinberg, *Trends Cogn. Sci.* **9**, 69 (2005).

34. We are grateful to S. Bowles and W. T. Harbaugh for valuable comments; R. H. Hansen and G. Myhrvold of the school authorities in Bergen for their cooperation; L. J. Eckhoff, T. Eriksen, M. Frøysok, A. Furu, C. Haugsnes, A. D. Hole, J. Håtuft, K. A. Karlstad, M. Ludvigsen, K. Risvand Mo, C. Nygård, K. E. Stokke, J. N. L. Sønsteby, I. Søreide, and E. Wærstad for research assistance. This project was supported by the Centre for the Study of Mind in Nature (CSMN) at the University of Oslo and the Research Council of Norway, grant 185831.

Supporting Online Material

www.sciencemag.org/cgi/content/full/328/5982/1176/DC1
Materials and Methods
SOM Text
Fig. S1
Tables S1 to S4
References

20 January 2010; accepted 12 April 2010
10.1126/science.1187300

SMALL-CAPACITY INCUBATORS

The Midi 40 is a small-capacity carbon dioxide incubator that delivers the reliable culturing performance of a full-sized incubator in a convenient, space-saving footprint. The Midi 40 is suitable for researchers who lack space or require separate, undisturbed incubation conditions due to the contamination risk associated with shared incubators. Additional benefits include reduced energy and gas consumption as well as lower heat output. The incubation parameters can be easily managed through the incubator's bright, vacuum fluorescent display and easy-to-navigate membrane keypad. The unit features a noncorrosive, stainless steel chamber with 40 liters of culture space, and a heated humidity pan to generate relative humidity values of up to 95 percent.

Thermo Fisher Scientific

For info: 508-742-5254 | www.thermo.com/incubators

PULSELESS LIQUID FLOW

The Mitos P-pump provides a pulseless liquid flow via a precise pressure-driven pumping mechanism. With its excellent response time and accuracy, the pressure-driven flow is suitable for microfluidic systems in which stable flow is required for applications such as droplet formation. Operating over a wide pressure range of 0–10 bar, the pump is suitable for use with systems of high fluidic resistance. The design features a lockable pressure chamber for safety, which is easily accessible and accommodates a wide range of standard and nonstandard fluid vessels. With the ability to contain samples from 100 l to 30 ml, the pump uses fluid directly from the container, producing no mess or waste. The pump can work with a laboratory nitrogen or argon supply, gas bottle, or compressor.

Dolomite

For info: +44-1763-242491 | www.dolomite-microfluidics.com

EXTENDED RANGE PROTEIN STANDARD

A new addition to the Precision Plus Protein line of protein standards, the Precision Plus Protein Dual Xtra standard provides 12 reference bands, from 2 kD to 250 kD. The new standard allows researchers to perform electrophoresis experiments with proteins of varying sizes, without the need to use two lanes in a gel to load two different markers for measurement of proteins in the high and low molecular weight range. The extended range of the new standard allows researchers to use just one molecular weight standard, whether they need to assess proteins with a wide molecular weight range or to focus on the low range only. The new dual standard offers the same sharp, bright, evenly spaced bands as the rest of the Precision Plus Protein family of standards.

Bio-Rad

For info: 800-424-6723 | www.bio-rad.com

OPTICAL OXYGEN SENSOR

The NeoFox Sport is a portable, handheld optical oxygen sensor for measuring dissolved and gaseous oxygen pressure in a variety of media. The sensor makes use of a proprietary sol-gel coating that is embedded with an oxygen indicator and can be applied to patches or probes. Patches are useful for measuring headspace gases and other parameters inside packages and containers. Probe options range from slender, 300- m–diameter fiber assemblies for fine spatial resolution applications to robust, quarter-inch stainless steel configurations for process environments. Coating formulations are available for general lab use, high-sensitivity applications, and hydrocarbon-rich sample environments. The NeoFox Sport fluorescence-based optical oxygen system includes an onboard microprocessor with a low-power organic LED display, a user interface, and a battery pack.

Ocean Optics

For info: 727-733-2447 | www.OceanOptics.com

MICROARRAY

The HumanOmniExpress BeadChip is part of the Omni family of microarrays for genomewide association studies. Designed in a 12-sample format, the OmniExpress allows interrogation of more than 700,000 variants per sample, for more than 8 million data points on a single chip. When used with the Illumina iScan System, OmniExpress allows processing of more than 1,400 samples per week. The markers on the OmniExpress incorporate an optimized set of single nucleotide polymorphisms chosen from all three phases of the International HapMap Project.

Illumina

For info: 858-882-6822 | www.illumina.com/OmniExpress

PROTEIN A KIT AND IMMOBILIZATION STATION

The Dip and Read Residual Protein A Detection Kit is for use on ForteBio's Octet platform. The new assay enables drug developers to measure levels of Protein A quickly with minimal hands-on time. The kit consists of biosensors and all the reagents required to quantitate Protein A or biosimilars in the presence of human immunoglobulin G. Another addition to the Octet platform, the Sidekick Offline Biosensor Immobilization Station, enables offline loading of reagents on biosensors in tandem with any Octet instrument. The station provides simultaneous and uniform sample loading on all 96 biosensors on a biosensor tray and shakes the samples while keeping the biosensors immobile, which decreases the incubation time by half. This process significantly increases the sensitivity of sandwich assays.

Fortebio

For info: 650-289-6800 | www.fortebio.com

Electronically submit your new product description or product literature information! Go to **www.sciencemag.org/products/newproducts.dtl** for more information.

Newly offered instrumentation, apparatus, and laboratory materials of interest to researchers in all disciplines in academic, industrial, and governmental organizations are featured in this space. Emphasis is given to purpose, chief characteristics, and availability of products and materials. Endorsement by *Science* or AAAS of any products or materials mentioned is not implied. Additional information may be obtained from the manufacturer or supplier.